EVALUATION OF COMPACTION SENSITIVITY OF SASKATCHEWAN ASPHALT MIXES

Thesis Submitted to the College of

Graduate Studies and Research

in Partial Fulfillment of the Requirements

for the Degree of Masters of Science

in the Department of Civil and Geological Engineering

University of Saskatchewan

Saskatoon

By

Aziz Salifu

PERMISSION TO USE

In presenting this thesis in partial fulfillment of the requirements for a Postgraduate degree from the University of Saskatchewan, the author has agreed that the Libraries of this University may make it freely available for inspection. The author has further agreed that permission for copying of this thesis in any manner, in whole or in part, for scholarly purposes may be granted by the professor or professors who supervised the thesis work or, in their absence, by the Head of the Department or the Dean of the College in which the thesis work was done. It is understood that any copying, publication, or use of this thesis or parts thereof for financial gain shall not be allowed without the author's written permission. It is also understood that due recognition shall be given to the author and to the University of Saskatchewan in any scholarly use which may be made of any material in this thesis.

Requests for permission to copy or to make other use of material in this thesis in whole or part should be addressed to:

Head of the Department of Civil Engineering

University of Saskatchewan

Saskatoon, Saskatchewan S7N 5A9

ABSTRACT

Saskatchewan Ministry of Highway and Infrastructure (SMHI) currently use the Marshall compaction method for the preparation of hot-mix asphalt laboratory samples. Due to increases in commercial truck traffic on most provincial highways, there has been an observed increasing trend in the occurrence of permanent deformation within the hot-mix asphalt concrete (HMAC) layer. One of the most important material properties found to influence the resistance of HMAC to structural permanent deformation is volumetric air voids within the mix.

End product air voids within a hot mix asphalt concrete pavement in the field is simulated by the method of compaction used during the laboratory design process. Based on findings of the Strategic Highway Research Program (SHRP), the gyratory compactor is believed to better simulate field compaction of asphalt mixes at the time of construction, as well as better predict mix consolidation over the field performance period. However, the Superpave^{TM} sample preparation protocol specifies a fixed angle of gyratory compaction, which may not be the optimal parameters to evaluate Saskatchewan hot-mix asphalt concrete mixes during the laboratory mix design phase.

The primary objective of this research was to investigate the relationship between laboratory characterization and field evaluation of Saskatchewan SPS-9A asphalt mixes across alternate laboratory compaction protocols. A second objective of this research was to quantify the effect of gyratory and Marshall compaction energy on the physical and mechanical properties of Saskatchewan SPS-9A asphalt mixes in the laboratory. The third objective of this research was to compare field ground penetrating radar dielectric permittivity profiles and rutting performance across Saskatchewan SPS-9A test sections.

The hypothesis of this research is that gyratory laboratory compaction will provide improved sensitivity in the characterization of physical asphaltic mix properties. It is also hypothesized that varied volumetric properties of HMAC mixes influence the mechanistic triaxial frequency sweep material properties of both conventional Saskatchewan and Superpave^{TM} dense graded HMAC mixes.

The laboratory portion of this research included volumetric and mechanical properties of the seven Saskatchewan SPS-9A asphaltic mixes.

The scope of this research included an investigation of the Saskatchewan Specific Pavement Study-9A (SPS-9A) asphalt mixes constructed in Radisson Saskatchewan in 1996. Physical volumetric properties as well as mechanistic triaxial frequency sweep properties were characterized across all seven Radisson SPS-9A mixes. Rutting after ten years of performance in the field was quantified as well as *in situ* ground penetrating radar dielectric permittivities of the Radisson SPS-9A test sections.

Based on the findings of the study, there was a significant reduction in VTM with an increase in Marshall compaction energy from 50 to 75 blows. Marshall stability was observed to be higher at 75 blow compared to 50 blows across the test sections.

Similarly, with regards to gyratory sample preparation, there was an observed reduction in VTM with an increase in gyratory compaction energy. VTM of Superpave^{TM} mixes were higher than VTM SMHI Marshall mixes. VTM of the Superpave^{TM} mixes were above acceptable SMHI limits at all angles of gyration at N_{design}. Superpave^{TM} gyratory compactor accurately predicted field air voids of the Radisson SPS-9A asphalt after ten years of traffic loading at 2.00° angle of gyration.

In general, this research showed significant sensitivity of volumetric material properties across both Marshall and gyratory compaction energy.

This research also demonstrated that there was an improvement in the triaxial mechanistic material properties of the Radisson SPS-9A HMAC mixes with an increase in gyratory compaction energy. Dynamic moduli across all test section mixes increased with an increase in gyratory compaction energy. Similarly, it was shown that Poisson's ratio generally increased with an increase in compaction energy across all test sections. Phase angle also increased with an increase in gyratory compaction energy. Radial microstrain (RMS) displayed the most significant sensitivity to increased gyratory compaction energy.

This research concluded that compaction energy in the laboratory can significantly influence the volumetric and mechanistic properties of hot-mix asphalt concrete mixes. As indicated by the field performance of the Radisson SPS-9A test sections, it is known that both volumetric and mechanistic properties can influence field performance. Mechanical material properties of HMAC may be improved by increasing compaction energy, as long as volumetric properties are adhered to. The use of rapid triaxial frequency sweep testing demonstrated the ability to characterize mechanistic material properties as a function of varied compaction energy.

Based on the findings of this research, it is recommended that Saskatchewan asphalt mixes, both Marshall and Superpave^{TM} types, be characterized using gyratory compaction with 2.00° angle of gyration and the SHRP specified number of gyrations. Further, the gyratory compacted samples provide the ability to characterize the mechanistic material constitutive properties of asphaltic mixes for mechanistic based road structural design purposes.

Future research should evaluate the relationship of laboratory material properties to the field performance of various Saskatchewan asphalt mixes across various field state conditions.

ACKNOWLEDGEMENTS

I am most grateful to the Almighty for granting me good health and protection during my study.

I would like to express my sincere gratitude to Dr. Curtis F. Berthelot P. Eng. who has helped and inspired me in diverse ways in the process of my research work. I am not only grateful for your encouragement and continued guidance but I am also grateful for your dedication to discipline and hard work.

My sincere gratitude also goes to the other members of my master's committee: Dr. Jim Kells P. Eng., Dr. Leon Wegner P. Eng., and Dr. Mohammed Boulfiza P. Eng., for their support and input into my master's degree.

I would also like to thank the Saskatchewan Ministry of Highways and Infrastructure and NSERC for their financial help during my master's program.

I would also like to thank Mr. Brent Marjerison P. Eng. and Ms. Ania Anthony P. Eng. of the Saskatchewan Ministry of Highways and Infrastructure for their support and advice throughout my master's program and also as members of my master's committee.

My thank you also goes to Ms. Debbie Forgie, Mr. Alex Kozlow, Mr. Jing Xu, Mr. Joseph Chan and Ms. Diana Podborochynski for their help in the course of my study. I will like to say thank you to Mr. Abukhater Basel of Stantec, and Mr. Dennis Klimochko P. Eng. of Saskatchewan Ministry of Highways and Infrastructure for helping me with field data during my Master's program.

I want to say thank you to Mr. Mukasa Bagonluri, my cousins and friends for their support in my study.

Finally I thank my mother Frances Kazine, my father Abubakar Salifu, Mr. Martin Abu, my wife Niamatu Yakubu, my daughters Tamira and Nasira and my brothers and sisters whose goodwill was motivational in the course of my study.

TABLE OF CONTENTS

LIST OF FIGURES

LIST OF TABLES

LIST OF ABREVIATIONS

AAMAS –Asphalt Aggregates Mixture Analysis System
AASHTO –American Association of State Highway and Transportation Officials
ANOVA –Analysis of Variance
ASTM –American Society of Testing and Materials
CBR –California Bearing Ratio
ESAL –Equivalent Single Axle Load
FR –Fully Reversed
G_{mb} –Bulk Specific Gravity
G_{mm} –Theoretical Maximum Specific Gravity
G_{sb} –Bulk Specific Gravity of Aggregate
HMAC –Hot Mix Asphalt Concrete
IDT –Indirect Tensile Tester
LTPP –Long Term Performing Pavements
LVDT –Linear Variable Differential Transducer
NCHRP –National Co-operative Highway Research Program
N_{des} or N_{design} –Design Number of Gyrations
N_{ini} or $N_{initial}$ –Initial Number of Gyrations
N_{max} or $N_{maximum}$ –Maximum Number of Gyrations
P_s –Aggregate content by weight of mix
PG –Performance Grading
RaTT –Rapid Triaxial Tester
SGC –Superpave™ gyratory compactor
SHRP –Strategic Highway Research Program
SMHI –Saskatchewn Ministry of Highway and Infrastructure
SPS-9A –Strategic Pavement Study 9A
SPT –Simple Performance Test
STP –Standard Test Procedure
Superpave™ –*Per*forming Asphalt *Pave*ments
RMS –Radial Microstrain
VFA –Voids Filled with Asphalt
VMA –Voids in Mineral Aggregates
VTM –Voids in Total Mix

CHAPTER 1 INTRODUCTION

The method used to compact asphalt concrete mixes in the laboratory is known to influence the volumetric and mechanical properties of laboratory compacted asphaltic concrete specimens (Ziauddin et al. 1998, Harvey et al. 1993). Laboratory characterization of compacted HMAC samples is used for the design as well as field performance prediction of asphalt concrete mixes. As a result, it is important to produce compacted asphalt specimens in the laboratory that have similar volumetric and mechanical properties as those obtained from field compaction and long term trafficking of the asphaltic mix (Von Quintus et al. 1991, Sousa et al. 1991).

The underlying objective of asphalt mix design is to design an asphalt mix that is mechanically and climatically durable for the field state conditions upon which it will be expected to perform. Engineering mix design processes typically employ physical mix properties to select the optimum asphalt content that satisfies the required voids in total mix (VTM), voids in mineral aggregates (VMA) and voids filled with asphalt (VFA) (SMHI STP 2001, Asphalt Institute 1996). These physical mix properties are known to be directly related to the field performance of asphalt concrete pavements (Berthelot 2003, Roberts et al. 1996, Asphalt Institute 1996). The VTM, VMA and VFA have also been found to influence the laboratory mechanical and climatic durability properties of hot-mix asphalt concrete (HMAC) (Berthelot 2003, Kandhal and Chakraborty 1996).

1.1 Background

The primary structural distresses of concern with regards to hot-mix asphalt pavement performance in the field are permanent deformation (rutting) and fatigue cracking (Berthelot 2003, Roberts et al. 1996). Figure 1.1 shows typical viscoplastic rutting of an HMAC pavement and Figure 1.2 shows typical fatigue cracking of an HMAC pavement. These distresses are visible on many highways across Saskatchewan. Failures of HMAC pavements are largely attributed to improper volumetric properties of the compacted HMAC, and /or inadequate structural design or construction of the pavement structure (Berthelot 2003, Roberts et al. 1996, Asphalt Institute 1996).

Figure 1.1 Rutting of Hot-Mix Asphalt Pavement

Figure 1.2 Top-Down Edge of Wheelpath Fatigue Cracking of Hot-Mix Asphalt Pavement

High VTM can result in excessive differencial consolidation and / or susceptibility to fatique cracking of the HMAC layer under traffic loading immediately after construction. However, too low VTM can result in viscoplastic flow of the asphalt mix in high temperatures. Viscoplastic rutting occurs due to thermomechanical expansion of the asphalt binder in hot weather, which can force the aggregate skeleton apart (Berthelot 2003, Roberts et al. 1996, Asphalt Institute 1996). VMA has been found to dictate the volumetric properties of compacted asphalt mixes (Heinrichsen and Heggen 1996, Kandhal and Chakraborty 1996). Adequate VMA in turn ensures adequate VTM and VFA, hence preventing excessive consolidation, viscoplastic flow and bleeding of asphalt pavements.

Traditionally, Saskatchewan Ministry of Highways and Infrastructure (SMHI) use the Marshall mix design method for hot-mix asphalt concrete design and construction quality control (SMHI 2001). The Marshall mix design method involves the use of the Marshall compaction hammer at various blows at a standardized drop height as specified in ASTM 1559. To help mitigate rutting, Saskatchewan Ministry of Highways and Infrastructure adopted the 75 Marshall blow mix design method in order to better simulate heavy traffic loading that occurs on many Saskatchewan HMAC pavements during their service life (Anthony 2007).

Gyratory compaction has been used extensively worldwide for decades, and is being used increasingly in North America to compact HMAC mixes in the laboratory (TexDOT 2005, SHRP 1994). It is believed that gyratory compaction better simulates field compaction of asphalt mixes in terms of volumetric and mechanical properties (Harman et al. 2002, Mallick 1999, Butcher 1995). An evaluation of alternate compaction methods reported that HMAC compacted using gyratory compaction showed better resistance to permanent deformation in the field due to a more accurate prediction of volumetric mix properties under heavy traffic (Von Quintus et al. 1989).

The Strategic Highway Research Program (SHRP) introduced the Superpave^{TM} mix design method with the gyratory compactor as an integral part of the mix design process (Harman et al. 2001, SHRP 1994). The Superpave^{TM} gyratory compaction method is a

combined modification of the Texas and French gyratory compaction equipment and protocols. The SHRP gyratory compactor is intended to better simulate the increasing loads and tire pressures of typical modern heavy vehicles operating on pavements. Superpave™ gyratory compaction has also been found to be sensitive in identifying changes in asphalt mix properties particularly asphalt binder content, voids in total mix and voids in mineral aggregates than Marshall compaction method (Harman et al. 1995, Anderson et al. 1995). An additional benefit to the SHRP gyratory compaction of HMAC is the Superpave™ gyratory compaction protocol specifies 150 mm diameter by 150 mm high continuum specimens. The larger gyratory compaction sample size provides improved continuum representation of the volumetric mix properties and has been found to be efficient for characterizing mechanical material properties of HMAC in the laboratory (Gould et al. 2003, Berthelot et al. 1999). However, because of the widespread use of the Marshall drop hammer compaction method, many highway agencies across Canada have not yet adopted the Superpave™ gyratory compaction asphaltic mixes. Therefore, there is a need to show the improved mix design and analysis capabilities of gyratory compaction in the laboratory to evaluate volumetric material properties and performance of asphalt mixes.

1.2 Research Goal

The goal of this research is to investigate alternative laboratory mix compaction and analysis protocols to better characterize the volumetric and mechanical mix properties of typical Saskatchewan asphalt mixes.

1.3 Research Objectives

The objectives of this study are:

1. To characterize and compare the sensitivity of laboratory volumetric properties of the Radisson Specific Pavement Study (SPS-9A) asphalt mixes across varied Marshall and gyratory compaction energies.

2. To characterize and compare the sensitivity of the triaxial frequency sweep mechanical properties of the Radisson SPS-9A asphalt mixes asphalt concrete mixes across various laboratory gyratory compaction energies.

3. To compare field hot mix pavement measures such as ground penetrating radar and rutting performance across Radisson SPS-9A test sections.

1.4 Research Hypothesis

It is hypothesized that gyratory laboratory compaction will provide improved sensitivity in characterization of physical asphaltic mix properties. It is also hypothesized that varied volumetric properties of HMAC mixes influence the mechanistic triaxial frequency sweep material properties of both conventional Saskatchewan and Superpave™ dense graded HMAC mixes.

1.5 Scope of Research

This research considered seven dense graded asphalt mixes that were used in the construction of the SPS-9A test sections near Radisson Saskatchewan. The asphalt concrete mixes used in the construction of the Radisson SPS-9A test sections consisted of two SMHI mixes designed with SMHI conventional Marshall mix design method, four mixes designed with the Superpave™ mix design method, and one recycled asphalt concrete mix also designed with Superpave™ mix design method. Table 1.1 shows the mix design method and binder specifications of each respective Radisson SPS-9A test section. Figure 1.3 shows the site layout plan of the Radisson SPS-9A test site.

Table 1.1 Asphalt Binder and Mix Design Method across Radisson SPS-9A Test Sections

SPS-9A Test Section Number	Specified Asphalt Binder	Mix Design Method
901M	PG 52-28 (AC 150/200)	SMHI Marshall Mix Design
961M	PG 52-34 (AC 200/300)	SMHI Marshall Mix Design
903S	PG 52-34 (AC 200/300)	Superpave™ Mix Design
959S	PG 52-28 (AC 150/200)	Superpave™ Mix Design
960S	PG 46-34 (AC300/400)	Superpave™ Mix Design
902S	PG 52-40	Superpave™ Mix Design
962SR	PG 52-40	Superpave™ Recycled Mix Design

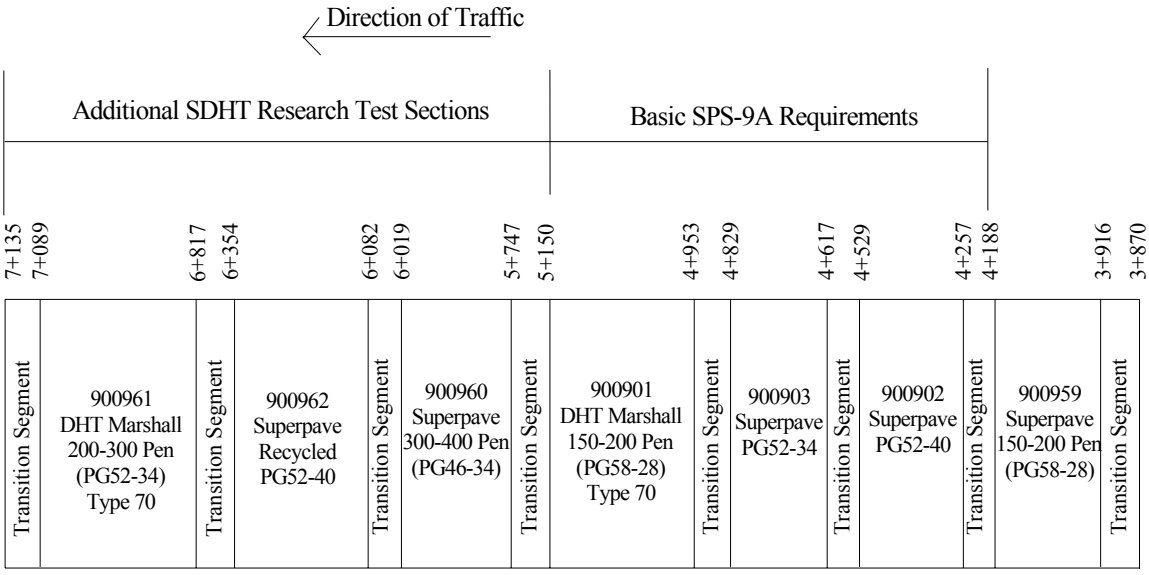

Figure 1.3 Radisson SPS-9A Test Site Layout

The seven Radisson SPS-9A test sections considered in this research were all designed and built with the same structural design cross section as shown in Figure 1.4. The Superpave™ test sections employed mixes with aggregates gradations meeting the Superpave™ coarse mix gradation requirements. The two Saskatchewan Ministry of Highways and Infrastructure mixes met the dense gradation requirements for a typical SMHI Type-71 asphalt concrete mix (SMHI 2000).

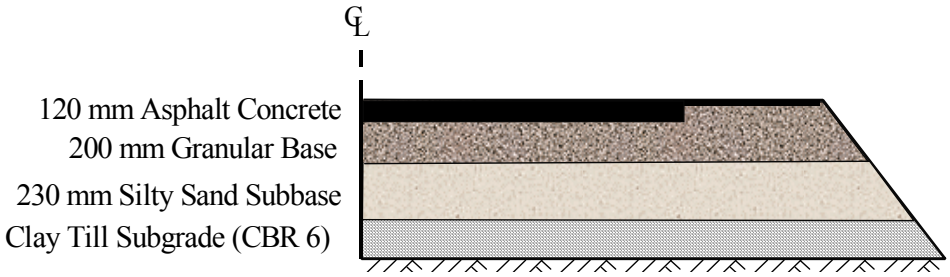

Figure 1.4 Typical Radisson SPS-9A Pavement Structural Cross Section

Field structural quality testing of the Radisson SPS-9A test sections included pavement distress data collection in the form of rut depth measurements across test sections. Rut depth data was collected and provided by SMHI as part of their annual field evaluation of the Radisson SPS-9A test site. Field surface mix properties were also evaluated using ground penetrating radar profiles taken laterally across each test section lane.

Compaction sensitivity of conventional SMHI dense graded and Superpave™ mixes was evaluated using 50 and 75 blow Marshall compaction effort and varied Superpave™ gyratory compaction angles of 1.25°, 2.00°, and 2.75°. Volumetric properties including VMA, VFA and VTM were determined across the compacted specimens.

Marshall stability and flow characterization was performed on Marshall compacted samples. Mechanistic characterization employing rapid triaxial frequency sweep characterization across various load frequencies, stress states and temperatures typical of the field state conditions experienced in Saskatchewan was performed on the gyratory compacted samples. Material properties determined from triaxial frequency sweep test included dynamic modulus, Poisson's ratio and phase angle.

1.6 Research Methodology

The methodology employed in this research is summarized in the following project elements and tasks.

1.6.1 Project Element 1: Background and Literature Review

Task1: Literature review to evaluate various laboratory compaction methods employed to characterize volumetric properties of asphaltic mixes.

Task 2: Literature review of the effects of volumetric properties have on mechanical and field performance of asphalt mixes.

Task 3: Literature review of alternative mix design methods, including Marshall, Hveem and Superpave™.

Task 4: Literature review of SMHI and Superpave™ mix design specifications.

Task 5: Literature review of mechanical performance characterization of asphalt mixes.

1.6.2 Project Element 2: Field Data Collection

Task 1: Pavement distress survey was conducted to include rut depth measurements across the Radisson SPS-9A test sections.

Task 2: Ground penetrating radar profiles were used to determine the differential dielectric permittivities of the asphalt mixes across the Radisson SPS-9A test sections.

1.6.3 Project Element 3: Marshall Laboratory Characterization

Task 1: Four repeat Marshall specimens of each Radisson SPS-9A asphaltic mix were compacted from the original plant produced asphalt concrete mix at each of 50 and 75-blows Marshall compactive effort as specified in SMHI 204-8 after ASTM D-1559.

Task 2: Volumetric properties of the laboratory compacted Marshall specimens were determined as specified in ASTM D-2726.

Task 3: Marshall stability and flow characterization as specified in SMHI 204-8 after ASTM D-1559 were performed across the laboratory compacted Marshall specimens.

1.6.4 Project Element 4: Gyratory Laboratory Characterization

Task 1: Three repeat gyratory compacted specimens were prepared across gyration angles of 1.25°, 2.00°, and 2.75° at a vertical stress of 600kPa as specified in AASHTO TP4. The gyration angle was varied to evaluate the volumetric sensitivity to compaction energy.

Task 2: The volumetric properties of the gyratory laboratory compacted specimens were determined as specified in ASTM D-2726.

1.6.5 Project Element 5: Triaxial Frequency Sweep Characterization

Task 1: Triaxial frequency sweep characterization was performed across the gyratory compacted samples at test temperatures of 20°C and frequency range of 0.5Hz to 10Hz, to evaluate sensitivity to traffic speed. Triaxial deviatoric stress states were applied to be representative of field state loading conditions. Dynamic modulus, Poisson's ratio and phase angle were calculated using the triaxial frequency sweep analysis results.

1.6.6 Project Element 6: Data Comparison and Statistical Analysis of Laboratory and Field Data

Statistical analysis was conducted across various combinations of dependent and independent variables obtained in this research and included: graphical-visual analysis; statistical analysis of variance; and Tukey's pairwise comparison. The following comparisons were performed on the Radisson SPS-9A asphalt mix test results.

Comparison 1: Volumetric properties, VTM, VMA and VFA of Marshall compacted samples with respect to 50 and 75 Marshall compaction blows.

Comparison 2: Volumetric properties, VTM, VMA and VFA of Superpave™ gyratory compacted samples as a function of 1.25°, 2.00°, and 2.75° gyratory angle.

Comparison 3: Volumetric properties, VTM, VMA and VFA of Superpave™ gyratory compacted samples and Marshall compacted samples across various compactive efforts.

Comparison 4: Marshall stability and flow across 50 and 75-blow Marshall compactive efforts.

Comparison 5: Triaxial frequency sweep material constitutive properties, dynamic modulus, Poisson's ratio and phase angle as a function of 1.25°, 2.00°, and 2.75° gyratory angle.

Comparison 6: Rut depth and ground penetrating radar profiles in the wheel paths and outside the wheel paths of each Radisson SPS-9A test section in the field.

1.6.7 Project Element 7: Summary, Conclusions and Future Recommendations.

1.6.8 Layout of Thesis

This research is presented in six chapters. Chapter 1 presents background, goal, objectives, hypothesis, scope and methodology of this research. Chapter 2 presents a literature review regarding the background to laboratory compaction of hot-mix asphalt concrete and laboratory testing of physical and mechanical properties of hot-mix asphalt concrete. Chapter 2 also presents a summary of the effect of mix design on field performance of asphalt mixtures. Chapter 3 summarizes volumetric mix properties of Marshall and Superpave™ gyratory compacted hot-mix asphalt samples obtained from the Radisson SPS-9A test site across various compactive efforts. Chapter 4 presents the mechanical test results from Marshall stability and flow of the laboratory Marshall compacted samples. Chapter 4 also presents material constitutive properties obtained from triaxial frequency sweep testing on gyratory compacted samples across varying angles of gyration. Chapter 5 presents the results of the field evaluation of the SPS-9A test sites including field rut depth and ground penetrating radar dielectric permittivities. Chapter 6 presents the summary, conclusions and recommendations based on the

findings of this research. Recommendations for future research are also presented in Chapter 6.

CHAPTER 2 LITERATURE REVIEW AND BACKGROUND STUDY

Chapter two summarizes a literature review regarding asphalt mix design methods, laboratory compaction of hot-mix asphalt, and mechanistic material characterization of hot-mix asphalt mixtures.

2.1 Hot-Mix Asphalt Composition

The objectives of any asphalt mix design method are to combine asphalt cement, mineral aggregates and sometimes additives in their correct proportions to provide optimum balance between life cycle functionality, structured performance and material costs. Asphalt concrete pavements are mostly designed to withstand traffic loading and environmental conditions. The factors affecting the performance of asphalt mixes in the field include: inadequate design of hot-mix asphalt, inadequate construction process, traffic loading and environmental conditions (Roberts et al. 1996, Berthelot 2000). Inadequate design of hot-mix asphalt will be considered in this study.

Hot-mix asphalt is a four phase particulate composite system, as shown in Figure 2.1, consisting of:

- Asphalt cement,
- Aggregates,
- Air voids and
- Asphalt/ Aggregates interface.

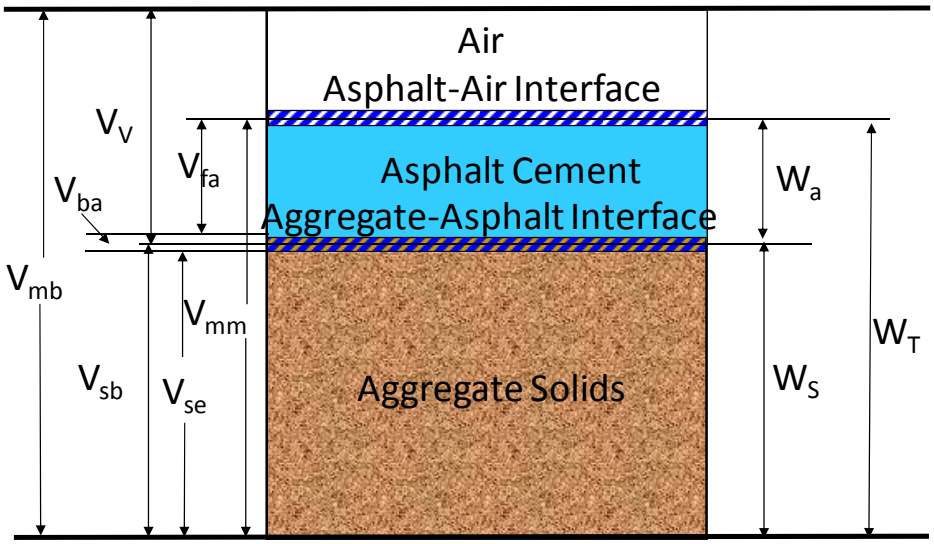

Figure 2.1 Volumetric Mix Design

In this figure, V_{mb} represents bulk volume of asphalt concrete mix, V_{fa} is voids filled with asphalt, V_{se} is effective viods in mineral aggregates, V_{sb} is bulk volume of mineral aggregates, V_{ba} is volume of absorbed asphalt, V_V is total air voids, W_T is total mass of asphalt-aggregate mix, W_a is mass of asphalt cement and W_s is mass of mineral aggregates.

The design of HMAC involves the selection of the composite materials, of the desirable qualities, in their correct proportions according to specifications to obtain a mix that will withstand traffic loading and environmental conditions without damage. Asphalt cement and aggregate are combined to give the optimum asphalt content, voids in mineral aggregates, voids filled with asphalt, voids in total mix and interaction between asphalt-aggregate interfaces. Figure 2.2 shows a cross-section of asphalt aggregates interface with air voids.

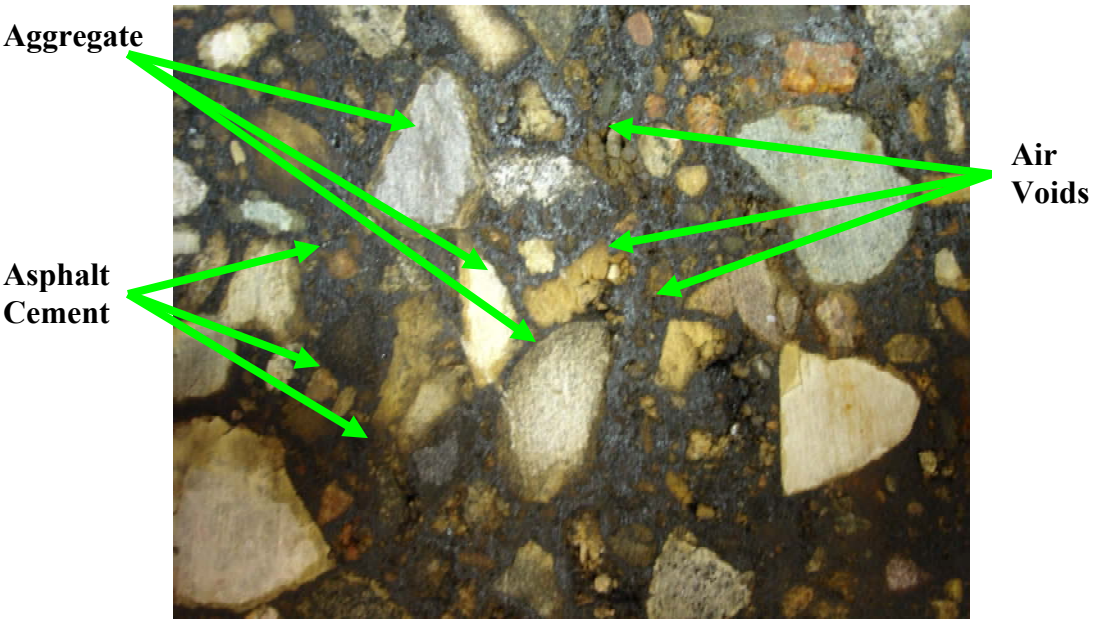

Figure 2.2 Cross-Section of Asphalt Aggregates Interface with Air Voids

2.1.1 Asphalt Cement

Asphalt cement comprises between five to six percent by weight (ten to twelve percent by volume) of the total asphalt concrete mix. Asphalt cement performs the primary roles of bonding mastic for the aggregate skeleton, as well as waterproofing the pavement layers. However, asphalt cement is a thermo viscoelastoplastic material (Roberts et al. 1996, Berthelot 2000). The selection of asphalt cement for pavement construction should therefore take into consideration the temperatures that are likely to be encountered both on the high and low sides based on the penetration and viscosity grading of the asphalt or performance grading as used by Superpave^{TM} method (Asphalt Institute 1996). Two main properties of asphalt cement important to engineers are viscosity and temperature susceptibility.

2.1.2 Aggregates

Aggregate comprises ninety percent by weight (eighty percent by volume) of the total asphalt concrete mix. The main role of aggregates in HMAC is to provide supporting skeleton for the distribution of stresses across the lower layers of the road

structure. The desired physical properties of aggregates related to performance for use in asphalt mixes have been identified as (Roberts et al. 1996, Berthelot 2000):

- Gradation and size,
- Cubical shape,
- Low porosity,
- Proper surface texture and
- Hydrophobic.

Superpave™ mix design involves the selection of aggregate based on specified consensus properties and source aggregate properties to achieve desirable performance of HMAC. Consensus and source aggregate properties are identified by Superpave™ as (Asphalt Institute 1996, Berthelot 2000):

1. Consensus properties
    - Coarse aggregate angularity;
    - Fine aggregate angularity;
    - Flat and elongated particles; and
    - Clay content.
2. Source aggregate properties
    - Toughness;
    - Soundness; and
    - Deleterious materials.

SHRP coarse aggregate and fine aggregate angularity specification was intended to mitigate permanent deformation of asphalt pavements by ensuring high degree of coarse aggregate and fine aggregate internal friction in HMAC mixtures. The requirement for coarse aggregate and fine aggregate angularity specification depends on the design traffic level as shown in Table 2.1 and Table 2.2 respectively.

Table 2.1 SHRP Superpave™ Coarse Aggregate Angularity Criteria (After Asphalt Institute)

Design Traffic (Million ESALs)	Depth From Surface	
	<100 mm (X_1/X_2)	> 100 mm (X_1/X_2)
<0.3	55/-	-/-
<1	65/-	-/-
<3	75/-	50/-
<10	85/80	60/-
<30	95/90	80/75
<100	100/100	95/90
>100	100/100	100/100

Note: X_1 denotes aggregate with one or more fractured faces
X_2 denotes aggregate with two or more fractured faces

Table 2.2 SHRP Superpave™ Fine Aggregate Angularity Criteria (After Asphalt Institute)

Design Traffic (Million ESALs)	Depth From Surface	
	<100 mm	> 100 mm
<0.3	-	-
<1	40	-
<3	40	40
<10	45	40
<30	45	40
<100	45	45
>100	45	45

Criteria is percentage air voids in loosely compacted fine aggregate

2.1.3 Asphalt-Aggregate Interface

Asphalt-aggregate interface defines the matrix of asphalt cement and aggregate and comprises air voids, effective asphalt binder, permeable and non-permeable voids and absorbed asphalt. The strength of HMAC is developed from the interactions between the aggregates surfaces, as a way of internal friction, and the asphalt cement (Roberts et al. 1996, Berthelot 2000). The asphalt-aggregate interface develops bonding and adhesion that increase resistance to moisture damage and ravelling of HMAC.

2.1.4 Voids in Total Mix (VTM)

Air voids is a physical property of asphalt concrete which is often correlated to in-field rutting performance of asphalt pavements. The stability and durability of asphalt pavements is significantly affected by the amount of air voids in the HMAC mixture (Huber and Herman 1987, Miller 1988, Brown and Cross 1989). The primary role of air voids in HMAC is to provide room for thermal expansion of asphalt cement between aggregate skeleton. When in-place air voids in asphalt pavements decrease to a critical value, rutting of HMAC pavements is likely to occur. HMAC with higher air voids will generally be prone to oxidation leading to pavement distresses such as cracking and ravelling (Roberts et al. 1996, Berthelot 2000). SMHI specifies air voids range of 3.0 – 5.0 percent for laboratory compacted specimen and 4.0 – 9.0 percent for field compacted HMAC pavement (SMHI Specification 4100). Higher initial air voids for field compacted HMAC usually results in rapid consolidation of the mix due to traffic loading during early service life of the HMAC pavement.

Air voids in HMAC is a function of voids in mineral aggregates and voids filled with asphalt. The method of laboratory compaction of HMAC has also been found to affect the air voids in HMAC (Ziauddin et al., 1998, Roberts et al. 1996, Berthelot 2000). Desired mineral aggregates properties have been found to provide the air voids requirements of aggregate-asphalt mixtures without sacrificing other engineering properties (Abdullah et al. 1998). Previous research also indicated that the voids in mineral aggregates affect the fatigue and rutting performance of both fine and coarse graded asphalt mixtures (Anderson and Bentsen 2001). VTM is calculated as shown in equation 2.1 below (ASTM 2726, SMHI STP 204):

$$VTM = \left(1 - \frac{G_{mb}}{G_{mm}}\right) * 100 \qquad \textbf{2.1}$$

where: VTM is total air voids in the compacted asphalt mix; G_{mb} is bulk specific gravity of asphalt concrete mixture and G_{mm} is maximum theoretical specific gravity of loose asphalt aggregate mixture.

2.1.5 Voids in the Mineral Aggregate (VMA)

Void in the Mineral Aggregate (VMA) is defined as the volume of inter-granular void space between the aggregate particles of a compacted paving mixture including the volume occupied by asphalt cement (Roberts et al. 1996). VMA also describes the portion of space in the compacted asphalt mixture which is not occupied by the mineral aggregate. VMA is expressed as a percentage of the total volume of the asphalt mixture. VMA affects the durability of compacted asphalt pavements (Aschenbrener et al. 1994, Roberts et al. 1996, Berthelot 2000, Chadbourn et al. 2002). Establishing adequate VMA during mix design and in the field will help establish adequate air voids and film thickness without excessive asphalt bleeding or flushing.

The primary role of the VMA is to provide room for thermal expansion of the asphalt cement between the aggregate skeleton. Thermal expansion requirement for asphalt cement and mineral aggregate has been specified below (Berthelot 2000);

- Typical Asphalt cement $= 60 \times 10^{-6}$ /°F
- Typical Aggregate = 3 to 6×10^{-6} /°F.

The SMHI specifies minimum VMA at 14 percent. SHRP specifies minimum VMA at design air void content of four percent as a function of nominal maximum aggregate size for the Superpave^{TM} mix design protocol as seen in Table 2.3 (Asphalt Institute 1996). VMA is calculated as shown in equation 2.2 below (ASTM 2726, SMHI STP 204):

$$VMA = 1 - \frac{G_{mb} P_s}{G_{sb}} \qquad \textbf{2.2}$$

where: VMA is voids in the mineral aggregate; G_{mb} is bulk specific gravity of asphalt concrete mix and P_s is aggregate content by weight of mix, G_{sb} is bulk specific gravity of aggregate.

Table 2.3 SHRP VMA Criteria

Nominal Maximum Aggregate Size (mm)	Minimum VMA (percent)
9.5	15.0
12.5	14.0
19.0	13.0
25.0	12.0
37.5	11.0

2.1.6 Voids Filled with Asphalt (VFA)

Voids filled with asphalt (VFA) is the part of the VMA that is coated with asphalt not including the asphalt absorbed into permeable pores of the mineral aggregate. The factors affecting VFA are the number of permeable and impermeable pores in the mineral aggregates and the aggregate structure (Roberts et al. 1996, Berthelot 2000). VFA is directly related to aging and rutting characteristic of compacted asphalt mixture. High VFA can result in viscoplastic flow and premature rutting (Asphalt Institute 1996). The SMHI acceptable range of VFA is 65.0 to 78.0 percent. VFA is evaluated in the laboratory using the equation below (ASTM 2726, SMHI STP 204):

$$VFA = \frac{VMA - VTM}{VMA} * 100 \qquad \textbf{2.3}$$

where: VFA is voids filled with asphalt; VMA is voids in mineral aggregate and VTM is voids in total mix.

2.2 Hot-Mix Asphalt Concrete Field Performance

Failure or damage of asphalt pavements can be a result of inadequate design in one or all of the physical properties of the mix. Failure of asphalt concrete pavement can be in the form of (Roberts et al. 1996, Berthelot 2000):

1) Mix disintegration:

- Segregation/ Ravelling;

- Flushing/ Bleeding; and
- Stripping (Moisture damage).

2) Fracture:

- Fatigue cracking;
- Thermal (Transverse) cracking; and
- Longitudinal cracking.

3) Viscoplastic flow:

- Rutting; and
- Shoving (Corrugation).

2.2.1 Permanent Deformation (Rutting) of HMAC Pavements

Permanent deformation or rutting in asphalt pavement manifests as longitudinal bowl-shaped depressions along wheel paths. Permanent deformation can be short term consolidation in hot-mix asphalt as a result of traffic action and primarily attributed to high level of voids in total mix. Permanent deformation can also be in the form of viscoplastic flow of the hot-mix asphalt or the substructure layers, generally as a result of a weak subgrade. Figures 2.3 to 2.5 show the different types of permanent deformation experienced by asphalt pavements. Traffic loading and environmental factors such as temperature and moisture have been found to contribute to permanent deformation of HMAC pavements (Huber 1989, SHRP-A-415 1994, Tarefder et al. 2003).

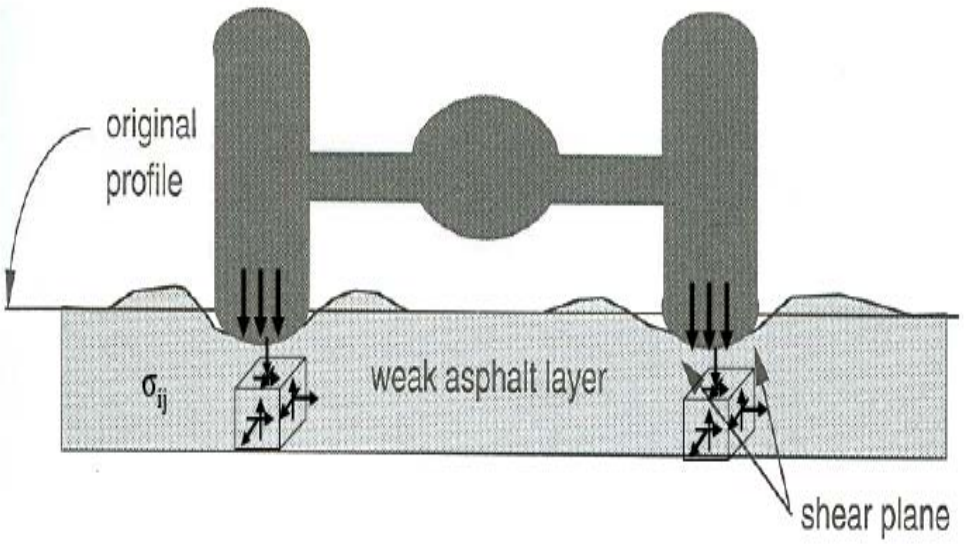

Figure 2.3 Rutting of HMAC material (SHRP 1996)

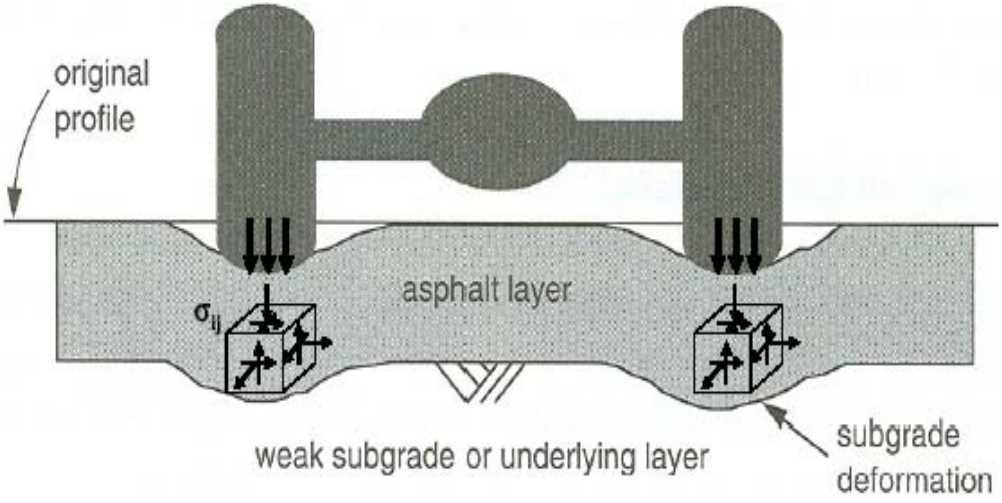

Figure 2.4 Structural Rutting of Asphalt Pavement

(SHRP 1996)

Figure 2.5 Typical Viscoplastic Rutting of Asphalt Pavement

Consolidation rutting is typically caused by high air voids in HMAC pavement resulting from lack of compaction or poor mix design. Repeated loading from traffic causes the HMAC in the wheelpaths to consolidate to lower air voids content. The use of excessive asphalt cement or too low a value of air voids in HMAC can also result in viscoplastic rutting in the form of lateral plastic flow. Too much asphalt cement content reduces internal friction between aggregates particles and compromises the load carrying ability of the HMAC (Roberts et al. 1996). Rutting of HMAC pavements can lead to failure of entire pavement structure.

2.3 Laboratory Design and Compaction of Hot-Mix Asphalt Concrete Mixtures

Hot-mix asphalt concrete mix design comprises the selection and the proportioning of asphalt cement, aggregates and additives to obtain the desired end product mix properties of HMAC placed in the field. The main objective of hot-mix asphalt design is to determine the most economical blend of the constituents and gradation of aggregate within the limits of the project specifications (Sousa et al. 1995, Roberts et al. 1996, Asphalt Institute 1996). Typical HMAC design specifications include:

1. Sufficient asphalt content to ensure a climatically durable pavement.

2. Sufficient mix stability to withstand plastic flow strains induced by traffic without permanent distortion or displacement.

3. Sufficient air voids in compacted mix to allow for expansion of asphalt and additional densification under traffic loading without flushing, bleeding and loss of stability, yet low enough air voids to resist harmful air and moisture infiltration.

4. Sufficient workability to permit effective placement of the hot-mix asphalt concrete without segregation or check cracking.

Asphalt mix design concepts have evolved from Hveem and Marshall mix design methods, which are both empirically based (Kandhal and Koehler 1985, Valerga and Lovering 1985). Asphalt Aggregates Mixture Analysis System (AAMAS) and SHRP mix design methods are intended to produce laboratory compacted hot-mix asphalt specimens that closely relate to performance of field compacted pavements (Roberts et al. 1996).

2.3.1 Hveem Mix Design Method

The Hveem mix design method was developed by Francis Hveem in the late 1920's. The Hveem mix design method is intended to produce hot-mix asphalt mixtures with sufficient asphalt cement for aggregate absorption, optimum film thickness and a compacted aggregate-asphalt cement mixture with sufficient stability to resist traffic (Kandhal and Koehler 1985, Roberts et al. 1996, Asphalt Institute 1997, Berthelot 2003). Hveem mix design method was intended for asphalt mixes being placed by mechanical pavers with nominal maximum aggregates size of 25 mm. Hveem designed mixtures that are less sensitive to percentage passing sieve number 0.075 mm (Hand et al. 2004).

Hveem mix design employs the California kneading compactor, shown in Figure 2.6, in the preparation of asphalt specimens (ASTM 1999, AASHTO 2000). The

California kneading compactor attempts to simulate in-field roller compaction of HMAC with a kneading compaction action. The preparation of laboratory compacted specimens using the Hveem mix design method is standardized in AASHTO T247 and ASTM D 1561. Standard test specimens 64 mm by 102 mm are prepared by the Hveem method with varying asphalt content both above and below the approximate design asphalt content. The approximate required asphalt content to provide adequate film thickness is determined by the centrifuge kerosene equivalent method (Asphalt Institute 1996).

The Hveem stabilometer, illustrated in Figure 2.7, is used to characterize the permanent deformation resistance and cohesion of the compacted specimens (AASHTO 2000). The Hveem stabilometer provides the key performance prediction measure for Hveem mix design method. The Hveem stabilometer measures the resistance to deformation of a compacted hot-mix asphalt specimen by measuring the lateral pressure developed from applying a vertical load.

Figure 2.6 California Kneading Compactor (FHWA)

Figure 2.7 Hveem Stabilometer

Hveem stabilometer test is a closed-system triaxial test which involves the application of an increasing load to the top of the sample at a predetermined rate. The load is increased and the lateral pressure is read at specified intervals. The lateral pressure can be varied to characterize the effect of various states of confinement. The Hveem stabilometer value is calculated as follows:

$$S = \frac{22.2}{\left[\frac{P_h \times D}{P_v - P_h}\right] - 0.222} \quad , \qquad \textbf{2.4}$$

where: S is stabilometer value; P_v is vertical pressure–typically 2800 kPa; P_h is horizontal pressure corresponding to P_v in kPa; D is displacement of specimen in 0.25 mm units.

Hveem stabilometer values range from 0 to 90. A stabilometer value of zero represents a poor mix condition where lateral pressure is equal to vertical pressure. A value of ninety indicates a stable mix condition of zero lateral pressure relative to axial pressure. Earlier research found the Hveem stabilometer to be able to distinguish significant differences between various asphalt concrete mixes and produce low mean coefficient of variance (Berthelot et al. 1999).

A limitation of the Hveem stabilometer is that it does not provide feedback control on multi-axial mechanistic measurements. In addition, the Hveem stabilometer specifies a small sample size and applies boundary tractions under curvilinear platens resulting in nonlinear stress-strain fields and lacks dynamic feedback control loading capabilities. Given the small sample size and the lack of traction feedback control, the Hveem stabilometer cannot be used to characterize the fundamental constitutive behaviour of asphalt concrete mixes across various stress and strain states, stress and strain rates, representative of those experienced in the field as required for mechanistic road-modelling.

The Hveem cohesiometer is used to measure the cohesion of the same compacted sample as in the stabilometer test by measuring the force required to break a sample as a cantilevered beam. The cohesiometer test is intended to provide some prediction about the ability of the hot-mix asphalt to resist ravelling under traffic loading. The hot-mix asphalt sample is bent as a cantilever beam until it fails and the cohesiometer value is calculated as follows:

$$C = \frac{L}{H}\left(0.20H + 0.044H^2\right), \qquad \textbf{2.5}$$

where: C is cohesiometer value; H is weight of shot (grams); D is diameter or width of specimens (inches) and H is height of specimens (inches).

2.3.2 Marshall Mix Design Method

The Marshall mix design method was developed in the 1930's by Bruce Marshall of the Mississippi State Highway Department. The Marshall mix design method was adopted and refined by the US Army Corps of engineers in the 1940's and 1950's. The main objective of Marshall mix design method was to design asphalt concrete mixture with optimum asphalt content and aggregate gradation to resist permanent deformation (Sousa et al. 1995, Roberts et al. 1996, Asphalt Institute 1997, Berthelot 2000).

Marshall specimens are compacted using a Marshall manual impact hammer or an automatic Marshall hammer. The compaction energy is determined by the number

of applied blows from a specified drop height of 457.2 mm depending on the level of traffic of the given pavement (Button et al. 1994, Roberts et al. 1996, Asphalt Institute 1997, Ziauddin et al. 1998, Berthelot 2000). The Marshall mix design method employs a 63.5 mm by 101.6 mm test sample which is characterized using the Marshall stabilometer. Marshall manual impact compaction has been found to produce consistently denser specimens with higher stability values than specimens prepared using automatic Marshall compaction (Ziauddin et al. 1998).

Permanent deformation characteristics of asphalt mixtures are characterized by the Marshall stabilometer in terms of Marshall flow and stability. The Marshall flow and stability tests are standardized in ASTM D 1559. The Marshall stability and flow of a test sample is measured by loading the sample in compression and measuring the maximum load supported by the test specimen at a loading rate of 50.8 mm per minute as seen in Figure 2.8. An attached dial gauge measures the plastic flow of the specimen as a result of loading. The maximum load applied to the test specimen is the Marshall stability and the maximum displacement is the Marshall flow (ASTM 1999). Marshall flow value is recorded in terms of 0.25 mm increments. The Marshall stability and flow test is performed at a temperature of 60°C, believed to be the temperature at which halt pavements are more prone to permanent deformation (Asphalt Institute 1997).

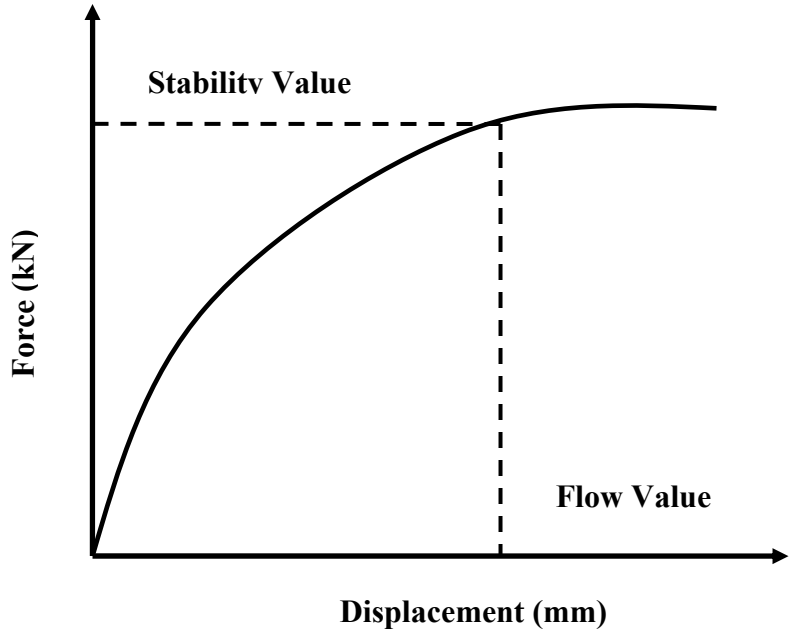

Figure 2.8 Marshall Stability and Flow Relationship

2.3.3 Asphalt-Aggregate Mixture Analysis System

Asphalt-Aggregate Mixtures Analysis System (AAMAS) was developed by the National Co-operative Highway Research Program (NCHRP) in the 1980's. The AAMAS study was intended to establish a performance specification. AAMAS was intended for both modified and unmodified binders (Kennedy et al. 1991). The main objective of AAMAS was to predict in-place properties of asphalt concrete in the laboratory during mix design stage to evaluate mixture behavior under traffic and environmental loads (Von Quintus et al. 1987). AAMAS was intended to characterize asphalt mixes based on engineering material properties which are different from empirical procedures employed by Hveem and Marshall mix design methods.

Earlier studies using AAMAS on typical HMAC test sections indicated that hot-mix asphalt properties were affected significantly by changes in air voids content (Hanson et al. 1994). Modification or alteration to existing performance related tests such as the indirect tension test, resilient modulus test and creep test were considered necessary for the AAMAS (Von Quintus et al. 1987, Monismith et al. 1991).

2.4 SHRP Superpave™ Level I Mix Design and Analysis

The Strategic Highway Research Program (SHRP) developed the *Su*perior *Per*forming Asphalt *Pave*ments (Superpave™) in 1987. SHRP comprises specifying asphalt binders and mineral aggregates, developing asphalt mixture design, analyzing and establishing pavement performance prediction models (Asphalt Institute 1996). Superpave™ mix design method specifies asphalt mixtures according to thermomechanical material properties in order to mitigate the primary pavement distresses of permanent deformation, fatigue cracking and low temperature transverse cracking.

Superpave™ mix design involves asphalt binder specification based on environmental conditions of the specific site, and performance tests to determine the thermo-rheological properties of the binder. Aggregate selection is based on source aggregates properties and consensus aggregates properties (Asphalt Institute 1996, Berthelot et al. 2000). Superpave™ mix design method involves the use of the Superpave™ gyratory compactor to compact laboratory specimens. The Superpave™ gyratory compactor specimens have been found to better replicate volumetrics and mechanistic properties of asphalt mixes under traffic in field (Button et al. 1994, Sousa et al. 1994, Asphalt Institute 1996, Roberts et al. 1996, Ziauddin et al. 1998, Carlberg et al. 2003).

Investigation of the volumetrics and mechanistic performance properties of Superpave™ mixtures showed that Superpave™ mixes are generally resistant to permanent deformation (Wang et al. 2000). However, a comparison of Superpave™ and Marshall mix performance in Alabama showed no significant variations in rutting between the two mix design methods (Watson et al. 2005).

Given the importance of volumetric mix properties in asphaltic concrete mixes, Superpave™ Level I mix design was intended for low-traffic-volume pavements, greater than or equal to 10^6 equivalent single axial loads (ESALs), and therefore was more focused on materials specification and volumetrics mix design of asphalt mixes as a way of ensuring satisfactory performance (Witczak et al. 2002, Myers and

D'Angelo 2005). For high-traffic-volume pavements, Superpave™ mix design method required a check for mechanistic material properties so as to characterize tertiary creep behaviour of asphalt mixes and evaluate the mix design's potential for permanent deformation, fatigue cracking and low-temperature cracking.

2.7.1 Superpave™ Gyratory Compaction

The Superpave™ gyratory compactor, shown in Figure 2.9, was included in the Superpave™ Level I mix design method to produce laboratory compacted specimens that better replicate volumetric and mechanistic material properties of in-field roller compacted asphalt mixes (SHRP 1994). The Superpave™ gyratory compactor uses a 150 mm (6 inch) diameter mold which makes it more suitable for compacting asphalt mixes with aggregate size of up to 50 mm maximum and 37.5 mm nominal size from a continuum mechanics perspective. The Superpave™ gyratory compactor was a modification of the Texas and French gyratory compactors. The SHRP gyratory compactor employs a lower angle of gyration and the number of gyrations per minute relative to the Texas gyratory compactor. Real time specimen height, bulk specific gravity and voids in total mix measurements are incorporated in the Superpave™ gyratory compactor (SHRP 1994, Asphalt Institute 1996, Roberts et al. 1996, Al-Khateeb et al. 2002).

Based on the French gyratory compaction protocols, the principle of the Superpave™ gyratory compactor is the application of 600 kPa vertical consolidation pressure on the test specimen through the vertical loading ram as displayed in Figure 2.10. Constant pressure is maintained during the compaction process by measuring the ram loading using a pressure gauge. The 150 mm diameter mold of the Superpave™ gyratory compactor is skewed at a fixed angle of 1.25° about the y-axis and rotates at 30 revolutions per minute throughout the compaction process. The number of gyrations reflects the level of traffic, (Asphalt Institute 1996, Roberts et al. 1996).

In-field roller compaction of hot-mix asphalt is simulated by the Superpave™ gyratory compactor by the application of a constant vertical consolidation pressure simulating the stress applied by the roller as shown in Figure 2.11, the angle made by

the hot-mix asphalt surface and the roller drum is simulated by the angle of gyration, the speed of the roller is simulated by the rate of gyration pre-set at revolutions per minute and the number of passes made by the roller to obtain desired air voids and density requirements in the field is simulated in the gyratory compactor by the number of gyrations at $N_{maximum}$ (Richard et al. 1995, Butcher 1998).

Figure 2.9 Superpave™ Gyratory Compactor with Mold

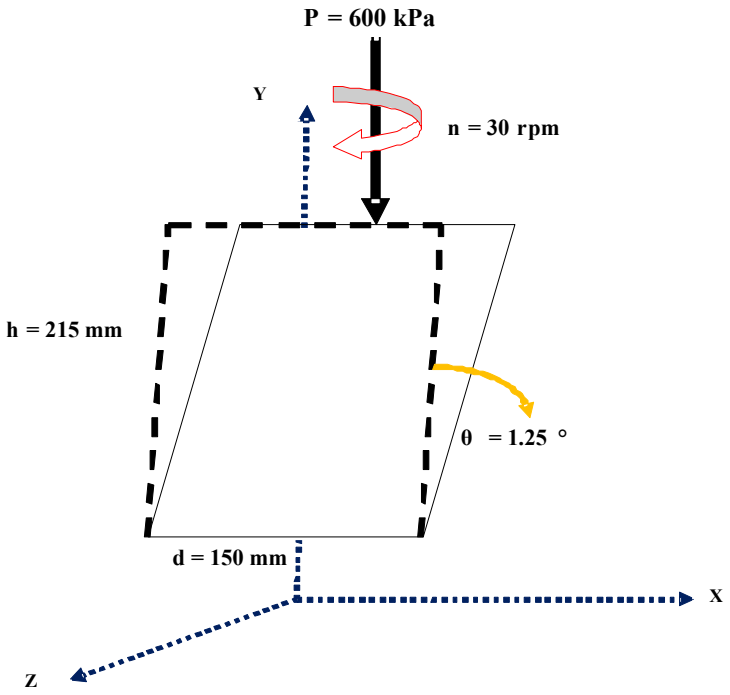

Figure 2.10 Schematic of Superpave™ Gyratory Compactor

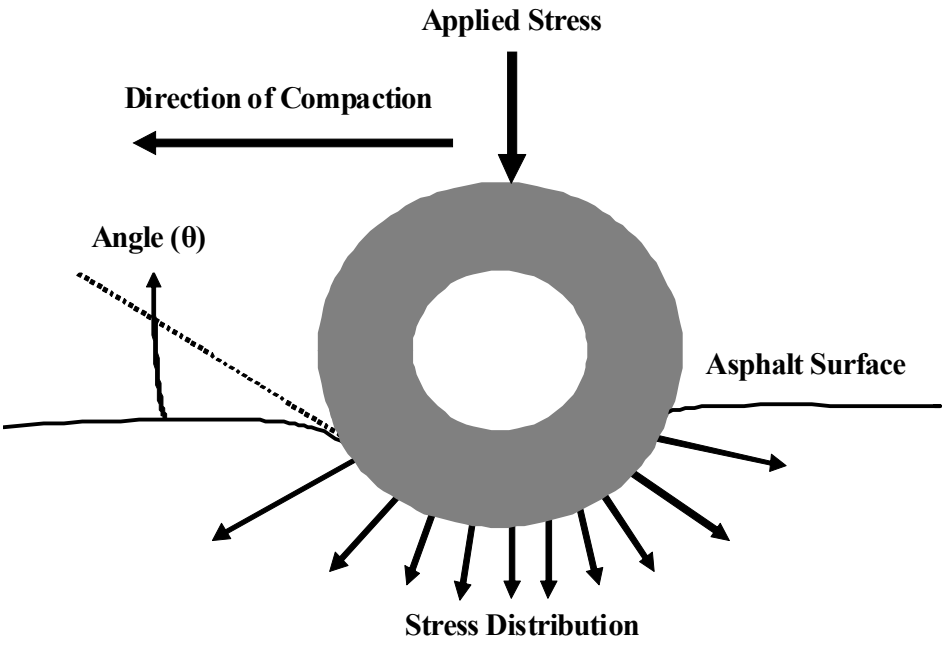

Figure 2.11 Schematic of Roller Compaction

Earlier research found that differences in laboratory compacted specimens using different types of Superpave^{TM} gyratory compactors were largely mix dependent (Hinrichsen 2001). Similar studies also compared different types of Superpave^{TM} gyratory compactors. The results from these studies indicated that increase in external angle of gyration results in a corresponding increase in sample density for individual compactors (Prowell et al. 2003).

An evaluation of the Superpave^{TM} compactor in simulating field density of asphalt mixes indicated that the Superpave^{TM} gyratory compactor is highly sensitive to changes in asphalt mix properties such as binder content, voids in total mix and voids in mineral aggregates (Harman et al. 1995). The Superpave^{TM} gyratory compactor applies compactive energy based on the number of gyrations. The number of gyrations required for asphalt mixes is a function of traffic level and climate. $N_{initial}$ (N_{ini}) is the number of gyrations used to indicate the initial compactibility of the asphalt mix. The air void content at N_{ini} should be more than 11.0 percent. N_{ini} was included in the Superpave^{TM} compaction protocol to eliminate tender mixes at initial compaction.

N_{design} (N_{des}) is used to indicate the number of gyrations required to compact asphalt samples in the laboratory having the same density as field compacted asphalt mixes after the design traffic level used to simulate ten years of compaction in the field. Superpave^{TM} specified air voids content at N_{des} should be approximately 4.0 percent. The properties of the compacted specimen are back-calculated from N_{max} to N_{des} number of gyrations (Vavrik and Carpenter. 1998). $N_{maximum}$ (N_{max}) represents the number of gyrations required to compact asphalt specimens to their maximum density, resulting in air void percent of less than 2.0. The density at N_{max} must not be exceeded in the field. The percent air voids in a design asphalt mix depends on the values of N_{ini}, N_{des} and N_{max} (SHRP 1994, WSDOT-Internet).

Densities of the laboratory prepared Superpave^{TM} gyratory compactor specimens were compared to densities of in-place pavements and recompacted asphalt samples in an attempt to evaluate the Superpave^{TM} gyratory compaction of HMAC (Brown et al.

1996). The number of gyration at N_{ini}, N_{des} and N_{max} were found to be high for lower traffic.

Earlier study shows that the Superpave™ gyratory compactor is highly sensitive to the angle of gyration (Corum and Forstie 1997, Ziauddin et al. 1998, Butcher 1998). However, the use of 1.25° angle of gyration in the Superpave™ gyratory compactor can help produce laboratory compacted specimens that better simulate mechanical properties of field compacted asphalt mixes as compared to Marshall compactor. The large sample size, 150 mm by 150 mm diameter produced by the Superpave™ gyratory compactor makes it more suitable than Marshall compactor in characterizing representative mechanistic material properties of asphalt mixes in conjunction with the rapid triaxial tester (Berthelot et al. 1999).

Superpave™ mix design method intends to characterize rutting performance of asphalt binders by specifying performance based asphalt binder with a rutting factor, G*/Sinδ, which signifies asphalt binder's stiffness or rut resistance at high field temperatures (Roberts et al. 1996, Asphalt Institute 1996, Berthelot 2000). An extensive study on five different asphalt binders to determine the correlation of superpave G*/Sinδ with rutting susceptibility from laboratory mixture tests found that rut depths were slightly higher compared with G*/Sinδ. They also observed that increased maximum aggregate size did not significantly reduce the effects of binder type on rutting susceptibility (Stuart and Izzo 1995).

In an effort to improve the rutting performance of HMAC, Superpave™ mix design method specifies desirable mineral aggregate properties including fine aggregates angularity, coarse aggregates angularity and aggregates gradation including the Superpave™ control points and restricted zone (Roberts et al. 1996, Asphalt Institute 1996, Berthelot 2000). Table 2.4 displays Superpave™ aggregate gradation for 25.0 mm nominal size and Figure 2.12 displays the Superpave™ gradation chart with the restricted zone and the control points.

Table 2.4 Superpave™ Specified 25.0 mm Nominal Size Gradation Limits

Sieve Size (mm)	Percentage Passing by Weight			
	Control Points		Restricted Zone Boundary	
			Minimum	Maximum
37.5		100.0		
25.0	90	100.0		
4.75	19.0	45.0	39.5	39.5
2.36			26.8	30.8
1.18			18.1	24.1
0.600			13.6	17.6
0.300			11.4	11.4
0.075	1.0	7.0		

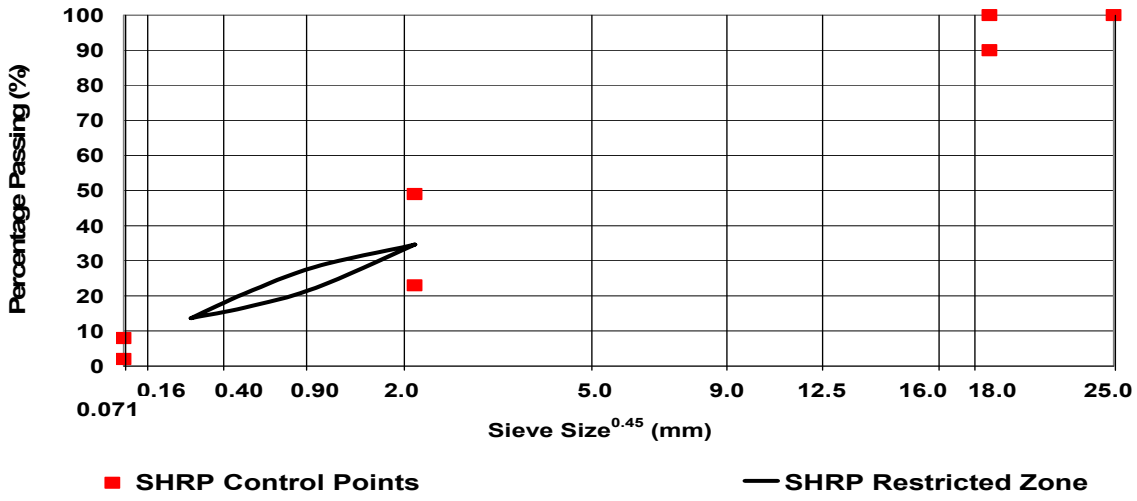

Figure 2.12 Superpave™ Specified 25.0 mm Nominal Size Gradation Limits

With increased axle loads, tire pressure and load repetitions, there is an urgent need for methodologies to predict rut depth before construction to minimize safety hazards and prevent premature failure of HMAC pavements. Therefore, there is a need for analysis procedures to estimate stresses, strains and deformations that arise from traffic loading and are the major cause of rutting of HMAC pavements (SHRP 1994). Analytically based, mechanistic or mechanistic-empirical procedures have been developed which have provisions for predicting rutting behavior.

A comparative evaluation of rutting resistance of coarse-graded versus fine-graded Superpave™ mixtures (Kandhal and Cooley 2002) was undertaken using three different rutting susceptible tests: asphalt pavement analyzer, Superpave™ shear tester and repeated load confined creep test. Statistical analysis of the data from the three tests indicated that there was no significant difference in rutting resistance between coarse-graded and fine-graded Superpave™ mixtures.

An extensive study on the effect of the Superpave™ restricted zone to the performance of HMAC mixes carried out by (Kandhal and Mallick 2001, Hand and Epps 2001) proved that asphalt mixes with aggregates gradations passing through the Superpave™ restricted zone do not display higher rutting when compared with asphalt mixes with aggregates gradations passing below or above the Superpave™ restricted zone.

The Superpave™ gyratory compactor (SGC), properties can be used to estimate rutting potential of asphalt mixtures (Butcher 1998, Anderson 2002). Anderson illustrated how to use the SGC properties to estimate the rutting potential of asphalt mixes from SPS-9 test sites, WesTrack test sites and GPS test sites. He compacted virgin asphalt samples from the various sites using a SGC with shear measurement capabilities. N-SR_{max} parameter was identified as the number of gyrations at which the ratio of shear stress to vertical stress (stress ratio) has a maximum value. The N-SR_{max} value was plotted against rutting rate (mm/$ESAL^{1/2}$) and rut depth (mm) for the various mixes. The ratio of the log N-SR_{max} to the log of N_{max} was used to determine a value of $N_{critical}$ which was between N_{max} and N_{des}. $N_{critical}$ was defined as the value at which the ratio of log N-SR_{max} to log N_{max} is greater than or equal to 0.95. The N-SR_{max} parameter was found to be able to evaluate high temperature performance of asphalt mixtures during design and construction quality control. The N-SR_{max} value can also be used to evaluate performance of different aggregate blends or evaluation of mix types at different asphalt binder contents.

The field cracking and rutting performance of SPS-9 test sites across the United States and Canada have been evaluated by using 2001 pavement distress data from the

Long-Term pavement Performance database. The study concluded that SPS-9 test sites do not have significant difference in rutting distress between Superpave™ binder sections and Superpave™ alternative binder sections after nine years of field performance (Kavanagh 2004).

The methods of predicting permanent deformation in HMAC pavements include viscoelastic, elastoplastic and linear elastic methods (Monismith 1976, Saraf et al. 1976). Current methods to determine permanent deformation of asphalt mixtures involve the use of material response parameters obtained from laboratory testing and used to evaluate and predict mixture performance (NCHRP-465 1994, SHRP-A-415 1994). A thorough understanding of the main attributes of permanent deformation behaviour of asphalt mixtures is needed before the development of constitutive models and relationships. Tertiary flow parameters, radial strain or axial strain have been found to have excellent correlation with field rut depth measurements (Kaloush and Witczak 2002).

2.5 Superpave™ Level II and III Mix Design

The Superpave™ Level II and III mix design are used for pavement design with traffic levels of up to ten million ESAL and above ten million ESAL, respectively (Asphalt Institute). Level II and III mix design procedures were included in the Superpave™ protocol to ensure mixtures produce acceptable performance in terms of permanent deformation, fatigue cracking and low temperature cracking from mechanistic testing of asphalt mixtures (Kenedy et al. 1994). Level II and III mix design procedures are also used in predicting pavement performance and development of performance models.

Mechanistic based Superpave™ Level II and III mix design testing, however, has been found to be too complex to perform and time consuming (Berthelot 1999). Earlier research has also indicated that Level III mix design testing was less consistent compared to other testing methods. As a result of the complexity of testing and analysis of test data, high cost of testing equipment and time consuming nature, Level II and III mix design methods are not used in pavement design by many infrastructure

agencies (Anderson et al. 1999, Berthelot 1999, Berthelot et al. 1999 and Brown et al. 2004).

2.5.1 Simple Performance Tests (SPT) for Superpave™ Mix Design

Simple performance tests (SPTs), were incorporated in the Superpave™ mix design method to serve as a mechanical proof test for asphalt mixes. One limitation of the Superpave™ level one mix design method was the lack of a mechanical test similar to Marshall stability and flow or Hveem stability tests employed by the two mix design methods to determine the mechanical stability of asphalt mixes. Several existing tests have been evaluated as potential SPTs in terms of their ability to (Witczak et al. 2002 Myers and D'Angelo 2005):

1. Accurately correlate HMAC response characteristics to actual field performance;
2. Reliability;
3. Ease of use; and
4. Reasonable equipment cost.

The SPTs include the following:

1. Dynamic modulus test;
2. Repeated load test; and
3. Static triaxial creep test.

2.5.2 Dynamic Modulus Test

The dynamic modulus test, standardized in ASTM D-3497, is used to determine the stiffness of HMAC mixtures under dynamic loading. The test consists of applying a uniaxial sinusoidal (haversine) compressive stress to an unconfined or confined HMAC cylindrical test specimen (Berthelot et al. 1999, Witczak et al. 2002, Myers and D'Angelo 2005). The dynamic modulus test is non-destructive and allows test specimens to be used at multiple temperatures and multiple load frequencies. The

stress-to-strain relationship under a continuous sinusoidal loading for linear viscoelastic materials is defined by a computed value called the complex modulus (E*). The dynamic modulus is defined as the absolute value of the complex modulus, |E*|. The dynamic modulus is mathematically defined as the ratio of the peak dynamic stress (σ_o) to peak recoverable axial strain (ε_o) (Berthelot et al. 1999, Witczak et al. 2002):

$$|E^*| = \frac{\sigma_o}{\varepsilon_o} = E_D \quad \textbf{2.5}$$

The real and imaginary portions of the complex modulus (E*) can be written as:

$$E^* = E' + iE'' \quad \textbf{2.6}$$

where: E′ is the real part of the complex modulus and is generally referred to as the storage or elastic modulus component of the complex modulus, while E″ is the imaginary part of the complex modulus and is usually referred to as the loss or viscous modulus. The phase angle, ϕ, is the angle by which ε_o lags behind σ_o. The phase angle indicates the viscous properties of the HMAC mixture. The complex modulus is expressed as:

$$E^* = |E^*|\cos\phi + i|E^*|\sin\phi \quad \textbf{2.7}$$

$$\phi = \frac{t_i}{t_p} \times 360 \quad \textbf{2.8}$$

where: t_i is time lag between a cycle of stress and a cycle of strain (sec.); t_p is time for a stress cycle (sec.) and *i* is imaginary unit.

For a pure elastic material, Ø = 0 and the complex modulus (E*) is equal to the absolute value, or the dynamic modulus. For a pure viscous material Ø = 90°.

There have been several attempts to develop dynamic modulus prediction models (Witczak and Fonseca 1996, Dogré et al. 2005, Zeghal et al. 2005). Among the regression models for predicting asphalt concrete dynamic modulus E_D, the models

developed by Witczak and Hirsch are found to be most reasonable in correlating predicted dynamic modulus values to laboratory measured dynamic modulus values (Witczak et al. 2002, Christensen 2002, Dongré et al. 2005).

The Witczak prediction model used a symmetrical sigmoidal function and is expressed as:

$$\log E_D = -1.249937 + 0.029232 P_{200} - 0.001767 (P_{200})^2 - 0.002841 P_4$$

$$- 0.058097\ V_a - \frac{0.802208\ V_{beff}}{V_{beff} + V_a} + \frac{3.871977 - 0.0021\ P_4 + 0.003958\ P_{38}}{1 + e^{(-0.603313 - 0.313351 \log f - 0.393523 \log \eta)}}$$

$$\frac{- 0.000017 (P_{38})^2 + 0.00547 P_{34}}{1 + e^{(-0.603313 - 0.313351 \log f - 0.393523 \log \eta)}} \qquad \textbf{2.9}$$

Where: E_D is dynamic modulus, in 10^5 psi; η is bitumen viscosity, 10^6 Poise; f is loading frequency, Hz; V_a is percentage air voids by volume; V_{beff} is percentage effective bitumen content by volume; P_{34} is cumulative percentage retained on ¾ inch sieve, by total aggregate weight; P_{38} is cumulative percentage retained on 3/8 inch sieve, by total aggregate weight; P_4 is cumulative percentage retained on number 4 sieve, by total aggregate weight and P_{200} is percentage passing the number 200 sieve, by total aggregate weight.

The Hirsch prediction model is as follows:

$$|E^*| = P_c \left[4{,}200{,}000 \left(1 - \frac{VMA}{100} \right) + 3 |G^*|_{binder} \left(\frac{VFA \times VMA}{10{,}000} \right) \right]$$

$$(1 - P_c) \left[\frac{1 - VMA/100}{4{,}200{,}000} + \frac{VMA}{3 VFA |G^*|_{binder}} \right]^{-1} \qquad \textbf{2.10}$$

$$P_c = \frac{\left(20 + \frac{VFA \times 3|G^*|_{binder}}{VMA}\right)^{0.58}}{650 + \left(\frac{VFA \times 3|G^*|_{binder}}{VMA}\right)^{0.58}} \quad \textbf{2.11}$$

where $|E^*|$ is dynamic modulus for asphalt mixture, psi; $|G^*|_{binder}$ is complex shear modulus for binder, psi; P_c is contact factor; VMA is voids in mineral aggregate, percent and VFA is voids filled with asphalt, percent.

2.5.3 Repeated Load Test

The repeated load test is used to simulate a heavy vehicle driven repeatedly over the asphalt pavement surface and determines the number of load cycles the pavement can withstand until it exhibits plastic deformations. To measure the permanent deformation characteristic of HMAC mixture, the repeated load test is repeated several thousand times and the cumulative permanent deformation is recorded as a function of the number of load cycles. Load cycle of 0.1-second haversine pulse load and 0.9-second rest time is applied for the test duration, generally three hours of testing comprising ten thousand loading cycles (Witczak et al. 2002).

Output of the repeated load test is generally in the form of a plot of the cumulative permanent strain (ε_p) versus number of loading cycles (N) as seen in Figure 2.13. The cumulative permanent strain (ε_p) curve can be divided into three zones:

1. The primary zone – this describes the portion in which strain rate decreases with loading time;

2. The secondary zone – this the zone in which the strain rate is constant with loading time and

3. The tertiary flow zone – this describes the portion in which the strain rate increases with loading time.

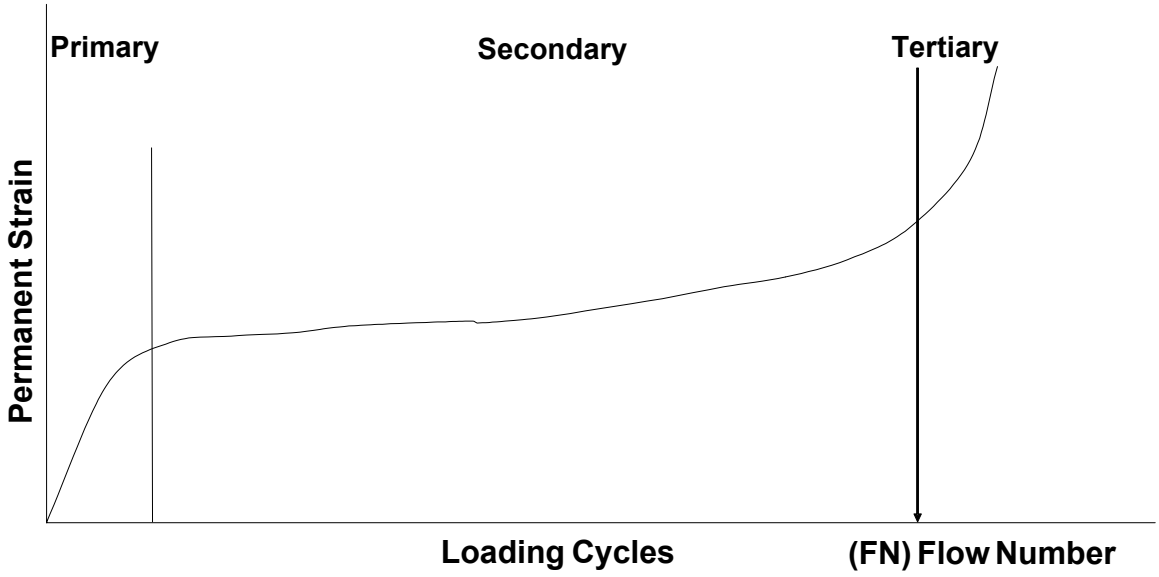

Figure 2.13 Typical Relationship between Permanent Strain and Loading Cycle

The classic power law model is used to analyze the test results:

$$\varepsilon_p = aN^b \qquad \textbf{2.12}$$

where ε_p is permanent strain; N is number of loading cycles; a is permanent strain at N=1 and b is rate of change of permanent strain as a function of the change in loading cycles (log [N]).

The parameters a and b are obtained from a regression analysis of the linear portion of the permanent strain versus number of load cycles plot (Witczak et al. 2002). Other HMAC mixture response parameters from the repeated load test that have been correlated to permanent deformation of in-field HMAC pavements are: resilient modulus (E_R), plastic strain (ε_p) per load cycle and strain ratio ($\varepsilon_p/\varepsilon_r$). ($\varepsilon_r$), is the resilient strain and represents the recoverable axial strain during the rest period of the load cycle.

2.5.4 Static Triaxial Creep Test

Static triaxial creep test was included as a simple performance test in Superpave™ Level II mix design to simulate a heavy vehicle standing on asphalt

pavements. Static creep loading loading can be seen in trucks stopping at traffic lights and intersections. The static triaxial creep test has the output of flow time which depicts the length of time HMAC pavement can withstand the steady pressure until flow occurs. In the static triaxial creep test, the total strain-time relationship of HMAC asphalt mixtures is determined under unconfined or confined conditions (Witczak et al. 2002). The static creep test can use one load and unload cycle or incremental load-unload cycles and provides information to determine the recoverable and irrecoverable time independent components as well as time dependent viscoelastic and viscoplastic components of material response. Analogous to repeated load test, the total compliance of HMAC mixes can be divided into three major zones: primary, secondary and tertiary flow zones.

The flow time of the test is defined as the starting point of tertiary flow and indicates the minimum point in the rate of compliance to loading time. The flow time, F_T, can therefore be defined as the time at which the shear deformation of HMAC under constant volume begins (Hafez 1997).

Earlier research (Bhasin et al. 2004) indicated that flow number value and flow time slope were better than dynamic modulus in correlating laboratory rutting depth of HMAC. The three material response properties were evaluated for their ability to correlate rutting of HMAC mixtures by comparing them with measured rut depths from the asphalt pavement analyzer and the Hamburg wheel tracking device.

The secondary phase of the creep compliance curve is modeled using power models (NCHRP Report-465 2002):

$$D' = D(t) - D_o = at^m \qquad \textbf{2.13}$$

where D′ is viscoelastic compliance component at any time; D(t) is total compliance at any time; D_o is instantaneous compliance; t is total loading time and a, m are material regression coefficients.

The regression coefficients a and m indicate the permanent deformation response of the HMAC mixture. The larger the value of a, the larger the compliance value, D(t),

the lower the modulus and the larger the permanent deformation of the particular mix. For a constant *a*-value, increase in slope of parameter *m* means higher permanent deformation of HMAC mix.

2.6 Rapid Triaxial Test (RaTT) Mechanistic Characterization

The RaTT cell test is used to characterize mechanistic material properties for structural models (Berthelot 1999, Berthelot et al. 1999, Crockford et al, Anthony and Berthelot 2004, Gould et al. 2003, Baumgartner 2005, Berthelot et al. 2005). RaTT cell mechanistic characterization of HMAC mixes is analogous to triaxial testing of soils and other engineering materials. The RaTT cell test can be performed at multiple frequencies as well as multiple stress states. This enables the RaTT cell test to quantify both time-dependent response and stress-dependent response of HMAC mixtures. The RaTT cell test has been used in quality control and quality assurance testing of HMAC because of its advantages over current SHRP SPTs and SHRP shear tester protocols. Advantages of the RaTT cell test include: (Berthelot et al. 1999, Gould et al. 2003):

- Short testing time;
- Ability to simulate multiple frequencies and multiple stress states representative of those in the field; and
- Ability to characterize 150 mm by 150 mm gyratory compactor specimen, hence reducing coefficient of variation in test data.

The RaTT cell machine, illustrated in Figure 2.14, is designed to use a pneumatic loading system to apply a constant confining pressure and a sinusoidal vertical load at various frequencies. The RaTT cell machine is capable of controlling the confining pressure at different levels and can therefore be used for hydrostatic compression testing. The computer automated system incorporated with the RaTT cell controls the cell movements, confining and axial stress, vertical and horizontal strain and test temperature. The strains in the test specimen are measured by means of an LVDT (Berthelot et al. 1999, Internet ipcglobal.com).

An evaluation of the rapid triaxial test method was carried out in the form of testing asphalt mixes with different nominal aggregates size, gradation, and asphalt content. Asphalt specimens compacted from the same mix but with different air voids as well as mixes with different percentage passing 0.075 mm sieve (Gould et al. 2003). The tests were performed at temperatures of 60°C and 100°C and frequencies of 1 Hz and 5 Hz respectively. A temperature of 100°C and frequency of 5 Hz were used to simulate pavement conditions under traffic travelling at highway speeds and a temperature of 60°C and 1 Hz were used for practical purposes.

The coefficients of variation of the dynamic modulus at 100°C and 1 Hz were compared with coefficients of variation of the dynamic modulus at 60°C and 5 Hz. They found that the coefficients of variation of results obtained from the test at 60°C and 1 Hz were significantly different from coefficients of variation at 100°C and 5 Hz.

Figure 2.14 Rapid Triaxial Test Cell at the University of Saskatchewan

Alternative test methods for predicting asphalt concrete rut performance included the evaluation of Marshall stability and flow, Hveem stability, Unconfined compressive strength, SHRP Level III tester and triaxial frequency properties (Berthelot et al. 1999). Seven different asphalt concrete mixes were tested using each of these rut characterization methods. After testing triplicate gyratory compactor samples, analysis of variance and Duncan pairwise comparison was carried out for the different asphalt mixes. It was found that the rapid triaxial tester determined the significant differences between the asphalt concrete mixes and can be employed as a complementary mechanistic characterization tool along side the SHRP gyratory compactor for asphalt concrete mix design and analysis.

Rapid triaxial testing has been found to be effective in HMAC quality control and quality assurance during pavement construction (Berthelot et al. 1999, Crockford et al 2002, Gould et al 2003, Anthony 2007). Fundamental material properties obtained from the rapid triaxial testing include:

- Dynamic Modulus
- Poisson's Ratio
- Radial Strain
- Vertical Strain
- Phase Angle

2.7 Chapter Summary

This chapter presented a discussion on different laboratory characterization methods of HMAC including compaction protocols, volumetric analysis and mechanistic property characterization. Previous research shows that the method of laboratory compaction used in the design of hot-mix asphalt has been found to affect the density and volumetric properties of asphalt mix. Failures of asphalt pavement due to poor compaction protocol have been observed in the form of permanent

deformation, thermal cracking and fatigue cracking. There is a need to design a compaction protocol that will be able to simulate increasing traffic loading as experienced on Saskatchewan highways and across highways all over North America.

Marshall stability and flow, as an empirical method, was found to be short in providing fundamental material properties. The rapid triaxial testing protocol was developed to simulate traffic loading on asphalt pavements and to provide fundamental pavement response properties. The fundamental material properties obtained from the rapid triaxial testing protocol were essential in predicting and modeling pavement performance.

The SHRP Superpave™ Level I mix design procedure incorporates the Superpave™ gyratory compaction protocol and has been found to be an effective way of simulating in field pavement density and volumetric properties. The gyratory compactor was found to produce specimens that are conveniently used for characterizing mechanistic material properties in the rapid triaxial testing device.

Voids in total mix is the primary volumetric mix property of importance. Void in mineral aggregates is documented as one of the most important void properties in asphalt mix design. Voids in mineral aggregates accommodates the thermal expansion of the asphalt binder. In order to produce mineral aggregates blend to meet sufficient air voids level for the total asphalt mix the SHRP Superpave™ Level I mix design procedure specifies coarse aggregates and fine aggregates requirements. The control points and restricted zone in the SHRP Superpave™ Level I mix design procedure was found to eliminate mineral aggregates blends that do not meet voids in mineral aggregates specification.

Based on the literature review, it was decided to employ gyratory compaction and Marshall compaction methods in laboratory sample preparation. The rapid triaxial frequency sweep tester and Marshall stabilometer were used to evaluate mechanical behaviour of the respective SPS-9A asphalt mixes across various laboratory compactive efforts.

CHAPTER 3 VOLUMETRIC PROPERTY CHARACTERIZATION OF MARSHALL AND GYRATORY COMPACTED SAMPLES

This study investigated seven hot-mix asphalt concrete mixtures from the Specific Pavement Study (SPS-9A) test site constructed near Radisson, Saskatchewan in 1996. The Radisson SPS-9A test sections were constructed to study the performance of different asphalt binders as well as compare conventional Saskatchewan Ministry of Highways and Infrastructure mixes to Superpave™ dense graded mixtures under the same field traffic and environmental conditions. The test sections were constructed as part of the Strategic Highway Research Program (SHRP) Long Term Pavement Performance Program (LTPP). For the purpose of analysis the last three digits of each test section are retained with letter M, S and SR denoting Marshall, Superpave™, Superpave™ recycled mix respectively. For example, SMHI Marshall designed test section 900901 becomes 901M while Superpave™ designed test section 900902 becomes 902S.

Typical asphalt binders used by the Saskatchewan Ministry of Highway and Infrastructure for pavement construction were selected for the test sections. Superpave™ Performance Graded (PG) asphalt binders were selected to meet the Superpave™ requirements of temperature, traffic speed and loading for test sections 902S, 903S and 959S.

Three of the Radisson SPS-9A test section; 901M, 902S and 903S, were constructed to meet the SHRP mix design requirements. Section 901M was constructed using conventional Marshall mix design with aggregate gradation meeting Saskatchewan Ministry of Highways and Infrastructure Type 70 dense aggregate gradation requirements and conventional 150-200A asphalt binder. Section 902S was constructed using Superpave™ coarse aggregate gradation and asphalt binder that meets the temperature, traffic speed and loading requirements of the test site at 98 percent reliability. Section 903S was constructed using Superpave™ coarse aggregate gradation and asphalt binder that is on a lower temperature end than the required asphalt binder according to Superpave™ binder requirement for the Radisson SPS-9A

test site. Four additional test sections, including a Superpave™ recycled section, were constructed to evaluate typical asphalt binders use by SMHI for pavement construction.

The seven test sections considered in this study were designed to the same structural integrity using the SMHI California Bearing Ratio (CBR) nomograph design procedure (SMHI 2001). The design life of the segment of Highway 16 near Radisson was 15 years and the traffic loading was predicted to be 6.1×10^6 equivalent single axle loads, (ESAL)s.

The structural cross-section was uniform across all test sections to ensure that any variations in performance of the test sections is due to the hot-mix asphalt properties and not due to differences in structural properties (SHRP 1994). The test sections consist of 120 mm of hot-mix asphalt concrete, 200 mm of Type 33 granular base and 230 mm of subbase. The underlying clay-till subgrade was prepared to a CBR of six.

Aggregates used for the construction of the Radisson test sections were manufactured from a local single source consisting of glacial gravel deposit (Berthelot and Anthony 2003, Berthelot et al. 1999). Sections 901M and 961M were constructed using the Saskatchewan Ministry of Highways and Infrastructure standard Marshall mix design method with aggregate gradation meeting SMHI Type 70 dense gradation requirements (SMHI Specification). The Superpave™ sections were constructed using Superpave™ Level I mix design procedure with aggregate gradation meeting Superpave™ coarse gradation requirements (Asphalt Institute 1996). As seen in Figure 3.1, the SMHI Type 70 dense gradation plotted on a Superpave™ 0.45 power chart passes through the SHRP restricted zone and lies close to the SMHI maximum limits of gradation envelope at the larger sieve sizes. Figure 3.2 illustrates the Superpave™ coarse aggregate gradation plotted on a Superpave™ gradation chart. As seen in Figure 3.2, the Superpave™ mix aggregate gradations all passed below the SHRP restricted area.

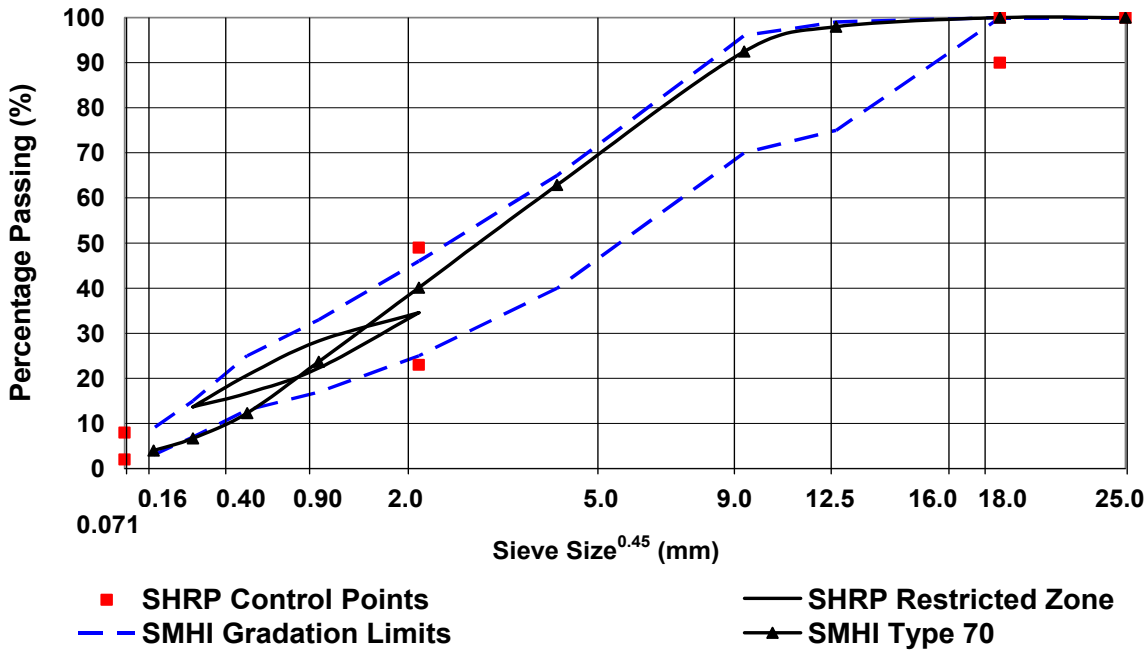

Figure 3.1 Aggregate Gradation for SMHI Type 70 Marshall Mix Design Method

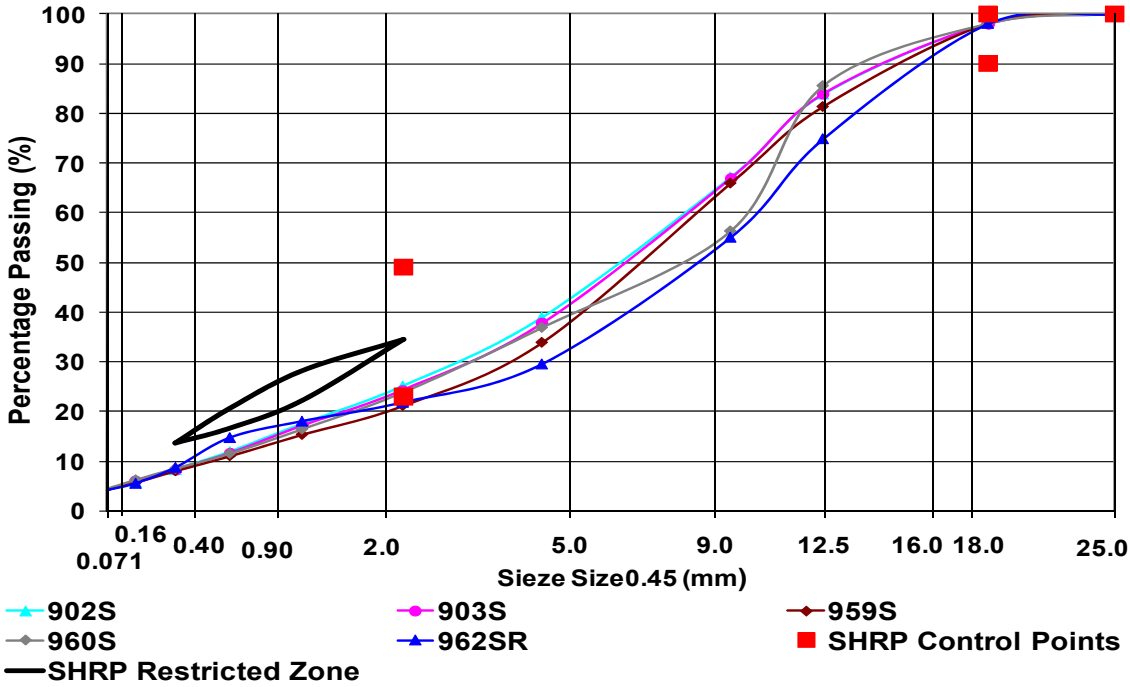

Figure 3.2 Aggregate Gradations for Superpave™ Mix Design Test Sections

To prepare hot-mix asphalt samples from each Radisson SPS-9A test site for laboratory testing, standard 50 and 75-blow Marshall and Superpave^{TM} Level I gyratory compaction protocols were employed (SMHI 2001, Berthelot 1999, Asphalt Institute 1996, Kandhal and Koehler 1985). Asphalt concrete from different locations within each test section were sampled, combined and stored in sealed pails during the construction of the Radisson SPS-9A test sections in 1996. The amount of hot-mix asphalt needed to compact the required repeat samples per test section was reheated in the pails to a temperature 90°C until it was workable and was uniformly mixed in a larger container. The uniformly combined hot-mix asphaltic concrete was then spread in pans and covered with aluminum foil and placed in the oven at the specified compaction temperature for each mix for a period of four hours prior to compaction as specified in the Superpave^{TM} Level I mix design procedure (Asphalt Institute 1996, SHRP 1994).

3.1 SMHI Marshall Compaction and Volumetric Property Characterization

SMHI commonly use conventional Marshall mix design methodology with 75-blow Marshall compaction for the design of Saskatchewan high traffic mixes as specified in STP 204 after ASTM D1559 (ASTM 1996, SMHI 1992). For the purposes of this research, four repeat samples were compacted at each of the 50 and 75-blow Marshall compaction energy representing light traffic loading and heavy traffic loading, respectively.

Volumetric property characterization was performed on the Marshall compacted specimens. Bulk specific gravity measurements were performed after ASTM D2726 (ASTM 1996). The Rice specific gravity of each asphaltic mix was determined as specified in ASTM D2041 (ASTM 1996). Voids in the total mix, voids in the mineral aggregates and voids filled with asphalt were determined for the compacted specimens based on the results of the volumetric property tests. Detailed data for the volumetric properties of the Marshall compacted samples can be found in Appendix A.

Marshall stability and flow tests were also performed on the samples to determine the relative resistance of the compacted hot-mix asphalt specimens to permanent deformation after ASTM D1559 (ASTM 1996).

3.1.1 Voids in the Total Mix (VTM)

Table 3.1 summarizes the average Marshall VTM and the respective coefficient of variation across the four repeat Marshall specimens at 50 and 75-blow Marshall across each Radisson SPS-9A test section asphalt concrete mix. Figure 3.3 illustrates the mean VTM with respect to varying compaction effort across each Radisson SPS-9A test section. The error bars displayed in Figure 3.3 represent ± two standard deviations from the mean of the four repeat samples compacted for each test section.

VTM was found to be lower for 75-blow Marshall compaction as compared to 50-blow Marshall. This trend was expected because of the resultant increase in compactive energy with increase in number of blows from the Marshall hammer. The decrease in VTM with increasing number of Marshall blows illustrates the effect of increased compactive effort resulting in more voids in the asphalt aggregate matrix being filled with asphalt binder. As seen in Table 3.1 and Figure 3.3, VTM of the conventional SMHI Marshall mix design sections 901M and 961M were found to be lower at 75-blow Marshall mix design criterion relative to the Superpave™ mix samples.

It should be noted that only section 961M met the SMHI air void criteria at 50-blow Marshall design criterion. Sections 902S and 903S also met the SMHI air void criteria at 75-blow Marshall compactive effort. It is interesting to note that of the Radisson SPS-9A mixes that did not meet the SMHI specified VTM criterion, the Marshall mixes were below acceptable VTM limits while the Superpave™ mixes were observed to be above the SMHI acceptable limits.

Table 3.1 Average Voids in Total Mix at 50 and 75-Blow Marshall Compaction across Radisson SPS-9A Asphalt Mixes

Test Section Number	50-Blow Marshall (% Air Voids)	Coefficient of Variation (%)	75-Blow Marshall (% Air Voids)	Coefficient of Variation (%)
901M	2.9	3.9	2.7	17.9
961M	3.4	9.1	2.8	9.7
903S	6.1	3.3	4.9	7.3
959S	6.2	10.3	5.3	5.3
960S	6.3	8.6	5.1	7.8
902S	5.5	7.5	4.3	10.2
962SR	5.7	8.7	5.3	1.6

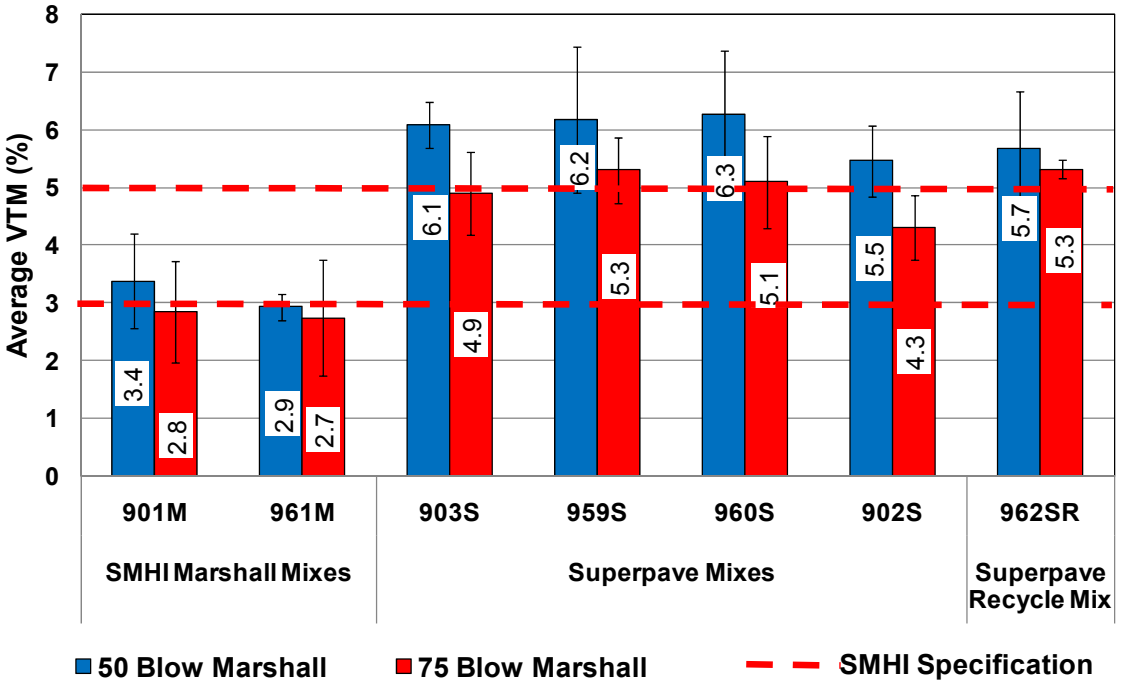

Figure 3.3 Average Voids in Total Mix at 50 and 75-Blow Marshall Compaction across Radisson SPS-9A Asphalt Mixes (± 2 SD)

Statistical analysis of variance was performed on the VTM values across 50 and 75-blow Marshall compaction within each Radisson SPS-9A test section and the results are presented in Table 3.2. As seen in Table 3.2, there was significant difference in VTM across 50 and 75-blow Marshall compaction. Table 3.3 presents Tukey's groups

of VTM across 50 and 75-blow Marshall compaction within each Radisson SPS-9A test section. As seen in Table 3.3, there was significance in VTM at 50-blow Marshall compared to 75-blow Marshall within all test sections except test sections 901M and 962SR.

Table 3.2 Analysis of Variance for VTM at 50 and 75-Blow Marshall Compaction across Radisson SPS-9A Asphalt Mixes

Parameter	Sum of Squares	Degrees of Freedom	Mean Squares	F-Test Statistic	P-value	Sig.
Between Groups	4.7	6	2.3	14	0.02	Yes
Within Groups	1.5	1	0.2			
Total	6.2	11				
Error	0.8					

Table 3.3 Tukey's Homogeneous Groups for VTM at 50 and 75-Blow Marshall Compaction across Radisson SPS-9A Asphalt Mixes

Test Section	Marshall Blow	Mean VTM (%)	Tukey's Homogeneous Groups	
901M	50	2.9	A	
	75	2.7	A	
961M	50	3.4	A	
	75	2.8		B
903S	50	6.1	A	
	75	4.9		B
959S	50	6.2	A	
	75	5.3		B
960S	50	6.3	A	
	75	5.1		B
902S	50	5.5	A	
	75	4.3		B
962SR	50	5.7	A	
	75	5.3	A	

Statistical analysis of variance was performed on the VTM values in order to investigate the variability of VTM across the Radisson SPS-9A asphalt mixes and the results are presented in Table 3.4 and Table 3.6 for 50-blow Marshall and 75-blow

Marshall compaction respectively. As seen in Table 3.4 and Table 3.5, analysis of variance shows significant differences in the VTM values at 50 and 75-blow Marshall across the Radisson SPS-9A mixes, as the F-Test is larger than one and the probability factor, P, is smaller than 0.05. Table 3.5 and Table 3.7 present Tukey's groups of VTM of Marshall compacted samples of the Radisson SPS-9A test sections at 50 and 75-blow Marshall compaction respectively. The conventional SMHI Marshall mix, test sections 901M and 961M have similar VTM values at 50-blow Marshall, compared to the Superpave™ mixes as shown in Table 3.5. There are no significant differences in the VTM for the Superpave™ mixes at 50-blow Marshall. It should also be noted that conventional SMHI Marshall mix, test sections 901M and 961M have similar VTM at 75-blow Marshall compared to the Superpave™ mixes as shown in Table 3.7. The Superpave™ mixes have similar VTM shown by the interaction in the Tukey's homogeneous groups. The only significant differences noted between VTM of the Superpave™ mixes were test sections 959S and 962SR (average VTM values of 5.3 percent) and test section 902S (average VTM value of 4.3 percent). From the statistical analysis it was concluded that VTM is sensitive to the mix type and compaction energy.

Table 3.4 Analysis of Variance for VTM at 50-Blow Marshall Compaction across Radisson SPS-9A Asphalt Mixes

Parameter	Sum of Squares	Degrees of Freedom	Mean Squares	F-Test Statistic	P-value	Sig.
Between Groups	47	6	8			
Within Groups	4	21	0.2	44	0.00	Yes
Total	50	27				
Error	0.3					

Table 3.5 Tukey's Homogeneous Groups for VTM at 50-Blow Marshall Compaction across Radisson SPS-9A Asphalt Mixes

Test Section	Mean VTM (%)	Tukey's Homogeneous Groups	
901M	2.9	A	
961M	3.4	A	B
902S	5.5		B
962SR	5.7		B
903S	6.1		B
959S	6.2		B
960S	6.3		B

Table 3.6 Analysis of Variance for VTM at 75-Blow Marshall Compaction across Radisson SPS-9A Asphalt Mixes

Parameter	Sum of Squares	Degrees of Freedom	Mean Squares	F-Test Statistic	P-value	Sig.
Between Groups	31	6	5			
Within Groups	3	21	0.1	40	0.00	Yes
Total	33	27				
Error	0.2					

Table 3.7 Tukey's Homogeneous Groups for VTM at 75-Blow Marshall Compaction across Radisson SPS-9A Asphalt Mixes

Test Section	Mean VTM (%)	Tukey's Homogeneous Groups		
901M	2.7	A		
961M	2.8	A		
902S	4.3		B	
903S	4.9		B	C
960S	5.1		B	C
959S	5.3			C
962SR	5.3			C

3.1.2 SMHI Marshall Voids in the Mineral Aggregate (VMA)

Table 3.8 summarizes the average Marshall VMA and the respective coefficient of variation across the four repeat Marshall specimens at 50 and 75-blow Marshall across each Radisson SPS-9A test section asphalt concrete mix. Figure 3.4 displays the mean VMA with respect to varying compaction effort cross each Radisson SPS-9A test section. The error bars displayed in Figure 3.4 represent ± two standard deviations from the mean of the four repeat samples compacted for each test section.

As seen in Table 3.6 and Figure 3.4, VMA was observed to be lower at 75-blow Marshall relative to 50-blow Marshall. The increase compactive effort results in the asphalt cement being forced into the permeable voids of the mineral aggregates hence the decrease in VMA. The conventional SMHI Marshall mixes have low VMA at both 50 and 75-blow Marshall compared with the Superpave^{TM} mixes.

It should be noted that sections 901M, 961M and 962SR met the SMHI VMA criteria at 50-blow Marshall. However, sections 902S, 903S and 959S had VMA values higher than the upper limit of the SMHI VMA criteria at 50-blow Marshall. It was also observed that only Section 959S did not meet the SMHI VMA criteria at 75-blow Marshall. The higher VMA values for the Superpave^{TM} mixes is due to the presence of higher crush coarse aggregate particles which increases the total surface area of the mineral aggregates and consequently increase the total voids in the mineral aggregates. This implies that the Superpave^{TM} mixes would provide sufficient voids for adhesion and thermal expansion of the asphalt cement within the asphalt aggregates matrix and will therefore be more resistant to bleeding and viscoplastic flow under the same field conditions.

Table 3.8 Average Voids in Mineral Aggregates at 50 and 75-Blow Marshall Compaction across Radisson SPS-9A Asphalt Mixes

Test Section Number	50-Blow Marshall (% Air Voids)	Coefficient of Variation (%)	75-Blow Marshall (% Air Voids)	Coefficient of Variation (%)
901M	14.2	0.7	14.0	3.1
961M	14.6	1.9	14.1	1.7
903S	16.5	1.1	15.4	2.1
959S	16.8	3.4	15.9	1.6
960S	16.4	2.9	15.4	2.3
902S	15.6	2.3	14.6	2.7
962SR	15.3	2.9	15.0	0.5

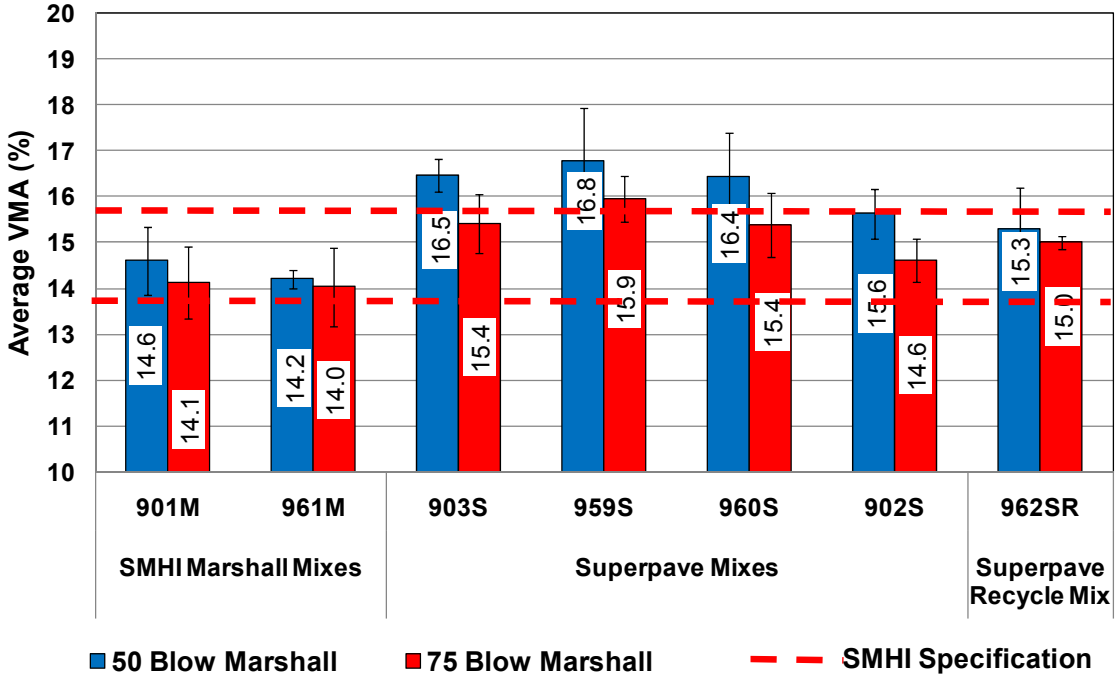

Figure 3.4 Average Voids in Mineral Aggregates at 50 and 75-Blow Marshall Compaction across Radisson SPS-9A Asphalt Mixes (± 2 SD)

Statistical analysis of variance was performed on the VMA values across 50 and 75-blow Marshall compaction within each Radisson SPS-9A test section and the results are presented in Table 3.9. As seen in Table 3.9, there was significant difference in VMA across 50 and 75-blow Marshall compaction. Table 3.10 presents Tukey's groups

of VMA across 50 and 75-blow Marshall compaction within each Radisson SPS-9A test section. As seen in Table 3.10, there was significance in VMA at 50-blow Marshall compared to 75-blow Marshall within all Superpave™ mixes. However, test sections 901M, 961M and 962SR did not show any significance in VMA at 50-blow Marshall compared to 75-blow Marshall compaction.

Table 3.9 Analysis of Variance for VMA at 50 and 75-Blow Marshall Compaction across Radisson SPS-9A Asphalt Mixes

Parameter	Sum of Squares	Degrees of Freedom	Mean Squares	F-Test Statistic	P-value	Sig.
Between Groups	1.6	6	0.8	11	0.00	Yes
Within Groups	0.6	1	0.6			
Total	2.1	11				
Error	0.7					

Table 3.10 Tukey's Homogeneous Groups for VMA at 50 and 75-Blow Marshall Compaction across Radisson SPS-9A Asphalt Mixes

Test Section	Marshall Blow	VTM (%)	Tukey's Homogeneous Groups	
901M	50	14.2	A	
	75	14.0	A	
961M	50	14.6	A	
	75	14.1	A	
903S	50	16.5	A	
	75	15.4		B
959S	50	16.8	A	
	75	15.9		B
960S	50	16.4	A	
	75	15.4		B
902S	50	15.6	A	
	75	14.6		B
962SR	50	15.3	A	
	75	15.0	A	

Statistical analysis of variance was performed on the VMA values in order to investigate the variability of VMA across the Radisson SPS-9A asphalt mixes and the results are presented in Table 3.11 and Table 3.13 for 50-blow Marshall and 75-blow

Marshall compaction respectively. As seen in Table 3.11 and Table 3.13, analysis of variance shows that there are significant differences in the VMA measured at 50 and 75-blow Marshall across the Radisson SPS-9A mixes, as the F-Test is larger than 1 and the probability factor, P, is smaller than 0.05. Table 3.12 and Table 3.14 show Tukey's homogeneous groups of VMA values at 50 and 75-blow Marshall Compaction respectively.

As seen in Table 3.12, there are similar VMA values between the conventional SMHI Marshall mix design sections 901M and 961M and the Superpave™ recycled mix design section 962SR at 50-blow Marshall. It should be noted that there is no significant difference in the VMA of the Superpave™ mixes shown by the interactions in the Tukey's multiple comparisons as seen in Table 3.12 and Table 3.14. Superpave™ recycled mix design section 962SR have no significant difference in VMA compared to the conventional SMHI Marshall mix design sections 901M and 961M at 75-blow Marshall. Superpave™ mixes show no significant difference in the VMA at 75-blow Marshall, as seen in Table 3.14.

Only Superpave™ mix design section 902S has similar VMA values compared to the Superpave™ recycled mix design section 962SR at 50 and 75-blow Marshall. It was therefore concluded that VMA is sensitive to the mix type and compaction energy.

Table 3.11 Analysis of Variance for VMA at 50-Blow Marshall Compaction across Radisson SPS-9A Mixes

Parameter	Sum of Squares	Degrees of Freedom	Mean Squares	F-Test Statistic	P-value	Sig.
Between Groups	23	6	4			
Within Groups	3	21	0.1	27	0.00	Yes
Total	26	27				
Error	0.2					

Table 3.12 Tukey's Homogeneous Groups for VMA at 50-Blow Marshall Compaction across Radisson SPS-9A Mixes

Test Section	Mean VMA (%)	Tukey's Homogeneous Groups				
901M	14.2	A				
961M	14.6	A	B			
962SR	15.3		B	C		
902S	15.6			C	D	
960S	16.4				D	E
903S	16.5				D	E
959S	16.7					E

Table 3.13 Analysis of Variance for VMA at 75-Blow Marshall Compaction across Radisson SPS-9A Mixes

Parameter	Sum of Squares	Degrees of Freedom	Mean Squares	F-Test Statistic	P-value	Sig.
Between Groups	12	6	2			
Within Groups	2	21	0.1	20	0.00	Yes
Total	14	27				
Error	0.1					

Table 3.14 Tukey's Homogeneous Groups for VMA at 75-Blow Marshall Compaction across Radisson SPS-9A Mixes

Test Section	Mean VMA (%)	Tukey's Homogeneous Groups				
901M	14.0	A				
961M	14.1	A				
962SR	14.6	A	B			
902S	15.0		B	C		
960S	15.4			C	D	
903S	15.4			C	D	
959S	15.9				D	

3.2.3 SMHI Marshall Voids Filled with Asphalt (VFA)

Table 3.15 summarizes the average Marshall VFA and the respective coefficient of variation across the four repeat Marshall compactor samples at 50 and 75-blow Marshall across each Radisson SPS-9A test section asphalt concrete mix. Figure 3.5 illustrates the mean VFA with respect to varying compaction effort across each Radisson SPS-9A test sections. The error bars displayed in Figure 3.5 represent ± two standard deviations from the mean of the four repeat samples compacted for each test section.

The VFA was observed to be higher for samples compacted with 75-blow Marshall relative to 50-blow Marshall compactor samples. The higher VFA values at 75-blow Marshall could be due to overall increase in compactive energy with increase in the number of blows from the Marshall hammer. More asphalt binder is forced into the permeable voids in the mineral aggregates and the voids in the asphalt-aggregate matrix.

It should be noted that the conventional SMHI Marshall mixes, Sections 901M and 961M, had the highest VFA values compared with the Superpave^{TM} mixes. The higher VFA values for the conventional SMHI Marshall mixes is due to the high asphalt content, 5.21 percent, resulting in high film thickness and sufficient coating of the mineral aggregates (Kandhal and Chakraborty 1996). Only sections 902S and 961M met the SMHI VFA criteria at 50-blow Marshall. Sections 902S, 903S, 959S and 960S all met the SMHI VFA criteria at 75-blow Marshall. However, sections 901M and 961M had VFA values that were higher than the upper limit of the SMHI VFA bandwidth. Section 962SR did not meet the SMHI VFA criteria for both 50 and 75-blow Marshall.

Table 3.15 Average Voids Filled with Asphalt at 50 and 75-Blow Marshall Compaction across Radisson SPS-9A Asphalt Mixes

Test Section Number	50-Blow Marshall	Coefficient of Variation (%)	75-Blow Marshall	Coefficient of Variation (%)
901M	79.4	0.8	80.6	3.8
961M	76.9	2.2	79.7	2.0
903S	63.1	1.3	68.2	2.5
959S	63.1	4.0	66.8	1.9
960S	61.9	3.4	66.9	2.7
902S	65.2	2.7	70.6	3.2
962SR	63.1	3.4	64.6	0.6

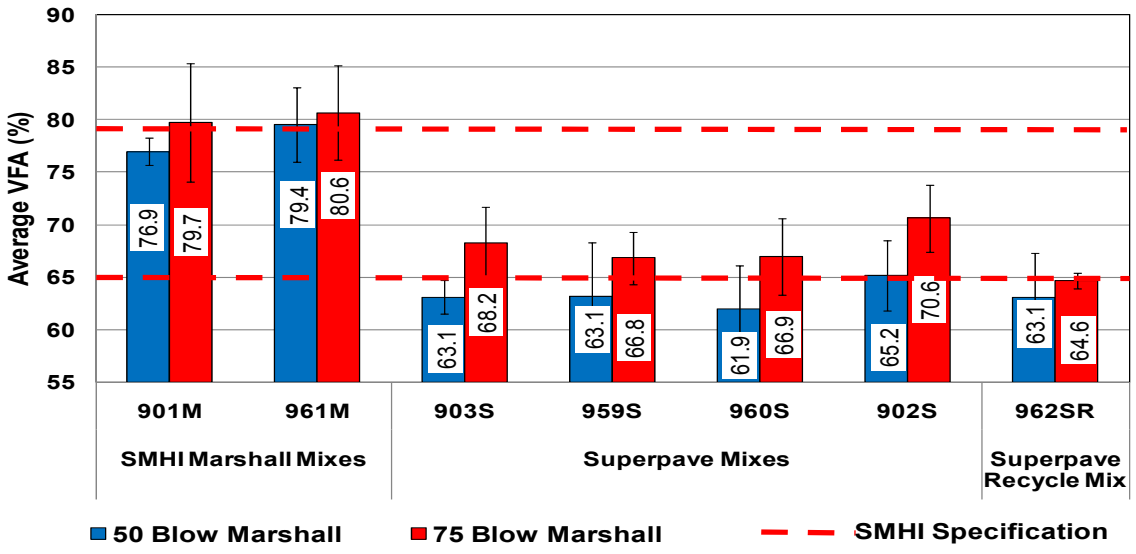

Figure 3.5 Average Voids Filled with Asphalt at 50 and 75-Blow Marshall Compaction across Radisson SPS-9A Asphalt Mixes (± 2 SD)

Statistical analysis of variance was performed on the VFA values across 50 and 75-blow Marshall compaction within each Radisson SPS-9A test section and the results are presented in Table 3.16. As seen in Table 3.16, there was significant difference in VFA across 50 and 75-blow Marshall compaction. Table 3.17 presents Tukey's groups of VFA across 50 and 75-blow Marshall compaction within each Radisson SPS-9A test section. As seen in Table 3.17, there was significance in VFA at 50-blow Marshall compared to 75-blow Marshall within test sections except test sections 901M and 962SR.

Table 3.16 Analysis of Variance for VFA at 50 and 75-Blow Marshall Compaction across Radisson SPS-9A Asphalt Mixes

Parameter	Sum of Squares	Degrees of Freedom	Mean Squares	F-Test Statistic	P-value	Sig.
Between Groups	117	6	58.6	22	0.004	Yes
Within Groups	24	1	2.7			
Total	141	11				
Error	0.9					

Table 3.17 Tukey's Homogeneous Groups for VFA at 50 and 75-Blow Marshall Compaction across Radisson SPS-9A Asphalt Mixes

Test Section	Marshall Blow	VTM (%)	Tukey's Homogeneous Groups	
901M	50	79.4	A	
	75	80.6	A	
961M	50	76.9	A	
	75	79.7		B
903S	50	63.1	A	
	75	68.2		B
959S	50	63.1	A	
	75	66.8		B
960S	50	61.9	A	
	75	66.9		B
902S	50	65.2	A	
	75	70.6		B
962SR	50	63.1	A	
	75	64.6	A	

Statistical analysis of variance was performed on the VFA values in order to investigate the variability of VFA across the Radisson SPS-9A asphalt mixes and the results are presented in Table 3.18 and Table 3.20 for 50-blow Marshall and 75-blow Marshall compaction respectively. As seen in Table 3.18 and Table 3.20, analysis of variance shows that there are significant differences in the VFA measured at 50 and 75-blow Marshall across the Radisson SPS-9A mixes, as the F-Test is larger than 1 and the probability factor, P, is smaller than 0.05. Table 3.19 and Table 3.21 show Tukey's homogeneous groups of VFA values at 50 and 75-blow Marshall Compaction respectively.

As seen in Table 3.19, there is significant difference in VFA between the conventional SMHI Marshall mixes, test sections 901M and 961M, compared to the Superpave™ mixes at 50-blow Marshall compaction. The Superpave™ mixes however, have similar VFA values compared to one another. Significant difference in VFA was noted that at 75-blow Marshall compaction between the conventional SMHI Marshall mixes, test sections 901M and 961M, compared to the Superpave™ mixes as seen in Table 3.21. The only significant difference between the Superpave™ mixes was between test section 962SR (average VFA value 64.6 percent) and 902S (average VFA value 70.6 percent). It was therefore conclude that VFA is sensitive to mix design method and compaction energy.

Table 3.18 Analysis of Variance for VFA at 50-Blow Marshall Compaction across Radisson SPS-9A Mixes

Parameter	Sum of Squares	Degrees of Freedom	Mean Squares	F-Test Statistic	P-value	Sig.
Between Groups	1306	6	218	68	0.00	Yes
Within Groups	6	21	3			
Total	1373	27				
Error	1					

Table 3.19 Tukey's Homogeneous Groups for VFA at 50-Blow Marshall Compaction across Radisson SPS-9A Mixes

Test Section	Mean VFA (%)	Tukey's Homogeneous Groups	
960S	61.9	A	
903S	63.1	A	
962SR	63.1	A	
959S	63.1	A	
902S	65.2	A	
961M	76.9		B
901M	79.4		B

Table 3.20 Analysis of Variance for VFA at 75-Blow Marshall Compaction across Radisson SPS-9A Mixes

Parameter	Sum of Squares	Degrees of Freedom	Mean Squares	F-Test Statistic	P-value	Sig.
Between Groups	1025.59	6	171	51	0.00	Yes
Within Groups	68.80	21	3			
Total	1095.39	27				
Error	1.20					

Table 3.21 Tukey's Homogeneous Groups for VFA at 75-Blow Marshall Compaction across Radisson SPS-9A Mixes

Test Section	Mean VTM (%)	Tukey's Homogeneous Group		
962SR	64.6	A		
959S	66.8	A	B	
960S	66.9	A	B	
903S	68.2	A	B	
902S	70.6		B	
961M	80.0			C
901M	80.6			C

3.2.4 SMHI Marshall Density

Table 3.22 summarizes the average Marshall density and the respective coefficient of variation across the four repeat Marshall specimens at 50 and 75-blow Marshall for each Radisson SPS-9A test sections asphalt concrete mix. Figure 3.6 illustrates the mean Marshall density with respect to varying compaction effort across each Radisson SPS-9A test sections. The error bars displayed in Figure 3.6 represent ± two standard deviations from the mean of the four repeat samples compacted for each test section.

As expected, the Marshall compactor samples displayed a trend of increasing Marshall density with increase in compaction effort. The increase in density from 50 to 75-blow Marshall would be due to increased compactive effort resulting in the hot-mix asphalt being compacted to a denser matrix.

The SMHI conventional Marshall mixes, sections 901M and 961M, were found to have higher Marshall densities compared with the Superpave™ coarse graded mixes. This indicates that SMHI Type 70 dense graded mixes are more workable and compact easily to a higher density as compared to the Superpave™ coarse graded mixes. The SMHI Marshall mixes will be expected to have lower VMA due to the overall larger bulk densities. Section 959S can be seen to have the lowest density for both 50 and 75-blow compacted specimens.

Table 3.22 Average Marshall Density at 50 and 75-Blow Marshall Compaction across Radisson SPS-9A Asphalt Mixes

Test Section Number	Density 50-Blow (kg/m^3)	Coefficient of Variation (%)	Density 75-Blow (kg/m^3)	Coefficient of Variation (%)
901M	2379	3.9	2384	17.9
961M	2368	9.1	2381	9.7
903S	2319	3.3	2348	7.3
959S	2314	10.3	2335	5.3
960S	2324	8.5	2353	7.8
902S	2337	7.5	2365	10.2
962SR	2341	8.7	2350	1.6

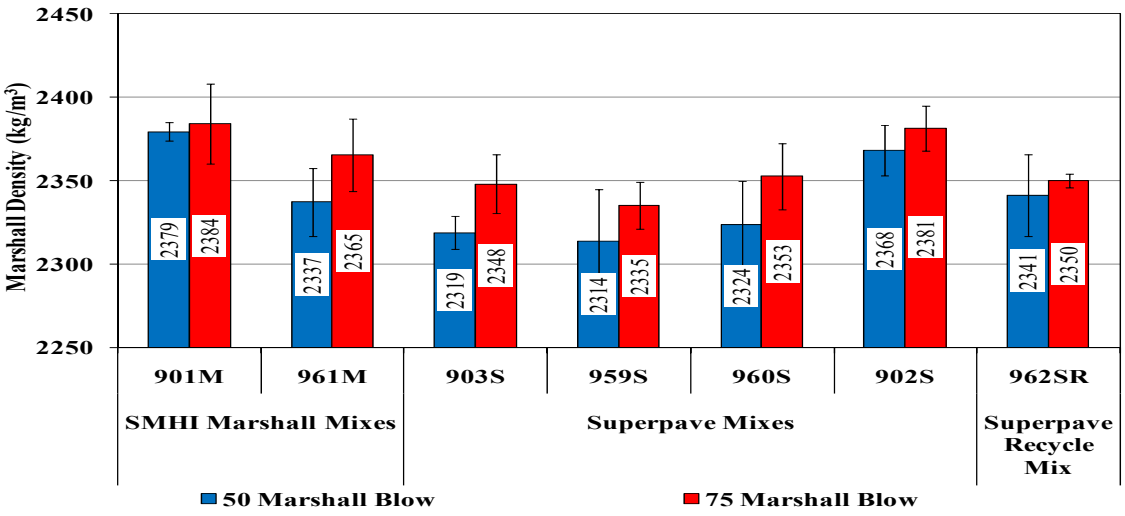

Figure 3.6 Average Marshall Density at 50 and 75-Blow Marshall Compaction across Radisson SPS-9A Asphalt Mixes (± 2 SD)

3.3 Superpave™ Level I Gyratory Compaction Volumetric Characterization

Three repeat samples were compacted for each of the seven asphalt mixes at gyratory angles of 1.25°, 2.00° and 2.75° using the Superpave™ gyratory compactor (SHRP 1994). The gyratory compaction hot-mix asphalt samples were compacted to a height of 150 ± 5 mm. The gyratory compaction samples were prepared using the compaction procedure designated in AASHTO TP4 (AASHTO 1995). The gyratory compaction samples were compacted to the number of gyration cycles specified at N_{ini}, N_{des} and N_{max} of 8, 96 and 152 gyrations, respectively. As required to meet the requirements of high air temperature and estimated traffic loading of the Radisson SPS-9A test site. Detailed data from the volumetric property evaluation from each gyratory compacted specimen is presented in Appendix B.

3.3.1 SHRP Superpave™ Voids in the Total Mix (VTM)

Table 3.23 summarizes the average SHRP Superpave™ VTM and the respective coefficient of variation across the three repeat gyratory compaction samples at the specified N_{ini}, N_{des} and N_{max} number of gyrations respectively for all the seven Radisson SPS-9A test sections and gyratory angles of 1.25°, 2.00° and 2.75°. Figure 3.7 to Figure 3.9 illustrate the average SHRP Superpave™ VTM with respect to varied gyratory angle of 1.25°, 2.00° and 2.75° at N_{ini}, N_{des} and N_{max} number of gyrations across each Radisson SPS-9A test sections. The error bars displayed in Figure 3.7 to Figure 3.9 represent ± two standard deviation from the mean of the three repeat samples at each angle of gyration for all the Radisson SPS-9A test sections.

The gyratory compactor samples showed a trend of decreasing VTM with increasing angle of gyration for all the Radisson SPS-9A test sections at N_{ini}, N_{des} and N_{max} number of gyrations. The decrease in the VTM with increasing angle of gyration would be as a result of a corresponding increase in gyratory shear action. The increase in gyratory shear action results in the asphalt binder being pushed into the asphalt-aggregate matrix and the voids in the mineral aggregates. It should be noted that the average VTM for each Radisson SPS-9A test section is lower at N_{max} relative to N_{des} and was observed to be lower at N_{des} than N_{ini} as expected.

The average VTM of all the Superpave™ mixes were slightly higher than the upper limits of the SMHI air void criteria at N_{des} for all the angles of gyration. Only Superpave™ mix design test section 902S meet the SMHI air void criteria at N_{des} for 2.75° the angle of gyration. However, it was observed that the conventional SMHI Marshall mixes, test sections 901M and 961M, generally yield lower VTM relative to the Superpave™ mixes. Test section 901M did not meet the SMHI air void criteria at N_{des} for 2.00° and 2.75° angles of gyration.

The average VTM of all Superpave™ mixes were slightly high and did not meet the SMHI air void criteria at N_{max} for 1.25° angle of gyration. However, it should be noted that all the Superpave™ mix design test sections meet the SMHI air void criteria at N_{max} for 2.00° angle of gyration. Only test sections 902S and 959S did not meet the SMHI air void criteria at N_{max} for 2.75° angle of gyration. It should be noted that test section 901M did not meet the SMHI air void criteria at N_{max} for all angles of gyration. Test section 961M meet the SMHI air void criteria at N_{max} only for 1.25° angle of gyration.

Table 3.23 Superpave™ Gyratory Compacted Voids in Total Mix at $N_{initial}$, N_{design} and $N_{maximum}$ across Radisson SPS-9A Asphalt mixes

Test Section Number	1.25° Angle of Gyration	Coefficient of Variation (%)	2.00° Angle of Gyration	Coefficient of Variation (%)	2.75° Angle of Gyration	Coefficient of Variation (%)
$N_{initial}$						
901M	10.9	4.8	9.8	4.3	9.1	5.9
961M	12.2	1.1	11.1	2.8	10.8	3.5
903S	17.0	2.0	16.0	4.9	14.8	2.1
959S	17.7	4.8	16.5	3.2	15.7	4.0
960S	17.3	2.7	16.2	2.3	15.3	5.2
902S	15.6	11.3	15.5	4.7	12.4	7.4
962SR	17.0	0.9	15.8	2.2	15.6	3.9
N_{design}						
901M	3.6	15.8	2.8	18.1	2.4	27.8
961M	5.0	4.1	3.9	4.2	3.9	4.8
903S	8.0	4.8	6.3	9.7	5.5	2.2
959S	8.3	11.0	6.3	6.3	5.6	13.9
960S	7.9	5.0	6.6	5.5	5.7	13.1
902S	6.7	28.1	6.3	7.3	4.4	14.4
962SR	7.2	5.4	5.8	5.8	5.6	4.7
$N_{maximum}$						
901M	1.8	5.7	0.8	18.0	0.4	31.9
961M	3.6	4.8	2.4	3.4	2.1	3.9
903S	6.1	5.0	4.0	11.3	3.1	6.7
959S	6.0	5.0	4.0	10.2	2.9	17.8
960S	6.0	5.0	4.0	3.0	3.4	4.0
902S	5.1	8.0	4.0	15.8	2.1	18.3
962SR	5.2	6.9	3.7	13.5	3.1	3.3

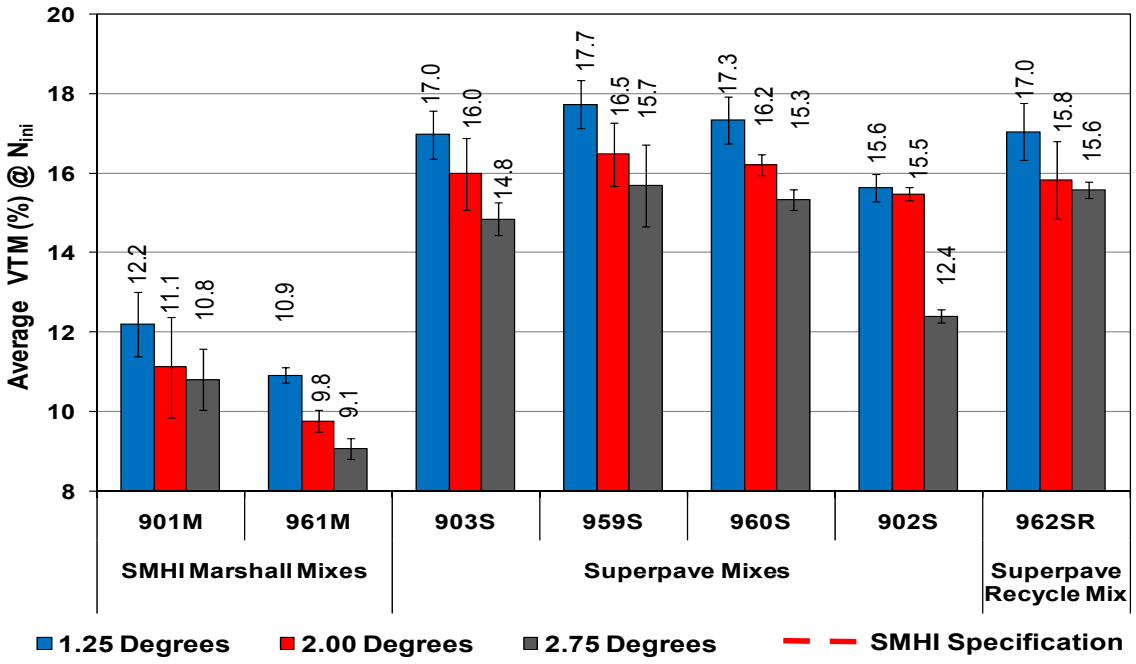

Figure 3.7 Superpave™ Gyratory Compacted Voids in Total Mix at $N_{initial}$ across Radisson SPS-9A Asphalt Mixes (± 2 SD)

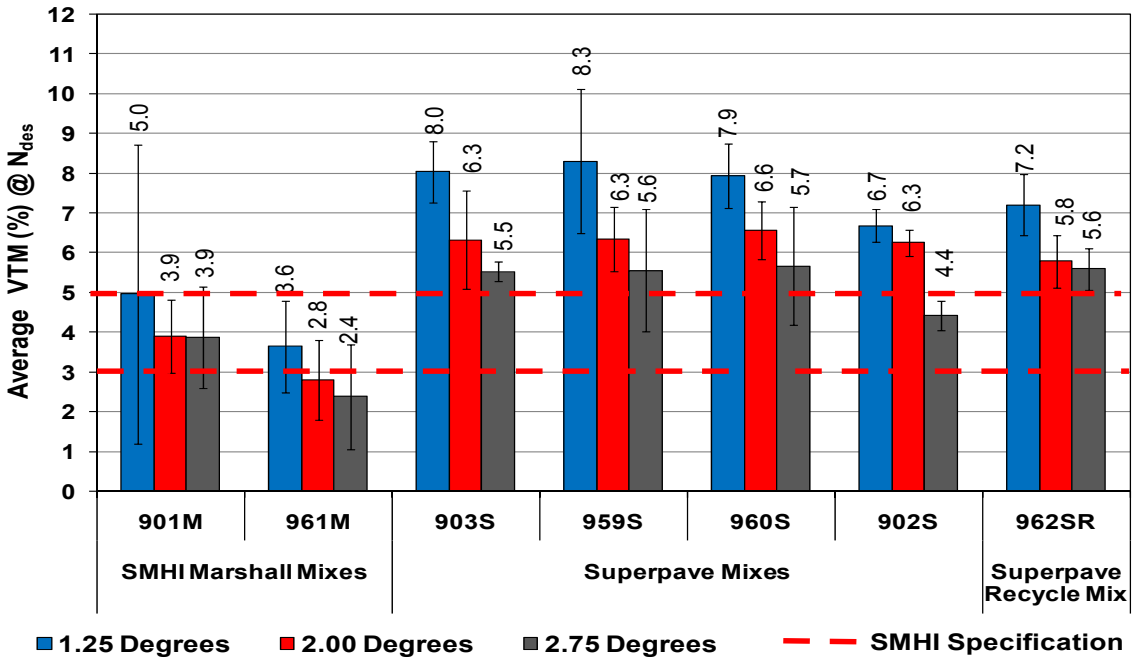

Figure 3.8 Superpave™ Gyratory Compacted Voids in Total Mix at N_{design} across Radisson SPS-9A Asphalt Mixes (± 2 SD)

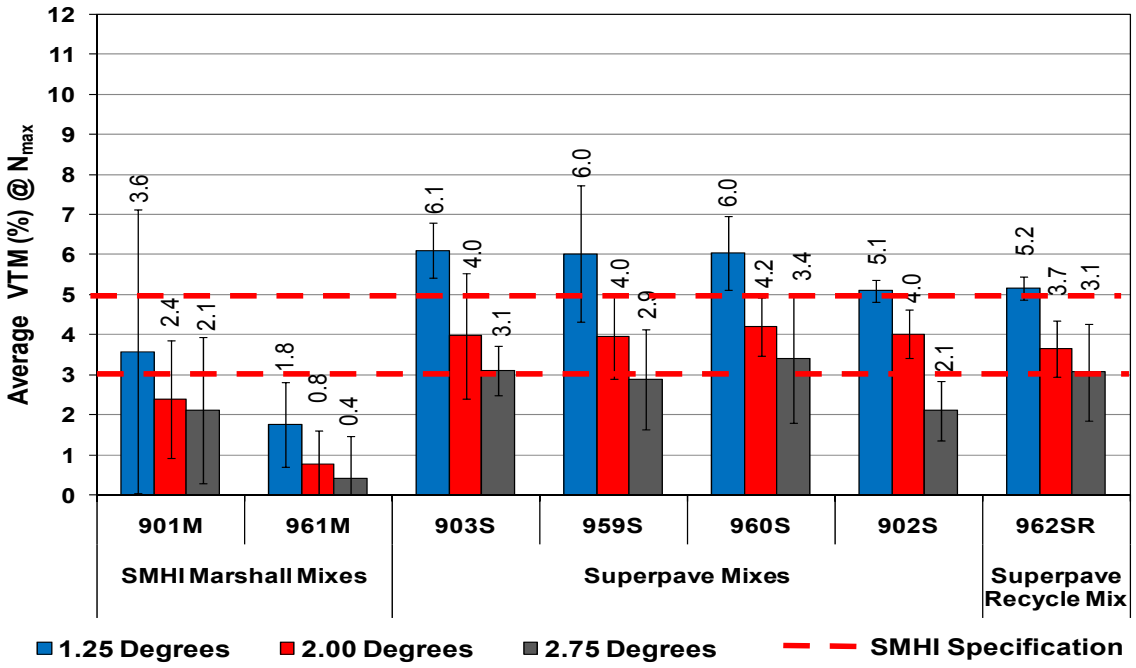

Figure 3.9 Superpave™ Gyratory Compacted Voids in Total Mix at $N_{maximum}$ across Radisson SPS-9A Asphalt Mixes (± 2 SD)

Statistical analysis of variance was conducted on the VTM results of gyratory compacted samples at N_{ini}, N_{des} and N_{max} across 1.25°, 2.00° and 2.75° angles of gyration. Tukey's pairwise comparison was performed where there was significant difference in volumetric properties across angle of gyration.

Tables 3.24, 3.26 and 3.28 summarize analysis of variance of VTM gyratory compacted samples at N_{ini}, N_{des} and N_{max} respectively, and Tables 3.25, 3.27 and 3.29 present the Tukey's groups of VTM for gyratory compacted samples at N_{ini}, N_{des} and N_{max}, respectively across 1.25°, 2.00° and 2.75° angles of gyration. As seen in Tables 3.24, 3.26 and 3.28, significant differences exist in VTM of gyratory compacted samples at N_{ini}, N_{des} and N_{max}.

VTM at 2.00° angle of gyration of the conventional SMHI Marshall mix 961M was similar to VTM at both 1.25° and 2.75° angles of gyration at N_{ini} as seen in Table 3.25. It should be noted that VTM at 1.25° angle of gyration was different compared to VTM at 2.75° angle of gyration across all test sections at N_{ini}.

It should be noted that VTM was different at all angles of gyrations across all test sections at N_{des}, as seen in Table 3.27. Only conventional SMHI Marshall mix 901M was not different at all angles of gyration. VTM at N_{max} was significantly different across the range of angles of gyration across all test sections, as seen in Table 3.29.

Table 3.24 Analysis of Variance for VTM of Gyratory Compacted Samples at $N_{initial}$ across Radisson SPS-9A Mixes

Parameter	Sum of Squares	Degrees of Freedom	Mean Squares	F-Test Statistic	P-value	Sig.
VTM	569	3	28	77		
Angle of Gyration	15918	2	15918	43220	0.000	YES
VTM*Angle of Gyration	518	6	29	78		
Error	21	36	0.4			

Table 3.25 Tukey's Homogeneous Groups for VTM of Gyratory Compacted Samples at $N_{initial}$ across Radisson SPS-9A Mixes

Test Section	Gyratory Angle (°)	VTM @ $N_{initial}$ (%)	Tukey's Homogeneous Groups	
901M	1.25	10.9	A	
	2.00	9.8	A	B
	2.75	9.1		B
961M	1.25	12.2	A	
	2.00	11.1		B
	2.75	10.8		B
903S	1.25	17.0	A	
	2.00	16.0	A	
	2.75	14.8		B
959S	1.25	17.7	A	
	2.00	16.5	A	B
	2.75	15.7		B
960S	1.25	17.3	A	
	2.00	16.2	A	
	2.75	15.3		B
902S	1.25	15.6	A	
	2.00	15.5	A	
	2.75	12.4		B
962SR	1.25	17.0	A	
	2.00	15.8		B
	2.75	15.6		B

Table 3.26 Analysis of Variance for VTM of Gyratory Compacted Samples at N_{design} across Radisson SPS-9A Mixes

Parameter	Sum of Squares	Degrees of Freedom	Mean Squares	F-Test Statistic	P-value	Sig.
VTM	210	3	10	31		
Angle of Gyration	2393	2	2393	7014	0.000	YES
VTM*Angle of Gyration	160	6	9	26		
Error	20	36	0.3			

Table 3.27 Tukey's Homogeneous Groups for VTM of Gyratory Compacted Samples at N_{design} across Radisson SPS-9A Mixes

Test Section	Gyratory Angle (°)	VTM @ N_{design} (%)	Tukey's Homogeneous Groups		
901M	1.25	3.6	A		
	2.00	2.8	A		
	2.75	2.4	A		
961M	1.25	5.0	A		
	2.00	3.9		B	
	2.75	3.9		B	
903S	1.25	8.0	A		
	2.00	6.3		B	
	2.75	5.5			C
959S	1.25	8.3	A		
	2.00	6.3		B	
	2.75	5.6			C
960S	1.25	7.9	A		
	2.00	6.6		B	
	2.75	5.7			C
902S	1.25	6.7	A		
	2.00	6.3		B	
	2.75	4.4		B	C
962SR	1.25	7.2	A		
	2.00	5.8		B	
	2.75	5.6		B	C

Table 3.28 Analysis of Variance for VTM of Gyratory Compacted Samples at $N_{maximum}$ across Radisson SPS-9A Mixes

Parameter	Sum of Squares	Degrees of Freedom	Mean Squares	F-Test Statistic	P-value	Sig.
VTM	203	3	10	115		
Angle of Gyration	954	2	954	10841	0.000	YES
VTM*Angle of Gyration	128	6	7	81		
Error	5	36	0.1			

Table 3.29 Tukey's Homogeneous Groups for VTM of Gyratory Compacted Samples at $N_{maximum}$ across Radisson SPS-9A Mixes

Test Section	Gyratory Angle (°)	VTM @ $N_{maximum}$ (%)	Tukey's Homogeneous Groups		
901M	1.25	1.8	A		
	2.00	0.8		B	
	2.75	0.4			C
961M	1.25	3.6	A		
	2.00	2.4		B	
	2.75	2.1			C
903S	1.25	6.1	A		
	2.00	4.0		B	
	2.75	3.1			C
959S	1.25	6.0	A		
	2.00	4.0		B	
	2.75	2.9			C
960S	1.25	6.0	A		
	2.00	4.2		B	
	2.75	3.4			C
902S	1.25	5.1	A		
	2.00	4.0		B	
	2.75	2.1			C
962SR	1.25	5.2	A		
	2.00	3.7		B	
	2.75	3.1			C

3.3.2 SHRP Superpave™ Voids in the Mineral Aggregates (VMA)

Table 3.30 summarizes the average SHRP Superpave™ VMA and the respective coefficient of variation across the three repeat gyratory compaction samples at the specified N_{ini}, N_{des} and N_{max} number of gyrations respectively for all the seven Radisson SPS-9A test sections and gyratory angles of 1.25°, 2.00° and 2.75°. Figure 3.10 to Figure 3.12 illustrate the average SHRP Superpave™ VMA with respect to varied gyratory angle of 1.25°, 2.00° and 2.75° at N_{ini}, N_{des} and N_{max} number of gyrations across each Radisson SPS-9A test sections. The error bars displayed in Figure 3.10 to Figure 3.12 represent ± two standard deviation from the mean of the three repeat samples at each angle of gyration for all the Radisson SPS-9A test sections.

The gyratory compactor specimens showed a trend of decreasing VMA at N_{ini}, N_{des} and N_{max} number of gyrations with increasing angle of gyration across all test

sections. The decrease in VMA with increasing angle of gyratory would be due to increase in the gyratory shear effort resulting from the increase in the angle of gyration. More asphalt binder is compacted into the permeable voids of the mineral aggregates resulting in the decrease in VMA that have been observed.

The VMA for each test section was found to be lower at N_{ini} relative VMA at N_{des} and was observed to be lower at N_{des} than $N_{max.}$ The trend would be expected because the hot-mix asphalt specimen would have been subjected to more gyrations at N_{des} and N_{max} and more compactive effort which will result in more binder getting into the permeable voids in the mineral aggregates.

The average VMA at N_{ini}, for all the Radisson SPS-9A test sections were slightly higher than the upper limits of the SMHI VMA criteria for all angles of gyration. It was observed that SMHI conventional Marshall mix design test sections all meet the SMHI VMA criteria at N_{des} for all angles of gyration except section 961M at 1.25° angle of gyration with VMA value of 16.2 percent. With regards to Superpave™ mix design test sections, only test sections 902S and 962SR meet the SMHI VMA criteria at gyratory angles of 2.75° with VMA values of 14.9 percent and 15.4 percent respectively.

The SMHI conventional Marshall mix design test section 901M did not meet the SMHI VMA criteria at N_{max} for all angles of gyration. However, conventional SMHI Marshall mix design test section 961M meets the SMHI VMA criteria at N_{max} for all angles of gyration. With regards to the Superpave™ mix design test sections, only test sections 902S and 962SR meet the SMHI VMA criteria at gyratory angles of 1.25° with VMA values of 15.5 percent and 15.1 percent respectively. It should be noted that all the Superpave™ mix design test sections meet the SMHI VMA criteria at N_{max} for 2.00° angle of gyration. Within the Superpave™ mix design test sections, only test sections 902S and 962SR did not meet the SMHI VMA criteria with lower VMA values of 12.8 percent and 13.2 percent respectively.

Table 3.30 Superpave™ Gyratory Compacted Voids in Mineral Aggregates at $N_{initial}$, N_{design} and $N_{maximum}$ across Radisson SPS-9A Asphalt mixes

Test Section Number	1.25° Angle of Gyration	Coefficient of Variation (%)	2.00° Angle of Gyration	Coefficient of Variation (%)	2.75° Angle of Gyration	Coefficient of Variation (%)
$N_{initial}$						
901M	21.5	2.2	20.5	1.8	19.9	2.4
961M	22.6	0.5	21.7	1.3	21.4	1.5
903S	26.3	1.2	25.5	2.7	24.4	1.1
959S	27.2	2.8	26.0	1.8	25.4	2.2
960S	26.5	1.6	25.5	1.3	24.7	2.9
902S	24.9	6.3	24.8	2.6	22.0	3.7
962SR	25.7	0.5	24.6	1.3	24.4	2.2
N_{design}						
901M	15.1	3.4	14.3	3.1	13.9	4.2
961M	16.2	1.1	15.3	1.0	15.3	1.1
903S	18.4	1.9	16.9	3.2	16.2	0.7
959S	18.8	4.3	17.1	2.1	16.4	4.2
960S	18.1	2.0	16.9	1.9	16.0	4.1
902S	16.9	9.9	16.5	2.5	14.1	3.8
962SR	16.9	2.1	15.6	1.9	15.4	1.5
$N_{maximum}$						
901M	13.4	0.7	12.5	1.0	12.2	0.9
961M	15.0	1.0	13.9	0.5	13.7	0.5
903S	16.7	1.6	14.8	2.7	14.0	1.3
959S	16.8	1.6	14.9	2.4	14.0	3.2
960S	16.4	1.6	14.8	0.8	14.1	0.9
902S	15.5	2.3	14.5	3.9	12.8	0.7
962SR	15.1	2.1	13.7	3.2	13.2	0.7

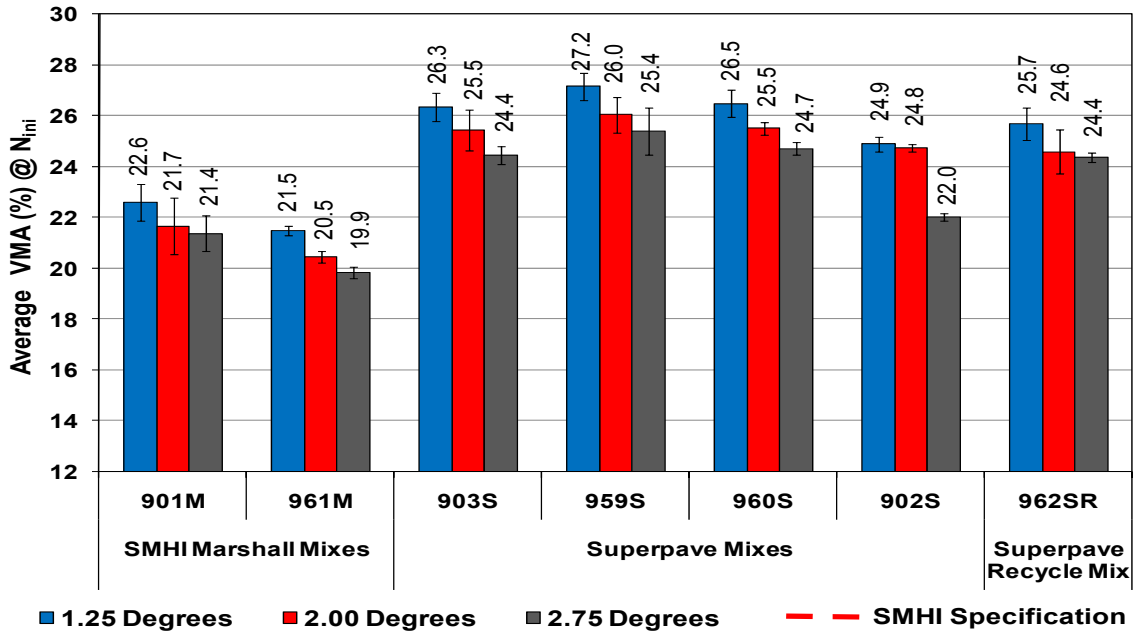

Figure 3.10 Superpave™ Gyratory Compacted Voids in Mineral Aggregates at $N_{initial}$ across Radisson SPS-9A Asphalt Mixes (± 2 SD)

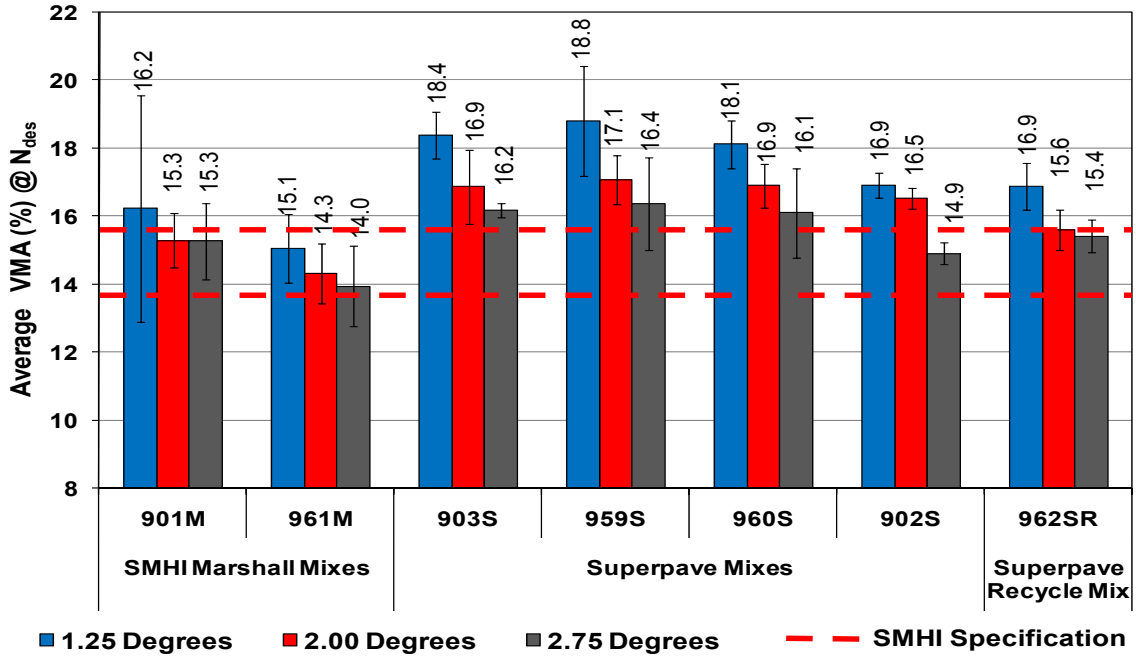

Figure 3.11 Superpave™ Gyratory Compacted Voids in Mineral Aggregates at N_{design} across Radisson SPS-9A Asphalt Mixes (± 2 SD)

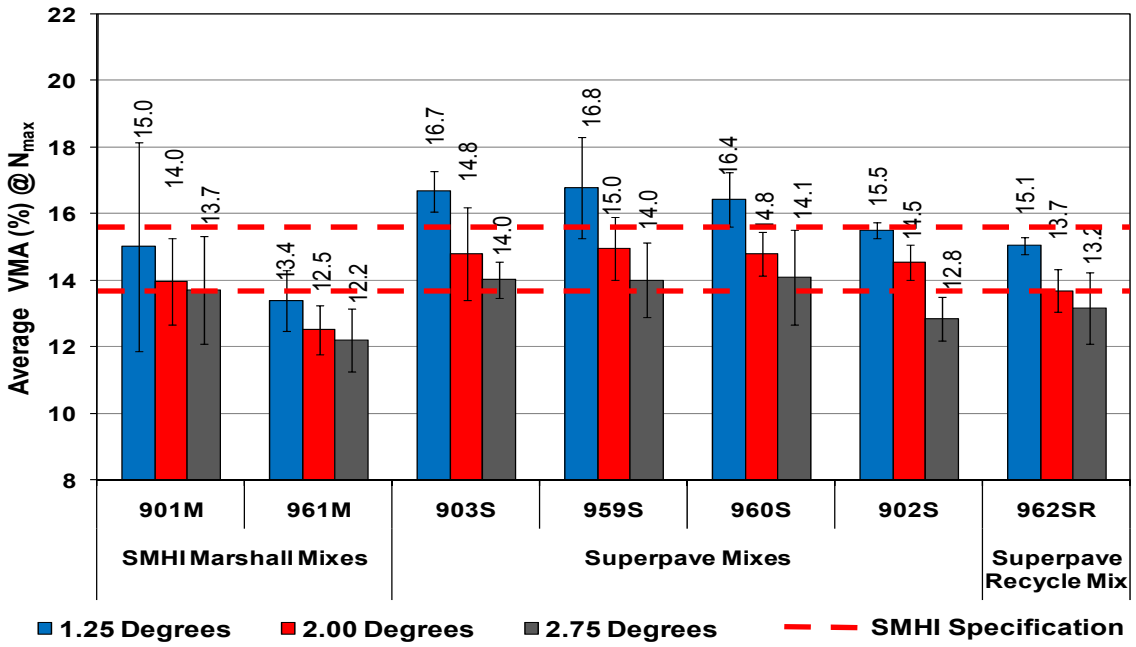

Figure 3.12 Superpave™ Gyratory Compacted Voids in Mineral Aggregates at $N_{maximum}$ across Radisson SPS-9A Asphalt Mixes (± 2 SD)

Based on the VMA results observed across the mix compaction efforts, it was observed that all mixes showed a decrease in VMA with respect to increasing compactive effort. In addition, it was observed that the SMHI dense graded mixes yielded a significantly lower VMA across all compactive efforts relative to the Superpave™ mixes.

Statistical analysis of variance was conducted on the VMA results of gyratory compacted samples at N_{ini}, N_{des} and N_{max} across 1.25°, 2.00° and 2.75° angles of gyration. Tukey's pairwise comparison was performed where there was significant difference in volumetric properties across angle of gyration.

Tables 3.31, 3.33 and 3.35 summarize analysis of variance of VMA gyratory compacted samples at N_{ini}, N_{des} and N_{max} respectively, and Tables 3.32, 3.34 and 3.36 present the Tukey's groups of VMA results for gyratory compacted samples at N_{ini}, N_{des} and N_{max}, respectively across 1.25°, 2.00° and 2.75° angles of gyration. As seen in Tables 3.31, 3.33 and 3.35, significant differences exist in VMA results of gyratory compacted samples at N_{ini}, N_{des} and N_{max}.

VMA was found to be significantly different at 1.25° angle of gyration compared to 2.00° and 2.75° angles of gyration for conventional SMHI test sections 901M and 961M at N_{ini}, as seen in Table 3.32. Similarly, Superpave™ recycle mix 962SR displayed VMA significantly different at 1.25° angle of gyration compared to 2.00° and 2.75° angles of gyration at N_{ini}. VMA was similar at 1.25° and 2.00° angles of gyration but different when compared to VMA at 2.75° angle of gyration for Superpave™ mix design test sections 960S and 902S. It was also noted that Superpave™ mix design test section 903S have VMA different at all three angles of gyration at N_{ini}, as seen in Table 3.32.

Conventional SMHI test sections 901M and 961M and Superpave™ recycle mix design test section 962SR have VMA significantly different at 1.25° angle of gyration compared to 2.00° and 2.75° angles of gyration at N_{des}, as seen in Table 3.34. Superpave™ mix design test sections 903S and 902S displayed VMA similar at 1.25° and 2.00° angles of gyration but different when compared to VMA at 2.75° angle of gyration N_{des}. It should be noted that VMA for Superpave™ mix design test sections 959S and 960S at 2.00° angle of gyration was similar to VMA at both 1.25° and 2.75° angles of gyration at N_{des}, as seen in Table 3.34.

VMA at N_{max} was found to be significantly different at all angles of gyration across all test sections except Superpave™ recycle mix design test section 962SR with VMA significantly different at 1.25° angle of gyration compared to 2.00° and 2.75° angles of gyration at N_{max}, as seen in Table 3.36.

Table 3.31 Analysis of Variance for VMA of Gyratory Compacted Samples at $N_{initial}$ across Radisson SPS-9A Mixes

Parameter	Sum of Squares	Degrees of Freedom	Mean Squares	F-Test Statistic	P-value	Sig.
VMA	383	3	19	67	0.000	YES
Angle of Gyration	44899	2	44899	156152		
VMA*Angle of Gyration	342	6	19	66		
Error	16	36	0.3			

Table 3.32 Tukey's Homogeneous Groups for VMA of Gyratory Compacted Samples at $N_{initial}$ across Radisson SPS-9A Mixes

Test Section	Gyratory Angle (°)	VMA @ $N_{initial}$ (%)	Tukey's Homogeneous Groups		
901M	1.25	21.5	A		
	2.00	20.5		B	C
	2.75	19.9		B	C
961M	1.25	22.6	A		
	2.00	21.7		B	C
	2.75	21.4		B	C
903S	1.25	26.3	A		
	2.00	25.5		B	
	2.75	24.4			C
959S	1.25	27.2	A		
	2.00	26.0	A	B	C
	2.75	25.4		B	C
960S	1.25	26.5	A	B	
	2.00	25.5	A	B	
	2.75	24.7			C
902S	1.25	24.9	A	B	
	2.00	24.8	A	B	
	2.75	22.0			C
962SR	1.25	25.7	A		
	2.00	24.6		B	
	2.75	24.4		B	C

Table 3.33 Analysis of Variance for VMA of Gyratory Compacted Samples at N_{design} across Radisson SPS-9A Mixes

Parameter	Sum of Squares	Degrees of Freedom	Mean Squares	F-Test Statistic	P-value	Sig.
VMA	383	3	19	67		
Angle of Gyration	44925	2	44925	156940	0.000	YES
VMA*Angle of Gyration	345	6	19	67		
Error	16	36	0.3			

Table 3.34 Tukey's Homogeneous Groups for VMA of Gyratory Compacted Samples at N_{design} across Radisson SPS-9A Mixes

Test Section	Gyratory Angle (°)	VMA @ N_{design} (%)	Tukey's Homogeneous Groups		
901M	1.25	15.1	A		
	2.00	14.3			B
	2.75	14.0			B
961M	1.25	16.2	A		
	2.00	15.3			B
	2.75	15.3			B
903S	1.25	18.4	A		
	2.00	16.9	A		
	2.75	16.2			B
959S	1.25	18.8	A		
	2.00	17.1	A		B
	2.75	16.4			B
960S	1.25	18.1	A		
	2.00	16.9	A		B
	2.75	16.1			B
902S	1.25	16.9	A		
	2.00	16.5	A		
	2.75	14.9			B
962SR	1.25	16.9	A		
	2.00	15.6			B
	2.75	15.4			B

Table 3.35 Analysis of Variance for VMA of Gyratory Compacted Samples at $N_{maximum}$ across Radisson SPS-9A Mixes

Parameter	Sum of Squares	Degrees of Freedom	Mean Squares	F-Test Statistic	P-value	Sig.
VMA	123	3	6	89		
Angle of Gyration	15879	2	15879	232120	0.000	YES
VMA*Angle of Gyration	65	6	4	52		
Error	4	36	0.7			

Table 3.36 Tukey's Homogeneous Groups for VMA of Gyratory Compacted Samples at $N_{maximum}$ across Radisson SPS-9A Mixes

Test Section	Gyratory Angle (°)	VMA @ $N_{maximum}$ (%)	Tukey's Homogeneous Groups		
901M	1.25	13.4	A		
	2.00	12.5		B	
	2.75	12.2			C
961M	1.25	15.0	A		
	2.00	14.0		B	
	2.75	13.7			C
903S	1.25	16.7	A		
	2.00	14.8		B	
	2.75	14.0			C
959S	1.25	16.8	A		
	2.00	15.0		B	
	2.75	14.0			C
960S	1.25	16.4	A		
	2.00	14.8		B	
	2.75	14.1			C
902S	1.25	15.5	A		
	2.00	14.5		B	
	2.75	12.8			C
962SR	1.25	15.1	A		
	2.00	13.7		B	C
	2.75	13.2		B	C

3.3.3 SHRP Superpave™ Voids Filled with Asphalt (VFA)

Table 3.37 summarizes the average Superpave™ VFA and the respective coefficient of variation across the three repeat gyratory compaction samples at the specified N_{ini}, N_{des} and N_{max} number of gyrations respectively for all the seven Radisson SPS-9A test sections and gyratory angles of 1.25°, 2.00° and 2.75°. Figure 3.13 to Figure 3.15 illustrate the average Superpave™ VFA with respect to varied gyratory angle of 1.25°, 2.00° and 2.75° at N_{ini}, N_{des} and N_{max} number of gyrations across each Radisson SPS-9A test sections. The error bars displayed in Figure 3.13 to Figure 3.15 represent ± two standard deviation from the mean of the three repeat samples at each angle of gyration for all the Radisson SPS-9A test sections.

The gyratory compactor specimens showed a trend of increasing VFA at N_{ini}, N_{des} and N_{max} number of gyrations with increasing angle of gyration across all test sections. The increase in VFA with increasing angle of gyratory would be due to increase in the gyratory shear effort resulting from the increase in the angle of gyration. More asphalt binder is compacted into the permeable voids in the mineral aggregates and the asphalt-aggregates matrix.

The VMA for each test section was found to be lower at N_{ini} relative to VMA at N_{des} and was observed to be lower at N_{des} than $N_{max.}$ The trend would be expected because the hot-mix asphalt specimen would have been subjected to more gyrations at N_{des} and N_{max} and more compactive effort which will result in more binder getting into the permeable voids in the mineral aggregates and the asphalt-aggregates matrix.

It was observed that the average VFA at N_{ini} were low and did not meet the SMHI VFA criteria at all three angles of gyration for all the Radisson SPS-9A test sections. It should be noted that only conventional SMHI Marshall mix design test section 901M meets the SMHI VFA criteria at 1.25° angle of gyration at N_{des}. It was also observed that conventional SMHI Marshall mix design test section 961M meets the SMHI VFA criteria at N_{des} for all angles of gyrations. The higher VFA values could be due to the fine nature of the SMHI conventional Marshall mixes which makes the mix more workable and allows more asphalt binder to be forced into the voids in the asphalt-aggregate matrix. The Superpave^{TM} mix design test sections did not meet the SMHI VFA criteria at for 1.25° and 2.00° angles of gyration. Within the Superpave^{TM} mix design test sections, only test section 962SR did not meet the SMHI VFA criteria at N_{des} for 2.75° angle of gyration with a VFA value of 63.8 percent.

The conventional SMHI Marshall mix design test section 901M has high VFA values and did not meet the SMHI VFA criteria. However, conventional SMHI Marshall mix design test section 961M meets the SMHI VFA criteria at N_{max} for 1.25° angle of gyration with average VFA value of 76.2 percent. Within the Superpave^{TM} mix design test sections it was noted that only test section 902S and 962SR meet the SMHI VFA criteria N_{max} for 1.25° angle of gyration with average VFA values of 67.2 percent

and 65.7 percent respectively. All the Superpave™ mix design test sections meet the SMHI VFA criteria at N_{max} and 2.00° angle of gyration. It was observed that Superpave™ mix design test sections 902S and 959S did not meet the SMHI VFA criteria at N_{max} for 2.75° angle of gyration with average VFA values of 83.7 percent and 79.5 percent respectively.

Table 3.37 Superpave™ Gyratory Compacted Voids Filled with Asphalt at $N_{initial}$, N_{design} and $N_{maximum}$ across Radisson SPS-9A Asphalt Mixes

Test Section Number	1.25° Angle of Gyration	Coefficient of Variation (%)	2.00° Angle of Gyration	Coefficient of Variation (%)	2.75° Angle of Gyration	Coefficient of Variation (%)
$N_{initial}$						
901M	49.2	2.7	52.3	2.3	54.3	3.0
961M	46.0	0.7	48.7	1.6	49.5	1.9
903S	35.6	1.6	37.3	3.7	39.3	1.5
959S	34.8	3.8	36.8	2.4	38.1	2.9
960S	34.6	2.1	36.4	1.7	38.0	3.8
902S	37.3	8.7	37.5	3.5	43.7	4.7
962SR	33.7	0.7	35.7	1.7	36.1	3.0
N_{design}						
901M	75.9	4.0	80.6	3.7	83.0	4.8
961M	69.4	1.3	74.5	1.1	74.6	1.3
903S	56.4	2.2	62.6	3.4	65.8	0.8
959S	55.9	5.1	62.9	2.5	66.2	4.9
960S	56.3	2.4	61.2	2.3	64.9	4.9
902S	61.0	12.4	62.2	2.9	70.4	4.4
962SR	57.3	2.5	62.9	2.3	63.8	1.8
$N_{maximum}$						
901M	86.9	0.8	93.9	1.1	96.7	1.1
961M	76.2	1.2	82.9	0.6	84.6	0.6
903S	63.5	2.0	73.2	3.1	77.9	1.5
959S	64.2	1.9	73.6	2.8	79.5	3.8
960S	63.3	1.9	71.6	0.9	75.9	0.9
902S	67.2	2.7	72.5	4.6	83.7	3.0
962SR	65.7	2.5	73.4	3.7	76.8	0.8

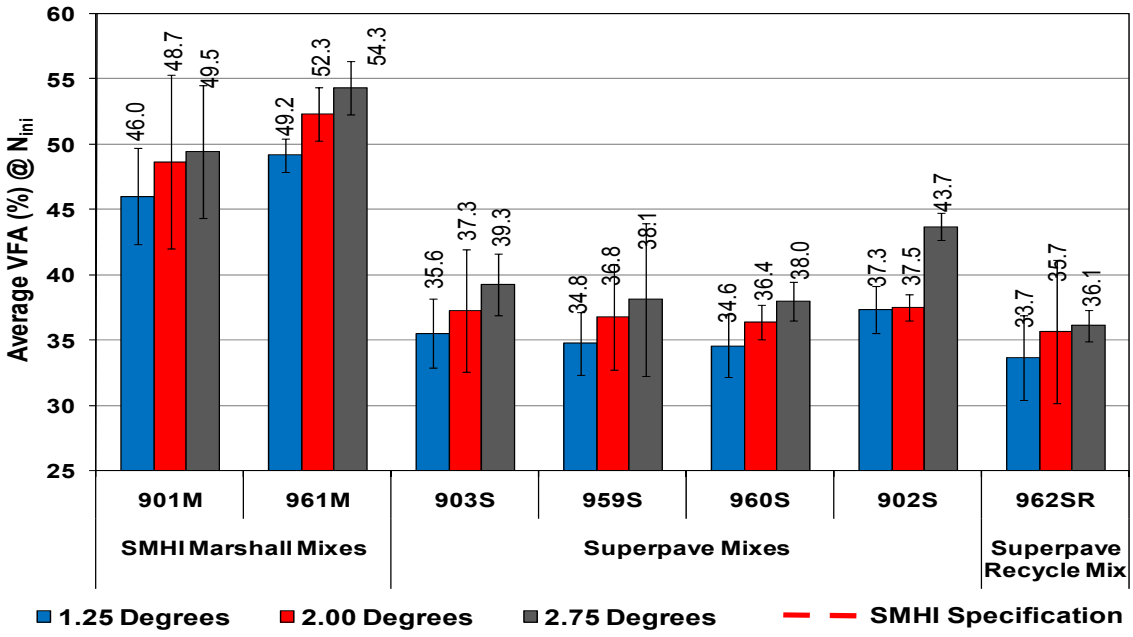

Figure 3.13 Superpave™ Gyratory Compacted Voids Filled with Asphalt at $N_{initial}$ across Radisson SPS-9A Asphalt Mixes (± 2 SD)

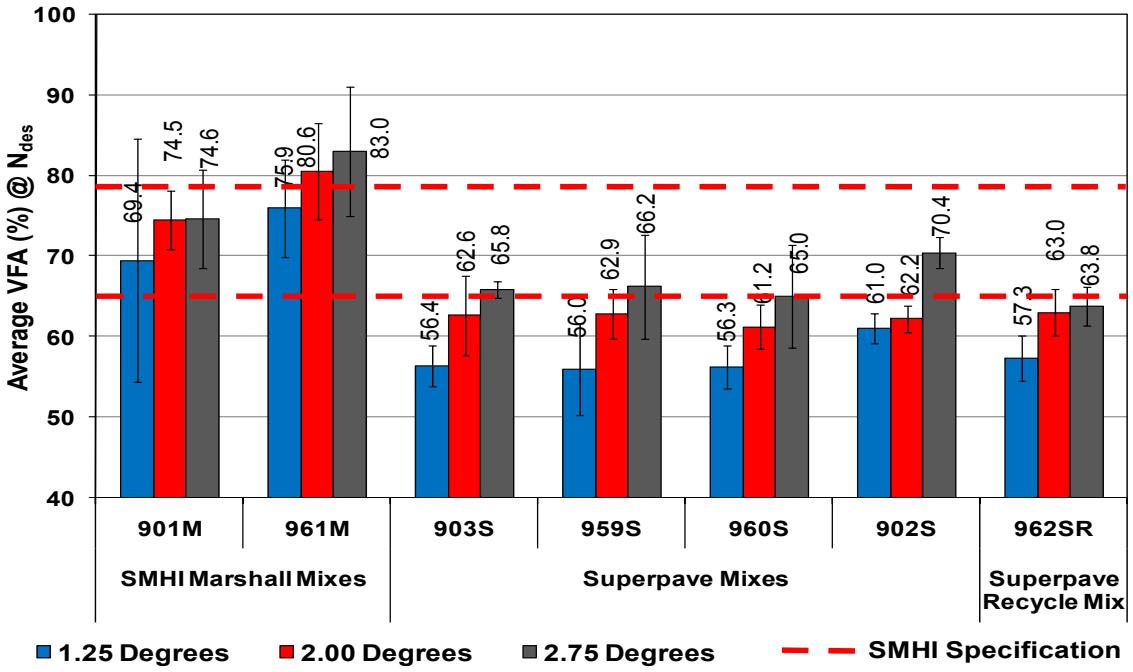

Figure 3.14 Superpave™ Gyratory Compacted Voids Filled with Asphalt at N_{design} across Radisson SPS-9A Asphalt Mixes (± 2 SD)

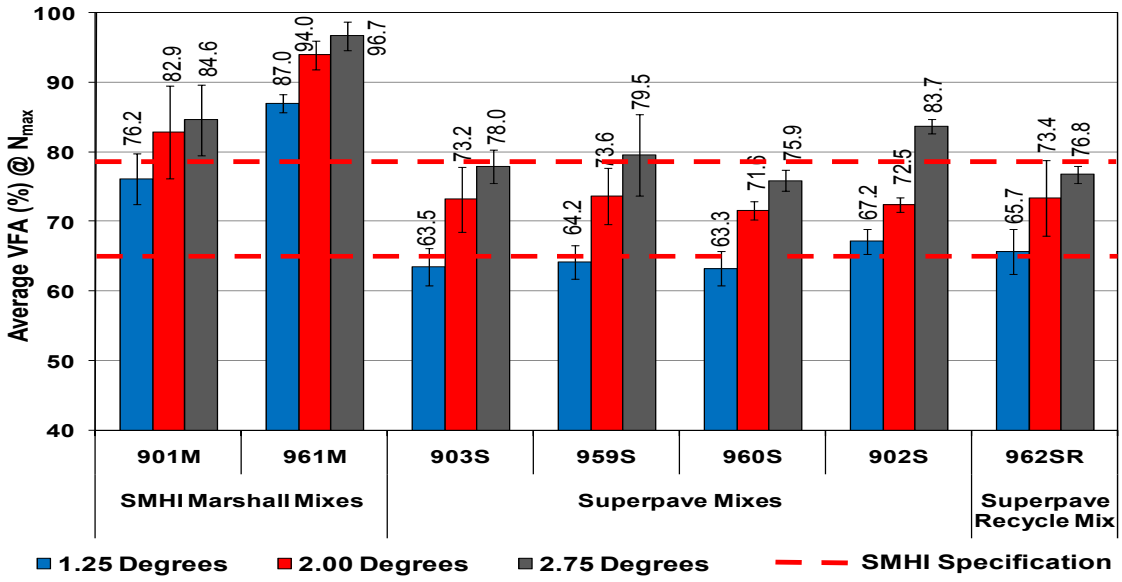

Figure 3.15 Superpave™ Gyratory Compacted Voids Filled with Asphalt at $N_{maximum}$ across Radisson SPS-9A Asphalt Mixes

Based on the VFA results observed across the mix compaction efforts, it was observed that all mixes showed an increase in VFA with respect to increasing compactive effort. In addition, it was observed that the SMHI dense graded mixes yielded a significantly higher VFA across all compactive efforts relative to the Superpave™ mixes.

Statistical analysis of variance was conducted on the VFA results of gyratory compacted samples at N_{ini}, N_{des} and N_{max} across 1.25°, 2.00° and 2.75° angles of gyration. Tukey's pairwise comparison was performed where there was significant difference in volumetric properties across angle of gyration.

Tables 3.38, 3.40 and 3.42 summarize analysis of variance of VFA results gyratory compacted samples at N_{ini}, N_{des} and N_{max} respectively, and Tables 3.39, 3.41 and 3.43 present the Tukey's groups of VFA results for gyratory compacted samples at N_{ini}, N_{des} and N_{max}, respectively across 1.25°, 2.00° and 2.75° angles of gyration. As seen in Tables 3.38, 3.40 and 3.42, significant differences exist in VMA results of gyratory compacted samples at N_{ini}, N_{des} and N_{max}.

VFA was significantly different at 1.25° angle of gyration compared to 2.00° and 2.75° angles of gyration at N_{ini} for test sections 961M, 960S and 962SR, as seen in Table 3.39. Superpave^{TM} mix design test sections 903S and 902S displayed VFA similar at 1.25° and 2.00° angles of gyration but different when compared to VFA at 2.75° angle of gyration N_{ini}. It should be noted that VFA for Superpave^{TM} mix design test section 959S and conventional SMHI mix test section 901M at 2.00° angle of gyration was similar to VFA at both 1.25° and 2.75° angles of gyration at N_{ini}, as seen in Table 3.39.

Superpave^{TM} mix design test sections 903S, 959S and 960S displayed VFA significantly different at all three angles of gyration at N_{des}, as seen in Table 3.41. VFA was significantly different at 1.25° angle of gyration compared to 2.00° and 2.75° angles of gyration at N_{des} for test sections 902S and 962SR.

VFA at N_{max} was found to be significantly different at all angles of gyration across all test sections except Superpave^{TM} recycle mix design test section 962SR with VFA significantly different at 1.25° angle of gyration compared to 2.00° and 2.75° angles of gyration at N_{max}, as seen in Table 3.43.

Table 3.38 Analysis of Variance for VFA of Gyratory Compacted Samples at $N_{initial}$ across Radisson SPS-9A Mixes

Parameter	Sum of Squares	Degrees of Freedom	Mean Squares	F-Test Statistic	P-value	Sig.
VFA	3073	3	154	108	0.000	YES
Angle of Gyration	129154	2	129154	90617		
VFA*Angle of Gyration	2871	6	159	112		
Error	81	36	1			

Table 3.39 Tukey's Homogeneous Groups for VFA of Gyratory Compacted Samples at $N_{initial}$ across Radisson SPS-9A Mixes

Test Section	Gyratory Angle (°)	VFA @ $N_{initial}$ (%)	Tukey's Homogeneous Groups	
901M	1.25	49.2	A	
	2.00	52.3	A	B
	2.75	54.3		B
961M	1.25	46.0	A	
	2.00	48.7		B
	2.75	49.5		B
903S	1.25	35.6	A	
	2.00	37.3	A	
	2.75	39.3		B
959S	1.25	34.8	A	
	2.00	36.8	A	B
	2.75	38.1		B
960S	1.25	34.6	A	
	2.00	36.4		B
	2.75	38.0		B
902S	1.25	37.3	A	
	2.00	37.5	A	
	2.75	43.7		B
962SR	1.25	33.7	A	
	2.00	35.7		B
	2.75	36.1		B

Table 3.40 Analysis of Variance for VFA of Gyratory Compacted Samples at N_{design} across Radisson SPS-9A Mixes

Parameter	Sum of Squares	Degrees of Freedom	Mean Squares	F-Test Statistic	P-value	Sig.
VFA	2031	3	101	27		
Angle of Gyration	459368	2	459368	119968	0.000	YES
VFA*Angle of Gyration	1516	6	84	22		
Error	218	36	3			

Table 3.41 Tukey's Homogeneous Groups for VFA of Gyratory Compacted Samples at N_{design} across Radisson SPS-9A Mixes

Test Section	Gyratory Angle (°)	VFA @ N_{design} (%)	Tukey's Homogeneous Groups		
901M	1.25	75.9	A	B	
	2.00	80.6		B	C
	2.75	83.0			C
961M	1.25	61.0	A	B	
	2.00	62.2			
	2.75	70.4			C
903S	1.25	56.4	A		
	2.00	62.6		B	
	2.75	65.8			C
959S	1.25	56.0	A		
	2.00	62.9		B	
	2.75	66.2			C
960S	1.25	56.3	A		
	2.00	61.2		B	
	2.75	65.0			C
902S	1.25	69.4	A		
	2.00	74.5		B	C
	2.75	74.6		B	C
962SR	1.25	57.3	A		
	2.00	63.0		B	C
	2.75	63.8		B	C

Table 3.42 Analysis of Variance for VFA of Gyratory Compacted Samples at $N_{maximum}$ across Radisson SPS-9A Mixes

Parameter	Sum of Squares	Degrees of Freedom	Mean Squares	F-Test Statistic	P-value	Sig.
VFA	6797	3	340	145		
Angle of Gyration	447549	2	447549	191167	0.000	YES
VFA*Angle of Gyration	4766	6	265	113		
Error	133	36	2			

Table 3.43 Tukey's Homogeneous Groups for VFA of Gyratory Compacted Samples at $N_{maximum}$ across Radisson SPS-9A Mixes

Test Section	Gyratory Angle (°)	VFA @ $N_{maximum}$ (%)	Tukey's Homogeneous Groups		
901M	1.25	87.0	A		
	2.00	94.0		B	
	2.75	96.7			C
961M	1.25	76.2	A		
	2.00	82.9		B	
	2.75	84.6			C
903S	1.25	63.5	A		
	2.00	73.2		B	
	2.75	78.0			C
959S	1.25	64.2	A		
	2.00	73.6		B	
	2.75	79.5			C
960S	1.25	63.3	A		
	2.00	71.6		B	
	2.75	75.9			C
902S	1.25	67.2	A		
	2.00	72.5		B	
	2.75	83.7			C
962SR	1.25	65.7	A		
	2.00	73.4		B	C
	2.75	76.8		B	C

3.4 Chapter Summary

Chapter three presented the results of laboratory compaction and volumetric property characterization of Radisson SPS-9A asphalt mixes. Marshall and Superpave™ gyratory compaction procedures were employed. Volumetric properties obtained from the laboratory compacted specimen were compared to SMHI mix design specifications.

The average VTM of the Marshall compacted samples were found to be lower at 75-blow Marshall compared to 50-blow Marshall across all the SPS-9A test sections. Only SMHI conventional Marshall mix design test section 961M met the SMHI air voids criteria at 50-blow Marshall with average VTM value of 3.4 percent. It was further observed that of the Radisson SPS-9A mixes that did not meet the SMHI air

voids criteria, the conventional SMHI Marshall mixes were below acceptable VTM limits while the Superpave™ mixes were above acceptable VTM limits. Tukey's pairwise comparison indicated similar VTM values between the conventional SMHI Marshall mix design test sections. The Superpave™ mix design test sections also showed no significant difference in VTM.

The average VMA of the Marshall samples was found to be lower at 75-blow Marshall compared to 50-blow Marshall across all Radisson SPS-9A test sections. It was observed that conventional SMHI Marshall mix design test sections 901M and 961M have lower VMA values at both 50 and 75-blow Marshall relative to Superpave™ mix design test sections. Test sections 901M, 961M and 962SR met the SMHI VMA criteria at 50-blow Marshall with average VMA values of 14.2 percent, 14.6 percent and 15.3 percent. Superpave™ mixes show no significant difference in the VMA at 50 and 75-blow Marshall. It was concluded that VMA is sensitive to the mix design method.

The conventional SMHI Marshall mix design test sections, 901M and 961M, have higher VFA relative to the Superpave™ mix design test sections at both 50 and 75-blow Marshall. It was observed that only test sections 902S and 961M met the SMHI VFA criteria at 50-blow Marshall with average VFA values of 65.2 percent and 76.9 percent respectively. Superpave™ mix design test sections 902S, 903S, 959S and 960S all met the SMHI VFA criteria at 75-blow Marshall. The only difference between the Superpave™ mixes was between test section 962SR with average VFA value 64.6 percent and 902S with average VFA value 70.6 percent. It was conclude that VFA is sensitive to mix design method.

In terms of gyratory compaction, average VTM was found to decrease with an increase in the angle of gyration for all the Radisson SPS-9A test sections at N_{ini}, N_{des} and N_{max}. The VTM was found to be lower at N_{max} relative to N_{des} and was observed to be lower at N_{des} than N_{ini}. It was observed that none of the Radisson SPS-9A test sections meet the SMHI VTM criteria at N_{ini} for all the three angles of gyration. It was noted that only conventional SMHI Marshall mix design test sections 901M and 961M

met the SMHI VTM criteria at N_{des} at 1.25° angle of gyration with average VTM values of 3.6 percent and 5.0 percent respectively. It was further noted that only SMHI conventional Marshall mix design test section 961M met the SMHI VTM criteria at N_{des} at 2.00° angle of gyration with average VTM values of 3.9 percent. Superpave™ mix design test section 902S and conventional SMHI Marshall mix design test sections 901M and 961M were the only test sections that meet the SMHI VTM criteria at 2.75° angle of gyration N_{des} with average VTM values of 4.4 percent and 3.9 percent respectively.

Only conventional SMHI Marshall mix design test section 961M met the SMHI VTM criteria at N_{max} at 1.25° angle of gyration with average VTM values of 3.6 percent. It was observed that only the conventional SMHI Marshall mix design test sections 901M and 961M did not meet the SMHI VTM criteria at N_{max} at 2.00° angle of gyration with average VTM values of 0.8 percent and 2.4 percent respectively. At 2.75° angle of gyration, only Superpave™ mix design test sections 903S, 960S and 962SR met the SMHI VTM criteria at N_{max}.

The average VMA was found to decrease with an increase in the angle of gyration for all the Radisson SPS-9A test sections at N_{ini}, N_{des} and N_{max}. The VMA was found to be lower at N_{ini} relative to N_{des} and was observed to be lower at N_{des} than N_{max}. It was observed that none of the test sections met the SMHI VMA criteria at N_{ini} for the three angles of gyration.

It was observed that only conventional SMHI Marshall mix design test section 901M met the SMHI VMA criteria at N_{des} for 1.25° angle of gyration with average VMA value of 15.1 percent. It was also noted that the conventional SMHI Marshall mix design test sections 901M and 961M met the SMHI VMA criteria at N_{des} for 2.00° angle of gyration with average VMA values of 14.3 percent and 15.3 percent respectively. However, none of the Superpave™ mix design test sections met the SMHI VMA criteria at N_{des} for 2.00° angle of gyration. The Superpave™ mix design test sections 903S, 959S and 960S were the only test sections that did not meet the SMHI

VMA criteria at N_{des} for 2.75° angle of gyration with average VMA values of 16.2 percent, 16.4 percent and 16.1 percent, respectively.

All the Radisson SPS-9A test sections met the SMHI VMA criteria at N_{max} for all angles of gyration except Superpave™ mix design test sections 903S, 959S and 960S with slightly high average VMA values of 16.7 percent, 16.8 percent and 16.4 percent respectively.

The average VFA was found to increase with an increase in the angle of gyration for all the Radisson SPS-9A test sections at N_{ini}, N_{des} and N_{max}. The VFA was found to be lower at N_{ini} relative to N_{des} and was observed to be lower at N_{des} than N_{max}. It was observed that none of the Radisson SPS-9A test sections met the SMHI VFA criteria at N_{ini} for all angles of gyration.

The conventional SMHI Marshall mix design test section 901M met SMHI VFA criteria at N_{des} for 1.25° angle of gyration but failed to meet the SMHI VFA criteria for 2.00° and 2.75° angles of gyration at N_{des}. However, conventional SMHI Marshall mix design test section 961M met SMHI VFA criteria for all angles of gyration at N_{des}. With regards to the Superpave™ mix design test sections, only test section 902S, 903S, 959S and 960S met the SMHI VFA criteria for 2.75° angle of gyration at N_{des} with average VFA values of 70.4 percent, 65.8 percent, 66.2 percent and 65.0 percent.

It was observed that the conventional SMHI Marshall mix design test section 901M did not meet the SMHI VFA criteria for all three angles of gyration at N_{max}. However, the conventional SMHI Marshall mix design test section 961M met the SMHI VFA criteria for 1.25° angle of gyration at N_{max}, with average VFA value of 76.2 percent, but failed for 2.00° and 2.75° angles of gyration.

CHAPTER 4 MECHANICAL PROPERTIES CHARACTERIZATION OF MARSHALL AND GYRATORY COMPACTED SAMPLES

Mechanical characterization of the research mixes involved laboratory and field tests to determine the primary response behavior of the different asphalt mixes used in the Radisson SPS-9A test sections to varying mechanical loading. Marshall Stability and flow tests were employed to determine the resistance of the different Radisson SPS-9A asphalt mixes to permanent deformation (rutting) and viscoplastic flow. Permanent deformation in the field was measured in wheel path across the Radisson SPS-9A test sections.

The effect of varying angle of gyration on mechanistic material properties of the hot-mix asphalt mixes used on the Radisson SPS-9A test sections was investigated using the rapid triaxial tester (RaTT) at the University of Saskatchewan. The rapid triaxial frequency testing has been discussed and presented in detail in Chapter Two. The RaTT has been used successfully for characterizing mechanistic material properties of various road materials including asphalt mixtures and granular materials (Berthelot 1999, Berthelot et al. 1999, Anthony and Berthelot 2003, Baumgartner 2005, Anthony 2007).

4.1 Marshall Stability and Flow Characterization of Radisson SPS-9A Asphalt Mixes

Saskatchewan Ministry of Highway and Infrastructure (SMHI) currently use the Marshall mix design method for hot-mix asphalt design and construction quality control and quality assurance. The basic mechanical properties of hot-mix asphalt designed by the Marshall mix design method are evaluated by the Marshall stability and flow tests (ASTM D 1559, AASHTO T245, SMHI 2001). The results of the Marshall stability and flow tests performed on four repeat samples at 50 and 75-blow Marshall compactive effort for each test section are presented in this section.

4.1.1 Marshall Stability Characterization

Table 4.1 summarizes the average Marshall stability and the respective coefficient of variation across 50 and 75-blow Marshall respectively for all the seven Radisson

SPS-9A test sections. Figure 4.1 illustrates the average Marshall stability across each Radisson SPS-9A test section. The error bars displayed in Figure 4.1 represent ± two standard deviations from the mean of the four repeat samples at each compaction energy of 50 and 75-blow Marshall for all the Radisson SPS-9A test sections. Detailed results of Marshall stability testing are presented in Appendix C.

The average Marshall stability values were generally lower for the samples compacted with 50-blow Marshall compared with samples compacted with 75-blow Marshall. The increase in Marshall stability with increasing number of blows from the Marshall hammer is due to increase in aggregate interlock that results from orientation of the mineral aggregates into a more stable skeleton within the asphalt aggregates matrix.

The average Marshall stability of all the test sections met the SMHI criteria for Marshall stability of 5.0 kN at 50-blow Marshall. There was no visible trend in the stability value. However, Sections 901M, 902S and 960S had the highest stability values. Section 962SR had the lowest stability value of 5.63 kN at 50-blow Marshall. It can be seen in Figure 4.1 that all the section, except Section 962SR, had stability values above the upper limit of the SMHI Marshall stability specification of 7.0 kN. Sections 901M and 902S have the highest Marshall stability values for 75-blow Marshall compaction with Marshall stability values of 8.9 kN and 9.1 kN respectively.

Table 4.1 Marshall Stability at 50 and 75-Blow Marshall Compaction across Radisson SPS-9A Asphalt Mixes

Test Section Number	50-Blow (kN)	Coefficient of Variation (%)	75-Blow (kN)	Coefficient of Variation (%)
901M	6.8	11.4	8.9	8.7
961M	6.8	9.2	7.3	5.1
903S	6.6	5.2	7.4	4.9
959S	6.8	10.5	7.8	5.8
960S	7.0	11.1	7.3	10.2
902S	7.0	13.7	9.1	13.6
962SR	5.6	14.6	5.8	11.7

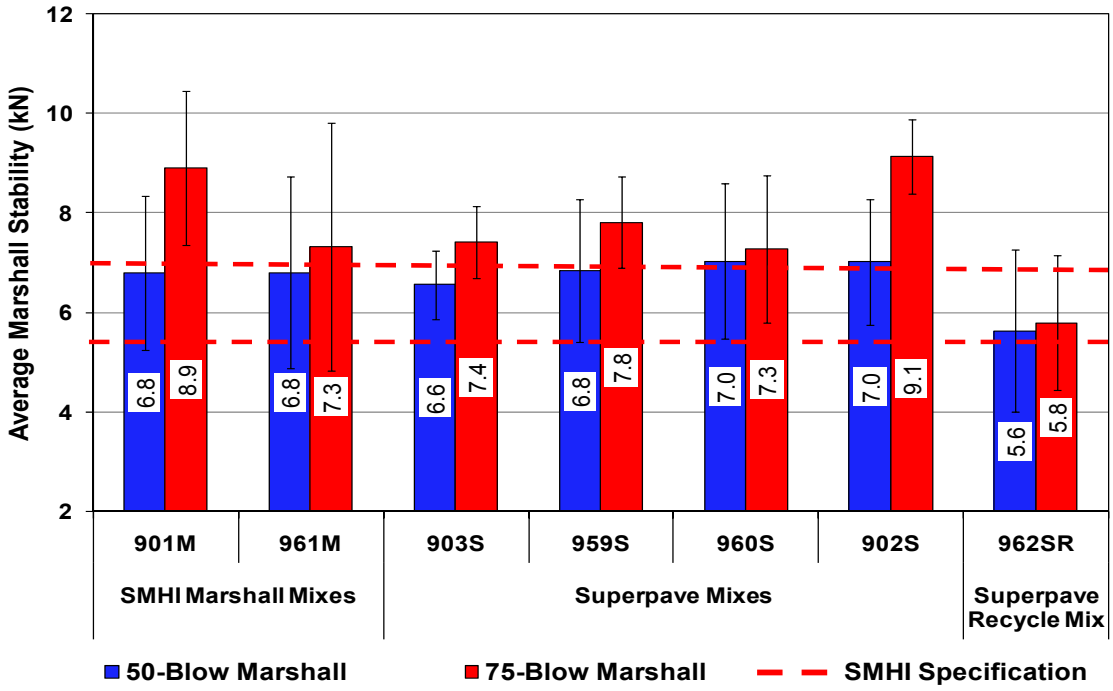

Figure 4.1 Marshall Stability at 50 and 75-Blow Marshall Compaction across Radisson SPS-9A Asphalt Mixes (± 2SD)

Statistical analysis of variance was performed on the Marshall stability values across 50 and 75-blow Marshall compaction within each Radisson SPS-9A test section and the results are presented in Table 4.2. As seen in Table 4.2, there was significant difference in Marshall stability across 50 and 75-blow Marshall compaction. Table 4.3 presents Tukey's groups of Marshall stability across 50 and 75-blow Marshall compaction within each Radisson SPS-9A test section. As seen in Table 4.3, there was significance in Marshall stability at 50-blow Marshall compared to 75-blow Marshall within test sections 901M, 903S and 902S. However there was no significance in Marshall stability at 50-blow Marshall compared to 75-blow Marshall within test sections 961M, 959S, 960S and 962SR.

Table 4.2 Analysis of Variance for Marshall Stability at 50 and 75-Blow Marshall Compaction across Radisson SPS-9A Asphalt Mixes

Parameter	Sum of Squares	Degrees of Freedom	Mean Squares	F-Test Statistic	P-value	Sig.
Between Groups	27212772	6	13606386	14	0.042	Yes
Within Groups	8710632	1	967848			
Total	35923405	11				
Error	522					

Table 4.3 Tukey's Homogeneous Groups for Marshall Stability at 50 and 75-Blow Marshall Compaction across Radisson SPS-9A Asphalt Mixes

Test Section	Marshall Blow	Marshall Stability (kN)	Tukey's Homogeneous Groups	
901M	50	6.8	A	
	75	8.9		B
961M	50	6.8	A	
	75	7.3	A	
903S	50	6.6	A	
	75	7.4		B
959S	50	6.8	A	
	75	7.8	A	
960S	50	7.0	A	
	75	7.3	A	
902S	50	7.0	A	
	75	9.1		B
962SR	50	5.6	A	
	75	5.8	A	

Statistical analysis of variance was performed on the Marshall stability values in order to investigate the variability of Marshall stability across the Radisson SPS-9A asphalt mixes and the results are presented in Table 4.4 and Table 4.5 for 50-blow Marshall and 75-blow Marshall compaction respectively. There was no significance in Marshall stability across all the test sections at 50-blow Marshall compaction as seen in the ANOVA Table 4.4. There was however significance in Marshall stability values at 75-blow Marshall compaction as seen in the ANOVA Table 4.5. Tukey's test was

performed on the Marshall stability values at 75-blow Marshall compaction to determine similar groups among the test sections.

Table 4.6 presents Tukey's groups of Marshall stability at 75-blow Marshall compaction with interaction between test sections 960S, 961M and 903S in subsets A and B. it should also be noted that there is interaction between test sections 959S and 901M in subsets B and C.

Table 4.4 Analysis of Variance for Marshall Stability at 50-Blow Marshall Compaction across Radisson SPS-9A Asphalt Mixes

Parameter	Sum of Squares	Degrees of Freedom	Mean Squares	F-Test Statistic	P-value	Sig.
Between Groups	5655470	3	942578	2	0.2	No
Within Groups	11455532	21	545501			
Total	17111002	27				
Error	522					

Table 4.5 Analysis of Variance for Marshall Stability at 75-Blow Marshall Compaction across Radisson SPS-9A Asphalt Mixes

Parameter	Sum of Squares	Degrees of Freedom	Mean Squares	F-Test Statistic	P-value	Sig.
Between Groups	30354759	3	5059127	10	0.000	Yes
Within Groups	10878299	21	518014			
Total	41233058	27				
Error	508					

Table 4.6 Tukey's Homogeneous Groups for Marshall Stability at 75-Blow Marshall Compaction across Radisson SPS-9A Asphalt Mixes

Test Section	Marshall Stability (kN)	Tukey's Homogeneous Groups		
962SR	5.8	A		
960S	7.3	A	B	
961M	7.3	A	B	
903S	7.4	A	B	
959S	7.8		B	C
901M	8.9		B	C
902S	9.1			C

4.1.2 Marshall Flow Characterization

The Marshall compacted samples were tested in the Marshall stability and flow meter using the test procedure specified in the ASTM manual. The Marshall flow of each repeat sample was recorded to indicate the resistance of the sample to permanent deformation. Table 4.7 summarizes the average Marshall flow recorded for each test section. The coefficients of variance of the four repeat samples are also shown in the table below. Figure 4.2 illustrates plots of average Marshall flow values at 50 and 75-blow Marshall for each test section. The error bars displayed show variation of ± two standard deviation from the mean. Detailed results of Marshall flow testing are presented in Appendix C.

The Marshall flow values obtained met the SMHI criteria for Marshall flow at 50-blow Marshall for all the test sections except Section 960S with a value of 3.6 mm. It should also be noted that only Section 962SR did not meet the Saskatchewan Ministry of Transportation specification for Marshall flow at 75-blow Marshall. There was no notable trend in the Marshall flow values from 50-blow Marshall to 75-blow Marshall within each test section. This could be a result of inaccuracies in testing equipment or errors in testing procedure.

Table 4.7 Marshall Flow at 50 and 75-Blow Marshall Compaction across Radisson SPS-9A Asphalt Mixes

Test Section Number	50-Blows (mm)	Coefficient of Variation (%)	75-Blows (mm)	Coefficient of Variation (%)
901M	2.9	5.1	2.7	11.6
961M	3.3	12.6	3.5	7.0
903S	2.8	12.8	3.3	6.3
959S	3.4	12.9	3.0	10.4
960S	3.6	6.7	3.3	24.4
902S	2.9	18.1	3.5	14.9
962SR	3.1	12.4	3.8	12.2

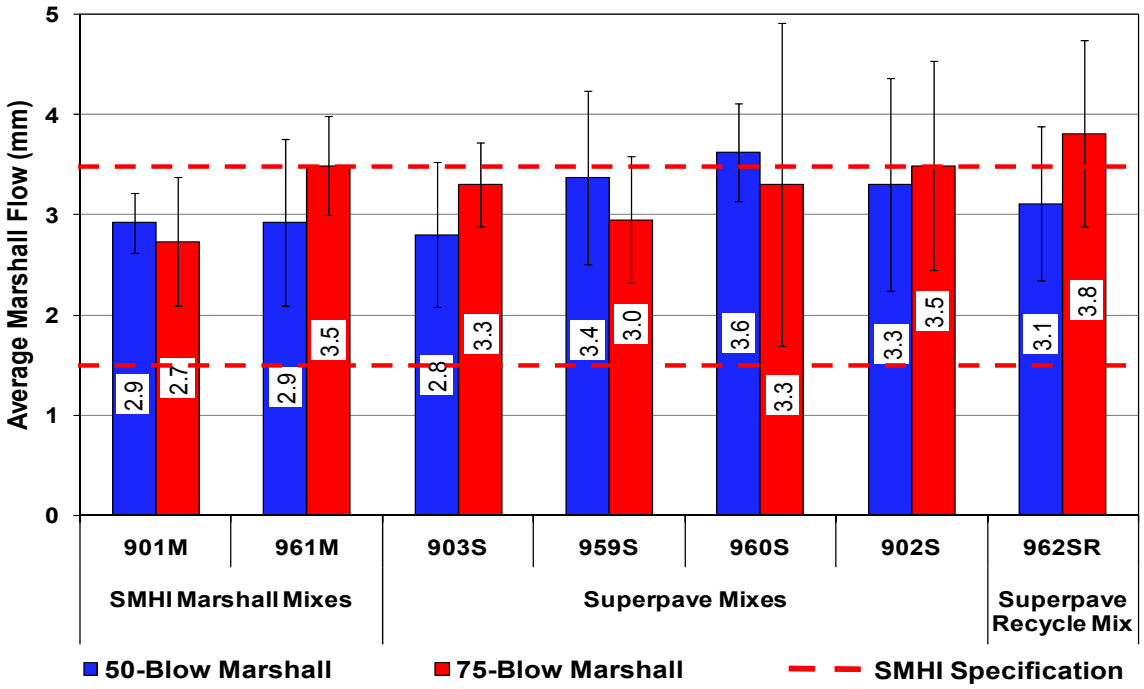

Figure 4.2 Marshall Flow at 50 and 75-Blow Marshall Compaction across Radisson SPS-9A Asphalt Mixes (± 2SD)

Statistical analysis of variance was performed on the Marshall flow values across 50 and 75-blow Marshall compaction within each Radisson SPS-9A test section and the results are presented in Table 4.8. As seen in Table 4.8, there was no significant difference in Marshall flow across 50 and 75-blow Marshall compaction. Table 4.9 presents Tukey's groups of Marshall flow across 50 and 75-blow Marshall compaction

within each Radisson SPS-9A test section. As seen in Table 4.9, there was no significance in Marshall flow at 50-blow Marshall compared to 75-blow Marshall within all the SPS-9A test sections.

Table 4.8 Analysis of Variance for Marshall Flow at 50 and 75-Blow Marshall Compaction across Radisson SPS-9A Asphalt Mixes

Parameter	Sum of Squares	Degrees of Freedom	Mean Squares	F-Test Statistic	P-value	Sig.
Between Groups	1.1	6	0.3	2	0.018	No
Within Groups	2.5	1	0.1			
Total	3.6	11				
Error	0.8					

Table 4.9 Tukey's Homogeneous Groups for Marshall Flow at 50 and 75-Blow Marshall Compaction across Radisson SPS-9A Asphalt Mixes

Test Section	Marshall Blow	Marshall Flow (mm)	Tukey's Homogeneous Group
901M	50	2.9	A
	75	2.7	A
961M	50	3.3	A
	75	3.5	A
903S	50	2.8	A
	75	3.3	A
959S	50	3.4	A
	75	3.0	A
960S	50	3.6	A
	75	3.3	A
902S	50	2.9	A
	75	3.5	A
962SR	50	3.1	A
	75	3.8	A

Statistical analysis of variance was performed on the Marshall flow values and the results are presented in Table 4.10 and Table 4.11 for 50-blow Marshall and 75-blow Marshall compaction respectively. There was no significance in Marshall flow

values across all the test sections at 50-blow Marshall compaction as seen in the ANOVA Table 4.10. There was however significance in Marshall flow values at 75-blow Marshall compaction as seen in the ANOVA Table 4.11. Tukey's test was performed on the Marshall flow values at 75-blow Marshall compaction to determine similar groups among the test sections. Table 4.12 presents Tukey's homogeneous groups of Marshall flow across the test sections with the only interaction occurring among test sections 959S, 960S, 903S and 961M. Marshall flow values for test section 901M were significantly different compared to test section 902S and 962SR.

Table 4.10 Analysis of Variance for Marshall Flow at 50-Blow Marshall Compaction across Radisson SPS-9A Asphalt Mixes

Parameter	Sum of Squares	Degrees of Freedom	Mean Squares	F-Test Statistic	P-value	Sig.
Between Groups	2	3	0.3	2	0.1	No
Within Groups	3	21	0.1			
Total	5	27				
Error	0.3					

Table 4.11 Analysis of Variance for Marshall Flow at 75-Blow Marshall Compaction across Radisson SPS-9A Asphalt Mixes

Parameter	Sum of Squares	Degrees of Freedom	Mean Squares	F-Test Statistic	P-value	Sig.
Between Groups	3	3	0.5	2.5	0.1	Yes
Within Groups	4	21	0.2			
Total	8	27				
Error	0.3					

Table 4.12 Tukey's Homogeneous Groups for Marshall Flow at 75-Blow Marshall Compaction across Radisson SPS-9A Asphalt Mixes

Test Section	Marshall Flow (mm)	Tukey's Homogeneous Groups	
901M	2.7	A	
959S	3.0	A	B
960S	3.3	A	B
903S	3.3	A	B
961M	3.5	A	B
902S	3.5		B
962SR	3.8		B

4.2 Mechanistic Triaxial Frequency Sweep Characterization of Radisson SPS-9A Asphalt Mixes

This chapter is a presentation and discussion of the results obtained from the rapid triaxial frequency sweep characterization of the Radisson SPS-9A asphalt mixes. Detailed test results and statistical analysis across stress states and loading frequencies obtained from the rapid triaxial frequency sweep characterization can be found in Appendix D. The test specimens used in the rapid triaxial frequency sweep characterization were created using the Superpave^{TM} gyratory compactor. Volumetric properties of the Superpave^{TM} gyratory compactor specimens have been presented and discussed in Chapter Three. All charts illustrate the mean of three repeat gyratory compactor samples tested, with the error bars representing minimum and maximum deviations from the mean.

Mechanistic material properties that are obtained from the RaTT cell, for the purposes of this research, include:

- Dynamic Modulus, E_d
- Poisson's Ratio, ν
- Phase Angle, δ
- Recoverable Radial Microstrain

The RaTT cell is capable of testing gyratory compactor samples 150 mm diameter and height of 150 ± 5 mm. The large sample employed by the RaTT enables the removal of significant error and disparity usually encountered in testing small asphalt mix samples. The RaTT cell features independent closed-loop feedback control of the vertical and confining stresses exerted on the gyratory compacted samples of 150 mm height. The sample is inserted into a rubber membrane, which is used to create radial confinement pneumatically. Sinusoidal axial loading is applied at a specified frequency, and the resulting strains on the sample are measured by two axial and four radially located linear variable differential transducers (LVDT) (Berthelot 1999). The RaTT cell is capable of varying test parameters in order to simulate conditions similar to in-field asphalt pavements. The varied test parameters and the conditions simulated include:

- Magnitude of axial load application (simulates varying vehicle loadings).
- Frequency of axial load application (simulates varying traffic speeds).
- Magnitude of radial confinement (simulates different locations within the pavement structure).
- Testing temperature (simulates varying atmospheric temperatures).

The testing protocol used in this research involves testing each sample at room temperature across three stress states and four frequencies as shown in Table 4.13 and Figures 4.3, 4.4 and 4.5. The stress invariants, deviatoric stress and shear stress used in this research are further explained in Equations 4.1 to 4.4.

Table 4.13 RaTT Cell Testing Protocols for Radisson SPS-9A Asphalt Mixes

Stress State	Max Axial Traction σ_1 (kPa)	Max Axial Traction σ_2 (kPa)	Confining Traction σ_3 (kPa)	Max Stress I_1 (kPa)	Max Stress J_2 (kPa)	Max Dev Stress σ_D (kPa)	Max Shear Stress τ_{max} (kPa)
One	450	250	250	950	13333	200	100
Two	650	50	50	750	120000	600	300
Three (Fully Reversed)	450	250	250	950	13333	200	100

$$I_1 = 2\sigma_2 + \sigma_1 \quad \textbf{4.1}$$

$$J_2 = \frac{1}{3}(\sigma_1 - \sigma_2)^2 \quad \textbf{4.2}$$

$$\sigma_D = \sigma_1 - \sigma_2 \quad \textbf{4.3}$$

$$\tau_{max} = \frac{1}{2}\sigma_D \quad \textbf{4.4}$$

where: I_1 is the first stress invariant of stress tensor; J_2 is second stress invariant of deviatoric stress tensor; σ_D is deviatoric stress; τ_{max} is maximum shear stress; σ_1 is applied axial traction and σ_2 is applied confining traction.

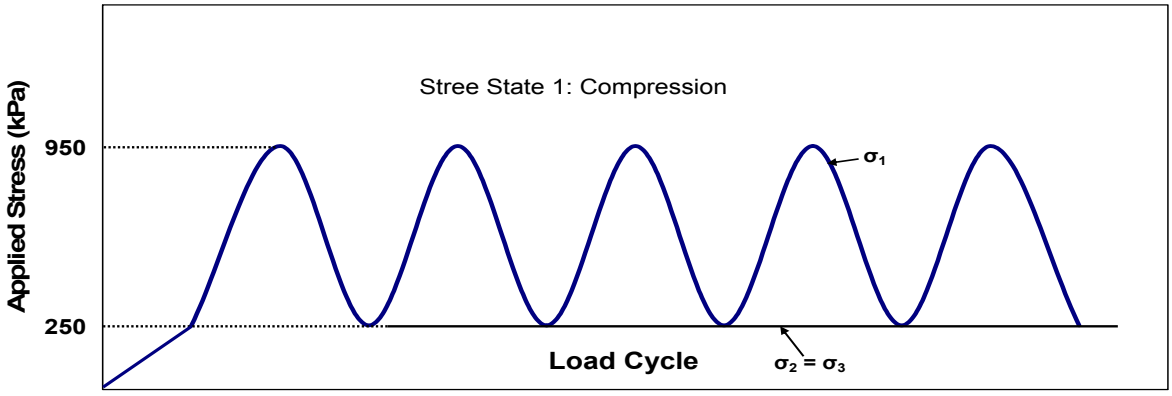

Figure 4.3 Triaxial Frequency Sweep Stress State One

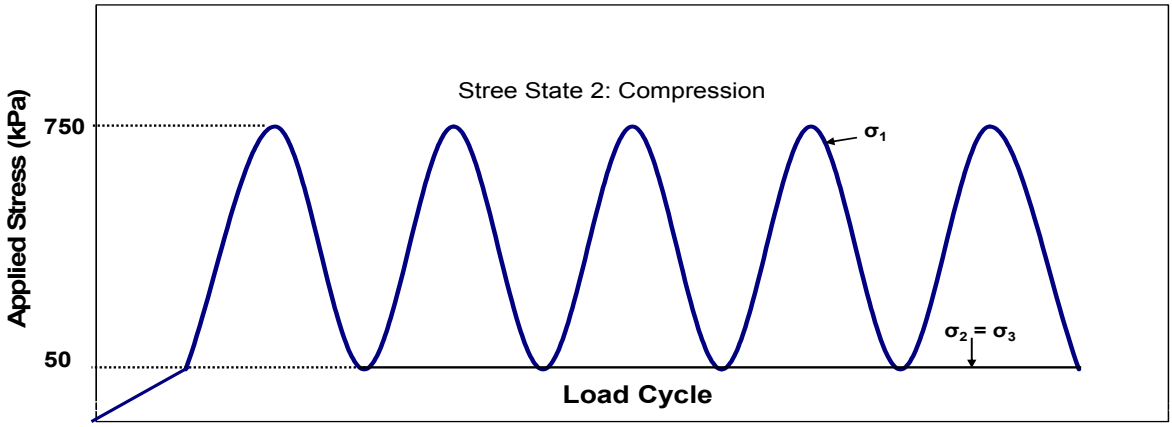

Figure 4.4 Triaxial Frequency Sweep Stress State Two

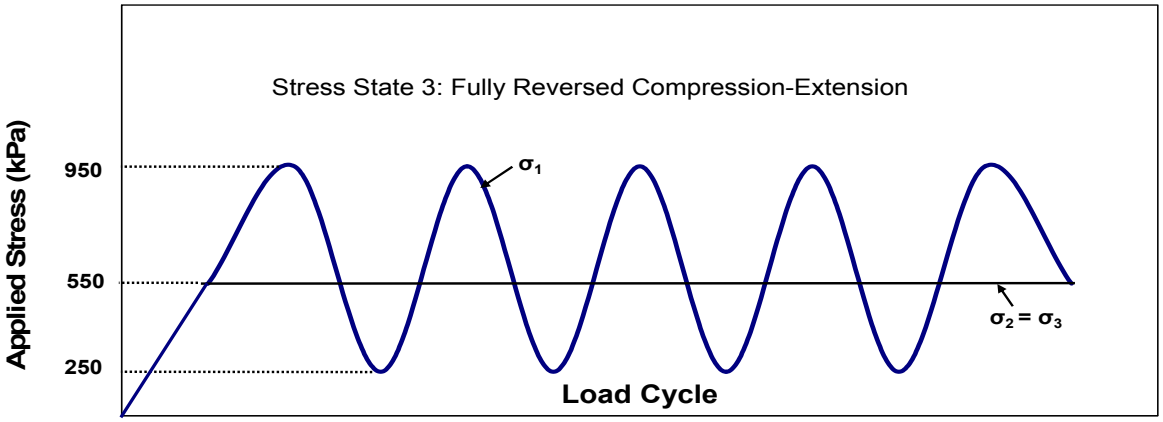

Figure 4.5 Triaxial Frequency Sweep Stress State Three

All samples were subjected to the same testing sequence beginning with the least damage-causing low stresses and high frequencies, and progressively applying increasing damage-causing high stresses and low frequencies, as shown in Table 4.14.

Table 4.14 Triaxial Frequency Sweep Testing Sequence

Testing Sequence	Peak Axial Traction (kPa)	Peak Radial Traction (kPa)	Deviatoric Stress σ_D (kPa)	Axial Load Frequency (Hz)
1	450	250	200	10
2	450	250	200	5
3	450	250	200	1
4	450	250	200	0.5
5	650	50	600	10
6	650	50	600	5
7	650	50	600	1
8	650	50	600	0.5
9	450	250	200	10
10	450	250	200	5
11	450	250	200	1
12	450	250	200	0.5

4.2.1 Dynamic Modulus Characterization of Radisson SPS-9A Mixes

Dynamic modulus, E_d, is a measure of stiffness of hot-mix asphalt sample under frequency sweep characterization. As outlined in Chapter Two, dynamic modulus is represented in the RaTT cell by the ratio of the absolute value of peak stress to peak strain under specified test conditions. Dynamic modulus is used in modeling stress-strain relationship in pavement structure under applied loading. Higher dynamic modulus values are an indication that applied stress results in lower strain in the hot-mix asphalt material.

The effects of varying angle of gyration on the measured dynamic modulus of the Radisson SPS-9A hot-mix asphalt mixtures at 20°C across varying deviatoric stresses and test frequency of 10 Hz are presented and discussed below. The dynamic modulus sensitivity was evaluated at 10 Hz to simulate the results obtained at highway speed given that the Radisson SPS-9A test site is a high-speed highway application.

Table 4.15 to Table 4.17 and Figure 4.6 to Figure 4.8 show the dynamic modulus and variation from the mean of research mixes at 10 Hz and 20°C across three levels of deviatoric stresses. The error bars shown in Figure 4.6 to Figure 4.8 represent minimum

and maximum deviation from the mean dynamic modulus of three gyratory compactor samples used in the frequency sweep characterization.

Dynamic modulus was found to decrease respectively from 200 kPa through 600 kPa to 200 kPa fully reversed deviatoric stress states across all gyratory angles for all test sections. The conventional SMHI Marshall mix design test section 901M has the highest average dynamic modulus compared to all other test sections across all deviatoric stress states and angles of gyration as displayed in Figure 4.6 to Figure 4.8. The high dynamic modulus recorded for the SMHI test section 901M is an indication of the stiffness of the asphalt mix used in the construction of the test section. The highest average dynamic modulus was recorded at 2.75° angle of gyration and 200 kPa deviatoric stress state with a value of 3975 MPa as shown in Figure 4.8. Superpave™ mix design test section 959S displayed the highest average dynamic modulus value compared to the other Superpave™ mix design test sections as shown in Figure 4.6 to Figure 4.8.

Superpave™ recycled mix design test section 962SR displayed less stiffness with lowest average dynamic modulus value across all deviatoric stress states and angles of gyrations as can be seen in Figure 4.6 to Figure 4.8. The lowest average dynamic modulus was recorded at 1.25° angle of gyration and 200 kPa fully reversed deviatoric stress state with a value of 1584 MPa as shown in Figure 4.6.

Table 4.15 Dynamic Modulus across Deviatoric Stress States at 1.25° Angle of Gyration and 10 Hz

SPS-9A Test Section	Deviatoric Stress (kPa)	Dynamic Modulus (MPa)	Deviation from Mean (MPa)	
			Minimum	Maximum
901M	200	3722	3677	3810
	600	3305	3120	3405
	200 (FR)	3229	3037	3386
961M	200	3044	3020	3062
	600	2362	2337	2398
	200 (FR)	2290	2272	2303
903S	200	2755	2714	2832
	600	2094	2035	2197
	200 (FR)	2033	1951	2117
959S	200	3216	3096	3312
	600	2714	2648	2791
	200 (FR)	2632	2572	2691
960S	200	2924	2823	3089
	600	2209	2159	2299
	200 (FR)	2151	2116	2206
902S	200	2840	2804	2885
	600	2172	2057	2308
	200 (FR)	2093	1994	2173
962SR	200	2224	2155	2312
	600	1618	1529	1756
	200 (FR)	1584	1510	1694

Table 4.16 Dynamic Modulus across Deviatoric Stress States at 2.00° Angle of Gyration and 10 Hz

SPS-9A Test Section	Deviatoric Stress (kPa)	Dynamic Modulus (MPa)	Deviation from Mean	
			Minimum	Maximum
901M	200	3788	3580	3851
	600	3317	3233	3378
	200 (FR)	3230	3117	3366
961M	200	3144	2891	3148
	600	2573	2301	2394
	200 (FR)	2478	2253	2344
903S	200	3022	2451	2983
	600	2392	1928	2196
	200 (FR)	2343	1912	2096
959S	200	3557	2969	3351
	600	3075	2653	2790
	200 (FR)	3011	2510	2777
960S	200	2765	2919	2932
	600	2325	2131	2281
	200 (FR)	2293	2132	2189
902S	200	2848	2651	2960
	600	2189	1930	2454
	200 (FR)	2134	1885	2293
962SR	200	2657	2142	2382
	600	1935	1539	1759
	200 (FR)	1830	1509	1682

Table 4.17 Dynamic Modulus across Deviatoric Stress States at 2.75° Angle of Gyration and 10 Hz

SPS-9A Test Section	Deviatoric Stress (kPa)	Dynamic Modulus (MPa)	Deviation from Mean	
			Minimum	Maximum
901M	200	3975	3541	3977
	600	3517	3085	3416
	200 (FR)	3295	3141	3346
961M	200	3150	2944	3131
	600	2676	2306	2411
	200 (FR)	2555	2265	2333
903S	200	3186	2652	2868
	600	2576	2078	2113
	200 (FR)	2554	1979	2071
959S	200	3184	3034	3522
	600	2922	2539	2902
	200 (FR)	2976	2498	2780
960S	200	3157	2864	2958
	600	2627	2138	2241
	200 (FR)	2570	2064	2215
902S	200	3182	2582	2988
	600	2676	2143	2206
	200 (FR)	2656	1923	2206
962SR	200	2954	2196	2243
	600	2183	1539	1680
	200 (FR)	1971	1582	1585

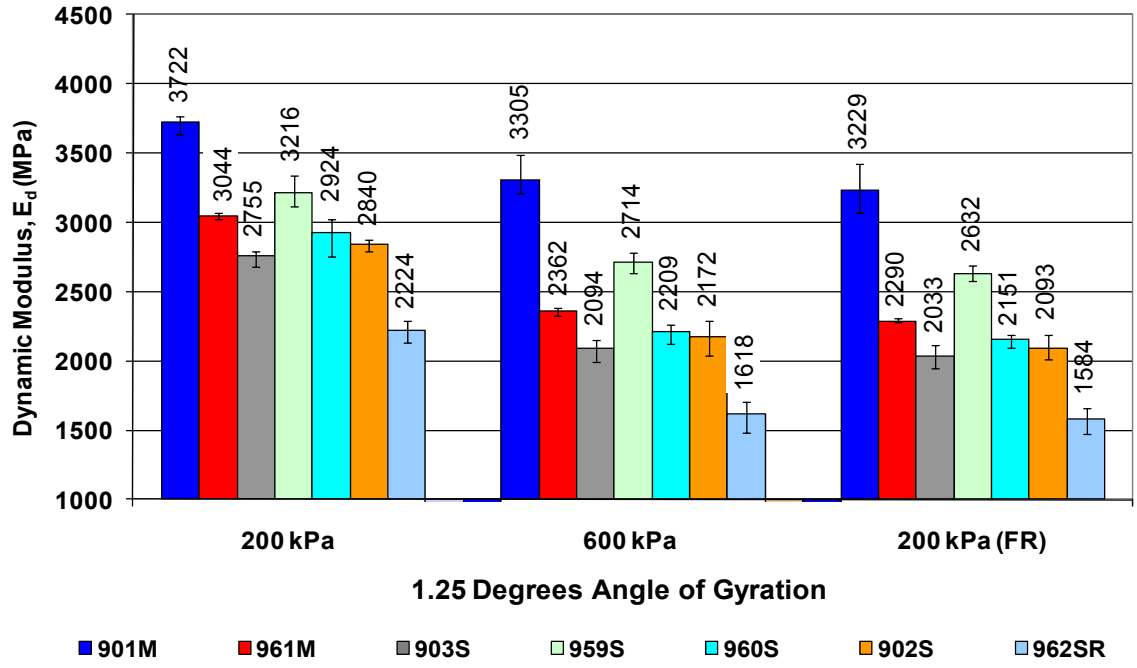

Figure 4.6 Dynamic Modulus across Deviatoric Stress States at 1.25° Angle of Gyration and 10 Hz

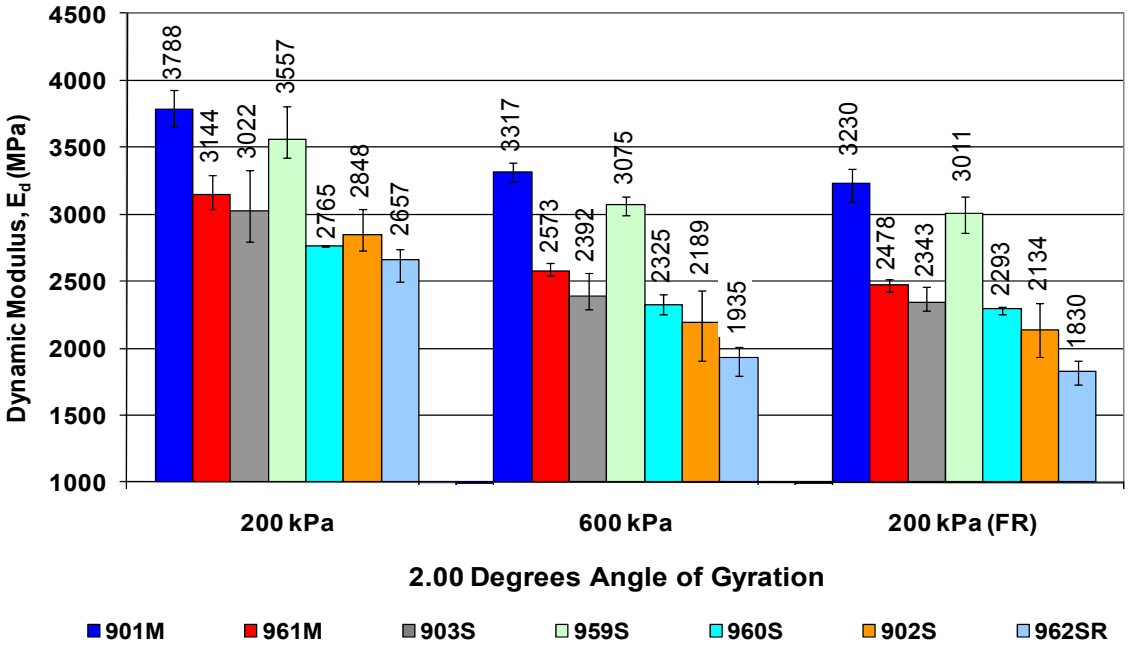

Figure 4.7 Dynamic Modulus across Deviatoric Stress States at 2.00° Angle of Gyration and 10 Hz

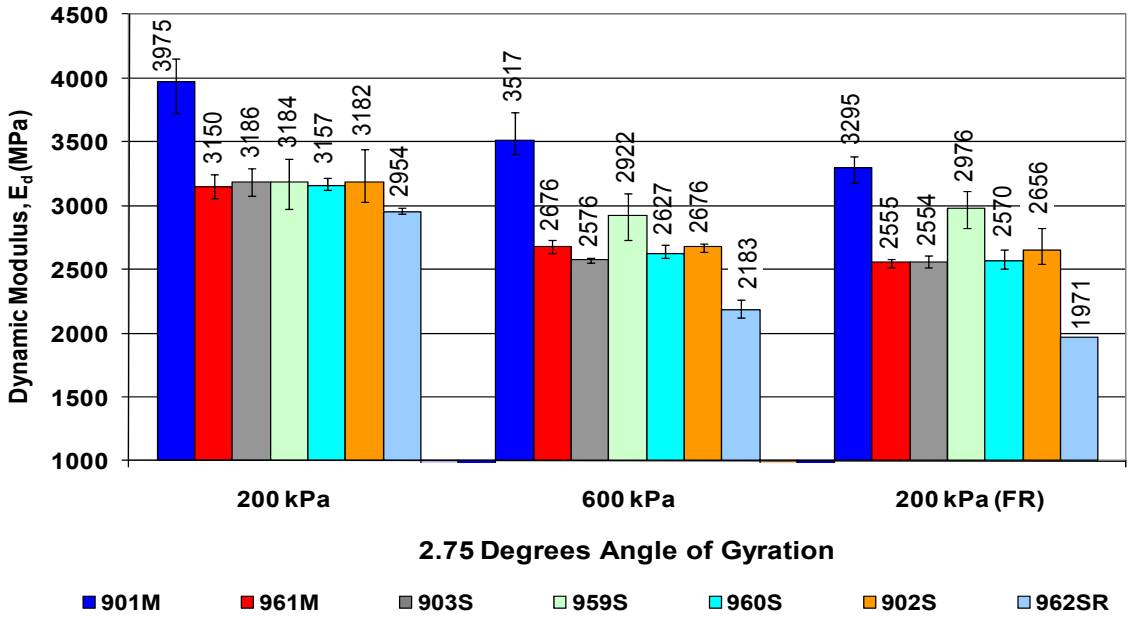

Figure 4.8 Dynamic Modulus across Deviatoric Stress States at 2.75° Angle of Gyration and 10 Hz

The effects of varying angle of gyration on the Dynamic modulus of the SPS-9A asphalt mixes have been investigated across three deviatoric stress states of 200 kPa, 600 kPa and 200 kPa (FR) and the results are presented in Figure 4.9 to Figure 4.11. The Superpave™ recommended angle of gyration 1.25° is set as a base for the analysis. The difference in dynamic modulus from 1.25° to 2.00° angles of gyration was compared to difference in dynamic modulus from 1.25° to 2.75° angles of gyration and the results are presented for each test section in Figure 4.9 to Figure 4.11.

There was significant increase in dynamic modulus from 1.25° to 2.00° angles of gyration to 1.25° to 2.75° angles of gyration across all test sections and deviatoric stress states except Superpave™ mix design test section 959S. The Superpave™ mix design test section 959S displayed reduced difference in dynamic modulus from 1.25° to 2.00° angles of gyration to 1.25° to 2.75° angles of gyration across all deviatoric stress states, Figure 4.9 to Figure 4.11. It should be noted that difference in dynamic modulus from 1.25° to 2.00° angles of gyration and 1.25° to 2.75° angles of gyration was highest at 200 kPa deviatoric stress compared to the other deviatoric stress states of 600 kPa and

200 kPa fully reversed. There was no significant effect of the fully reversed frequency sweep testing on the difference in dynamic modulus recorded.

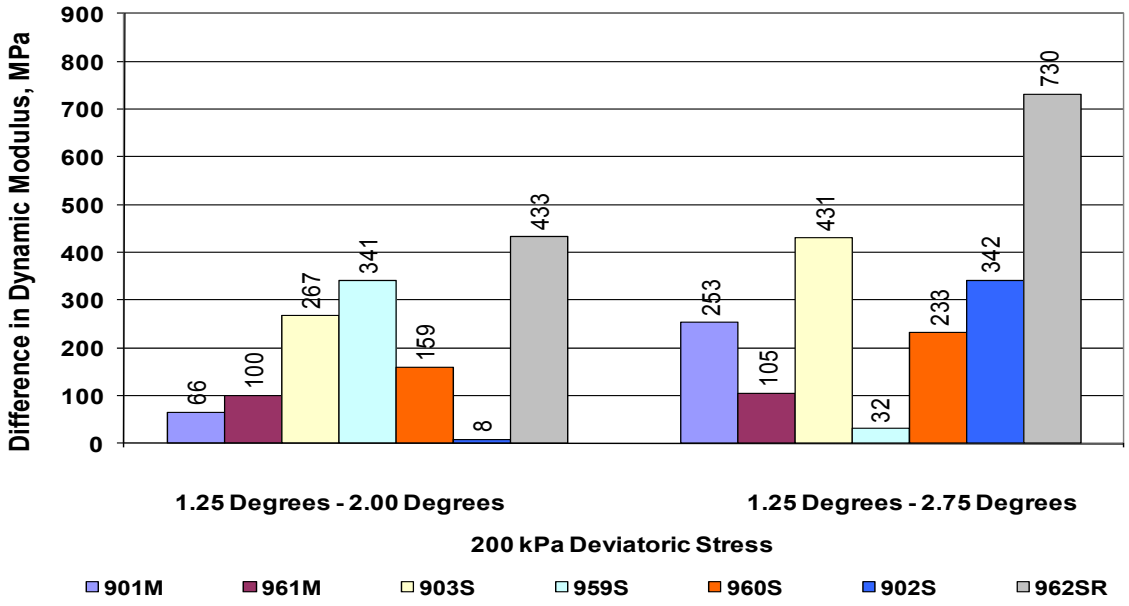

Figure 4.9 Effect of Gyratory Angle on Dynamic Modulus at 200 kPa Deviatoric Stress States and 10 Hz

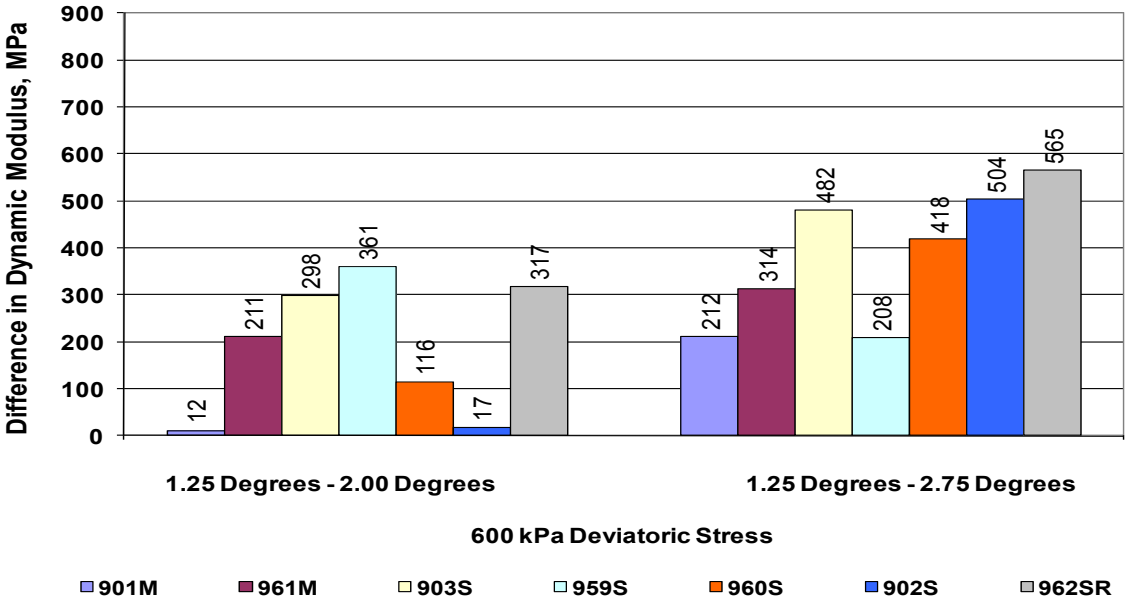

Figure 4.10 Effect of Gyratory Angle on Dynamic Modulus at 600 kPa Deviatoric Stress States and 10 Hz

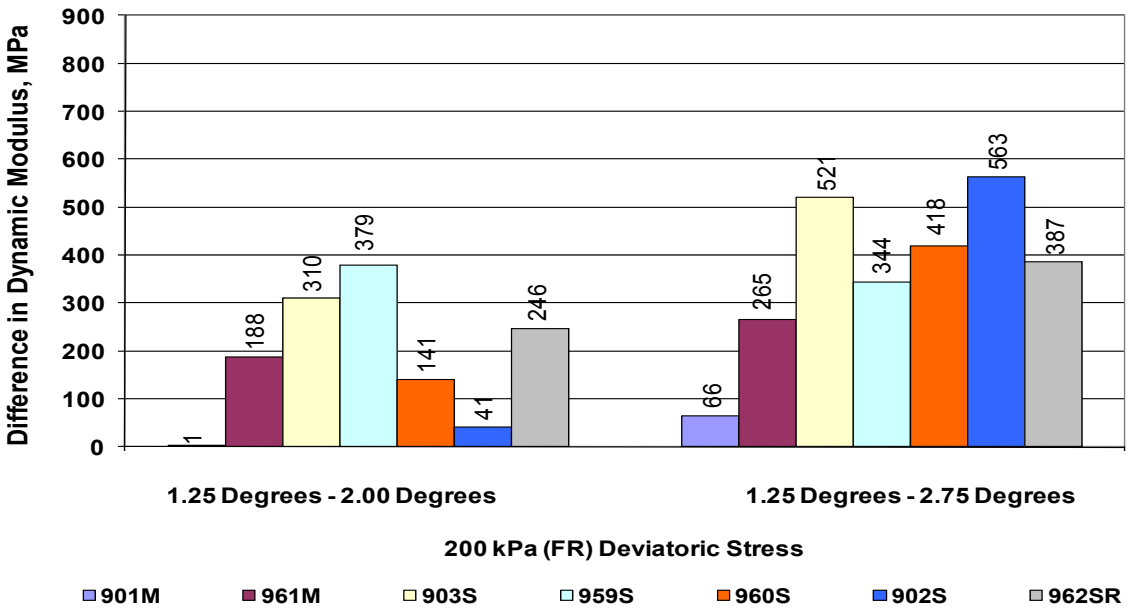

Figure 4.11 Effects of Gyratory Angle on Dynamic Modulus at 200 kPa (FR) Deviatoric Stress States and 10 Hz

The effects of varying deviatoric stress on the dynamic modulus of the SPS-9A asphalt mixes was investigated across three angles of gyration 1.25°, 2.00° and 2.75° and the results are presented in Figure 4.12 to Figure 4.14.

There was increase in difference in dynamic modulus from 200 kPa to 600 kPa and 200 kPa to 200 kPa (FR) deviatoric stress for 1.25°, 2.00° and 2.75° angles of gyration across all test sections as can be seen in Figure 4.12 to Figure 4.14. It should however be noted that the difference in dynamic modulus from 200 kPa to 600 kPa is not significantly different from 200 kPa to 200 kPa (FR) deviatoric stress for 1.25° angle of gyration. There was an observed decrease in difference in dynamic modulus from 200 kPa to 600 kPa and 200 kPa to 200 kPa (FR) deviatoric stress at 2.75°, for test section 959S as seen in Figure 4.14.

4.2.1.1 Staistical Sensitivity of Dynamic Modulus across Gyration Angle

Statistical analysis of variance (ANOVA) was performed on dynamic modulus results to evaluate statistical significance at 95 percent confidence level across angle of gyration and mix type. The ANOVA of dynamic modulus results are shown in Tables 4.18, 4.20 and 4.22 at deviatoric stresses 200 kPa, 600 kPa and 200 kPa fully reversible respectively. As shown in Table 4.18, 4.20 and 4.22 significant differences of dynamic modulus values exist across angle of gyration for the Radisson SPS-9A test sections at deviatoric stresses of 200 kPa, 600 kPa and 200 kPa fully reversed.

In order to identify which angle of gyration yielded statistical difference in dynamic modulus results, Tukey's homogeneous group analysis was performed at a confidence level of 95 percent on the dynamic modulus results. Similar dynamic modulus across angle of gyration was put under the same homogeneous group for each Radisson SPS-9A test section. The Tukey's homogeneous group analysis results are shown in Tables 4.19, 4.21 and 4.23. As seen in Tables 4.19, 4.21 and 4.23, significant differences generally existed between dynamic modulus results across angle of gyration for the Raddisson SPS-9A test sections. Dynamic modulus results at 1.25° angle of gyration was significantly different compared to dynamic modulus results at 2.75° angle of gyration across most of the Raddisson SPS-9A test sections. There was however, noted similarity in dynamic modulus results at 2.00° angle of gyration compared to dynamic modulus results at 2.75° angle of gyration.

Table 4.18 Analysis of Variance for Dynamic Modulus at 200 kPa Deviatoric Stress across Radisson SPS-9A Asphalt Mixes

Parameter	Sum of Squares	Degrees of Freedom	Mean Squares	F-Test Statistic	P-value	Sig.
Mix Type	19736594	6	986829	109		
Angle of Gyration	405607957	2	47957	44799	0.000	
Mix Type*Angle of Gyration	6019401	12	429957	47	0.000	Yes
Error	380263	15	9054			

Table 4.19 Tukey's Homogeneous Groups for Dynamic Modulus at 200 kPa Deviatoric Stress across Radisson SPS-9A Asphalt Mixes

Test Section	Angle of Gyration (°)	Dynamic Modulus (MPa)	Tukey's Homogeneous Groups		
901M	1.25	3722	A	B	C
	2.00	3788		B	C
	2.75	3975			C
961M	1.25	3044	A		
	2.00	3144	A		
	2.75	3150	A		
903S	1.25	2755	A	B	C
	2.00	3022		B	C
	2.75	3186			C
959S	1.25	3216		B	C
	2.00	3557		B	C
	2.75	3184			C
960S	1.25	2924	A	B	
	2.00	2765		B	
	2.75	3157			C
902S	1.25	2840	A		
	2.00	2848	A		
	2.75	3182	A		
962SR	1.25	2224	A		
	2.00	2657		B	
	2.75	2954			C

Table 4.20 Analysis of Variance for Dynamic Modulus at 600 kPa Deviatoric Stress across Radisson SPS-9A Asphalt Mixes

Parameter	Sum of Squares	Degrees of Freedom	Mean Squares	F-Test Statistic	P-value	Sig.
Mix Type	285249580	6	390657	93		
Angle of Gyration	4297224	2	40560	67769	0.000	
Mix Type*Angle of Gyration	418391	12	52299	12	0.000	Yes
Error	101020	15	4209			

Table 4.21 Tukey's Homogeneous Groups for Dynamic Modulus at 600 kPa Deviatoric Stress across Radisson SPS-9A Asphalt Mixes

Test Section	Angle of Gyration (°)	Dynamic Modulus (MPa)	Tukey's Homogeneous Groups		
901M	1.25	3305	A		
	2.00	3317	A		
	2.75	3517	A		
961M	1.25	2362	A		
	2.00	2573		B	C
	2.75	2676		B	C
903S	1.25	2094	A	B	
	2.00	2392		B	C
	2.75	2922			C
959S	1.25	2714	A	B	
	2.00	3075		B	C
	2.75	2922			C
960S	1.25	2209	A	B	
	2.00	2325	A	B	
	2.75	2627			C
902S	1.25	2172	A	B	
	2.00	2189		B	C
	2.75	2676			C
962SR	1.25	1618	A		
	2.00	1935		B	C
	2.75	2183		B	C

Table 4.22 Analysis of Variance for Dynamic Modulus at 200 kPa Fully Reversed Deviatoric Stress across Radisson SPS-9A Asphalt Mixes

Parameter	Sum of Squares	Degrees of Freedom	Mean Squares	F-Test Statistic	P-value	Sig.
Mix Type	367271672	6	460519	20		
Angle of Gyration	5065705	2	36772	16140	0.000	
Mix Type*Angle of Gyration	1107842	12	138480	6	0.000	Yes
Error	546153	15	22756			

Table 4.23 Tukey's Homogeneous Groups for Dynamic Modulus at 200 kPa Fully Reversed Deviatoric Stress across Radisson SPS-9A Asphalt Mixes

Test Section	Angle of Gyration (°)	Dynamic Modulus (MPa)	Tukey's Homogeneous Groups		
901M	1.25	3229	A		
	2.00	3230	A		
	2.75	3295	A		
961M	1.25	2290	A		
	2.00	2478		B	C
	2.75	2555		B	C
903S	1.25	2033	A		C
	2.00	2343		B	C
	2.75	2976		B	C
959S	1.25	2632	A		
	2.00	3011	A		
	2.75	2976	A		
960S	1.25	2151	A	B	
	2.00	2293	A	B	
	2.75	2570			C
902S	1.25	2093	A	B	
	2.00	2134		B	C
	2.75	2656		B	C
962SR	1.25	1584	A	B	
	2.00	1830		B	C
	2.75	1971		B	C

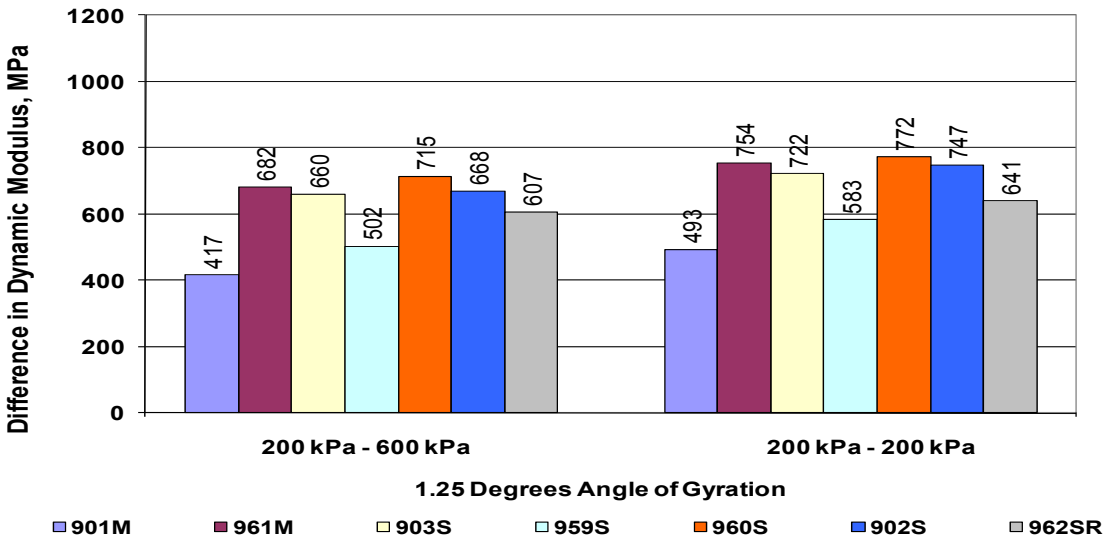

Figure 4.12 Effects of Deviatoric Stress States on Dynamic Modulus at 1.25° Angle of Gyration and 10 Hz

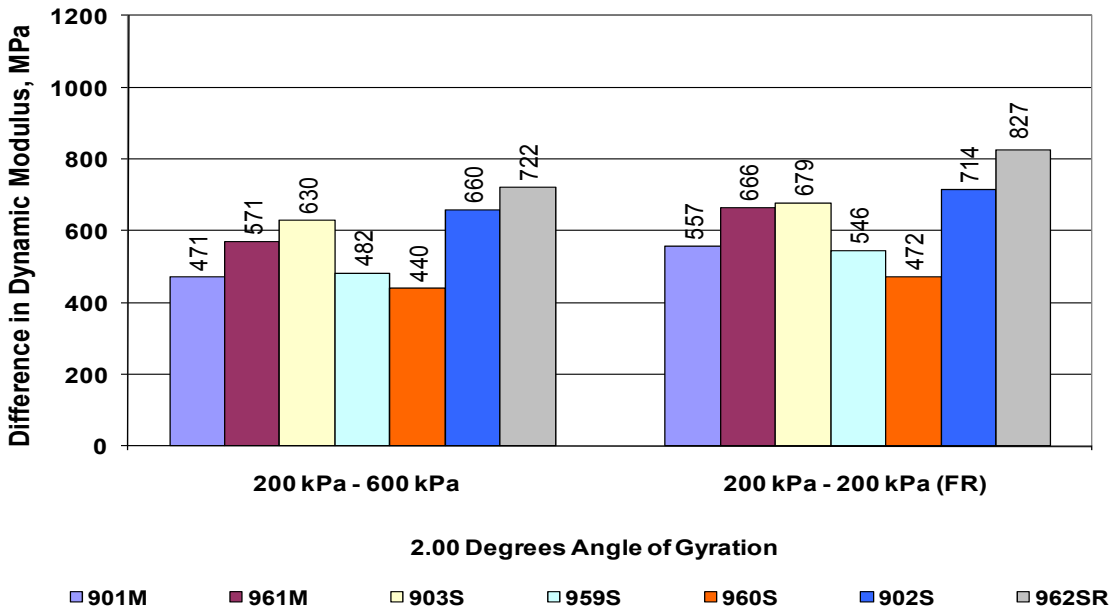

Figure 4.13 Effects of Deviatoric Stress States on Dynamic Modulus at 2.00° Angle of Gyration and 10 Hz

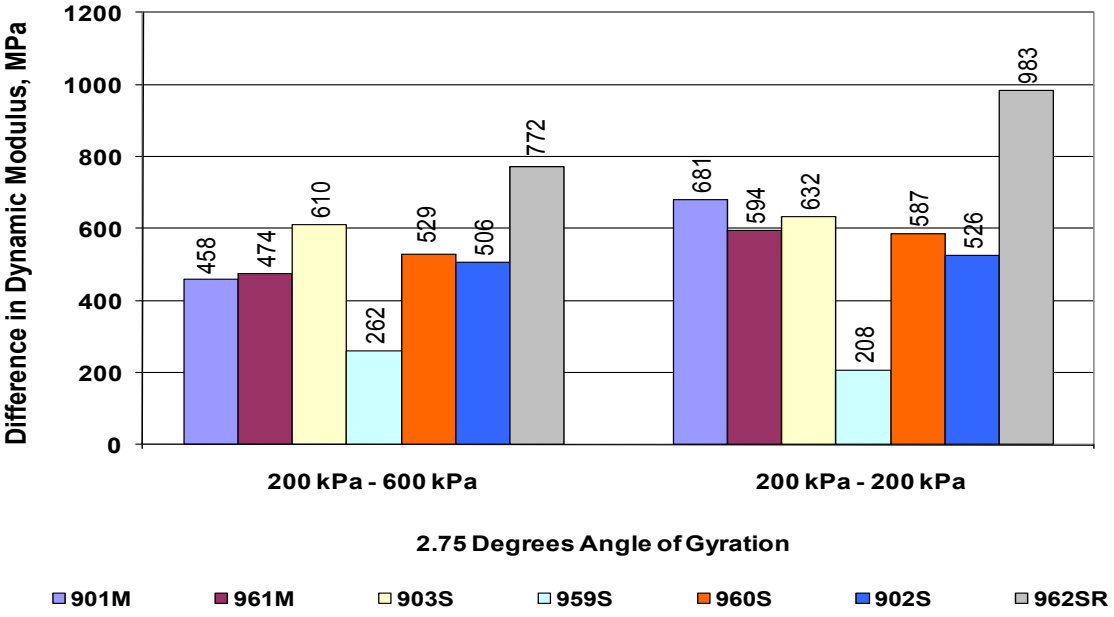

Figure 4.14 Effects of Deviatoric Stress States on Dynamic Modulus at 2.75° Angle of Gyration and 10 Hz

4.2.1.2 Staistical Sensitivity of Dynamic Modulus across Deviatoric Stress

Statistical analysis of variance was performed on dynamic modulus values in order to investigate the sensitivity of the Radisson SPS-9A asphalt mixes to varied deviatoric stress. Analysis of variance for Dynamic modulus characterization is summarized in Tables 4.24, 4.26 and 4.28 and Tukey's groups are presented in Tables 4.25, 4.27 and 4.29. As seen in Tables 4.24, 4.26 and 4.28, there was significant difference in dynamic modulus as a function of deviatoric stress at all angles of gyration across most of the Radisson SPS-9A test sections.

Dynamic modulus at 200 kPa deviatoric stress was significantly different compared to dynamic modulus at 600 kPa and 200 kPa fully reversed deviatoric stresses at 1.25° angle of gyration across most of the test sections, as seen in Table 4.25. Only test section 961M has difference in dynamic modulus across all three deviatoric stresses at 1.25° angle of gyration.

Similarly, dynamic modulus at 200 kPa deviatoric stress was significantly different compared to dynamic modulus at 600 kPa and 200 kPa fully reversed deviatoric stresses at 2.00° angle of gyration across most of the test sections, as seen in Table 4.27. It should be noted that test section 903S did not show any significant difference in dynamic modulus across all deviatoric stresses at 2.00° angle of gyration.

Dynamic modulus at 200 kPa deviatoric stress was significantly different compared to dynamic modulus at 600 kPa and 200 kPa fully reversed deviatoric stresses at 2.75° angle of gyration across test sections 901M, 961M, 903S and 960S, as seen in Table 4.29. Test sections 959S and 902S have different dynamic modulus across all three deviatoric stresses at 2.75° angle of gyration. It should be noted that test section 962SR did not show any significant difference in dynamic modulus across all deviatoric stresses at 2.75° angle of gyration.

Table 4.24 Analysis of Variance for Dynamic Modulus at 1.25° Angle of Gyration across Radisson SPS-9A Asphalt Mixes

Parameter	Sum of Squares	Degrees of Freedom	Mean Squares	F-Test Statistic	P-value	Sig.
Dynamic Modulus	19736594	2	986829	109		
Deviatoric Stress	405607957	2	47957	44799	0.000	
Dynamic Modulus*Deviatoric Stress	6019401	4	429957	47		Yes
Error	380263	16	9054			

Table 4.25 Tukey's Homogeneous Groups for Dynamic Modulus at 1.25° Angle of Gyration across Radisson SPS-9A Asphalt Mixes

Test Section	Deviatoric Stress (kPa)	Dynamic Modulus (MPa)	Tukey's Homogeneous Groups		
901M	200	3722	A		
	600	3305		B	C
	200 (FR)	3229		B	C
961M	200	3044	A		
	600	2362		B	
	200 (FR)	2290			C
903S	200	2755	A		
	600	2094		B	C
	200 (FR)	2033		B	C
959S	200	3216	A		
	600	2714		B	C
	200 (FR)	2632		B	C
960S	200	2924	A		
	600	2209		B	C
	200 (FR)	2151		B	C
902S	200	2840	A		
	600	2172		B	C
	200 (FR)	2093		B	C
962SR	200	2224	A		
	600	1618		B	C
	200 (FR)	1584		B	C

Table 4.26 Analysis of Variance for Dynamic Modulus at 2.00° Angle of Gyration across Radisson SPS-9A Asphalt Mixes

Parameter	Sum of Squares	Degrees of Freedom	Mean Squares	F-Test Statistic	P-value	Sig.
Dynamic Modulus	285249580	2	390657	93		
Deviatoric Stress	4297224	2	40560	67769	0.000	
Dynamic Modulus*Deviatoric Stress	418391	4	52299	12		Yes
Error	101020	16	4209			

Table 4.27 Tukey's Homogeneous Groups for Dynamic Modulus at 2.00° Angle of Gyration across Radisson SPS-9A Asphalt Mixes

Test Section	Deviatoric Stress (kPa)	Dynamic Modulus (MPa)	Tukey's Homogeneous Groups	
901M	200	3788	A	
	600	3317		B
	200 (FR)	3230		B
961M	200	3144	A	
	600	2573		B
	200 (FR)	2478		B
903S	200	3022	A	
	600	2392	A	
	200 (FR)	2343	A	
959S	200	3557	A	
	600	3075		B
	200 (FR)	3011		B
960S	200	2765	A	
	600	2325		B
	200 (FR)	2293		B
902S	200	2848	A	
	600	2189		B
	200 (FR)	2134		B
962SR	200	2657	A	
	600	1935		B
	200 (FR)	1830		B

Table 4.28 Analysis of Variance for Dynamic Modulus at 2.75° Angle of Gyration across Radisson SPS-9A Asphalt Mixes

Parameter	Sum of Squares	Degrees of Freedom	Mean Squares	F-Test Statistic	P-value	Sig.
Dynamic Modulus	367271672	2	460519	20		
Deviatoric Stress	5065705	2	36772	16140	0.000	
Dynamic Modulus*Deviatoric Stress	1107842	4	138480	6		Yes
Error	546153	16	22756			

Table 4.29 Tukey's Homogeneous Groups for Dynamic Modulus at 2.75° Angle of Gyration across Radisson SPS-9A Asphalt Mixes

Test Section	Deviatoric Stress (kPa)	Dynamic Modulus (MPa)	Tukey's Homogeneous Groups		
901M	200	3975	A		
	600	3517		B	C
	200 (FR)	3295		B	C
961M	200	3150	A		
	600	2676		B	C
	200 (FR)	2555		B	C
903S	200	3186	A		
	600	2576		B	C
	200 (FR)	2554		B	C
959S	200	3184	A		
	600	2922	A		
	200 (FR)	2976	A		
960S	200	3157	A		
	600	2627		B	C
	200 (FR)	2570		B	C
902S	200	3182	A		
	600	2676	A		
	200 (FR)	2656	A		
962SR	200	2954	A		
	600	2183		B	
	200 (FR)	1971			C

4.2.2 Poisson's Ratio Characterization of Radisson SPS-9A Mixes

Poisson's Ratio has been defined in Chapter Two as the relationship between lateral strain and axial strain. Poisson's Ratio can be obtained from the RaTT cell as the ratio of recoverable radial microstrain to recoverable axial microstrain. Table 4.30 to Table 4.32 and Figure 4.15 to Figure 4.17 show the Poisson's ratio and variation from the mean of research mixes at 10 Hz and 20°C across three levels of deviatoric stresses. The error bars shown in Figure 4.15 to Figure 4.17 represent minimum and maximum deviation from the mean Poisson's ratio of three gyratory compactor samples used in the frequency sweep characterization. The average Poisson's ratio for all the asphalt mixes used in this research was 0.32 which is close to the Poisson's ratio of 0.35 specified for asphalt mixtures for design and modeling purposes.

Poisson's ratio was not sensitive to varying deviatoric stress. The conventional SMHI Marshall mix design test section 961M has the highest Poisson's ratio compared across all test sections and angles of gyration at 600 kPa and 200 kPa (FR) deviatoric stress as shown in Figure 4.15 to Figure 4.17. The highest Poisson's ratio was recorded as 0.41 at 600 kPa deviatoric stress and 1.25° angle of gyration for test section 961M. The Poisson's ratio for test section 961M was however low at 200 kPa deviatoric stress for 2.00° and 2.75° angles of gyration, Figures 4.16 and 4.17. It should be noted that Superpave^{TM} mix design test section 959S recorded low average Poisson's ratio at all angles of gyration and deviatoric stresses. The lowest Poisson's ratio was recorded as 0.25 at 200 kPa fully reversed deviatoric stress and 2.75° angle of gyration for test section 959S.

Table 4.30 Poisson's Ratio across Deviatoric Stress States at 1.25° Angle of Gyration and 10 Hz

SPS-9A Test Section	Deviatoric Stress (kPa)	Poisson's Ratio	Deviation from Mean	
			Minimum	Maximum
901M	200	0.28	0.25	0.30
	600	0.32	0.31	0.33
	200 (FR)	0.31	0.29	0.33
961M	200	0.32	0.30	0.35
	600	0.38	0.37	0.39
	200 (FR)	0.36	0.34	0.38
903S	200	0.28	0.27	0.29
	600	0.35	0.35	0.35
	200 (FR)	0.31	0.30	0.32
959S	200	0.29	0.27	0.31
	600	0.28	0.28	0.28
	200 (FR)	0.27	0.27	0.27
960S	200	0.27	0.27	0.27
	600	0.31	0.30	0.32
	200 (FR)	0.32	0.29	0.34
902S	200	0.26	0.25	0.28
	600	0.27	0.25	0.29
	200 (FR)	0.28	0.26	0.30
962SR	200	0.31	0.30	0.32
	600	0.32	0.31	0.33
	200 (FR)	0.34	0.32	0.36

Table 4.31 Poisson's Ratio across Deviatoric Stress States at 2.00° Angle of Gyration and 10 Hz

SPS-9A Test Section	Deviatoric Stress (kPa)	Poisson's Ratio	Deviation from Mean	
			Minimum	Maximum
901M	200	0.36	0.35	0.38
	600	0.33	0.33	0.34
	200 (FR)	0.34	0.34	0.34
961M	200	0.33	0.33	0.33
	600	0.38	0.36	0.39
	200 (FR)	0.37	0.36	0.39
903S	200	0.29	0.28	0.31
	600	0.35	0.33	0.36
	200 (FR)	0.37	0.35	0.38
959S	200	0.27	0.25	0.28
	600	0.29	0.29	0.29
	200 (FR)	0.26	0.23	0.29
960S	200	0.27	0.25	0.28
	600	0.32	0.30	0.35
	200 (FR)	0.34	0.32	0.37
902S	200	0.27	0.26	0.28
	600	0.28	0.27	0.29
	200 (FR)	0.30	0.29	0.31
962SR	200	0.32	0.31	0.33
	600	0.33	0.31	0.35
	200 (FR)	0.37	0.36	0.39

Table 4.32 Poisson's Ratio across Deviatoric Stress States at 2.75° Angle of Gyration and 10 Hz

SPS-9A Test Section	Deviatoric Stress (kPa)	Poisson's Ratio	Deviation from Mean	
			Minimum	Maximum
901M	200	0.39	0.38	0.40
	600	0.37	0.34	0.40
	200 (FR)	0.38	0.36	0.39
961M	200	0.35	0.34	0.37
	600	0.41	0.39	0.42
	200 (FR)	0.38	0.35	0.40
903S	200	0.31	0.28	0.34
	600	0.36	0.35	0.37
	200 (FR)	0.39	0.37	0.42
959S	200	0.25	0.22	0.27
	600	0.27	0.24	0.29
	200 (FR)	0.25	0.24	0.25
960S	200	0.30	0.29	0.31
	600	0.33	0.32	0.34
	200 (FR)	0.37	0.36	0.38
902S	200	0.28	0.27	0.29
	600	0.28	0.28	0.28
	200 (FR)	0.30	0.28	0.32
962SR	200	0.37	0.33	0.39
	600	0.36	0.33	0.38
	200 (FR)	0.38	0.38	0.38

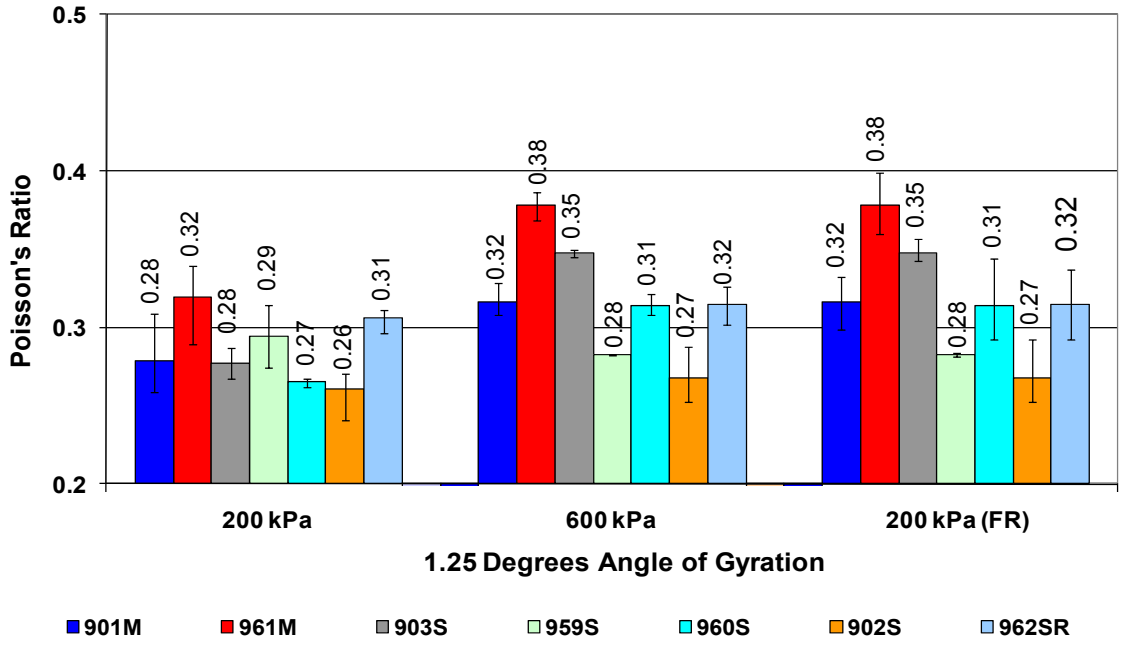

Figure 4.15 Poisson's Ratio across Deviatoric Stress States at 1.25° Angle of Gyration and 10 Hz

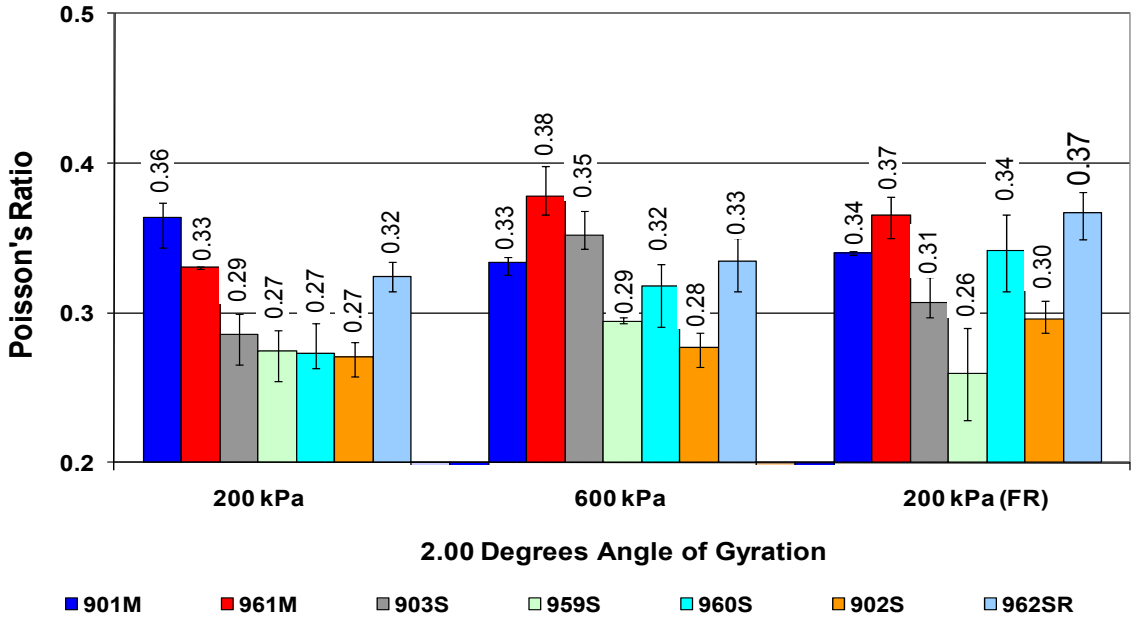

Figure 4.16 Poisson's Ratio across Deviatoric Stress States at 2.00° Angle of Gyration and 10 Hz

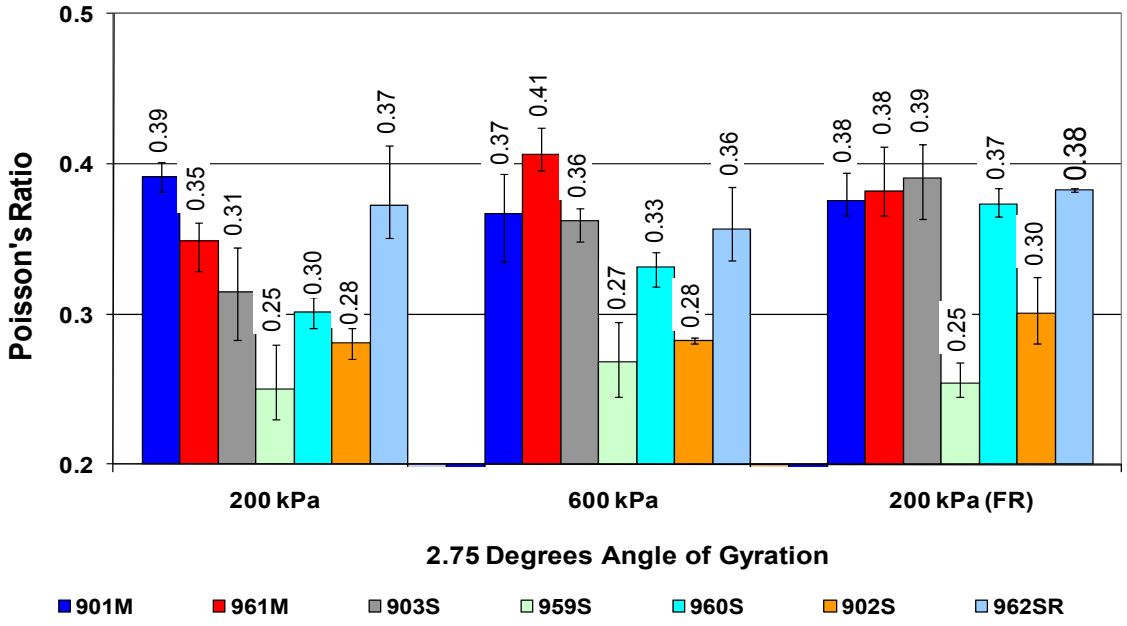

Figure 4.17 Poisson's Ratio across Deviatoric Stress States at 2.75° Angle of Gyration and 10 Hz

The effects of varying angle of gyration on the Poisson's ratio of the SPS-9A asphalt mixes have been investigated across three deviatoric stress states of 200 kPa, 600 kPa and 200 kPa (FR) and the results are presented in Figure 4.18 to Figure 4.20. The Superpave™ recommended angle of gyration 1.25° is set as a base for the analysis. The difference in Poisson's ratio from 1.25° to 2.00° angles of gyration was compared to difference in Poisson's ratio from 1.25° to 2.75° angles of gyration and the results are presented for each test section.

Poisson's ratio was found to be sensitive to varying angle of gyration as shown by the increase in the difference in Poisson's ratio from 1.25° to 2.00° angles of gyration compared to difference in Poisson's ratio from 1.25° to 2.75° angles of gyration as shown in Figure 4.18 to Figure 4.20. There was a higher difference in Poisson's ratio for 1.25° to 2.75° angles of gyration compared to 1.25° to 2.00° angles of gyration. This is evidence that increasing the angle of gyration results in gyratory compacted samples that resist change in volume as a result of applied axial stress. The conventional SMHI Marshall mix design test section 901M was observed to have the highest change in Poisson's ratio as seen in Figures 4.18 and 4.19.

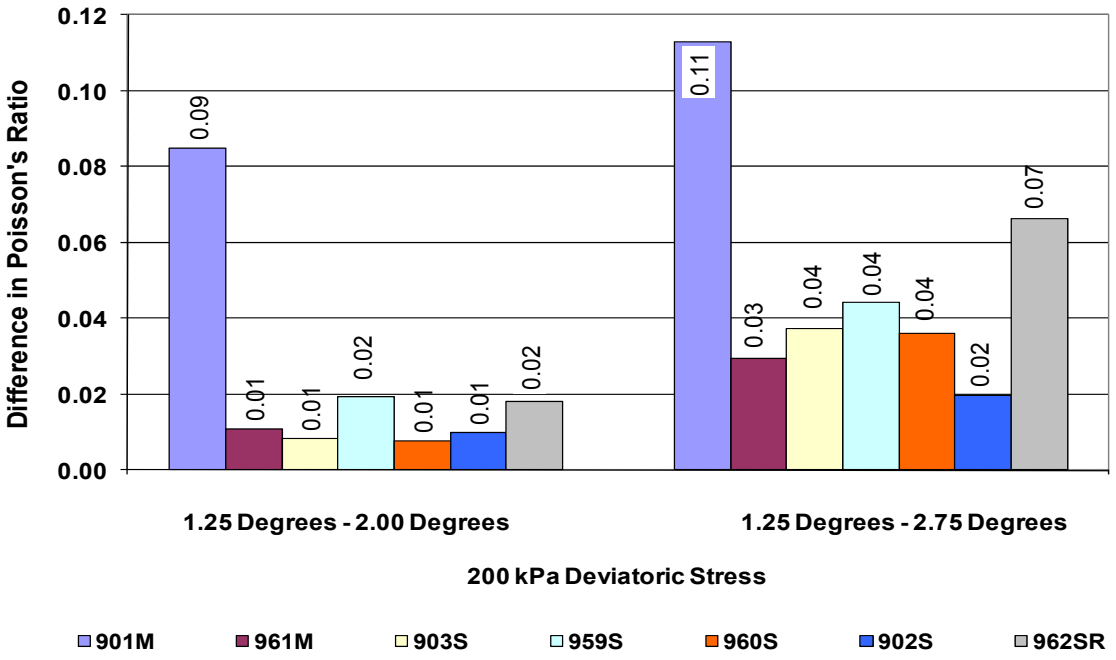

Figure 4.18 Effects of Gyratory Angle on Poisson's Ratio at 200 kPa Deviatoric Stress States and 10 Hz

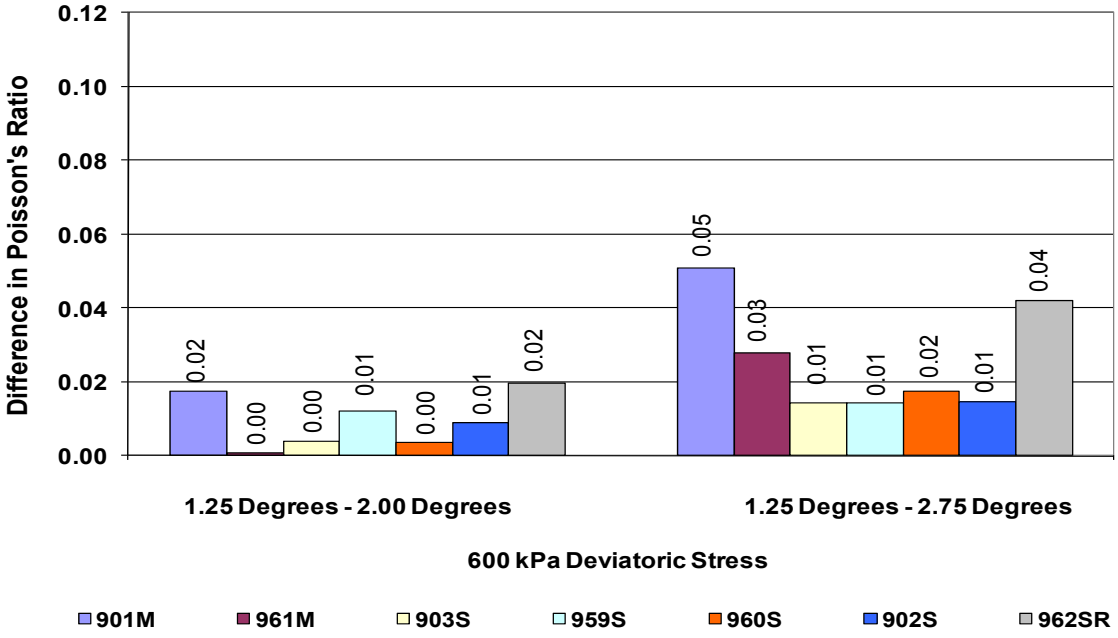

Figure 4.19 Effects of Gyratory Angle on Poisson's Ratio at 600 kPa Deviatoric Stress States and 10 Hz

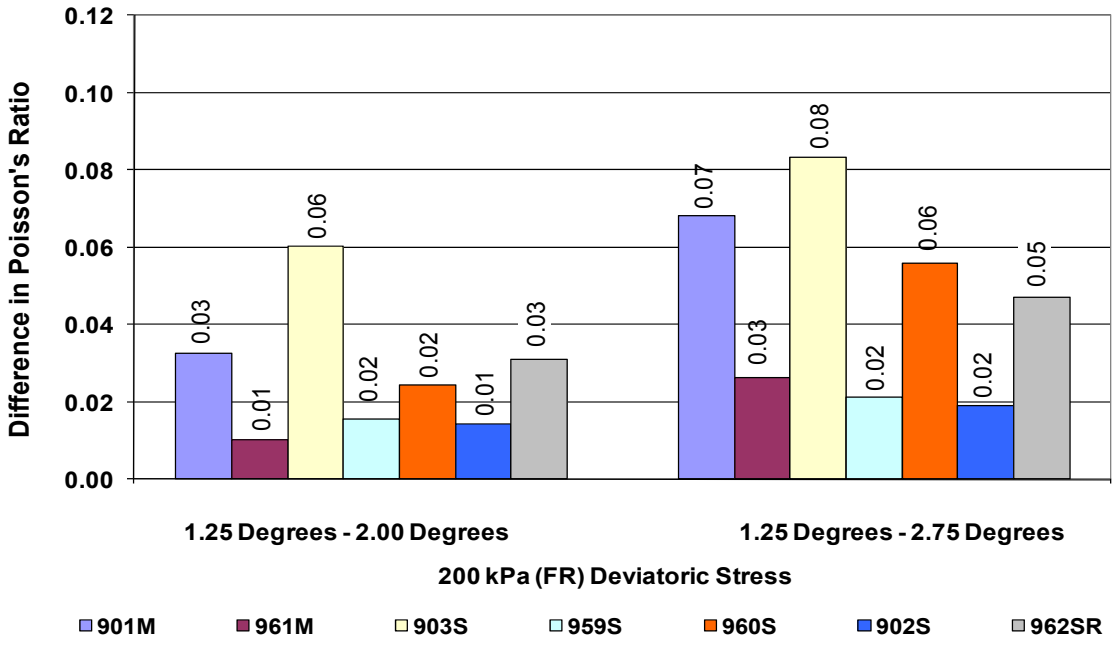

Figure 4.20 Effects of Gyratory Angle on Poisson's Ratio at 200 kPa (FR) Deviatoric Stress States and 10 Hz

The effects of varying deviatoric stress on the Poisson's ratio of the SPS-9A asphalt mixes was investigated across three angles of gyration 1.25°, 2.00° and 2.75° and the results are presented in Figure 4.21 to Figure 4.23.

The conventional SMHI Marshall mix design test sections recorded a decrease in change in Poisson's ratio from 200 kPa to 600 kPa and 200 kPa to 200 kPa (FR) deviatoric stresses at all three angles of gyration as can be seen in Figure 4.21 to Figure 4.23. The Superpave™ mixes however did not show any trend in the difference in Poisson's ratio from 200 kPa to 600 kPa and 200 kPa to 200 kPa (FR) deviatoric stresses at all three angles of gyration. It should however be seen that Superpave™ mix design test section 903S recorded the highest difference in Poisson's ratio from 200 kPa to 600 kPa and 200 kPa to 200 kPa (FR) deviatoric stresses at all three angles of gyration except at 1.25° angle of gyration and 200 kPa to 200 kPa (FR) deviatoric stress, Figure 4.21.

4.2.2.1 Staistical Sensitivity of Poisson's Ratio across Gyration Angle

Statistical analysis of variance (ANOVA) was performed on Poisson's ratio results to evaluate statistical significance at 95 percent confidence level across angle of gyration and mix type. The ANOVA of Poisson's ratio results are shown in Tables 4.33, 4.35 and 4.37 at deviatoric stresses 200 kPa, 600 kPa and 200 kPa fully reversible respectively.

Tukey's homogeneous group analysis for Poisson's ratio results are shown in Tables 4.34, 4.36 and 4.38. There was no significant difference in poisson's ratio results of the Radisson SPS-9A test sections across varied gyratory angle at 200 kPa deviatoric stress except sections 903S which shows significant differences in Poisson's ratio across all three angles of gyration as seen in Table 4.34. It was also noted that only test section 962SR show significant differences in Poisson's ratio results across varied angle of gyration at 600 kPa deviatoric stress as seen in Table 4.36. Test sections 961M, 959S and 902S did not show any significant difference in Poisson's ratio results across varied angle of gyration at 200 kPa fully reversed deviatori stress.

Table 4.33 Analysis of Variance for Poisson's Ratio at 200 kPa Deviatoric Stress across Radisson SPS-9A Asphalt Mixes

Parameter	Sum of Squares	Degrees of Freedom	Mean Squares	F-Test Statistic	P-value	Sig.
Mix Type	0.029	6	0.004	5	0.002	
Angle of Gyration	0.017	2	0.002	4	0.003	
Mix Type*Angle of Gyration	0.027	12	0.003	11	0.086	No
Error	0.013	15	0.001			

Table 4.34 Tukey's Homogeneous Groups for Poisson's Ratio at 200 kPa Deviatoric Stress across Radisson SPS-9A Asphalt Mixes

Test Section	Angle of Gyration (°)	Poisson's Ratio	Tukey's Homogeneous Groups		
901M	1.25	0.28	A		
	2.00	0.36	A		
	2.75	0.39	A		
961M	1.25	0.32	A		
	2.00	0.33	A		
	2.75	0.35	A		
903S	1.25	0.28	A		
	2.00	0.29		B	
	2.75	0.31			C
959S	1.25	0.29	A		
	2.00	0.27	A		
	2.75	0.25	A		
960S	1.25	0.27	A		
	2.00	0.27	A		
	2.75	0.30	A		
902S	1.25	0.26	A		
	2.00	0.27	A		
	2.75	0.28	A		
962SR	1.25	0.31	A		
	2.00	0.32	A		
	2.75	0.37	A		

Table 4.35 Analysis of Variance for Poisson's Ratio at 600 kPa Deviatoric Stress across Radisson SPS-9A Asphalt Mixes

Parameter	Sum of Squares	Degrees of Freedom	Mean Squares	F-Test Statistic	P-value	Sig.
Mix Type	0.015	6	0.002	2	0.017	No
Angle of Gyration	0.014	2	0.017	3	0.369	
Mix Type*Angle of Gyration	0.017	12	0.001	1	0.880	
Error	0.013	15	0.001			

Table 4.36 Tukey's Homogeneous Groups for Poisson's Ratio at 600 kPa Deviatoric Stress across Radisson SPS-9A Asphalt Mixes

Test Section	Angle of Gyration (°)	Poisson's Ratio	Tukey's Homogeneous Groups		
901M	1.25	0.32	A		
	2.00	0.33	A		
	2.75	0.37	A		
961M	1.25	0.38	A		
	2.00	0.38	A		
	2.75	0.41	A		
903S	1.25	0.35	A		
	2.00	0.35	A		
	2.75	0.36	A		
959S	1.25	0.28	A		
	2.00	0.29	A		
	2.75	0.27	A		
960S	1.25	0.31	A		
	2.00	0.32	A		
	2.75	0.33	A		
902S	1.25	0.27	A		
	2.00	0.28	A		
	2.75	0.28	A		
962SR	1.25	0.32	A	B	C
	2.00	0.33		B	C
	2.75	0.36			C

Table 4.37 Analysis of Variance for Poisson's Ratio at 200 kPa Fully Reversed Deviatoric Stress across Radisson SPS-9A Asphalt Mixes

Parameter	Sum of Squares	Degrees of Freedom	Mean Squares	F-Test Statistic	P-value	Sig.
Mix Type	0.013	6	0.004	3	0.036	Yes
Angle of Gyration	0.003	2	0.002	7	0.315	
Mix Type*Angle of Gyration	0.002	12	0.001	2	0.953	
Error	0.032	15	0.001			

Table 4.38 Tukey's Homogeneous Groups for Poisson's Ratio at 200 kPa Fully Reversed Deviatoric Stress across Radisson SPS-9A Asphalt Mixes

Test Section	Angle of Gyration (°)	Poisson's Ratio	Tukey's Homogeneous Groups		
901M	1.25	0.31	A		
	2.00	0.34		B	C
	2.75	0.38		B	C
961M	1.25	0.36	A		
	2.00	0.37	A		
	2.75	0.38	A		
903S	1.25	0.31	A		
	2.00	0.37		B	C
	2.75	0.39		B	C
959S	1.25	0.27	A		
	2.00	0.26	A		
	2.75	0.25	A		
960S	1.25	0.32	A	B	
	2.00	0.34	A	B	
	2.75	0.37			C
902S	1.25	0.28	A		
	2.00	0.30	A		
	2.75	0.30	A		
962SR	1.25	0.34	A		
	2.00	0.37		B	C
	2.75	0.38		B	C

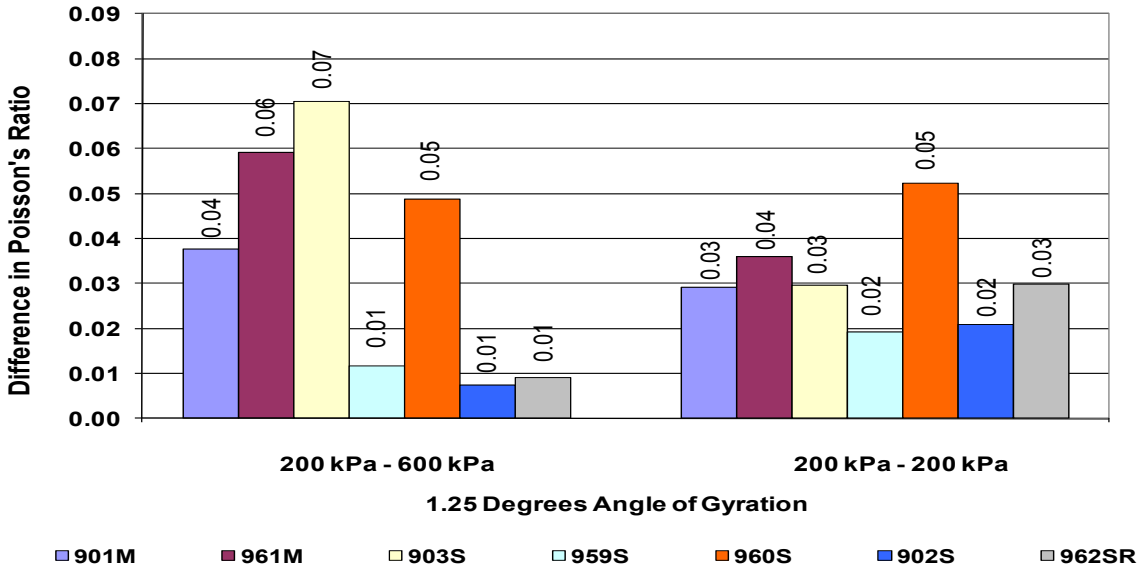

Figure 4.21 Effects of Deviatoric Stress States on Poisson's Ratio at 1.25° Angle of Gyration and 10 Hz

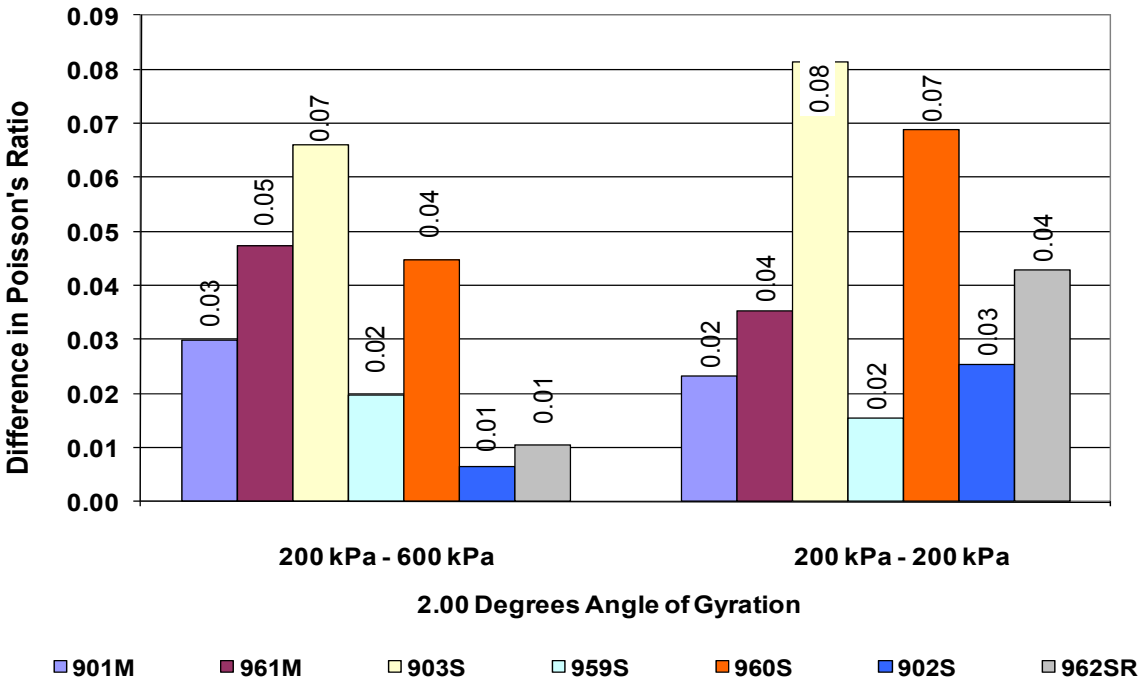

Figure 4.22 Effects of Deviatoric Stress States on Poisson's Ratio at 2.00° Angle of Gyration and 10 Hz

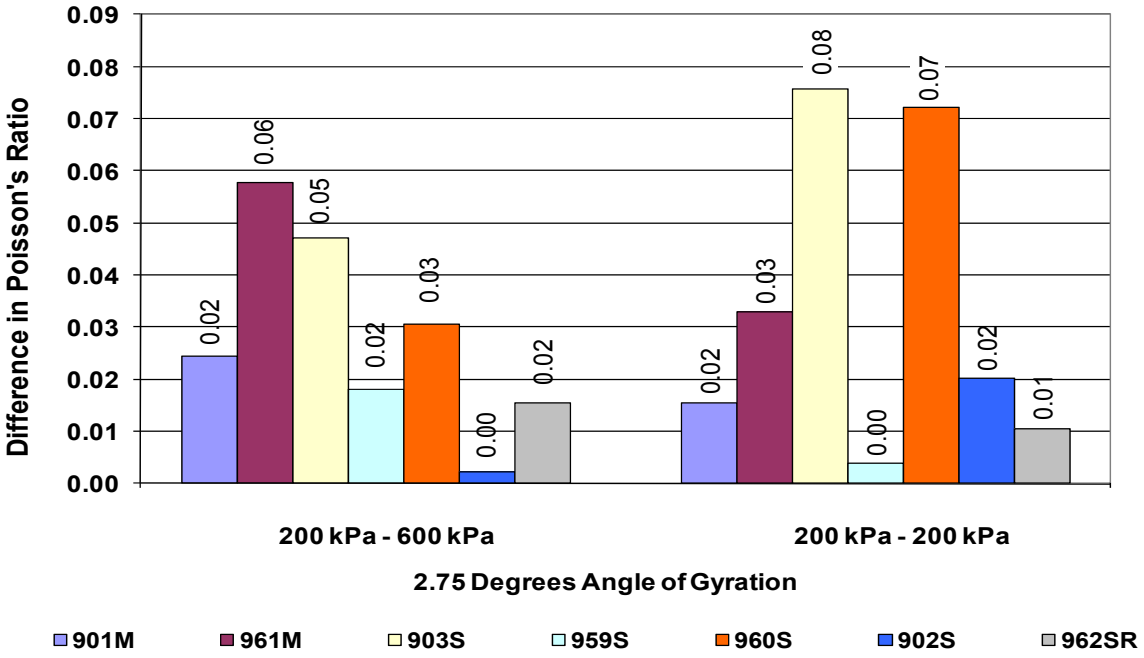

Figure 4.23 Effects of Deviatoric Stress States on Poisson's Ratio at 2.75° Angle of Gyration and 10 Hz

4.2.2.2 Staistical Sensitivity of Poisson's Ratio across Deviatoric Stress

Statistical analysis of variance was performed on Poisson's ratio values in order to investigate the sensitivity of the Radisson SPS-9A asphalt mixes to varied deviatoric stress. Analysis of variance for Poisson's ratio characterization is summarized in Tables 4.39, 4.41 and 4.43 and Tukey's groups are presented in Tables 4.40, 4.42 and 4.44. As seen in Tables 4.39, 4.41 and 4.43, there was significant difference in Poisson's ratio as a function of deviatoric stress at all angles of gyration across most of the Radisson SPS-9A test sections.

It was noted that there was no significance in Poisson's ratio at all deviatoric stresses across most of the test sections at 1.25° angle of gyration, as seen in Table 4.40. Test section 903S showed significance in Poisson's ratio across all deviatoric stresses at 1.25° angle of gyration.

Test sections 901M, 959S, 960S and 902S did not show any significance in Poisson's ratio across all deviatoric stresses at 2.00° angle of gyration, as seen in Table 4.42. There was interaction between Poisson's ratio at 200 kPa and 600 kPa and 200 kPa fully reversed deviatoric stresses for test section 961M at 2.00° angle of gyration. Test section 903S displays Poisson's ratio significantly different at 200 kPa relative to 600 kPa and 200 kPa fully reversed deviatoric stresses at 2.00° angle of gyration.

Poisson's ratio at 2.75° angle of gyration was not different at all deviatoric stresses across test sections 901M, 959S, 9009060 and 902S, as seen in Table 4.44. There was interaction between Poisson's ratio at 200 kPa and 600 kPa and 200 kPa fully reversed deviatoric stresses for test section 961M and 962SR at 2.75° angle of gyration. Test section 903S displays Poisson's ratio significantly different at 200 kPa relative to 600 kPa and 200 kPa fully reversed deviatoric stresses at 2.75° angle of gyration.

Table 4.39 Analysis of Variance for Poisson's Ratio at 1.25° Angle of Gyration across Radisson SPS-9A Asphalt Mixes

Parameter	Sum of Squares	Degrees of Freedom	Mean Squares	F-Test Statistic	P-value	Sig.
Poisson's Ratio	0.002	2	0.001	0.96	0.000	
Deviatoric Stress	0.033	2	0.016	25.62	0.000	
Poisson's Ratio *Deviatoric Stress	0.008	4	0.001	2.15	0.000	Yes
Error	0.015	16	0.001			

Table 4.40 Tukey's Homogeneous Groups for Poisson's Ratio at 1.25° Angle of Gyration across Radisson SPS-9A Asphalt Mixes

Test Section	Deviatoric Stress (kPa)	Poisson's Ratio	Tukey's Homogeneous Groups		
901M	200	0.28	A		
	600	0.32	A		
	200 (FR)	0.31	A		
961M	200	0.32	A		
	600	0.38	A		
	200 (FR)	0.36	A		
903S	200	0.28	A		
	600	0.35		B	
	200 (FR)	0.31			C
959S	200	0.29	A		
	600	0.28	A		
	200 (FR)	0.27	A		
960S	200	0.27	A		
	600	0.31	A		
	200 (FR)	0.32	A		
902S	200	0.26	A		
	600	0.27	A		
	200 (FR)	0.28	A		
962SR	200	0.31	A		
	600	0.32	A		
	200 (FR)	0.34	A		

Table 4.41 Analysis of Variance for Poisson's Ratio at 2.00° Angle of Gyration across Radisson SPS-9A Asphalt Mixes

Parameter	Sum of Squares	Degrees of Freedom	Mean Squares	F-Test Statistic	P-value	Sig.
Poisson's Ratio	0.006	2	0.002	3.713	0.025	Yes
Deviatoric Stress	0.034	2	0.017	32.542	0.000	
Poisson's Ratio *Deviatoric Stress	0.001	4	0.001	0.387	0.880	
Error	0.013	16	0.001			

Table 4.42 Tukey's Homogeneous Groups for Poisson's Ratio at 2.00° Angle of Gyration across Radisson SPS-9A Asphalt Mixes

Test Section	Deviatoric Stress (kPa)	Poisson's Ratio	Tukey's Homogeneous Groups		
901M	200	0.36	A		
	600	0.33	A		
	200 (FR)	0.34	A		
961M	200	0.33	A		
	600	0.38	A		B
	200 (FR)	0.37			B
903S	200	0.29	A		
	600	0.35			B
	200 (FR)	0.37			B
959S	200	0.27	A		
	600	0.29	A		
	200 (FR)	0.26	A		
960S	200	0.27	A		
	600	0.32	A		
	200 (FR)	0.34	A		
902S	200	0.27	A		
	600	0.28	A		
	200 (FR)	0.30	A		
962SR	200	0.32	A		
	600	0.33	A		B
	200 (FR)	0.37			B

Table 4.43 Analysis of Variance for Poisson's Ratio at 2.75° Angle of Gyration across Radisson SPS-9A Asphalt Mixes

Parameter	Sum of Squares	Degrees of Freedom	Mean Squares	F-Test Statistic	P-value	Sig.
Poisson's Ratio	0.013	2	0.004	3.331	0.036	
Deviatoric Stress	0.003	2	0.002	21.13	0.315	
Poisson's Ratio *Deviatoric Stress	0.002	4	0.001	0.254	0.953	Yes
Error	0.032	16	0.001			

Table 4.44 Tukey's Homogeneous Groups for Poisson's Ratio at 2.75° Angle of Gyration across Radisson SPS-9A Asphalt Mixes

Test Section	Deviatoric Stress (kPa)	Poisson's Ratio	Tukey's Homogeneous Groups		
901M	200	0.39	A		
	600	0.37	A		
	200 (FR)	0.38	A		
961M	200	0.35	A		
	600	0.41	A		B
	200 (FR)	0.38			B
903S	200	0.31	A		
	600	0.36			B
	200 (FR)	0.39			B
959S	200	0.25	A		
	600	0.27	A		
	200 (FR)	0.25	A		
960S	200	0.30	A		
	600	0.33	A		
	200 (FR)	0.37	A		
902S	200	0.28	A		
	600	0.28	A		
	200 (FR)	0.30	A		
962SR	200	0.37	A		
	600	0.36			B
	200 (FR)	0.38	A		

4.2.3 Phase Angle Characterization of Radisson SPS-9A Mixes

Phase angle, δ, is the lag between applied stress and resultant strain. Phase angle is an indicator of visco-elastic material properties. Table 4.45 to Table 4.47 and Figure 4.24 to Figure 4.26 show the phase angle of research mixes at 10 Hz and 20°C across three levels of deviatoric stresses. The error bars shown in Figure 4.24 to Figure 4.26 represent minimum and maximum deviation from the mean phase angle of three gyratory compactor samples used in the frequency sweep characterization.

Phase angle was found to increase with increase in deviatoric stress at all three angles of gyration across all test sections as can be seen in Figure 4.24 to Figure 4.26. The highest average phase angle values were recorded at 200 kPa fully reversed deviatoric stress across all test sections. The highest average phase angle of 30.2° was recorded at 2.75° angle of gyration and 200 kPa fully reversed deviatoric stress, Figure 4.26.

It should be noted that the Superpave™ mix design test sections 959S and 902S have the lowest phase angle values at all three angles of gyration and deviatoric stresses.

Table 4.45 Phase Angle across Deviatoric Stress States at 1.25° Angle of Gyration and 10 Hz

SPS-9A Test Section	Deviatoric Stress (kPa)	Phase Angle δ (Degrees)	Deviation from Mean	
			Minimum	Maximum
901M	200	19.5	17.9	20.8
	600	21.0	20.4	21.4
	200 (FR)	25.2	23.6	26.2
961M	200	21.8	21.1	23.0
	600	24.3	23.6	25.0
	200 (FR)	28.4	27.4	29.1
903S	200	20.6	19.9	21.3
	600	23.2	22.9	23.6
	200 (FR)	25.1	24.5	25.9
959S	200	19.4	18.6	20.2
	600	21.0	20.3	21.4
	200 (FR)	23.9	23.6	24.2
960S	200	21.5	20.2	22.3
	600	23.6	23.4	23.9
	200 (FR)	26.5	25.0	28.1
902S	200	18.6	17.8	19.0
	600	21.9	21.5	22.1
	200 (FR)	24.2	22.7	25.1
962SR	200	19.4	19.3	19.5
	600	23.1	23.0	23.9
	200 (FR)	27.0	26.1	27.7

Table 4.46 Phase Angle across Deviatoric Stress States at 2.00° Angle of Gyration and 10 Hz

SPS-9A Test Section	Deviatoric Stress (kPa)	Phase Angle δ (Degrees)	Deviation from Mean	
			Minimum	Maximum
901M	200	23.0	22.3	23.7
	600	22.8	21.5	23.7
	200 (FR)	27.5	24.5	30.0
961M	200	23.2	22.4	24.5
	600	24.8	24.5	24.9
	200 (FR)	28.8	28.5	29.1
903S	200	20.4	20.0	21.8
	600	22.6	22.3	23.9
	200 (FR)	24.8	23.0	25.9
959S	200	18.0	17.2	19.6
	600	19.1	18.8	19.7
	200 (FR)	22.1	21.9	22.2
960S	200	19.9	19.6	20.3
	600	22.2	21.9	22.5
	200 (FR)	26.2	25.9	26.4
902S	200	18.6	17.8	19.0
	600	21.8	21.4	22.0
	200 (FR)	24.5	23.0	25.4
962SR	200	19.8	19.0	21.0
	600	23.1	22.6	23.6
	200 (FR)	27.9	27.6	28.4

Table 4.47 Phase Angle across Deviatoric Stress States at 2.75° Angle of Gyration and 10 Hz

SPS-9A Test Section	Deviatoric Stress (kPa)	Phase Angle δ (Degrees)	Deviation from Mean	
			Minimum	Maximum
901M	200	23.0	22.3	23.9
	600	23.3	23.2	23.4
	200 (FR)	28.1	26.7	30.7
961M	200	24.0	22.3	25.9
	600	24.9	24.7	25.2
	200 (FR)	30.2	29.1	31.5
903S	200	21.2	20.2	22.2
	600	23.4	23.0	23.7
	200 (FR)	27.8	26.5	28.6
959S	200	16.9	16.3	17.4
	600	18.3	18.2	18.5
	200 (FR)	21.8	20.8	22.8
960S	200	20.5	19.6	21.8
	600	22.6	22.4	23.0
	200 (FR)	28.4	26.7	29.3
902S	200	17.5	16.5	18.3
	600	20.0	19.2	21.1
	200 (FR)	23.3	22.1	24.3
962SR	200	20.9	20.4	21.4
	600	23.4	23.2	23.6
	200 (FR)	28.1	27.7	28.4

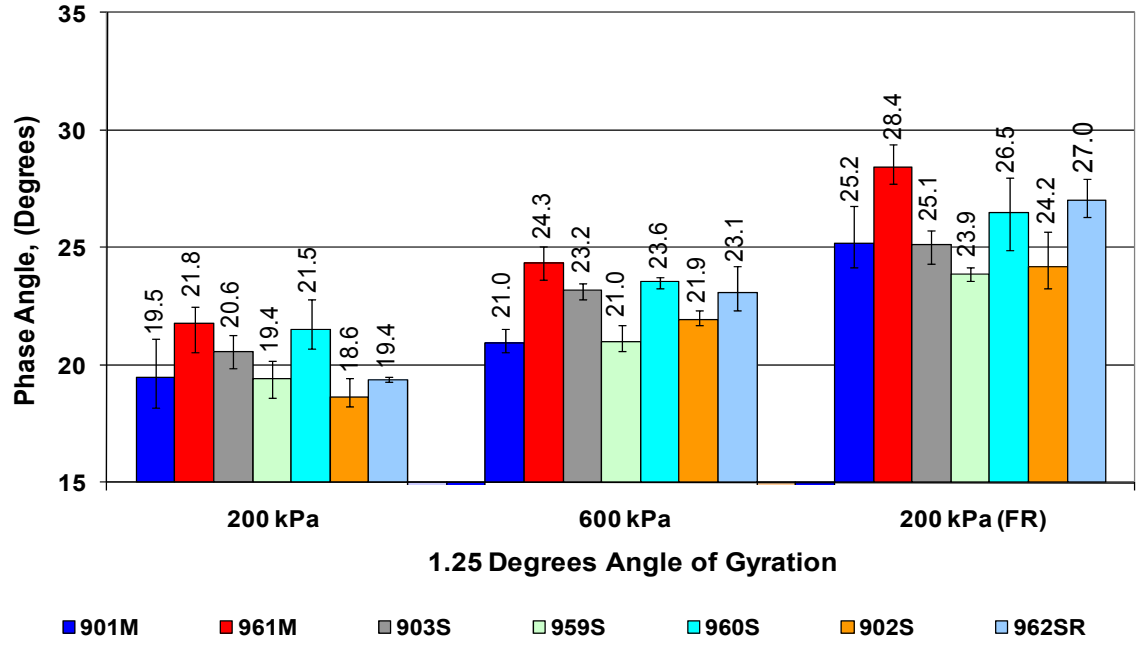

Figure 4.24 Phase Angle across Deviatoric Stress States at 1.25° Angle of Gyration and 10 Hz

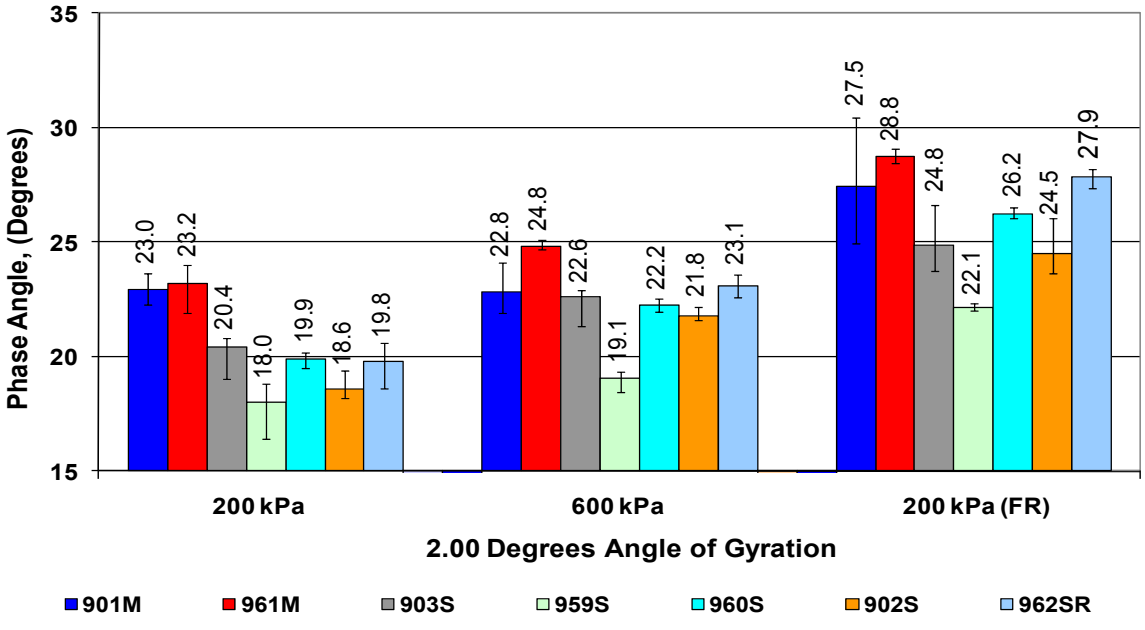

Figure 4.25 Phase Angle across Deviatoric Stress States at 2.00° Angle of Gyration and 10 Hz

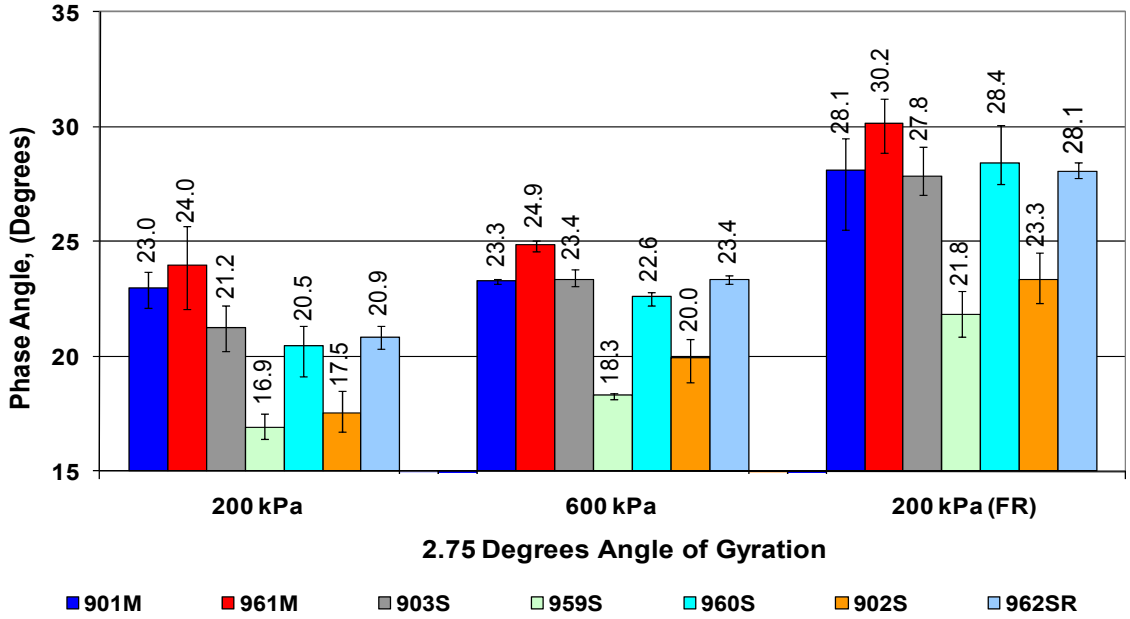

Figure 4.26 Phase Angle across Deviatoric Stress States at 2.75° Angle of Gyration and 10 Hz

The effects of varying angle of gyration on the phase angle of the SPS-9A asphalt mixes have been investigated across three deviatoric stress states of 200 kPa, 600 kPa and 200 kPa (FR) and the results are presented in Figure 4.27 to Figure 4.29. The Superpave^{TM} recommended angle of gyration 1.25° is set as a base for the analysis. The difference in phase angle from 1.25° to 2.00° angles of gyration was compared to difference in phase angle from 1.25° to 2.75° angles of gyration and the results are presented for each test section.

There was increase in difference in phase angle from 1.25° to 2.00° angles of gyration to 1.25° to 2.75° angles of gyration at 200 kPa and 200 kPa (FR) deviatoric stresses across all test sections as seen in Figures 4.27 and 4.29. It should however be seen that at 600 kPa deviatoric stress some test sections recorded decrease in difference in phase angle from 1.25° to 2.00° angles of gyration to 1.25° to 2.75° angles of gyration as seen in Figure 4.28.

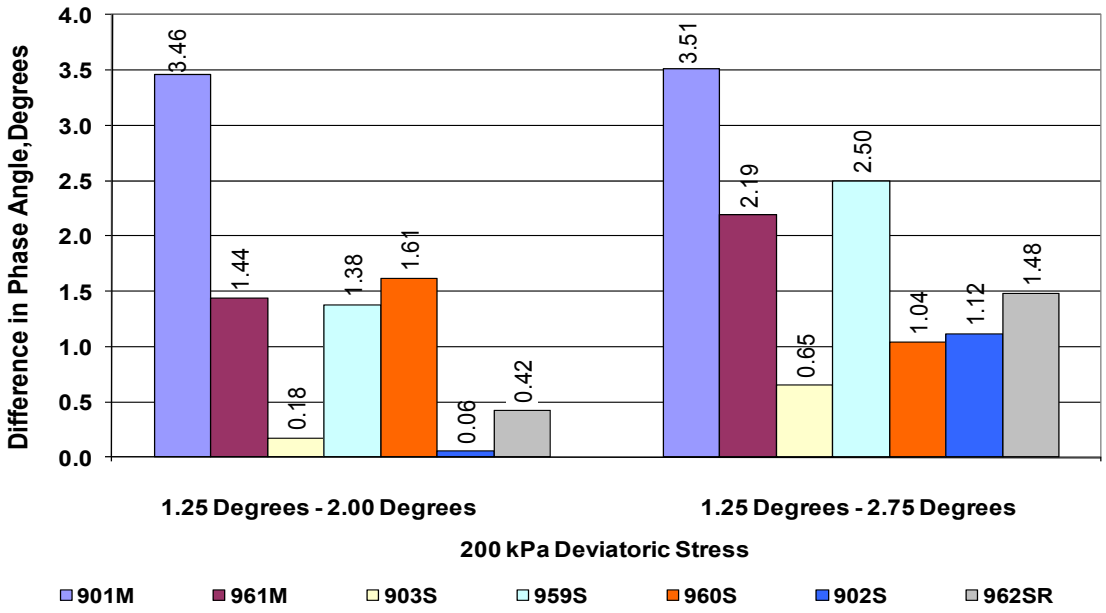

Figure 4.27 Effects of Gyratory Angle on Phase Angle at 200 kPa Deviatoric Stress States and 10 Hz

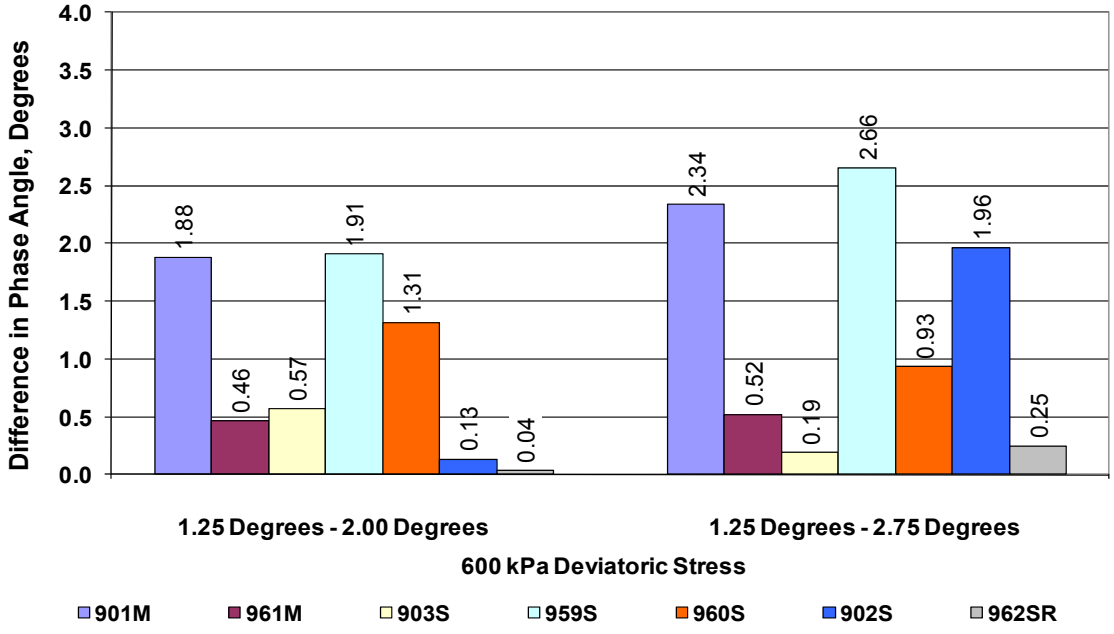

Figure 4.28 Effects of Gyratory Angle on Phase Angle at 600 kPa Deviatoric Stress States and 10 Hz

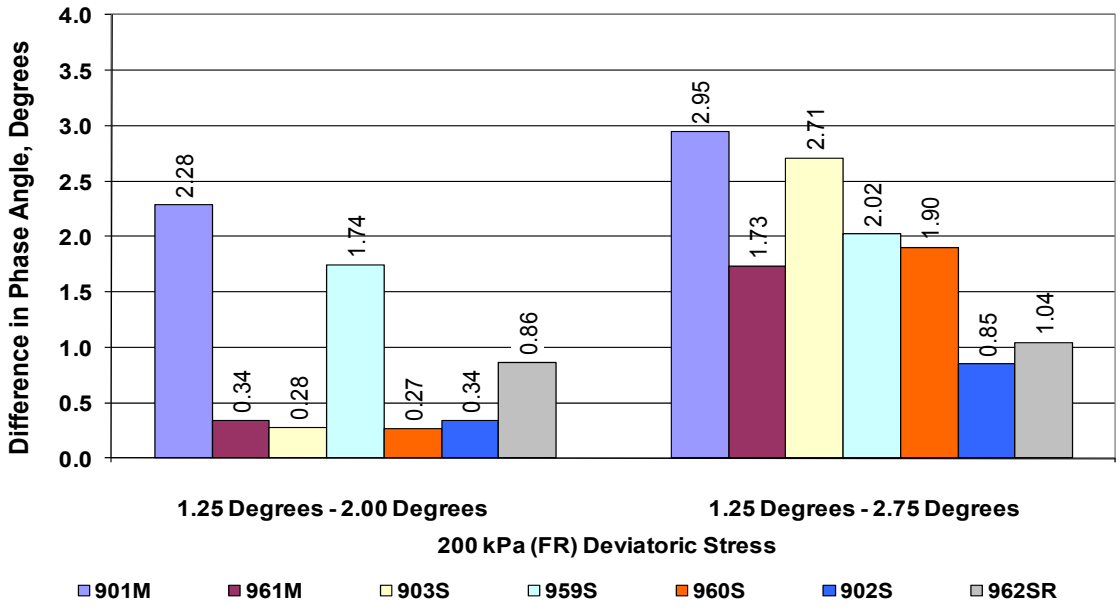

Figure 4.29 Effects of Gyratory Angle on Phase Angle at 200 kPa (FR) Deviatoric Stress States and 10 Hz

The effects of varying deviatoric stress on the phase angle of the Radisson SPS-9A asphalt mixes was investigated across three angles of gyration 1.25°, 2.00° and 2.75° and the results are presented in Figure 4.30 to Figure 4.32.

Phase angle was found to be sensitive to deviatoric stress as shown by the significant increase in difference in phase angle from 200 kPa to 600 kPa compared to 200 kPa to 200 kPa (FR) deviatoric stresses as seen in Figure 4.30 to Figure 4.32.

4.2.3.1 Staistical Sensitivity of Phase Angle across Gyration Angle

Statistical analysis of variance (ANOVA) was performed on phase angle results to evaluate statistical significance at 95 percent confidence level across angle of gyration and mix type. The ANOVA of phase angle results are shown in Tables 4.48, 4.50 and 4.52 at deviatoric stresses 200 kPa, 600 kPa and 200 kPa fully reversible respectively. As seen in Tables 4.48 and 4.50, there was no significant difference in phase angle values of the Radisson SPS-9A test sections across varied angle of gyration at 200 kPa and 600 kPa deviatoric stresses.

Tukey's homogeneous group analysis for Phase angle results are shown in Tables 4.49, 4.51 and 4.53. There was no significant difference in Phase angle results of the Radisson SPS-9A test sections across varied gyratory angle at 200 kPa deviatoric stress except sections 901M which shows significant differences in Phase angle at 1.25° angle of gyration compared to 2.00° and 2.75° angles of gyration as seen in Table 4.49. Only test section 902S shows significant difference in phase angle results across varied angle of gyration at 600 kPa deviatoric stress as seen in Table 4.51. Test sections 901M, 961M and 962SR did not show significant differences in phase angle results across varied angle of gyration at 200 kPa fully reversed deviatoric stress as seen in Table 4.53.

Table 4.48 Analysis of Variance for Phase Angle at 200 kPa Deviatoric Stress across Radisson SPS-9A Asphalt Mixes

Parameter	Sum of Squares	Degrees of Freedom	Mean Squares	F-Test Statistic	P-value	Sig.
Mix Type	191	6	24	25		
Angle of Gyration	198	2	25	13	0.030	
Mix Type*Angle of Gyration	136	12	17	7	0.602	No
Error	38	15	9			

Table 4.49 Tukey's Homogeneous Groups for Phase Angle at 200 kPa Deviatoric Stress across Radisson SPS-9A Asphalt Mixes

Test Section	Angle of Gyration (°)	Phase Angle (°)	Tukey's Homogeneous Groups		
901M	1.25	19.5	A		
	2.00	23.0		B	C
	2.75	23.0		B	C
961M	1.25	21.8	A		
	2.00	23.2	A		
	2.75	24.0	A		
903S	1.25	20.6	A		
	2.00	20.4	A		
	2.75	21.2	A		
959S	1.25	19.4	A		
	2.00	18.0	A		
	2.75	16.9	A		
960S	1.25	21.5	A		
	2.00	19.9	A		
	2.75	20.5	A		
902S	1.25	18.6	A		
	2.00	18.6	A		
	2.75	17.5	A		
962SR	1.25	19.4	A		
	2.00	19.8	A		
	2.75	20.9	A		

Table 4.50 Analysis of Variance for Phase Angle at 600 kPa Deviatoric Stress across Radisson SPS-9A Asphalt Mixes

Parameter	Sum of Squares	Degrees of Freedom	Mean Squares	F-Test Statistic	P-value	Sig.
Mix Type	219	6	15	28	0.000	
Angle of Gyration	168	2	52	17	0.704	
Mix Type*Angle of Gyration	11	12	13	6		No
Error	18	15	7			

Table 4.51 Tukey's Homogeneous Groups for Phase Angle at 600 kPa Deviatoric Stress across Radisson SPS-9A Asphalt Mixes

Test Section	Angle of Gyration (°)	Phase Angle (°)	Tukey's Homogeneous Groups		
901M	1.25	21.0	A		
	2.00	22.8	A		
	2.75	23.3	A		
961M	1.25	24.3	A		
	2.00	24.8	A		
	2.75	24.9	A		
903S	1.25	23.2	A		
	2.00	22.6	A		
	2.75	23.4	A		
959S	1.25	21.0	A		
	2.00	19.1	A		
	2.75	18.3	A		
960S	1.25	23.6	A		
	2.00	22.2	A		
	2.75	22.6	A		
902S	1.25	21.9	A	B	
	2.00	21.8	A	B	C
	2.75	20.0			C
962SR	1.25	23.1	A		
	2.00	23.1	A		
	2.75	23.4	A		

Table 4.52 Analysis of Variance for Phase Angle at 200 kPa Fully Reversed Deviatoric Stress across Radisson SPS-9A Asphalt Mixes

Parameter	Sum of Squares	Degrees of Freedom	Mean Squares	F-Test Statistic	P-value	Sig.
Mix Type	145	6	13	39		
Angle of Gyration	114	2	11	11	0.000	
Mix Type*Angle of Gyration	22	12	2	2	0.202	Yes
Error	9	15	1			

Table 4.53 Tukey's Homogeneous Groups for Phase Angle at 200 kPa Fully Reversed Deviatoric Stress across Radisson SPS-9A Asphalt Mixes

Test Section	Angle of Gyration (°)	Phase Angle (°)	Tukey's Homogeneous Groups		
901M	1.25	25.2	A		
	2.00	27.5	A		
	2.75	28.1	A		
961M	1.25	28.4	A		
	2.00	28.8	A		
	2.75	30.2	A		
903S	1.25	25.1	A		C
	2.00	24.8	A	B	
	2.75	27.8			C
959S	1.25	23.9	A	B	
	2.00	22.1	A	B	
	2.75	21.8			C
960S	1.25	26.5	A	B	
	2.00	26.2	A	B	
	2.75	28.4			C
902S	1.25	24.2	A	B	
	2.00	24.5	A	B	
	2.75	23.3			C
962SR	1.25	27.0	A		
	2.00	27.9	A		
	2.75	28.1	A		

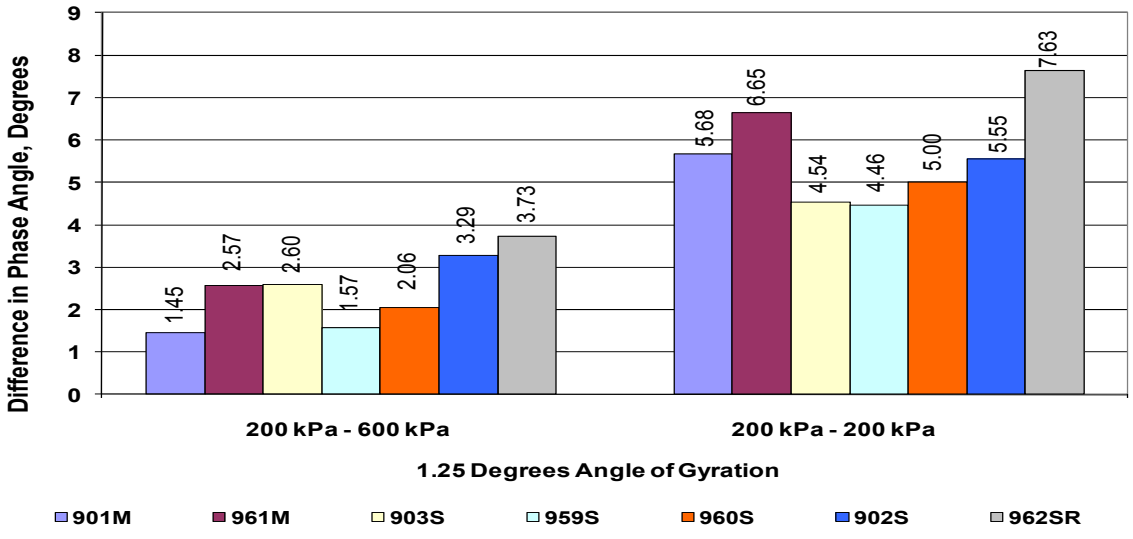

Figure 4.30 Effects of Deviatoric Stress States on Phase Angle at 1.25° Angle of Gyration and 10 Hz

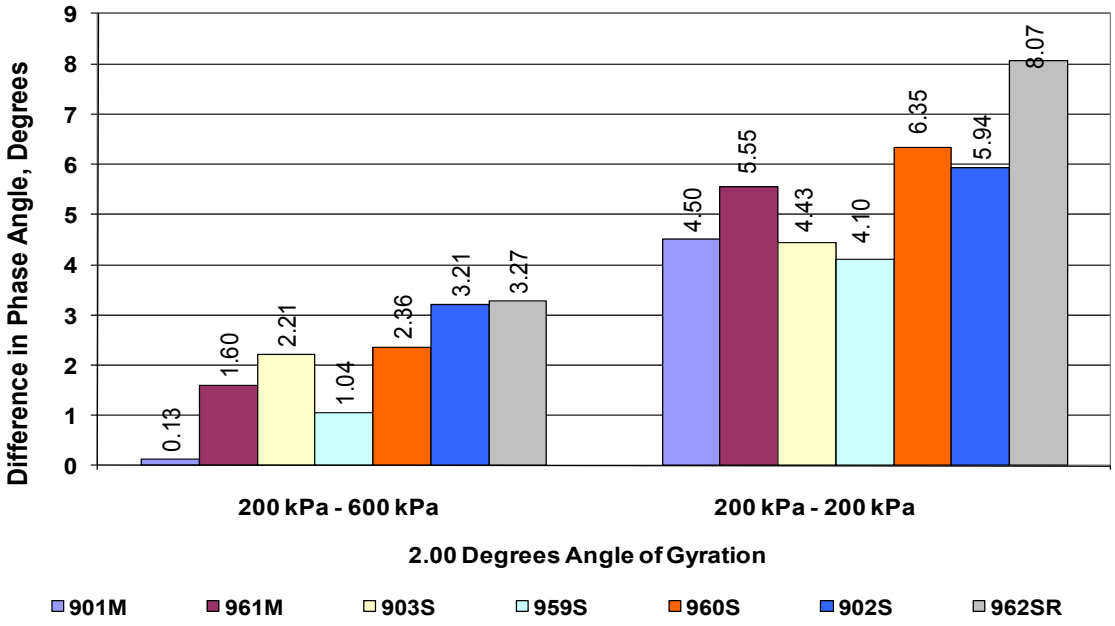

Figure 4.31 Effects of Deviatoric Stress States on Phase Angle at 2.00° Angle of Gyration and 10 Hz

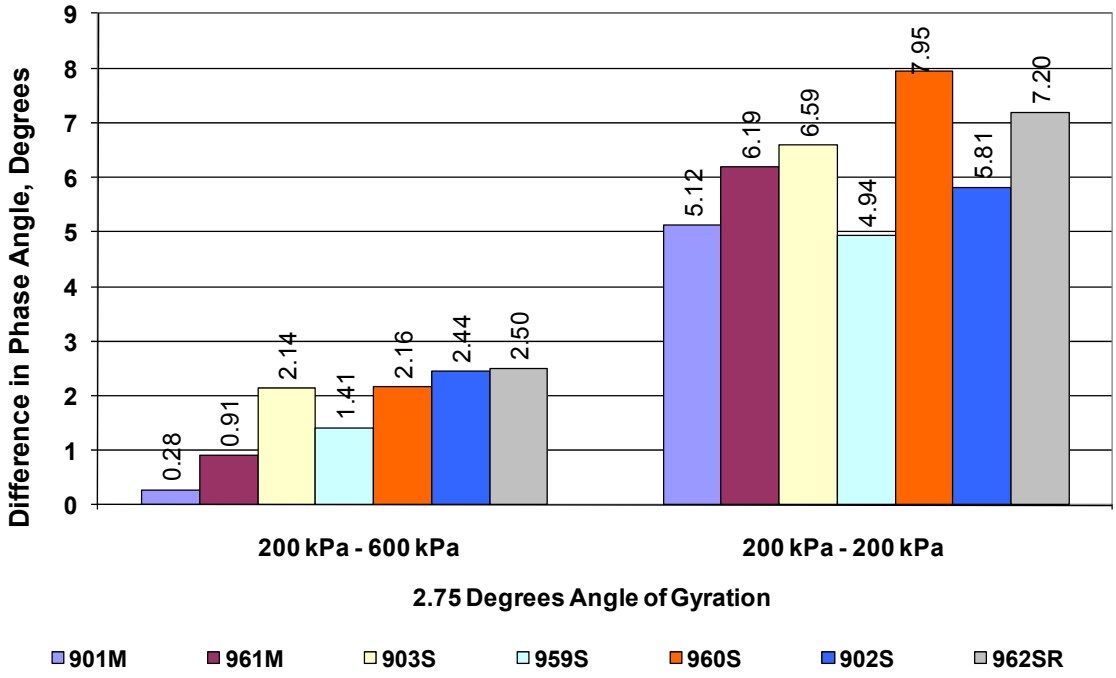

Figure 4.32 Effects of Deviatoric Stress States on Phase Angle at 2.75° Angle of Gyration and 10 Hz

4.2.3.2 Staistical Sensitivity of Phase Angle across Deviatoric Stress

Statistical analysis of variance was performed on phase angle values in order to investigate the sensitivity of the Radisson SPS-9A asphalt mixes to varied deviatoric stress. Analysis of variance for phase angle characterization is summarized in Tables 4.54, 4.56 and 4.58 and Tukey's groups are presented in Tables 4.55, 4.57 and 4.59. As seen in Tables 4.54, 4.56 and 4.58, there was significant difference in phase angle as a function of deviatory stress at all angles of gyration across most of the Radisson SPS-9A test sections.

Phase angle was significantly different across all deviatory stresses at 1.25° angle of gyration for test sections 961M, 903S, 902S and 962SR as seen in Table 4.55. However, phase angle across 200 kPa and 600 kPa deviatory stresses was significantly different relative to phase angle at 200 kPa fully reversed deviatory stress at 1.25° angle of gyration for test sections 901M and 960S. It should be noted that there was no significant difference in phase angle across all deviatory stresses at 1.25° angle of gyration for test section 959S.

Phase angle across 200 kPa and 600 kPa deviatory stresses was significantly different relative to phase angle at 200 kPa fully reversed deviatory stress at 2.00° angle of gyration for test sections 901M and 961M, as seen in Table 4.57. There was no significant difference in phase angle across all deviatory stresses at 2.00° angle of gyration for test section 903S and 959S. Phase angle was significantly different across all deviatory stresses at 2.00° angle of gyration for test sections 960S and 962SR. phase angle across 200 kPa fully reversed and 600 kPa deviatory stresses was significantly different relative to phase angle at 200 kPa deviatory stress at 2.00° angle of gyration for test sections 902S.

Phase angle across 200 kPa and 600 kPa deviatory stresses was significantly different relative to phase angle at 200 kPa fully reversed deviatory stress at 2.75° angle of gyration for most of the SPS-9A test sections. However, phase angle was significantly different across all deviatory stresses at 2.75° angle of gyration for test sections 962SR as seen in Table 4.59.

Table 4.54 Analysis of Variance for Phase Angle at 1.25° Angle of Gyration across Radisson SPS-9A Asphalt Mixes

Parameter	Sum of Squares	Degrees of Freedom	Mean Squares	F-Test Statistic	P-value	Sig.
Phase Angle	210	2	19	32		
Deviatoric Stress	153	2	51	16	0.000	
Phase Angle *Deviatoric Stress	52	4	26	0.4	0.854	Yes
Error	38	16	2			

Table 4.55 Tukey's Homogeneous Groups for Phase Angle at 1.25° Angle of Gyration across Radisson SPS-9A Asphalt Mixes

Test Section	Deviatoric Stress (kPa)	Phase Angle (Degree)	Tukey's Homogeneous Groups		
901M	200	19.5	A	B	
	600	21.0	A	B	
	200 (FR)	25.2			C
961M	200	21.8	A		
	600	24.3		B	
	200 (FR)	28.4			C
903S	200	20.6	A		
	600	23.2		B	
	200 (FR)	25.1			C
959S	200	19.4	A		
	600	21.0	A		
	200 (FR)	23.9	A		
960S	200	21.5	A	B	
	600	23.6	A	B	
	200 (FR)	26.5			C
902S	200	18.6	A		
	600	21.9		B	
	200 (FR)	24.2			C
962SR	200	19.4	A		
	600	23.1		B	
	200 (FR)	27.0			C

Table 4.56 Analysis of Variance for Phase Angle at 2.00° Angle of Gyration across Radisson SPS-9A Asphalt Mixes

Parameter	Sum of Squares	Degrees of Freedom	Mean Squares	F-Test Statistic	P-value	Sig.
Phase Angle	174.2	2	15.84	66.99	0.000	
Deviatoric Stress	158.4	2	52.81	7.17	0.004	
Phase Angle *Deviatoric Stress	11.3	4	5.65	0.96	0.473	Yes
Error	18.9	16	0.75			

Table 4.57 Tukey's Homogeneous Groups for Phase Angle at 2.00° Angle of Gyration across Radisson SPS-9A Asphalt Mixes

Test Section	Deviatoric Stress (kPa)	Phase Angle (Degree)	Tukey's Homogeneous Groups		
901M	200	23.0	A	B	
	600	22.8	A	B	
	200 (FR)	27.5			C
961M	200	23.2	A	B	
	600	24.8	A	B	
	200 (FR)	28.8			C
903S	200	20.4	A		
	600	22.6	A		
	200 (FR)	24.8	A		
959S	200	18.0	A		
	600	19.1	A		
	200 (FR)	22.1	A		
960S	200	19.9	A		
	600	22.2		B	
	200 (FR)	26.2			C
902S	200	18.6	A		
	600	21.8		B	C
	200 (FR)	24.5		B	C
962SR	200	19.8	A		
	600	23.1		B	
	200 (FR)	27.9			C

Table 4.58 Analysis of Variance for Phase Angle at 2.75° Angle of Gyration across Radisson SPS-9A Asphalt Mixes

Parameter	Sum of Squares	Degrees of Freedom	Mean Squares	F-Test Statistic	P-value	Sig.
Phase Angle	145	2	13	39		
Deviatoric Stress	114	2	11	11	0.000	
Phase Angle *Deviatoric Stress	22	4	2	2	0.202	Yes
Error	9	16	1			

Table 4.59 Tukey's Homogeneous Groups for Phase Angle at 2.75° Angle of Gyration across Radisson SPS-9A Asphalt Mixes

Test Section	Deviatoric Stress (kPa)	Phase Angle (Degree)	Tukey's Homogeneous Groups		
901M	200	23.0	A	B	
	600	23.3	A	B	
	200 (FR)	28.1			C
961M	200	24.0	A	B	
	600	24.9	A	B	
	200 (FR)	30.2			C
903S	200	21.2	A	B	
	600	23.4	A	B	
	200 (FR)	27.8			C
959S	200	16.9	A	B	
	600	18.3	A	B	
	200 (FR)	21.8			C
960S	200	20.5	A	B	
	600	22.6	A	B	
	200 (FR)	28.4			C
902S	200	17.5	A	B	
	600	20.0	A	B	
	200 (FR)	23.3			C
962SR	200	20.9	A		
	600	23.4		B	
	200 (FR)	28.1			C

4.2.4 Recoverable Radial Microstrain Characterization of Radisson SPS-9A Mixes

Recoverable radial microstrain (RMS) defines the recoverable portion of strain that results from dynamic loading along a horizontal at mid-height of the sample and perpendicular to the direction of the dynamic loading applied in the RaTT cell. RMS indicates the shear strength of the material being tested. The effect of varying angle of gyration on the measured RMS of the Radisson SPS-9A hot-mix asphalt mixtures at 20°C across varying deviatoric stresses and test frequency of 10 Hz are presented and discussed below.

Table 4.60 to Table 4.62 and Figure 4.33 to Figure 4.35 show the RMS and variation from the mean of research mixes at 10 Hz and 20°C across three levels of deviatoric stresses. The error bars shown in Figure 4.33 to Figure 4.35 represent minimum and maximum deviation from the mean RMS of three gyratory compactor samples used in the frequency sweep characterization.

RMS values were found to be highest at 600 kPa deviatoric stress for all test sections and across all gyratory angles as displayed in Figure 4.33 to Figure 4.35. RMS was found to be sensitive to varying deviatoric stress. Significantly low RMS values were recorded at 200 kPa deviatoric stress compared to 600 kPa and 200 kPa fully reversed deviatoric stresses. Superpave^{TM} recycle mix design test sections 962SR displayed the highest RMS values compared to the other test sections across all angles of gyration as displayed in Figure 4.33 to Figure 4.35.

Table 4.60 Radial Microstrain across Deviatoric Stress States at 1.25° Angle of Gyration and 10 Hz

SPS-9A Test Section	Deviatoric Stress (kPa)	Radial Microstrain	Deviation from Mean	
			Minimum	Maximum
901M	200	14.7	13.1	15.6
	600	58.7	55.0	63.1
	200 (FR)	37.9	35.7	39.7
961M	200	21.3	19.3	23.9
	600	93.3	90.1	96.9
	200 (FR)	61.7	58.6	65.6
903S	200	19.7	18.6	20.8
	600	97.0	92.2	99.7
	200 (FR)	60.1	58.5	63.2
959S	200	17.9	17.5	18.7
	600	60.7	59.0	62.2
	200 (FR)	41.5	40.4	42.4
960S	200	19.9	18.3	21.3
	600	88.8	87.2	91.4
	200 (FR)	58.7	53.9	63.7
902S	200	16.1	13.5	21.3
	600	68.9	65.1	73.7
	200 (FR)	50.2	45.3	52.5
962SR	200	27.1	26.8	27.7
	600	113.7	108.2	116.8
	200 (FR)	84.4	82.9	86.1

Table 4.61 Radial Microstrain across Deviatoric Stress States at 2.00° Angle of Gyration and 10 Hz

SPS-9A Test Section	Deviatoric Stress (kPa)	Radial Microstrain	Deviation from Mean	
			Minimum	Maximum
901M	200	17.0	15.2	20.3
	600	58.5	56.5	59.8
	200 (FR)	42.2	40.5	43.9
961M	200	20.5	19.8	21.5
	600	85.4	82.8	87.2
	200 (FR)	55.6	53.0	58.1
903S	200	18.5	17.1	19.6
	600	76.1	74.2	79.1
	200 (FR)	48.7	44.6	56.1
959S	200	15.2	13.6	17.0
	600	54.6	51.9	57.8
	200 (FR)	35.9	33.8	40.2
960S	200	20.9	16.8	23.7
	600	79.6	74.1	86.2
	200 (FR)	59.3	55.7	64.5
902S	200	17.7	14.6	20.3
	600	74.2	67.7	79.5
	200 (FR)	55.4	50.4	58.6
962SR	200	24.0	22.1	25.7
	600	100.7	99.2	102.4
	200 (FR)	79.8	77.8	82.3

Table 4.62 Radial Microstrain across Deviatoric Stress States at 2.75° Angle of Gyration and 10 Hz

SPS-9A Test Section	Deviatoric Stress (kPa)	Radial Microstrain	Deviation from Mean	
			Minimum	Maximum
901M	200	19.3	18.0	20.0
	600	60.7	57.6	64.2
	200 (FR)	45.4	41.5	47.9
961M	200	21.7	20.5	23.8
	600	88.4	82.9	91.8
	200 (FR)	59.4	53.7	62.4
903S	200	19.3	17.5	21.8
	600	81.9	80.2	85.4
	200 (FR)	54.4	53.5	55.0
959S	200	14.2	12.2	15.8
	600	53.5	48.1	57.5
	200 (FR)	33.9	33.4	34.6
960S	200	18.7	17.7	19.5
	600	73.6	70.3	75.7
	200 (FR)	57.7	56.8	58.4
902S	200	14.9	12.7	17.1
	600	61.6	60.7	62.2
	200 (FR)	44.9	44.2	46.0
962SR	200	24.7	22.0	26.1
	600	95.2	91.2	100.3
	200 (FR)	77.2	76.9	77.4

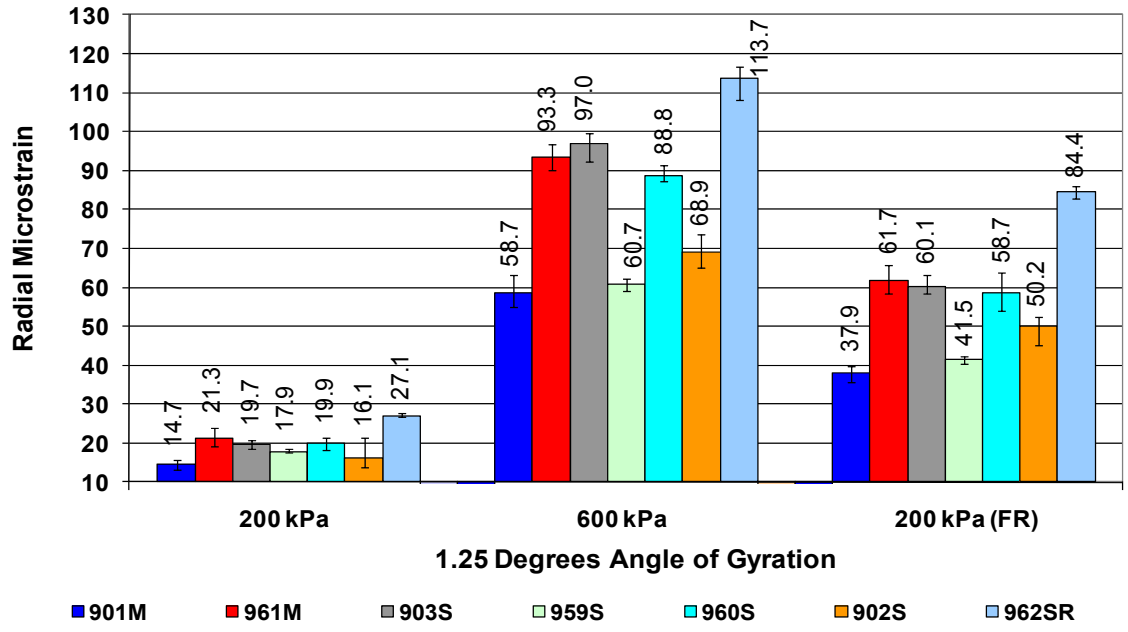

Figure 4.33 Radial Microstrain across Deviatoric Stress States at 1.25° Angle of Gyration and 10 Hz

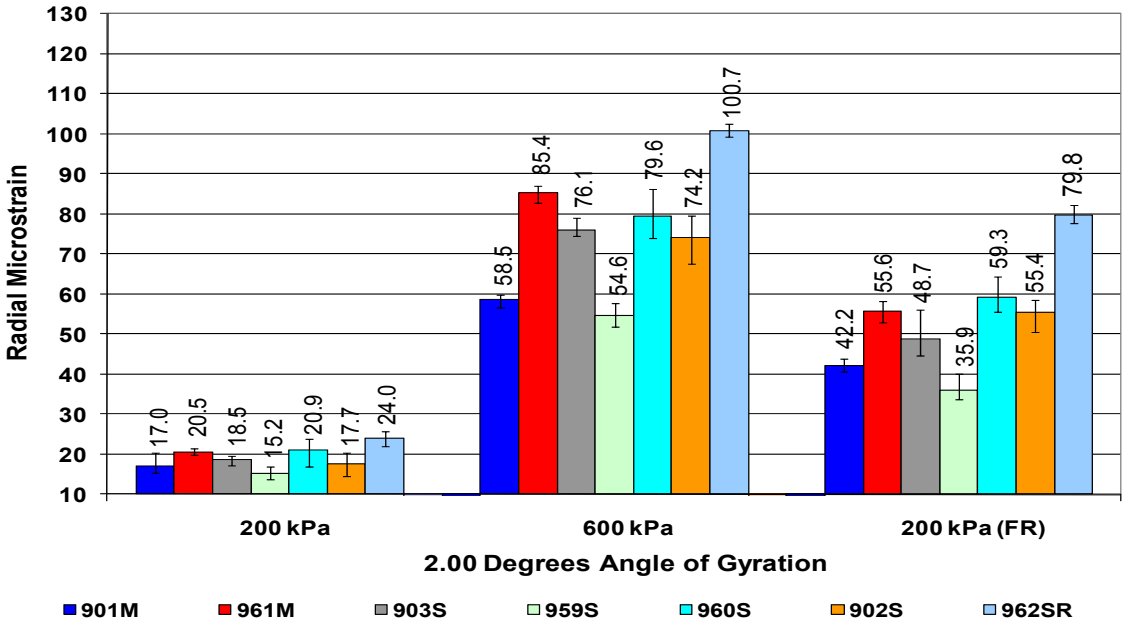

Figure 4.34 Radial Microstrain across Deviatoric Stress States at 2.00° Angle of Gyration and 10 Hz

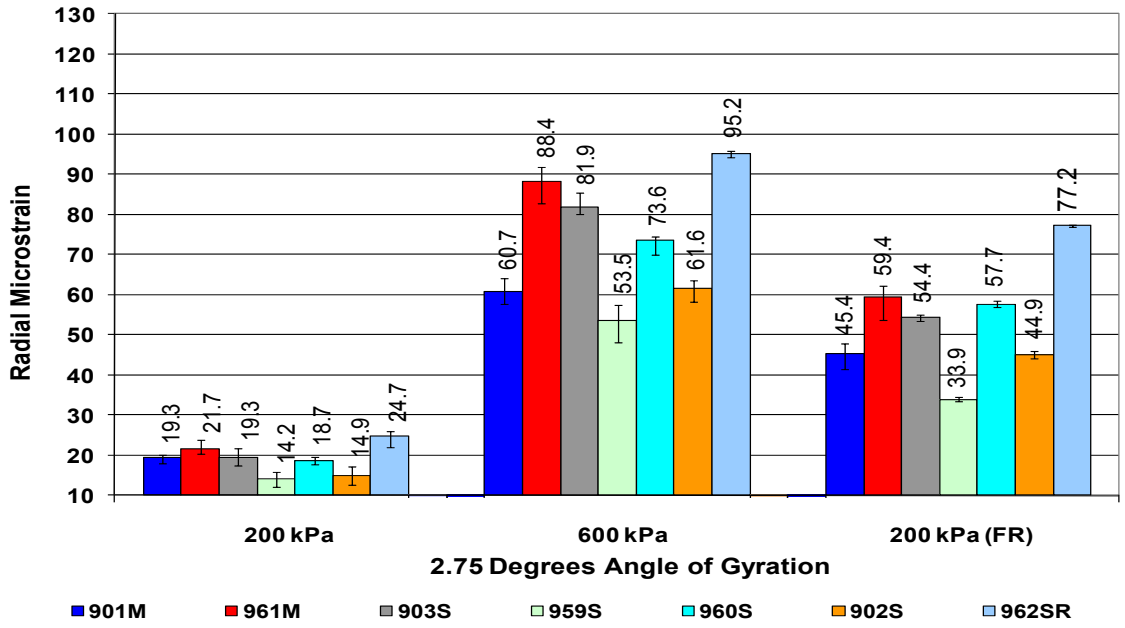

Figure 4.35 Radial Microstrain across Deviatoric Stress States at 2.75° Angle of Gyration and 10 Hz

The effects of varying angle of gyration on the RMS of the Radisson SPS-9A asphalt mixes have been investigated across three deviatoric stress states of 200 kPa, 600 kPa and 200 kPa (FR) and the results are presented in Figure 4.36 to Figure 4.38. The Superpave™ recommended angle of gyration 1.25° is set as a base for the analysis. The difference in RMS from 1.25° to 2.00° angles of gyration was compared to difference in RMS from 1.25° to 2.75° angles of gyration and the results are presented for each test section.

RMS was not sensitive to increase in angle of gyration across Radisson SPS-9A asphalt mixes compared at 200 kPa deviatoric stress as seen in Figure 4.36. The difference in RMS was however found to be significantly higher at 1.25° to 2.75° angles of gyration compared to 1.25° to 2.00° angles of gyration at 600 kPa deviatoric stress as seen in Figure 4.37. The difference in RMS compared between 1.25° to 2.00° angles of gyration and 1.25° to 2.75° angles of gyration did not produce a visible trend.

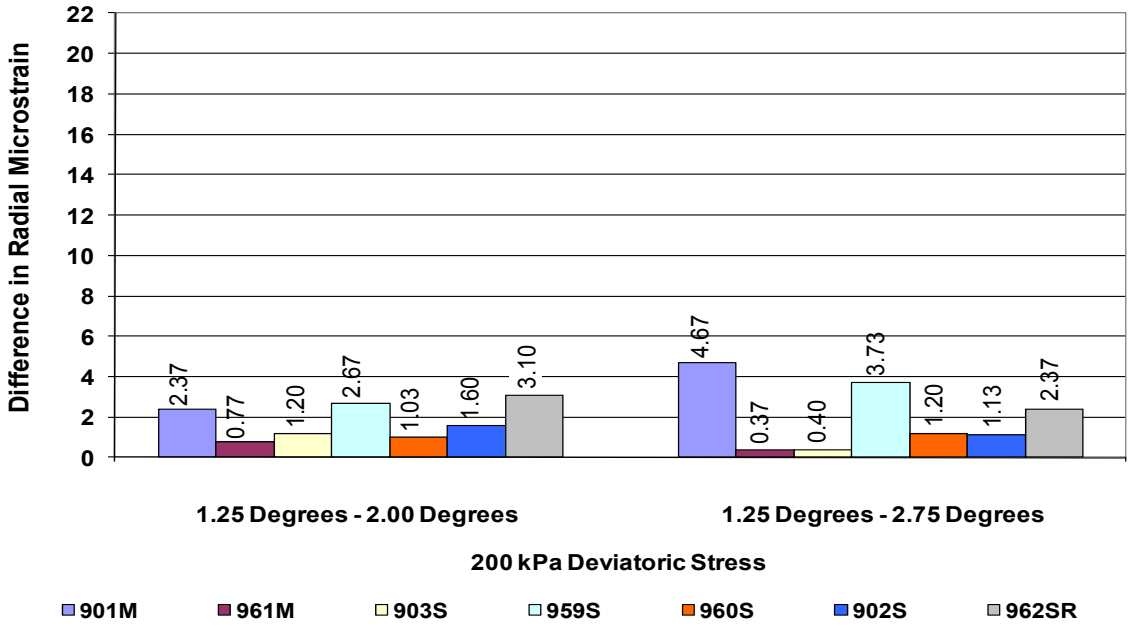

Figure 4.36 Effects of Gyratory Angle on Radial Microstrain at 200 kPa Deviatoric Stress and 10 Hz

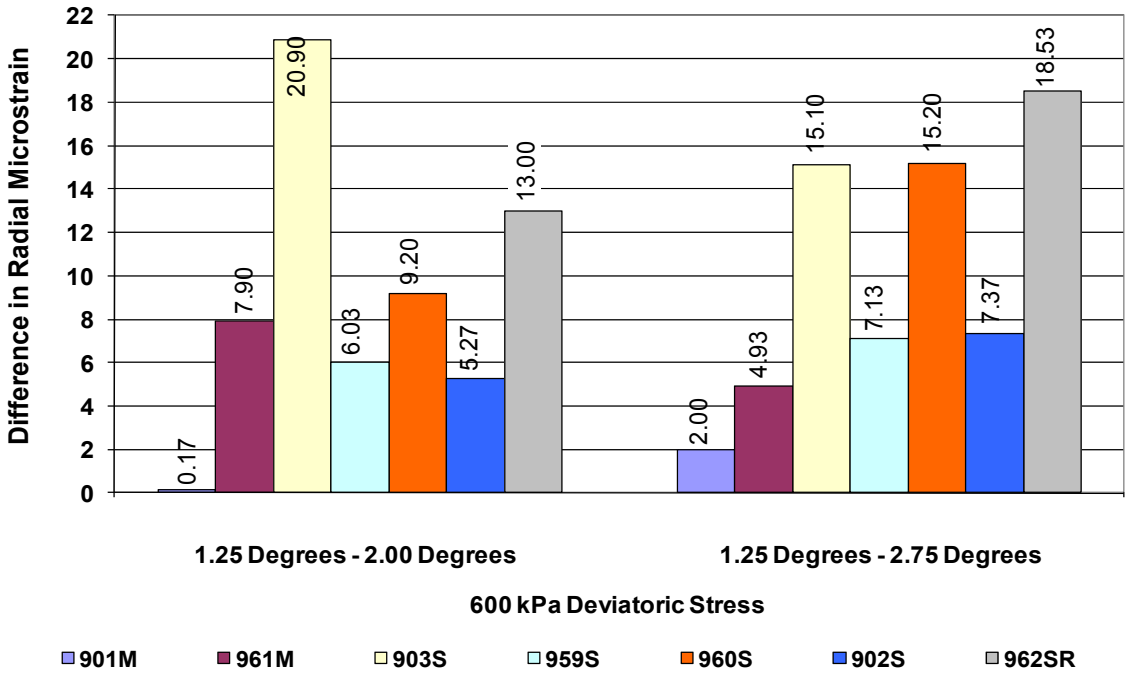

Figure 4.37 Effects of Gyratory Angle on Radial Microstrain at 600 kPa Deviatoric Stress and 10 Hz

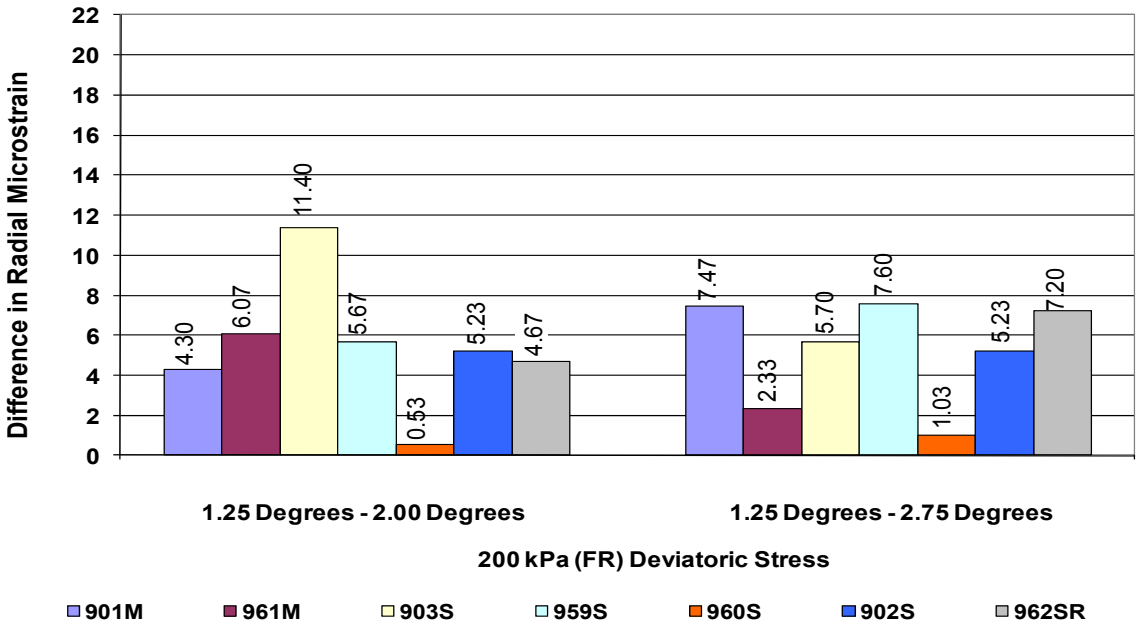

Figure 4.38 Effects of Gyratory Angle on Radial Microstrain at 200 kPa (FR) Deviatoric Stress and 10 Hz

4.2.4.1 Staistical Sensitivity of Radial Microstrain across Gyration Angle

Statistical analysis of variance (ANOVA) was performed on RMS results to evaluate statistical significance at 95 percent confidence level across angle of gyration and mix type. The ANOVA of RMS results are shown in Tables 4.63, 4.65 and 4.67 at deviatoric stresses 200 kPa, 600 kPa and 200 kPa fully reversible respectively. As seen in Tables 4.63, 4.65 and 4.67, there was significant difference in RMS values of the Radisson SPS-9A test sections across varied angle of gyration at 600 kPa and 200 kPa fully reversed deviatoric stresses.

Tukey's homogeneous group analysis for RMS results are shown in Tables 4.64, 4.66 and 4.68. Only test sections 902S and 962SR show significant difference in RMS results of the Radisson SPS-9A test sections across varied gyratory angle at 200 kPa deviatoric stress as seen in Table 4.64. As seen in Tables 4.66 and 4.68, significant difference in RMS results across varied angle of gyration was observed for all test sections at 600 kPa and 200 kPa fully reversed deviatoric stresses.

Table 4.63 Analysis of Variance for Radial Microstrain at 200 kPa Deviatoric Stress across Radisson SPS-9A Asphalt Mixes

Parameter	Sum of Squares	Degrees of Freedom	Mean Squares	F-Test Statistic	P-value	Sig.
Mix Type	8358	6	1044	231		
Angle of Gyration	145	2	2624	299	0.000	
Mix Type*Angle of Gyration	75	12	2517	39	0.049	Yes
Error	81	15	960			

Table 4.64 Tukey's Homogeneous Groups for Radial Microstrain at 200 kPa Deviatoric Stress across Radisson SPS-9A Asphalt Mixes

Test Section	Angle of Gyration (°)	Radial Microstrain	Tukey's Homogeneous Groups		
901M	1.25	14.7	A		
	2.00	17.0	A		
	2.75	19.3	A		
961M	1.25	21.3	A		
	2.00	20.5	A		
	2.75	21.7	A		
903S	1.25	19.7	A		
	2.00	18.5	A		
	2.75	19.3	A		
959S	1.25	17.9	A		
	2.00	15.2	A		
	2.75	14.2	A		
960S	1.25	19.9	A		
	2.00	20.9	A		
	2.75	18.7	A		
902S	1.25	16.1	A		
	2.00	17.7		B	C
	2.75	14.9		B	C
962SR	1.25	27.1	A		
	2.00	24.0		B	
	2.75	24.7			C

Table 4.65 Analysis of Variance for Radial Microstrain at 600 kPa Deviatoric Stress across Radisson SPS-9A Asphalt Mixes

Parameter	Sum of Squares	Degrees of Freedom	Mean Squares	F-Test Statistic	P-value	Sig.
Mix Type	7680	6	1896	132		
Angle of Gyration	17822	2	234	5	0.020	
Mix Type*Angle of Gyration	13355	12	56	1	0.392	Yes
Error	93	15	51			

Table 4.66 Tukey's Homogeneous Groups for Radial Microstrain at 600 kPa Deviatoric Stress across Radisson SPS-9A Asphalt Mixes

Test Section	Angle of Gyration (°)	Radial Microstrain	Tukey's Homogeneous Groups		
901M	1.25	58.7	A		
	2.00	58.5		B	C
	2.75	60.7		B	C
961M	1.25	93.3	A		
	2.00	85.4		B	
	2.75	88.4			C
903S	1.25	97.0	A		
	2.00	76.1		B	
	2.75	53.5			C
959S	1.25	60.7	A		
	2.00	54.6		B	
	2.75	53.5			C
960S	1.25	88.8	A		
	2.00	79.6		B	
	2.75	73.6			C
902S	1.25	68.9	A		
	2.00	74.2		B	
	2.75	61.6			C
962SR	1.25	113.7	A		
	2.00	100.7		B	
	2.75	95.2			C

Table 4.67 Analysis of Variance for Radial Microstrain at 200 kPa Fully Reversed Deviatoric Stress across Radisson SPS-9A Asphalt Mixes

Parameter	Sum of Squares	Degrees of Freedom	Mean Squares	F-Test Statistic	P-value	Sig.
Mix Type	85882	6	174	160		
Angle of Gyration	75176	2	73	29	0.000	
Mix Type*Angle of Gyration	35951	12	12	1	0.464	Yes
Error	88	15	5			

Table 4.68 Tukey's Homogeneous Groups for Radial Microstrain at 200 kPa Fully Reversed Deviatoric Stress across Radisson SPS-9A Asphalt Mixes

Test Section	Angle of Gyration (°)	Radial Microstrain	Tukey's Homogeneous Groups		
901M	1.25	37.9	A		
	2.00	42.2		B	
	2.75	45.4			C
961M	1.25	61.7	A		
	2.00	55.6		B	
	2.75	59.4			C
903S	1.25	60.1	A		
	2.00	48.7		B	
	2.75	33.9			C
959S	1.25	41.5	A		
	2.00	35.9		B	
	2.75	33.9			C
960S	1.25	58.7	A		
	2.00	59.3		B	
	2.75	57.7			C
902S	1.25	50.2	A		
	2.00	55.4		B	
	2.75	44.9			C
962SR	1.25	84.4	A		
	2.00	79.8		B	
	2.75	77.2			C

The effects of varying deviatoric stress on the RMS of the Radisson SPS-9A asphalt mixes was investigated across three angles of gyration 1.25°, 2.00° and 2.75° and the results are presented in Figure 4.39 to Figure 4.41.

RMS was observed to be sensitive to varying deviatoric stress across all test sections and at all angles of gyration as seen in Figure 4.39 to Figure 4.41. The difference in RMS was found to be higher at 200 kPa to 600 kPa compared to 200 kPa to 200 kPa fully reversed deviatoric stress. The Superpave™ recycle mix design test section 962SR recorded the highest difference in RMS compared to the other test sections across all angles of gyration seen in Figure 4.39 to Figure 4.41.

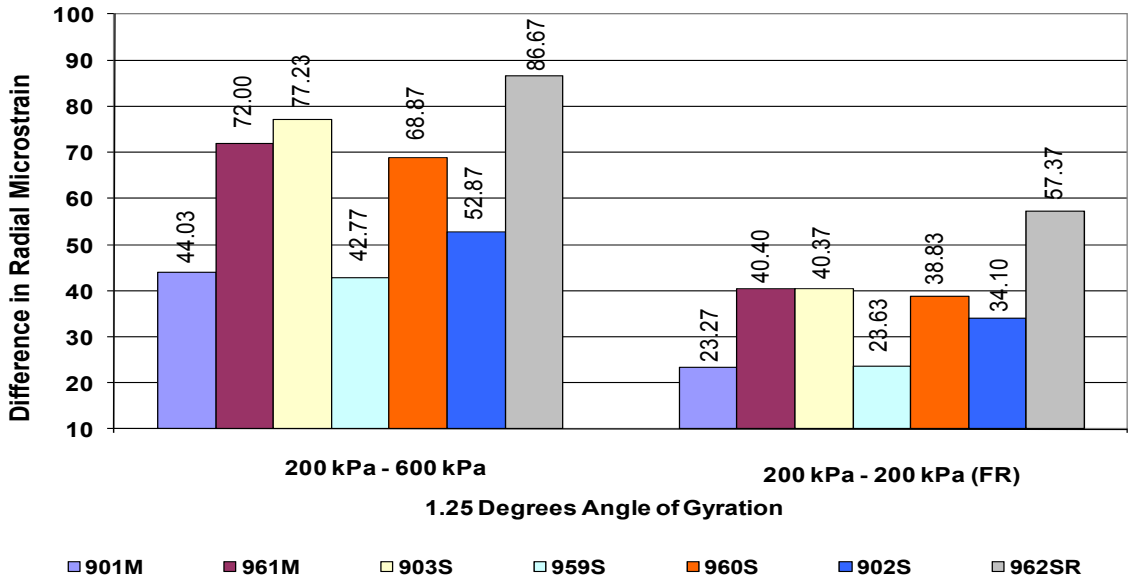

Figure 4.39 Effects of Deviatoric Stress States on Radial Microstrain at 1.25° Angle of Gyration and 10 Hz

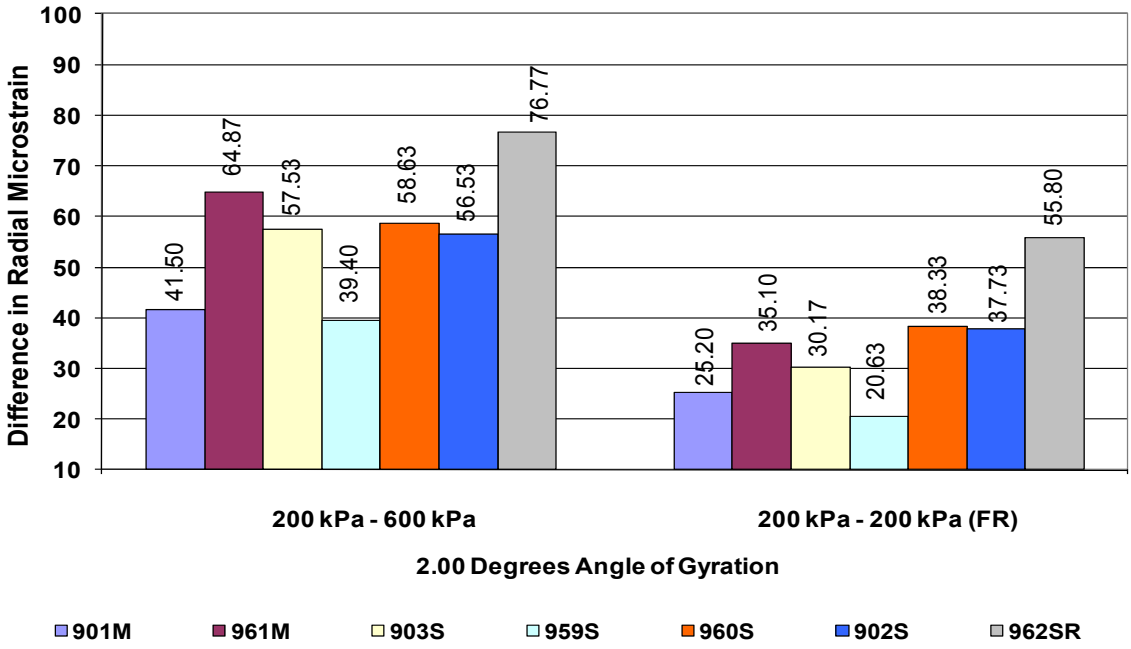

Figure 4.40 Effects of Deviatoric Stress States on Radial Microstrain at 2.00° Angle of Gyration and 10 Hz

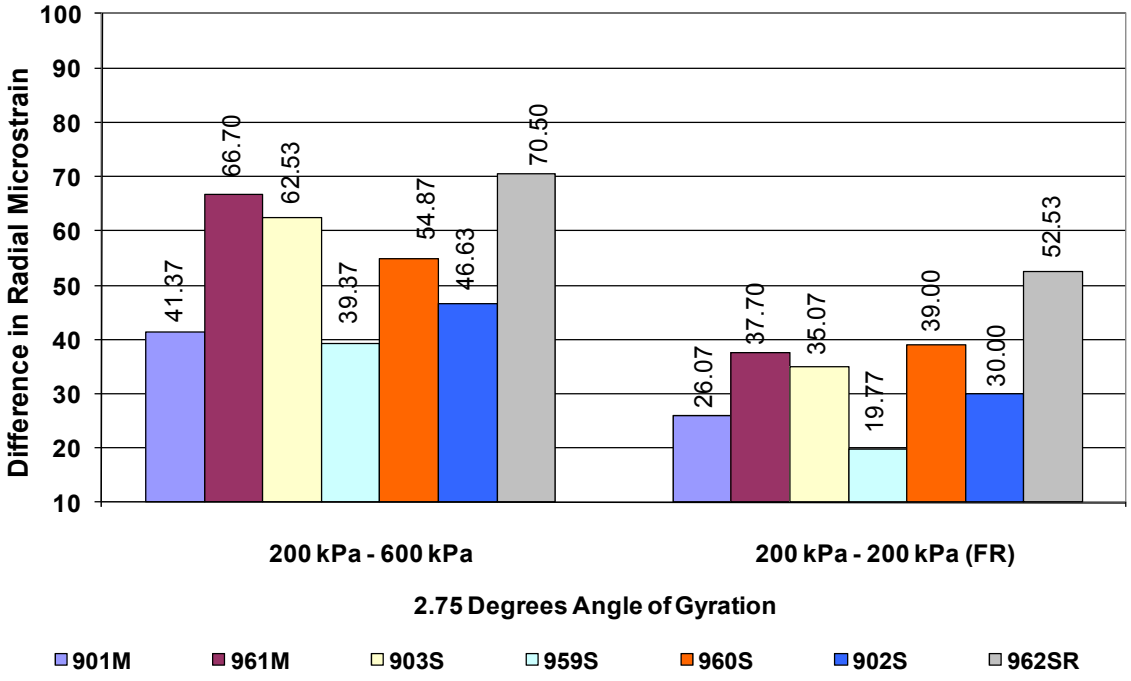

Figure 4.41 Effects of Deviatoric Stress States on Radial Microstrain at 2.75° Angle of Gyration and 10 Hz

4.2.4.2 Staistical Sensitivity of Radial Microstrain across Deviatoric Stress

Statistical analysis of variance was performed on RMS values in order to investigate the sensitivity of the Radisson SPS-9A asphalt mixes to varied deviatoric stress. Analysis of variance for RMS characterization is summarized in Tables 4.69, 4.71 and 4.73 and Tukey's homogeneous groups are presented in Tables 4.70, 4.72 and 4.74. As seen in Tables 4.69, 4.71 and 4.73, there was significant difference in RMS as a function of deviatoric stress at all angles of gyration across all the Radisson SPS-9A test sections.

RMS was found to be significantly different across all deviatory stresses for all the Radisson SPS-9A test sections at 1.25° angle of gyration, as seen in Table 4.70. Similarly, RMS was found to be significantly different across all deviatory stresses for most of the Radisson SPS-9A test sections at 2.00° angle of gyration, except test section 901M which has RMS at 200 kPa different compared to 600 kPa and 200 kPa fully reversed deviatory stresses, as seen in Table 4.72. RMS was found to be significantly different across all deviatory stresses for all the Radisson SPS-9A test sections at 2.75° angle of gyration, as seen in Table 4.74.

Table 4.69 Analysis of Variance for Radial Microstrain at 1.25° Angle of Gyration across Radisson SPS-9A Asphalt Mixes

Parameter	Sum of Squares	Degrees of Freedom	Mean Squares	F-Test Statistic	P-value	Sig.
RMS	8472	2	790	160		
Deviatoric Stress	145	2	73	15	0.000	
RMS *Deviatoric Stress	75	4	12	3	0.049	Yes
Error	119	16	5			

Table 4.70 Tukey's Homogeneous Groups for Radial Microstrain at 1.25° Angle of Gyration across Radisson SPS-9A Asphalt Mixes

Test Section	Deviatoric Stress (kPa)	Radial Microstrain	Tukey's Homogeneous Groups		
901M	200	14.7	A		
	600	58.7		B	
	200 (FR)	37.9			C
961M	200	21.3	A		
	600	93.3		B	
	200 (FR)	61.7			C
903S	200	19.7	A		
	600	97.0		B	
	200 (FR)	60.1			C
959S	200	17.9	A		
	600	60.7		B	
	200 (FR)	41.5			C
960S	200	19.9	A		
	600	88.8		B	
	200 (FR)	58.7			C
902S	200	16.1	A		
	600	68.9		B	C
	200 (FR)	50.2		B	C
962SR	200	27.1	A		
	600	113.7		B	
	200 (FR)	84.4			C

Table 4.71 Analysis of Variance for Radial Microstrain at 2.00° Angle of Gyration across Radisson SPS-9A Asphalt Mixes

Parameter	Sum of Squares	Degrees of Freedom	Mean Squares	F-Test Statistic	P-value	Sig.
RMS	20054	2	1896	132		
Deviatoric Stress	468	2	234	5	0.020	
RMS *Deviatoric Stress	334	4	56	1	0.392	Yes
Error	1217	16	51			

Table 4.72 Tukey's Homogeneous Groups for Radial Microstrain at 2.00° Angle of Gyration across Radisson SPS-9A Asphalt Mixes

Test Section	Deviatoric Stress (kPa)	Radial Microstrain	Tukey's Homogeneous Groups		
901M	200	17.0	A		
	600	58.5		B	C
	200 (FR)	42.2		B	C
961M	200	20.5	A		
	600	85.4		B	
	200 (FR)	55.6			C
903S	200	18.5	A		
	600	76.1		B	
	200 (FR)	48.7			C
959S	200	15.2	A		
	600	54.6		B	
	200 (FR)	35.9			C
960S	200	20.9	A		
	600	79.6		B	
	200 (FR)	59.3			C
902S	200	17.7	A		
	600	74.2		B	
	200 (FR)	55.4			C
962SR	200	24.0	A		
	600	100.7		B	
	200 (FR)	79.8			C

Table 4.73 Analysis of Variance for Radial Microstrain at 2.75° Angle of Gyration across Radisson SPS-9A Asphalt Mixes

Parameter	Sum of Squares	Degrees of Freedom	Mean Squares	F-Test Statistic	P-value	Sig.
RMS	7897	2	174	160		
Deviatoric Stress	248	2	73	29	0.000	
RMS *Deviatoric Stress	25	4	12	1	0.464	Yes
Error	102	16	5			

Table 4.74 Tukey's Homogeneous Groups for Radial Microstrain at 2.75° Angle of Gyration across Radisson SPS-9A Asphalt Mixes

Test Section	Deviatoric Stress (kPa)	Radial Microstrain	Tukey's Homogeneous Groups		
901M	200	19.3	A		
	600	60.7		B	
	200 (FR)	45.4			C
961M	200	21.7	A		
	600	88.4		B	
	200 (FR)	59.4			C
903S	200	19.3	A		
	600	81.9		B	
	200 (FR)	54.4			C
959S	200	14.2	A		
	600	53.5		B	
	200 (FR)	33.9			C
960S	200	18.7	A		
	600	73.6		B	
	200 (FR)	57.7			C
902S	200	14.9	A		
	600	61.6		B	
	200 (FR)	44.9			C
962SR	200	24.7	A		
	600	95.2		B	
	200 (FR)	77.2			C

4.3 Chapter Summary

This chapter presented the results of the laboratory mechanical characterization of Marshall compacted samples and triaxial frequency sweep mechanistic characterization gyratory compacted samples of the Radisson SPS-9A asphalt mixes used in this research. Marshall stability and flow were obtained from Marshall characterization. Dynamic modulus, Poisson's ratio and phase angle obtained from triaxial frequency sweep testing were presented and discussed.

Marshall stability values increased with increase in compaction energy across all test sections. There was significance in Marshall stability and flow values across test sections at 75-blow Marshall compaction. However, Marshall stability and flow values

compared at 50-blow Marshall compaction did not show any statistical significance among the test sections.

Dynamic modulus was observed to decrease respectively from 200 kPa through 600 kPa to 200 kPa fully reversed deviatoric stress states across all gyratory angles for all test sections. The conventional SMHI Marshall mix design test section 901M has the highest average dynamic modulus compared to all other test sections across all deviatoric stress states and angles of gyration. The Superpave™ mix design test section 959S displayed the highest average dynamic modulus values compared to the other Superpave™ mix design test sections. Superpave™ recycled mix design test section 962SR displayed less stiffness with lowest average dynamic modulus values across all deviatoric stress states and angles of gyrations. Dynamic modulus was sensitive to deviatoric stress state.

The average Poisson's ratio for all research asphalt mixes was 0.32. Poisson's ratio was sensitive to varying angle of gyration. The conventional SMHI Marshall mix design test section 961M has the highest Poisson's ratio compared across all test sections and angles of gyration at 600 kPa and 200 kPa (FR) deviatoric stress. Superpave™ mix design test section 959S recorded low average Poisson's ratio across all angles of gyration and deviatoric stresses compared to other test sections. The lowest Poisson's ratio was recorded as 0.25 at 200 kPa fully reversed deviatoric stress and 2.75° angle of gyration for test section 959S.

Phase angle increases with increase in deviatoric stress at all three angles of gyration across all test sections. The highest average phase angle values were recorded at 200 kPa fully reversed deviatoric stress across all test sections. The Superpave™ mix design test sections 959S and 902S have the lowest phase angle values at all three angles of gyration and deviatoric stresses compared to tother test sections. Phase angle was sensitive to deviatoric stress state and increased significantly with change in deviatoric stress. Phase angle also increased with an increase in angle of gyration across test sections.

RMS increase with increase in deviatoric stress. The highest RMS was recorded at 600 kPa deviatoric stress across all test sections and angles of gyration. RMS was sensitive to change in deviatoric stress and change in angle of gyration. Superpave™ recycle mix design test section 962SR recorded the highest RMS compared to the other test sections at all angles of gyration.

CHAPTER 5 FIELD PERFORMANCE DATA OF RADISSON SPS-9A TEST SECTIONS

This chapter presents field data collected from the Radisson SPS-9A test site after ten years of field performance. Rut depth measurements after each year of performance are presented across each test section. Average rut depth and ground penetrating radar dielectric permittivities are also presented across each SPS-9A test section. The results of the field air voids are compared to the laboratory air voids after Marshall and gyratory compaction.

5.1 Rutting Characterization of Radisson SPS-9A Asphalt Mixes

Rutting in hot mix asphalt pavement, as defined in Chapter Two, occurs when permanent deformation within the asphalt pavement layers occurs under load applications. Rutting is caused by a combination of densification of the asphalt mix and shear deformation that can occur in one or more of the structural layers.

Rutting occurring within the Radisson SPS-9A test sections has been measured annually by the Dipstick™ profiler since 1997. Table 5.1 summarizes the average inside and outside wheel path rut depth across the Radisson SPS-9A test sections. Figure 5.1 displays progress of rutting across the test sections by plotting the average of inside and outside wheel path rut measurements from six different locations within each test section. The cumulated equivalent single axle load (ESAL) corresponding to each year of rutting measurement are also shown in Figure 5.1. Average rut depths across each test section after ten years of service are presented in Figure 5.1.

As seen in Figure 5.1, the measured rut depths significantly increased in the first three years of life followed by seven years of progressively slower rate of rutting propagation. The high rate of rutting in the initial stages of service life of the test sections is in agreement with the concept of mix consolidation rutting.

As seen in Figure 5.1, the Superpave™ recycle mix design test section 962SR yielded the minimum rutting after ten years. The Superpave™ mix test sections generally yielded similar rutting performance, of 8.8 mm +/- 1.4 mm, regardless of the asphalt cement used. The similarity of the Superpave™ mixes in terms of rutting

performance can be attributed to the aggregate structure of the Superpave™ mix design method.

Table 5.1 Average Annual Rut Depths and Cumulated ESAL across Radisson SPS-9A Asphalt Test Sections

Year	Test Section Number							ESAL
	901M	961M	903S	959S	960S	902S	962SR	
1997	1.7	2.3	1.9	2.3	2.2	2.3	2.1	3.0E+05
1998	2.0	5.1	3.5	2.9	3.5	4.7	2.2	7.0E+05
1999	4.5	7.7	5.3	3.8	5.8	6.3	3.7	1.0E+06
2000	5.6	9.7	6.7	5.6	7.1	8.2	4.6	1.6E+06
2001	5.9	10.5	7.4	5.9	7.2	8.5	4.8	2.0E+06
2002	6.3	11.6	8.3	6.4	7.6	8.9	5.4	2.5E+06
2003	7.0	12.8	8.8	7.2	8.2	9.5	5.5	3.1E+06
2004	7.9	10.9	9.2	7.9	8.5	10	5.7	3.4E+06
2005	8.4	12.0	9.3	8.1	8.5	10.2	5.9	3.7E+06
2006	9.1	13.0	10.1	9.2	8.8	10.2	6.2	4.1E+06

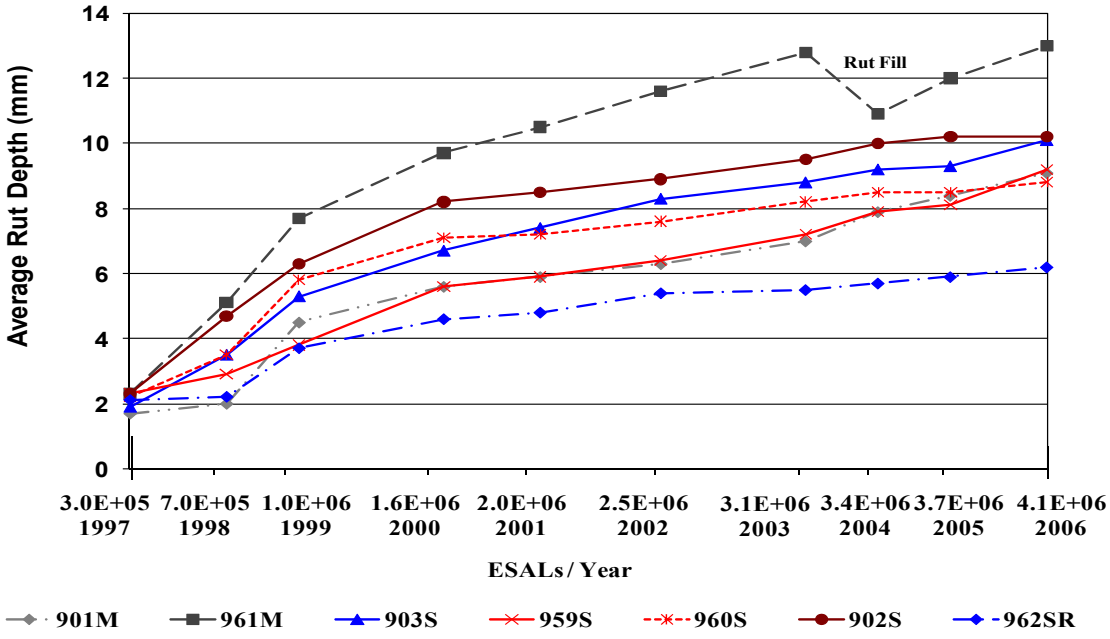

Figure 5.1 Average Annual Rut Depths and Cumulated ESAL across Radisson SPS-9A Asphalt Test Sections

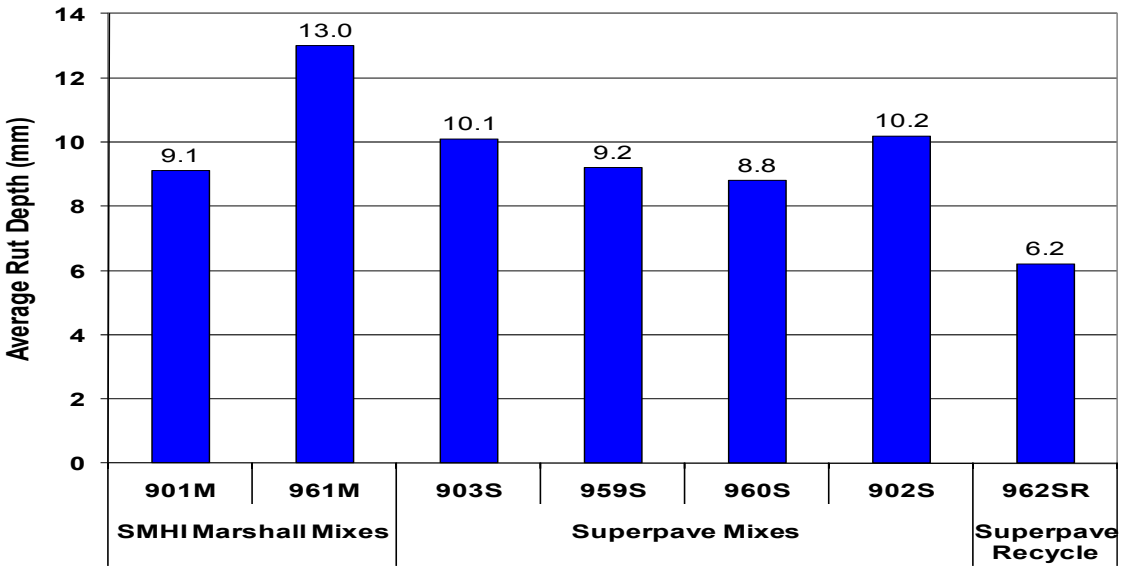

Figure 5.2 Average Rut Depths after Ten Years in Service across Radisson SPS-9A Asphalt Test Sections

The two conventional SMHI Marshall mixes were found to exhibit significantly different rutting behavior as a function of asphalt cement type and aggregate gradation as compared to the Superpave™ mixes. The conventional SMHI Marshall mixes seem to rely on the properties of the asphalt cement for rutting resistance with test section 901M, constructed with PG 52-28 (AC 150/200), showing more resistance to rutting compared with test section 961M, constructed with PG 52-34 (AC 200/300). It is also observed, in Figure 5.2, that the conventional SMHI Marshall mix design test sections 961M and Superpave™ mix design test section 903S show significant difference in average rut depth measurement even though both test sections were constructed with the same asphalt cement, PG 52-34 (AC 200/300).

It should be noted that a significant drop in rut depth measured on test section 961M in 2004 was observed due to routine maintenance works performed on the section. It is also interesting to noted that the rate of rutting in test section 961M was observed to continue after the routine maintenance work.

5.2 Dielectric Permittivity Characterization of SPS-9A Asphalt Mixes

Based on the ground penetrating radar profiles collected, the asphalt concrete surface dielectric permittivity is summarized in Table 5.2 and presented in Figure 5.3. The dielectric permittivity was measured in the wheelpaths and outside of the wheelpaths across the Radisson SPS-9A test sections. Figure 5.4 illustrates the difference between average asphalt concrete surface dielectric permittivity in the wheelpaths and between the wheelpaths across the Radisson SPS-9A test sections.

Table 5.2 Asphalt Concrete Surface Dielectric Permittivity across Radisson SPS-9A Test Sections

Test Section	Inner Wheelpath			Between Wheelpaths			Outside Wheelpath		
	Average	Min.	Max.	Average	Min.	Max.	Average	Min.	Max.
901M	5.1	4.8	5.5	6.1	4.9	6.9	5.3	4.9	6.6
961M	4.8	4.2	5.5	6.4	5.9	7.0	5.5	5.1	6.1
903S	5.6	5.1	6.4	5.9	5.4	7.0	5.4	4.7	6.5
959S	5.4	4.8	5.6	5.3	4.7	5.7	4.9	4.2	6.1
960S	5.2	4.9	5.7	5.9	4.8	6.9	5.2	4.9	5.7
902S	5.6	5.1	5.9	6.0	5.1	6.6	5.5	5.3	5.8
962SR	5.3	5.0	6.0	4.8	4.3	5.5	5.2	4.8	5.8

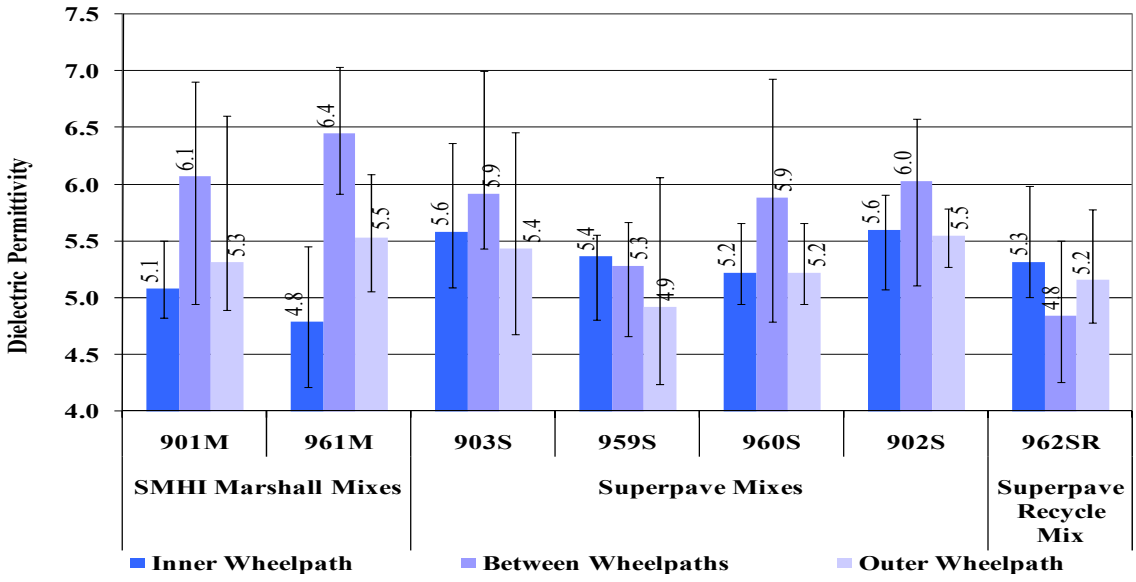

Figure 5.3 Asphalt Concrete Surface Dielectric Permittivity across Radisson SPS-9A Test Sections

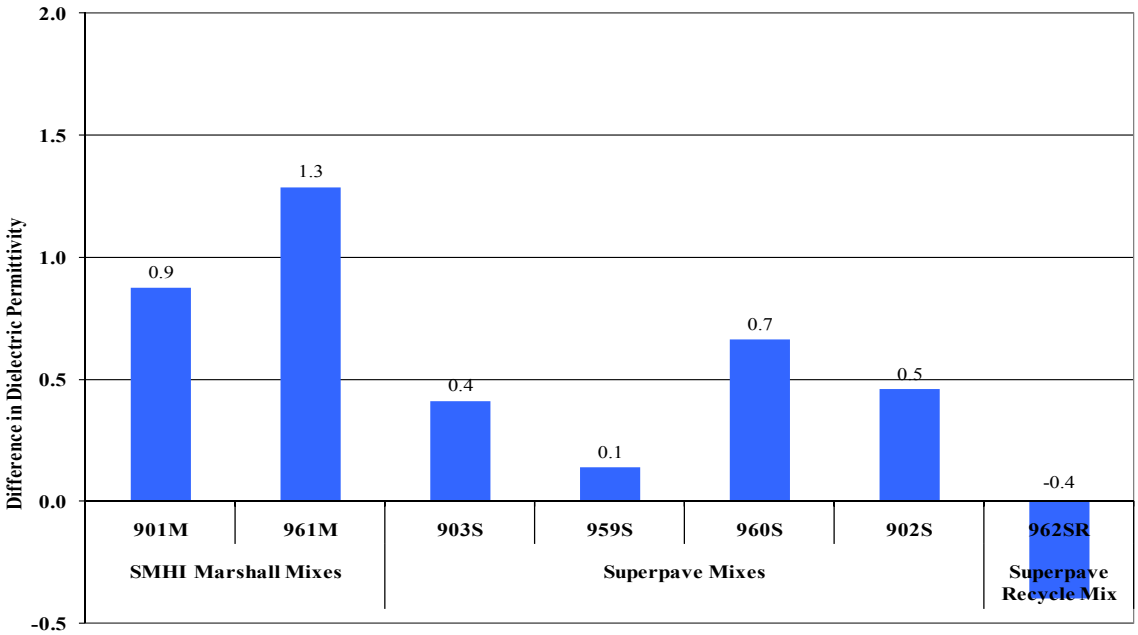

Figure 5.4 Difference in Asphalt Concrete Surface Dielectric Permittivity in Wheelpaths and Between Wheelpaths

As seen in Figure 5.3, the asphalt concrete surface dielectric permittivity in the wheelpaths was observed to be generally lower compared to the dielectric permittivity between the wheelpaths across the Radisson SPS-9A test sections, with the exception of the Superpave™ recycled mix 962SR. This relative decrease in surface dielectric permittivity indicates a difference in volumetric and / or moisture properties of the asphalt mix.

As seen in Figure 5.4, there was a difference in asphalt concrete surface dielectric permittivity in the wheelpaths and between the wheelpaths across most of the asphalt mixes. Only the Superpave™ recycled mix 962SR recorded a negative difference in asphalt concrete surface dielectric permittivity in the wheelpaths and between the wheelpaths. The SMHI dense graded mixes recorded a higher difference in surface dielectric permittivity in the wheelpaths relative to between the wheelpaths compared to the Superpave™ mixes.

The effect of consolidation of the Radisson SPS-9A asphalt mixes on dielectric permittivity was investigated by cross plotting rut depth measurements after ten years of field performance to the difference in dielectric permittivity with respect to inside the wheelpaths and between the wheelpaths across the Radisson SPS-9A asphalt mixes as seen in Figure 5.5.

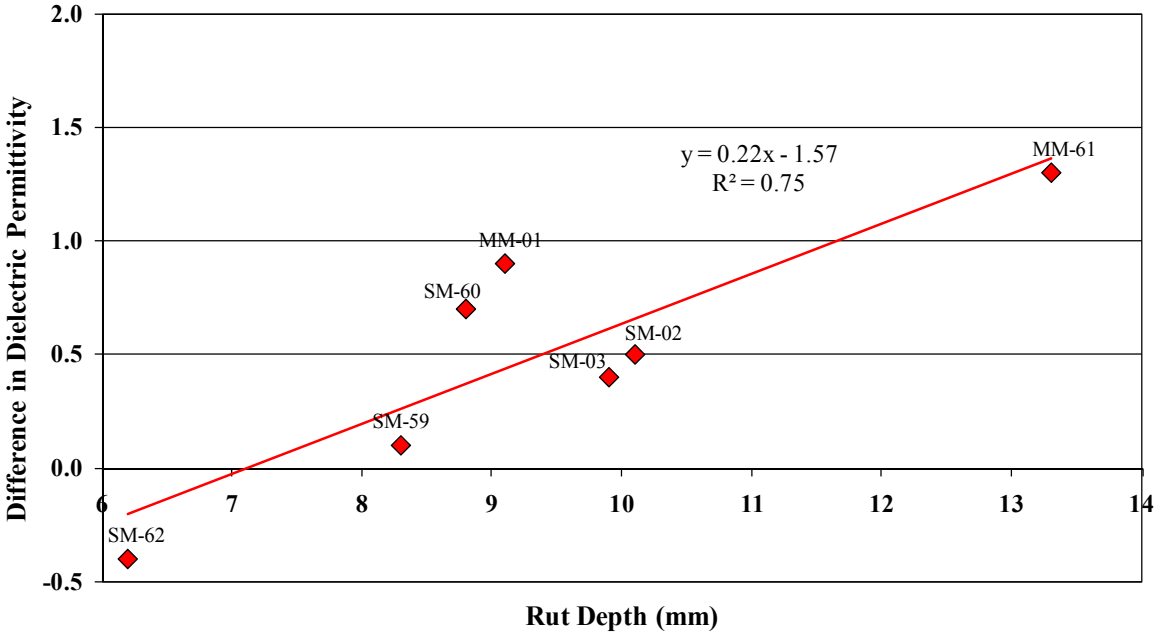

Figure 5.5 Dielectric Permittivity and Rut Depth across Radisson SPS-9A Test Sections

As seen in Figure 5.5, there appears to be a correlation between the difference in dielectric permittivity and rut depth across the Radisson SPS-9A asphalt mixes as shown be the regression line with a R^2 value of 0.75. Based on this relationship, there was a general increase in rut depth with an increase in dielectric permittivity difference between the wheelpaths and inside the wheelpaths across the Radisson SPS-9A asphalt mixes. This trend is assumed to be related to consolidation of the asphalt surfacing with respect to traffic loading. However, it should be noted that if the two mixes (961M and 962SR) were removed from the data set, a much less obvious trend would exist between the dielectric permittivity and rut depth.

5.3 Comparison of Laboratory and Field Air Voids

Air voids obtained from Marshall and gyratory laboratory compaction were compared to field air voids obtained from each Radisson SPS-9A test section.

Air voids after 50 and 75-blow Marshall compaction were ploted against field air voids of the Radisson SPS-9A test sections as shown in Figure 5.6 and Figure 5.7 respectively. At both 50 and 75-blow Marshall compaction air voids of the Superpave™ mixes were different compared to the SMHI Marshall mixes. This indicates the ability of the Marshall compactor to differentiate between the SMHI Marshall and Superpave™ mixes. Laboratory air voids of the Superpave™ mixes were higher at both 50 and 75-blow Marshall than the 4.0% air voids specified by the Superpave™ mix design criteria. However, the SMHI Marshall mixes displayed lower air voids at both 50 and 75-blow Marshall than the 4.0% air voids specified by the Superpave™ mix design criteria.

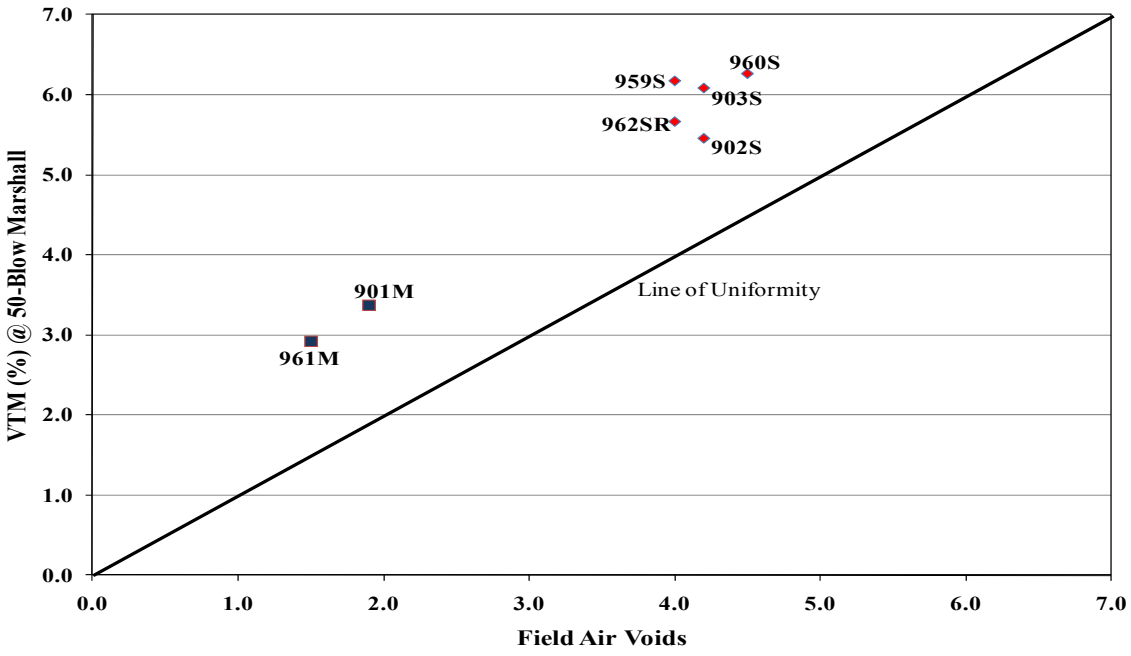

Figure 5.6 Air Voids at 50-Blow Marshall versus 10-Year Field Air Voids across Radisson SPS-9A Test Sections

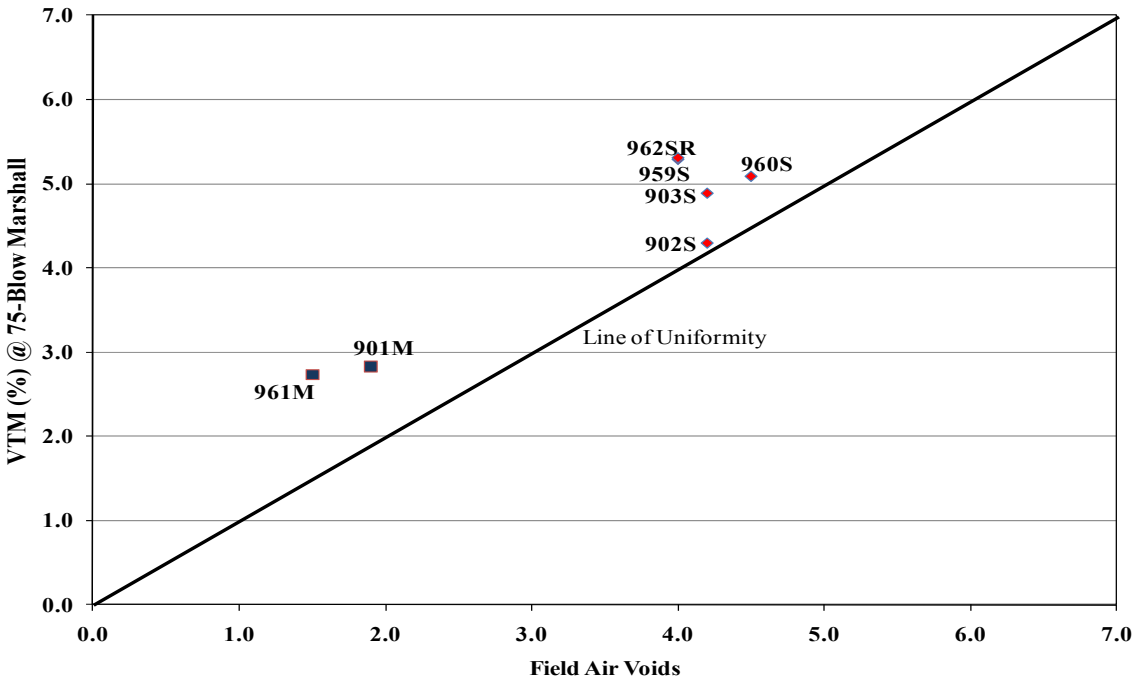

Figure 5.7 Air Voids at 75-Blow Marshall versus 10-Year Field Air Voids across Radisson SPS-9A Test Sections

Air voids after Superpave™ gyratory compaction were ploted at 1.25°, 2.00° and 2.75° angle of gyration against field air voids of the Radisson SPS-9A test sections as shown in Figures 5.8, 5.9 and 5.10 respectively. Similarly, air voids of the Superpave™ mixes were different compared to the SMHI Marshall mixes at all angles of gyration. This indicates the ability of the Superpave™ gyratory compactor to differentiate between the SMHI Marshall and Superpave™ mixes.

As seen in Figure 5.9, the Superpave™ gyratory compactor was able to accurately predict air voids of 4.0% at 2.00° angle of gyration which is the desired air voids specified by the Superpave™ mix design procedure. It is therefore concluded that a higher angle of gyration in compacting Saskatchewan asphalt mixes will be suitable to predict desired field air voids.

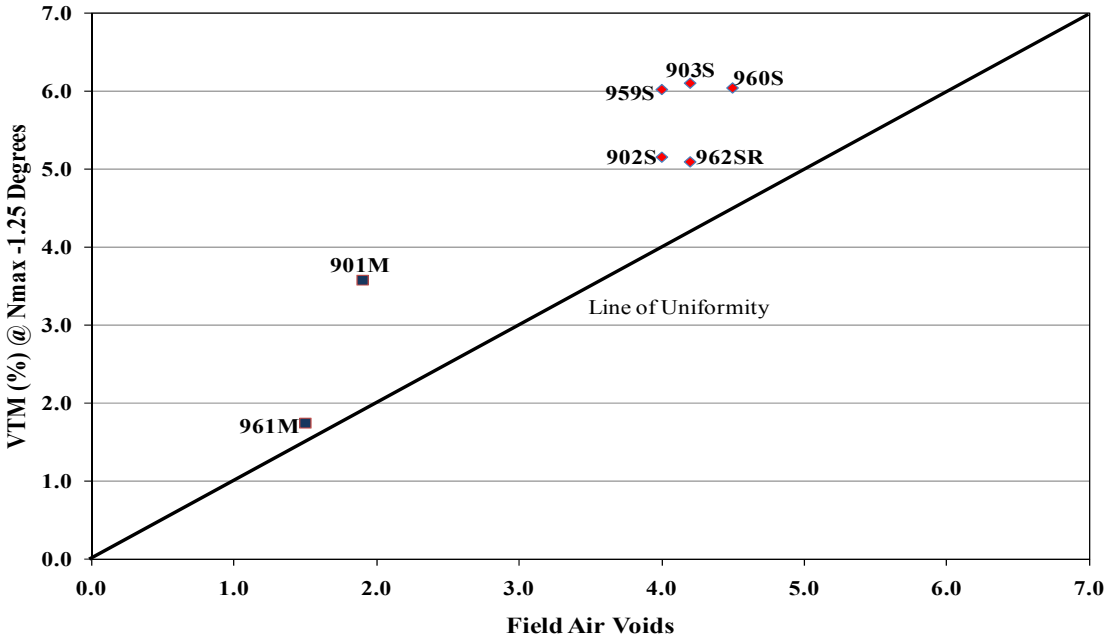

Figure 5.8 Air Voids at 1.25° versus 10-Year Field Air Voids across Radisson SPS-9A Test Sections

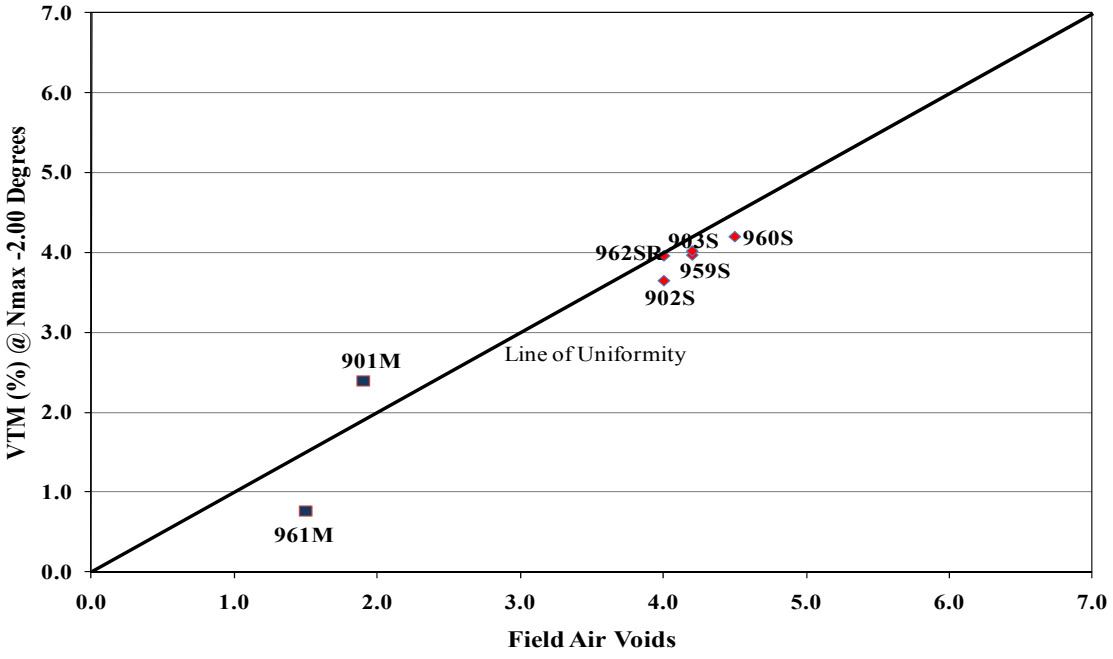

Figure 5.9 Air Voids at 2.00° versus 10-Year Field Air Voids across Radisson SPS-9A Test Sections

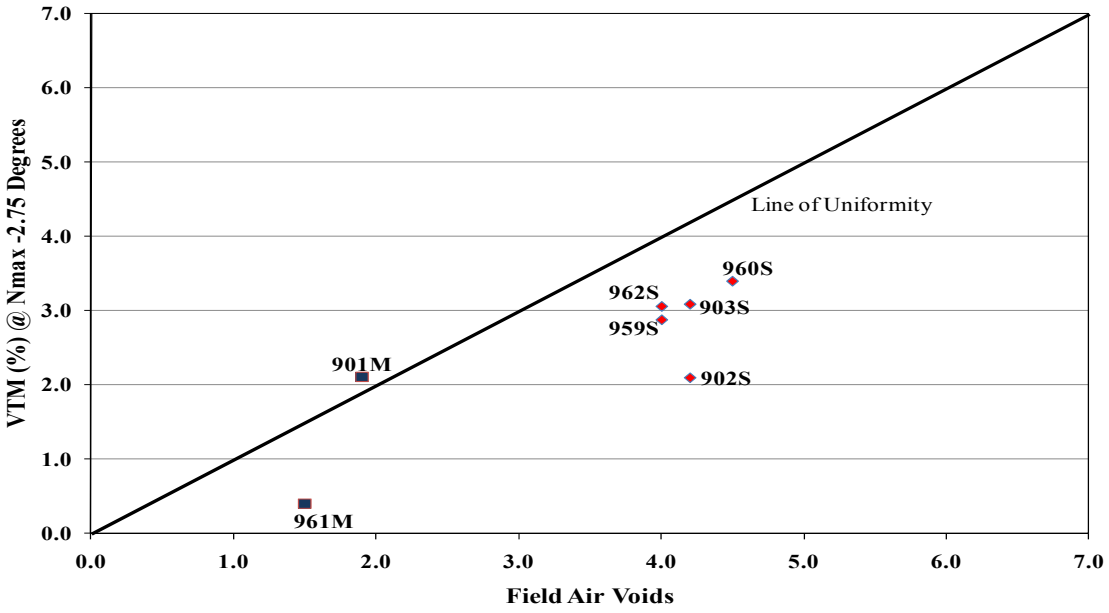

Figure 5.10 Air Voids at 2.75° versus 10-Year Field Air Voids across Radisson SPS-9A Test Sections

5.4 Chapter Summary

Chapter Five presented field data collected from the Radisson SPS-9A test site after ten years of field performance. Rut depths measurements after each year of performance are presented across each test section. Average rut depths after ten years of field performance are also presented across test sections.

Field measurement of rut depth indicates a significant rutting during initial years of construction of each test section with rut depths becoming steady with time. After ten years of traffic loading average rut depth was found to be highest for test sections 961M and 902S. There was a drop of rut depth from the year 2003 to 2004 for test section 961M due to maintenance works that has been carried out.

The asphalt concrete surface dielectric permittivity in the wheelpaths was observed to be generally lower compared to the dielectric permittivity outside the wheelpaths across the Radisson SPS-9A test sections. Based on the field data collected there appear to be an increase in rutting with an increase in asphalt concrete surface dielectric permittivity difference with respect to inside the wheelpaths and between the

wheelpaths across the Radisson SPS-9A asphalt mixes. However, it should be noted that if the two mixes (961M and 962SR) were removed from the data set, a much less obvious trend would exist between the dielectric permittivity and rut depth.

Both Marshall and Superpave™ compaction differentiate between SMHI Marshall and Superpave™ mixes. Laboratory air voids of the Superpave™ mixes were higher compared to field air voids after Marshall compaction. Superpave™ gyratory compactor accurately predicted field air voids at 2.00° angle of gyration.

CHAPTER 6 SUMMARY AND CONCLUSION

Saskatchewan Ministry of Highway and Infrastructure (SMHI) relies on the Marshall mix design protocol for hot-mix asphalt design. The Marshall mix design employs empirical correlation to physical properties of hot-mix asphalt. As such, Marshall mix design is not suitable for evaluating the performance based properties of diverse asphalt mixes, particularly those not typically employed in Saskatchewan. It is therefore necessary to adopt a laboratory mix design and compaction protocol which will be able to characterize and predict volumetric and mechanistic properties of asphalt mixes in the laboratory as obtained in the field compacted asphalt mixes. Therefore sensitivity of asphalt mixes to laboratory compaction properties needs to be accurately characterized.

The primary objective of this research was to characterize and compare the sensitivity of laboratory volumetric properties of conventional SMHI Marshall designed mixes as well as Superpave^{TM} dense graded mixes placed at the Radisson Specific Pavement Study (SPS)-9A test site. This research evaluated the Radisson SPS-9A mixes across varying Marshall and gyratory compaction energies. Secondly, this research was intended to characterize the triaxial frequency sweep mechanical properties of the Radisson SPS-9A asphalt concrete mixes across various laboratory compaction energies.

6.1 Summary of Test Results

The test results obtained with respect to the objectives of this research are presented below.

6.1.1 Objective 1: Characterize and Compare the Sensitivity of Laboratory Volumetric Properties of Conventional SMHI Marshall Mix Designed and Superpave^{TM} Dense Graded Mixes

The volumetric properties of the conventional SMHI Marshall mixes were found to be significantly different than the Superpave^{TM} mixes. Volumetric properties were also statistically significantly different at 50-blow Marshall compared to 75-blow Marshall across all test sections. The average VTM of the Marshall compacted samples

were found to be lower at 75-blow Marshall compared to 50-blow Marshall across all the Radisson SPS-9A test sections, as expected. Only conventional SMHI Marshall mix design test section 961M met the SMHI air voids criteria at 50-blow Marshall with average VTM value of 3.4 percent. The conventional SMHI Marshall mixes were found to have similar VTM. The Superpave^{TM} mixes also showed no significant difference in VTM.

The average VMA of the Marshall samples was found to be lower at 75-blow Marshall compared to 50-blow Marshall across all SPS-9A test sections. The conventional SMHI Marshall mixes have lower VMA values at both 50-blow and 75-blow Marshall relative to Superpave^{TM} mixes. Test sections 901M, 961M and 962SR met the SMHI VMA criteria at 50-blow Marshall with average VMA values of 14.2 percent, 14.6 percent and 15.3 percent respectively. Superpave^{TM} mixes show no significant difference in the VMA at 50 and 75-blow Marshall. VMA was concluded to be sensitive to the mix design method.

The conventional SMHI Marshall mixes 901M and 961M have higher VFA relative to the Superpave^{TM} mixes at both 50 and 75-blow Marshall. It was observed that only test sections 902S and 961M met the SMHI VFA criteria at 50-blow Marshall with average VFA values of 65.2 percent and 76.9 percent respectively. Superpave^{TM} mix design test sections 902S, 903S, 959S and 960S all met the SMHI VFA criteria at 75-blow Marshall. The only significant difference between the VFA of Superpave^{TM} mixes was between test section 962SR with average VFA value 64.6 percent and 902S with average VFA value 70.6 percent. It was concluded that VFA is sensitive to mix design method.

Average VTM of gyratory compacted samples was found to decrease with an increase in the angle of gyration for all the SPS-9A test sections at $N_{initial}$, N_{design} and $N_{maximum}$. The VTM was found to be lower at $N_{maximum}$ relative to N_{design} and was observed to be lower at N_{design} than $N_{initial}$. It was noted that only conventional SMHI Marshall mixes 901M and 961M met the SMHI VTM criteria at N_{design} at 1.25° angle of gyration with average VTM values of percent and 5.0 percent respectively.

The average VMA was found to decrease with an increase in the angle of gyration for all the SPS-9A test sections at $N_{initial}$, N_{design} and $N_{maximum}$. The VMA was found to be lower at $N_{initial}$ relative to N_{design} and was observed to be lower at N_{design} than $N_{maximum}$. None of the test sections met the SMHI VMA criteria at $N_{initial}$ for the three angles of gyration. Only conventional SMHI Marshall mix 901M met the SMHI VMA criteria at N_{design} for 1.25° angle of gyration with average VMA value of 15.1 percent. The conventional SMHI Marshall mixes 901M and 961M met the SMHI VMA criteria at N_{design} for 2.00° angle of gyration with average VMA values of 14.3 percent and 15.3 percent respectively. None of the Superpave™ mixes met the SMHI VMA criteria at N_{design} for 2.00° angle of gyration. The Superpave™ mixes 903S, 959S and 960S were the only test sections that did not meet the SMHI VMA criteria at N_{design} for 2.75° angle of gyration with average VMA values of 16.2 percent, 16.4 percent and 16.1 percent respectively. All the SPS-9A mixes met the SMHI VMA criteria at $N_{maximum}$ for all angles of gyration except Superpave™ mixes 903S, 959S and 960S.

The average VFA was found to increase with an increase in the angle of gyration for all the SPS-9A test sections at $N_{initial}$, N_{design} and $N_{maximum}$. None of the SPS-9A mixes met the SMHI VFA criteria at $N_{initial}$ for all angles of gyration. The conventional SMHI Marshall mix design test section 961M met SMHI VFA criteria for all angles of gyration at N_{design}. The Superpave™ mixes 902S, 903S, 959S and 960S met the SMHI VFA criteria for 2.75° angle of gyration at N_{design}. The conventional SMHI Marshall mix 961M met the SMHI VFA criteria for 1.25° angle of gyration at $N_{maximum}$, with average VFA value of 76.2 percent, but failed for 2.00° and 2.75° angles of gyration.

There was significant increase in density of both Marshall and gyratory compacted samples with increase in compaction energy.

Marshall stability was found to be significant at 50-blow compared to 75-blow Marshall compaction. The conventional SMHI Marshall mixes met the SMHI stability criteria with identical Marshall stability values of 6.8 kN at 50-blow Marshall. The Superpave™ mixes also met the SMHI stability criteria at 50-blow Marshall compaction. Marshall stability values at 75-blow Marshall were found to be above the

acceptable stability criteria for all research mixes except 962SR which recorded low stability values of 5.6 kN and 5.8 kN at 50 and 75-blow Marshall respectively. Marshall flow values were within the SMHI acceptable limits. Only mixes 960S and 962SR failed to meet acceptable criteria at 50-blow and 75-blow Marshall respectively.

6.1.2 Objective 2: Characterize Triaxial Frequency Sweep Mechanistic Properties of Radisson SPS-9A SMHI and Superpave™ Mixes

Dynamic modulus was lower at 200 kPa compared to 600 kPa and lower at 600 kPa compared to 200 kPa (FR) deviatoric stress states across all gyratory angles for all test sections. The conventional SMHI Marshall mix 901M has the highest average dynamic modulus compared to all other test sections across all deviatoric stress states and angles of gyration. Superpave™ recycled mix 962SR displayed less stiffness with lowest average dynamic modulus values across all deviatoric stress states and angles of gyration. Dynamic modulus was sensitive to angle of gyration and deviatoric stress state.

Poisson's ratio was sensitive to varying angle of gyration. The conventional SMHI Marshall mix design test section 961M has the highest Poisson's ratio compared to other test sections across angles of gyration at 600 kPa and 200 kPa (FR) deviatoric stress. Superpave™ mix 959S recorded low average Poisson's ratio of 0.25 at 200 kPa fully reversed deviatoric stress and 2.75° angle of gyration.

Phase angle increases with increased deviatoric stress at all three angles of gyration across all test sections. The highest average phase angle values were recorded at 200 kPa fully reversed deviatoric stress across all test sections. The Superpave™ mix design test sections 959S and 902S have the lowest phase angle values at all three angles of gyration and deviatoric stresses compared to other test sections. Phase angle was sensitive to deviatoric stress state and increased significantly with change in deviatoric stress.

Recoverable radial microstrain was found to be highest at 600 kPa deviatoric stress compared to 200 kPa and 200 kPa fully reversed deviatoric stresses at all angles

of gyrations across all test sections. Recoverable radial microstrain was sensitive to varying deviatoric stress. Recoverable radial microstrain was statistically significant across varied angle of gyration and varied deviatoric stress.

6.1.3 Objective 3: Compare rutting performance of Radisson SPS-9A test sections

Significant rutting was observed during initial years of service across all the Radisson SPS-9A test sections. The rate of rutting was found to stabilize with the aging of the pavement. The asphalt mixes design with soft binder recorded the highest rut depths. The conventional SMHI mix 961M recorded the highest rut depth of 13.0 mm.

The asphalt concrete surface dielectric permittivity in the wheelpaths was observed to be generally lower compared to the dielectric permittivity outside the wheelpaths across the Radisson SPS-9A test sections. There was a general trend of increase in rut depth with an increase in asphalt concrete surface dielectric permittivity across the Radisson SPS-9A test sections.

Both Marshall and Superpave^{TM} compaction differentiate between SMHI Marshall and Superpave^{TM} mixes. Laboratory air voids of the Superpave^{TM} mixes were higher compared to field air voids after Marshall compaction. Superpave^{TM} gyratory compactor accurately predicted field air voids at 2.00° angle of gyration.

6.2 Conclusions

This research hypothesized that gyratory laboratory compaction analysis will provide increased sensitivity in asphaltic mix properties. In addition, it was hypothesized that varied volumetric properties of HMAC mixes will influence the mechanistic triaxial frequency sweep material properties of both conventional Saskatchewan and Superpave^{TM} dense graded mixes.

Based on the increase in density and volumetric properties obtained at 50 and 75 blow Marshall compaction as well as 1.25°, 2.00° and 2.75° angles of gyration and the correlation of laboratory and filed air voids from the Radisson SPS-9A test sections, it is apparent that varying the laboratory compaction energy could be used to accurately predict volumetrics properties of field compacted asphalt mixes. The gyratory

compacted samples displayed significant variation in density and volumetric properties at N_{design} gyration across 1.25°, 2.00° and 2.75° angles of gyration. It was therefore concluded that using the gyratory compactor at a higher angle of gyration than specified by the SHRP protocol is better suited in predicting volumetric properties of Saskatchewan asphalt mixes as field compaction.

Further, varying the volumetric properties of laboratory compacted asphalt mixes significantly affects the stability and flow characteristics as shown by the higher Marshall stability values obtained at 75-blow compared to 50-blow Marshall compaction.

There was improvement in stiffness of the research asphalt mixes with varying volumetric properties as supported by the increase in dynamic modulus with increase in angle of gyration. The conventional SMHI mix 901M recorded the highest dynamic modulus at all angles of gyration. Poisson's ratio was affected by varying volumetric properties with higher Poisson's values at 2.00° and 2.75° angles of gyration compared to Poisson's ratio values at 1.25° angle of gyration. Phase angle increased with increase in angle of gyration and shows that varying the volumetric properties of asphalt mix affect the viscoelastic properties of the asphalt mix.

6.3 Future Research

This research characterized the volumetric and mechanistic material properties of asphalt mixes used in the construction of the Radisson SPS-9A test sections. Significant findings have been made in the conduct of this research which will help improve the compaction protocol used by the SMHI.

It is recommended that future research look into the aging of the asphalt binders used in the mix design of each test section.

Future research should investigate the relationship between the fully reversed deviatoric stress testing in the rapid frequency sweep test and recoverable radial microstrain to rut prediction in the field.

Future research should correlate field density and laboratory mix properties of Saskatchewan asphalt mixes.

LIST OF REFERENCES

AASHTO (1998). Resistance to Deformation and Cohesion of Bituminous Mixtures by Means of Hveem Apparatus. American Association of State Highway and Transportation Officials Provisional Standards.

AASHTO (2000). Compaction of Bituminous Mixture by Means of the Gyratory Compactor. American Association of State Highway and Transportation Officials Provisional Standards.

AASHTO (2000). Preparation of Test Specimens of Bituminous Mixtures by Means of the California Kneading Compactor. American Association of State Highway and Transportation Officials Provisional Standards.

Abdullah, W. S., Obaidat, M.T., Abu-Sa'da, N.M. (1998). Influence of Aggregate Type and Gradation on Voids of Asphalt Concrete Pavements. Journal of Materials in Civil Engineering, v10**:** pp.76-85.

Al-Khateeb, G., Paugh, C., Stuart, K., Harman, T., D'Angelo, J. (2002). Target and Tolerance Study for Angle of Gyration used in Superpave™ Gyratory Compactor. Transportation Research Board. Washington, D.C., n1789**:** pp.208-215.

Anderson, D. A., Maurer, D., Ramirez, T., Christensen, D.W., Marasteanu M.O., Mehta, Y. (1999). Field Performance of Modified Asphalt Binders Evaluated with Superpave™ Test Methods: I-80 Test Project. Transportation Research Board. Washington, D.C., n1661**:** pp.60-68.

Anderson, R. M., Bosley, R.D., Robert, D., Creamer, P.A (1995). Quality Management of HMA Construction Using Superpave™ Aquipment: A Case Study. Transportation Research Record. Washington, D.C., n1513**:** pp.18-24.

Anderson, R. M., and Bentsen, R.A. (2002). Influence of Voids in the Mineral Aggregate (VMA) on the Mechanical Properties of Coarse and Fine Asphalt Mixtures. Association of Asphalt Paving Technologists, v70**:** pp.1-37.

Anderson, R. M. (2002). Using Superpave™ Gyratory Compaction Properties to Estimate the Rutting Potential of Asphalt Mixtures. Association of Asphalt Paving Technologists, v71**:** pp.725-738.

Anthony, A. and Berthelot, C. (2004). Effect of Manufactured Fines on Physical and Mechanistic Properties of Fine Dense Graded Hot Mix Asphalt Pavement Mixes in Saskatchewan. Canadian Technical Asphalt Association Annual Conference, Montreal, Canada. pp.377-397.

Anthony, A. (2007). Effect of Manufactured Fine Aggregate on Physical And Mechanistic Properties of Saskatchewan Asphalt Concrete Mixes. MSc. Thesis, University of Saskatchewan, Department of Civil and Geological Engineering.

Aschenbrener T., M., C. (1994). Factors that Affect the Voids in the Mineral Aggregate of Hot-Mix Asphalt. Transportation Research Board. Washington, D.C., n1416**:** pp.1-8.

Asphalt-Institute (1996). Mix Design Methods for Asphalt Concrete and Other Hot-Mix Types.

Asphalt-Institute (1996). Superpave™ Mix Design.

ASTM-D1559 (1999). Standard Test Method for Resistance to Plastic Flow for Bituminous Mixtures Using Marshall Apparatus. Annual Book of ASTM Standards, American Society of Testing and Materials.

ASTM-D1561 (1999). Preparation of Test Specimens of Bituminous Mixtures by Means of the California Kneading Compactor. Annual Book of ASTM Standards, American Society of Testing and Materials.

ASTM-D2041 (2000). Standard Test Method for Maximum Theoretical Specific Gravity of Loose Asphalt Aggregates Mixture. Annual Book of ASTM Standards, American Society of Testing and Materials.

ASTM-D3549 (2003). Standard Test Method for Thickness or Height of Compacted Bituminous Paving Mixture Specimen. Annual Book of ASTM Standards, American Society of Testing and Materials.

ASTM-D6307 (2004). Standard Test Method for Asphalt Content of Hot-Mix Asphalt by Ignition Oven Method. Annual Book of ASTM Standards, American Society of Testing and Materials.

ASTM-D6927 (2006). Standard Test Method for Marshall Stability and Flow of Bituminous Mixtures. Annual Book of ASTM Standards, American Society of Testing and Materials.

ASTM-D6931 (2000). Standard Test Method for Indirect Tensile Strength of Bituminous Mixtures. Annual Book of ASTM Standards, American Society of Testing and Materials.

Bashin, A., Button, J.W., Chowdhury, A. (2004). Evaluation of Simple Performance Tests on Hot-Mix Asphalt Mixtures from South Central United States. Transportation Research Board. Washington, D.C., n1894**:** pp.174-181.

Baumgartner, E. D. (2005). Triaxial Frequency Sweep Characterization for Dense Graded Hot-Mix Asphalt Concrete Mix Design. M.Sc.Thesis, University of Saskatchewan, Department of Civil and Geological Engineering.

Berthelot, C. F., Crockford, B., Lytton, R (1999). Comparison of Alternative Test Methods for Predicting Asphalt Concrete Rut Performance. Canadian Technical Asphalt Association Proceedings, vXLVL**:** pp.405-434.

Berthelot, C.F., Anthony, A., Raducanu, C. **(**2005). Mechanistic Characterization of Effects of Anti Stripping Agents on Saskatchewan Asphalt Concrete Mixes. Transportation Association of Canada Annual Conference, CDRom Proceedings. Calgary, Canada. September, PP.18-21.

Berthelot, C. F. (1999). Mechanistic Modelling of Saskatchewan SPS-9A Asphalt Concrete Pavements. Ph.D. Dissertation, Texas A&M University, Department of Civil Engineering.

Berthelot, C. F. (2003). Pavement Materials and Design. Course Material for CE 417. University of Saskatchewan.

Brown, E. R., and Cross, S. (1989). A Study of In-Place Rutting of Asphalt Pavements. Association of Asphalt Paving Technologists, v58**.**

Bruce, A. C., Eugene, L.S., Jr., Benita, L.C., Samantha, S. (2000). Effect of Voids in Mineral Aggregates (VMA) on Hot-Mix Asphalt Pavement. Minnesota Department of Transportation.

Butcher, M. (1998). Determining Gyratory Compaction Characteristics using Servopac Gyratory Compactor. Transportation Research Board. Washington, D.C, n1630**:** pp.89-97.

Button, J. W., Little, D.N., Jagadam, V., Pendleton, O.J. (1994). Correlation of Selected Laboratory Compaction Methods with Field Compaction. Transportation Research Board. Washington, D.C., n1454**:** pp.193-204.

Carlberg, M., Berthelot, C, Richardson, N. (2003). Comparison of Marshall and Superpave Gyratory Volumetric Properties of Saskatchewan Asphalt Concrete Mixes. Transportation Association of Canada Annual Conference Proceedings. St. Johns, Canada. CDROM Proceedings.

Chadbourn, B. A., Eugene, L.S.Jr., Crow, B.L., Spindler, S. (2000). Effect of Voids in Mineral Aggregates (VMA) on Hot-Mix Asphalt Pavement. M. D. o. Transportation. Minnesota Department of Transportation.

Christensen, D. W., Pellinen, T., Bonaquist, R.F. (2002). Hirsh Model for Estimating the Modulus of Asphalt Concrete. Paper prepared for presentation at the Annual Meeting of the Highway Research Board.

Crockford, W. W., Berthelot, C.F., Tritt, B., Sinadinos, C. (2002). Triaxial Frequency Sweep Test. Association of Asphalt Paving Technologists, v71**:** pp.712-724.

Dongre, R., Myers, L., D'Angelo, J., Paugh, C., Christensen, D., Heitzman, M., Page, G., Dukatz, E., King, G. (2005). Field Evaluation of Witczak and Hirsch Models for Predicting Dynamic Modulus of Hot-Mix Asphalt. Association of Asphalt Paving Technologists, v74**:** pp.381-442.

Ford, M. C. J. (1988). Pavement Densification Related to Asphalt Mix Characteristics. Transportation Research Board. Washington, D.C., n1178**:** pp.9-15.

Forstie, D. A., and Corum, D.K. (1997). Determination of Key Gyratory Compaction Points for Superpave^{TM} Mix Design in Arizona. American Society for Testing and Materials, ASTM Special Technical Publication, v1322**:** pp.201-209

Gould, J. S., Nanagiri, Y.V., Mallick, R.B., Petruccelli, J.D., Crockford, W.C. (2003). Evaluation of Rapid Triaxial Test in Quality Control of Hot-Mix Asphalt. Transportation Research Board. Washington, D.C., n1832**:** pp.191-200.

Hand, A. J., and Epps, A.L. (2001). Impact of Gradation Relative to Superpave™ Restricted Zone on Hot-Mix Asphalt Performance. Transportation Research Board. Washington, D.C., n1767**:** pp.158-166.

Hand, A. J., Martin, A.E., Sebaaly, P.E., Weitzel, D (2004). Evaluating Field Performance: Case Study Including Hot-Mix Asphalt Performance-Related Specifications. Journal of Transportation Engineering, v130**:** pp.251-260.

Harman, T.P., Bukowsky, J.R., Moutier, F., Huber, G., McGennis, R. (2001). The History and Future Challenges of Gyratory Compaction 1939 – 2001.

Harman, T. P., D'Angelo, J., Bukowski, J.R. (1995). Evaluation of Superpave™ Gyratory Compactor in the Field Management of Asphalt Mixes: Four Simulation Studies. Transportation Research Board. Washington, D.C., n1513**:** pp.1-8.

Harman, T. P., D'Angelo, J., Paugh, C.W. (2002). Evaluation of Volumetric Properties and Gyratory Compaction Slope for the Quality Control of Hot-Mix Asphalt Production. Association of Asphalt Paving Technologists Technical Sessions, v70**:** pp.729-761.

Harvey, J., Eriksen, K., Sousa, J., Monismith, C.L. (1993). Effects of Laboratory Specimen Preparation on Aggregate-Asphalt Structure, Air-Void Content Measurement, and Repetitive Simple Shear Test Results. Transportation Research Board. Washington, D.C., n1454**:** pp.113-122.

Hinrichsen, J., and Heggen, J. (1996). Minimum VMA in HMA Based on Gradation and Volumetric Properties. Iowa Department of Transportation, v960410.

Hinrichsen, J. (2001). Comparison of Four Brands of Superpave™ Gyratory Compactors. Transportation Research Board. Washington, D.C., n1767**:** pp.167-172.

Huber, G. A., and Herman, G.H. (1987). Effect of Asphalt Concrete Parameters on Rutting Performance: A Field Investigation. Association of Asphalt Paving Technologists, v56**:** pp.33-61.

IPC-Global. Pavement Materials Testing, http://www.ipcglobal.com.au/pavement.html.

Kandhal, P. S., and Chakraborty, S. (1996). Evaluation of Voids in the Mineral Aggregate for HMA Paving Mixtures. National Center for Asphalt Technology, v96-4.

Kandhal, P. S., and Mallick, R.B. (2001). Effect of Mix Gradation on Rutting Potential of Dense-Graded Asphalt Mixtures. Transportation Research Board. Washington, D.C., n1767**:** pp.146-151.

Kandhal, P. S., and Cooley Jr., L.A. (2002). Coarse-Versus Fine-Graded Superpave™ Mixtures Comparative Evaluation of Resistance to Rutting. Transportation Research Board. Washington, D.C., n1789**:** pp.216-224.

Kandhal, P. S., and Koehler, W.S. (1985). Marshall Mix Design Method: Current Practices. Association of Asphalt Paving Technologists, v54**:** pp.284-303.

Kavanagh, L. N. (2004). A 9-Year Evaluation of Field Cracking and Rutting Performance of SPS-9 Superpave™ Experiment. Transportation Research Board. Washington, D.C., n1896**:** pp.138-146.

Kennedy, T. W., Von Quintus, H.L., Scherocman, J.A., Hughes, C.S. (1991). Asphalt-Aggregate Mixture Analysis System: AAMAS. Transportation Research Board. Washington, D.C., n339**:** pp.191-122.

Mallick, R. B. (1999). Use of Superpave™ Gyratory Compactor to Characterize Hot-Mix Asphalt. Transportation Research Board. Washington, D.C., n1681**:** pp.86-96.

Monismith, C. L. (1976). Rutting Prediction in Asphalt Concrete Pavements. Transportation Research Board. Washington, D.C., n616**:** pp.2-8.

Monismith, C. L., Sousa, J.B., Deacon, J.A. (1991). Effect of Laboratory Compaction Method on Permanent Deformation Characteristics of Asphalt-Aggregate Mixtures. Association of Asphalt Paving Technologists Technical Sessions, v60**:** pp.533-585.

Myers, L. A., and D'Angelo, J. (2005). Evaluating the Field Performance of Asphalt Mixtures in the Lab. Public Roads, v68**:** pp.38-43.

NCHRP-465. (1994). National Cooperative Highway Research Program.

Prowell, B. D., Brown, E.R., Huner, M.H. (2003). Evaluation of the Internal Angle of Gyration of Superpave™ Gyratory Compactors in Alabama. Association of Asphalt Paving Technologists Technical Sessions, v72**:** pp.533-586.

Roberts, F. L., Kandhal, P.S., Brown, E.R., Lee, D.Y., Kennedy, T.W. (1996). Hot Mix Asphalt Materials, Mixture Design, and Construction. NAPA Research and Education Foundation. Maryland, USA.

Saraf, C. L., Smith, W.F., Finn, F.N. (1976). Rut Depth Prediction. Transportation Research Board. Washington, D.C., n616**:** pp.9-14.

SHRP-A-408. (1994). Level One Mix Design: Materials Selection, Compaction, and Conditioning. Strategic Highway Research Program.

SHRP-A-415. (1994). Permanent Deformation Response of Asphalt Aggregate Mixes. Strategic Highway Research Program.

Sousa, J. B., Harvey, J.T., Bouldin, M.G., Azevedo, C. (1994). Application of SHRP Mix Performance-Based Specifications. Transportation Research Board. Washington, D.C., n1454**:** pp.154-162.

Sousa, J. B., Way, G., Harvey, J.T., Hines, M. (1995). Comparison of Mix Design Concepts. Transportation Research Board. Washington, D.C., n1492**:** pp.151-160.

STP-204-10. (2001). Standard Test Procedure for Marshall Mix Design Method. Saskatchewan Department of Highway and Transportation.

STP-204-27. (2000). Standard Test Procedure for Asphalt Content by Ignition Oven Method. Saskatchewan Department of Highway and Transportation.

Stuart, K. D., and Izzo, R.P. (1995). Correlation of G* / Sin Delta with Rutting Susceptibility from Laboratory Mixture Tests. Transportation Research Board. Washington D.C., n1492**:** pp.176 – 183.

Tandon, V., Kambham, B.S., Bonaquist, R., Solaimanian, M. (2004). Results of Integrating Simple Performance Tests and Environmental Conditioning System. Transportation Research Board. Washington, D.C., n1891**:** pp.140-152.

Tarefder, R. A., Zaman, M., Hobson, K. (2003). A Laboratory and Statistical Evaluation of Factors Affecting Rutting. International Journal of Pavement Engineering, v4**:** pp.59-68.

TexDOT (2005). Superpave Gyratory Compacting of Test Specimens of Bituminous Mixtures. Internet.

Vallerga, B.A. and Lovering, W.R. (1985). Evolution of Hveem Stabilometer Method of Designing Asphalt Paving Mixstures. Association of Asphalt Paving Technologists, v54**:** pp.243-265.

Vavrik, W. R., and Carpenter, S.H. (1998). Calculating Air Voids at Specified Number of Gyrations in Superpave™ Gyratory Compactor. Transportation Research Board. Washington, D.C., n1630**:** pp.117-125.

Von Quintus, H. L., Scherocman, J., Hughes, C. (1987). Asphalt- Aggregate Mixtures Analysis System: Philosophy of the Concept. ASTM Special Technical Publication n1041**:** pp.15.

Von Quintus, H. L., Little, D.N., Consuegra, A., Burati, J. (1989). Comparative Evaluation of Laboratory Compaction Devices Based on Their Ability to Produce Mixtures with Engineering Properties similar to those produced in the Field. Transportation Research Board. Washington, D.C., n1228**:** pp.80-87.

Wang, J., Kennedy, T.W., McGennis, R.B. (2000). Volumetric and Mechanical Performance Properties of Superpave™ Mixtures. Journal of Materials in Civil Engineering, v12**:** pp.238-244.

Watson, D. E., Brown, E.R., Moore, J. (2005). Comparison of Superpave™ and Marshall Mix Performance in Alabama. Transportation Research Board. Washington, D.C., n1929**:** pp.133-140.

Witczak, M. W., and Fonseca, O.A. (1996). Revised Predictive Model for Dynamic (Complex) Modulus of Asphalt Mixtures. Transportation Research Board. Washington, D.C., n1540**:** pp.15-23.

Witczak, M. W., Kaloush, K.E. Von Quintus, H. (2002). Pursuit of the Simple Performance Test for Asphalt Mixture Rutting. Association of Asphalt Paving Technologists, v71**:** pp.671-691.

WSDOT. Washington State Department of Transportation. http://www.wsdot.wa.gov/.

Zeghal, M., Adam, Y.E., Mohamed, H.H. (2005). Effectiveness of Predictive Models for Estimating Asphalt Concrete Complex Modulus. Annual Conerence – Canadian Society for Civil Engineering. TR-188-1-TR-188-10.

Ziauddin, Z. A., Al-Abdu Wahab, H.I., Asi, I., Ramadhan, R. (1998). Comparative Study of Asphalt Concrete Laboratory Compaction Methods to Simulate Field Compaction. Construction and Materials, v12**:** pp.337-384.

APPENDICES

APPENDIX A. VOLUMETRIC PROPERTIES OF MARSHAL COMPACTOR SAMPLES

Table A. 1 Volumetric Properties of Marshall Samples at 50 Blows Marshall for Section 901M

Asphalt Content, P_b(%) = 5.21

BSG Aggregates = 2.64

Theoretical Maximum Specific Gravity = 2.46

Sample Number	Weight in Air (g)	Weight in Water (g)	Weight Saturated Surface-Dry	BSG mix	Marshall Density (kg/m^3)	VTM (%)	VMA (%)	VFA (%)
1	1197.5	694.3	1198.0	2.38	2376.3	3.0	14.3	78.7
2	1198.3	695.3	1198.9	2.38	2378.3	3.0	14.2	79.2
3	1202.0	698.3	1202.5	2.39	2382.9	2.8	14.1	80.3
4	1198.8	695.7	1199.2	2.38	2379.8	2.9	14.2	79.6
Mean	1199.2	695.9	1199.7	2.4	2379.3	2.9	14.2	79.4
Std Dev	2.0	1.7	2.0	0.003	2.8	0.1	0.1	0.7
2 x Std Dev	3.9	3.4	3.9	0.01	5.5	0.2	0.2	1.3
Variance	3.9	2.9	3.9	0.00001	7.6	0.01	0.01	0.4
CV (%)	0.2	0.2	0.2	0.1	0.1	3.9	0.7	0.8

Table A. 2 Volumetric Properties of Marshall Samples at 75 Blows Marshall for Section 901M

Sample Number	Weight in Air (g)	Weight in Water (g)	Weight Saturated Surface-Dry	BSG mix	Marshall Density (kg/m^3)	VTM (%)	VMA (%)	VFA (%)
1	1202.5	700.6	1202.9	2.40	2392.8	2.4	13.7	82.7
2	1201.0	698.7	1201.2	2.39	2388.9	2.5	13.9	81.8
3	1206.7	697.5	1207.2	2.37	2366.3	3.5	14.7	76.5
4	1203.4	700.2	1203.9	2.39	2388.0	2.6	13.9	81.5
Mean	1203.4	699.3	1203.8	2.4	2384.0	2.7	14.0	80.6
Std Dev	2.4	1.4	2.5	0.01	12.0	0.5	0.4	2.8
2 x Std Dev	4.8	2.8	5.1	0.02	23.9	1.0	0.9	5.6
Variance	5.8	2.0	6.4	0.0001	143.3	0.2	0.2	7.9
CV (%)	0.2	0.2	0.2	0.5	0.5	17.9	3.1	3.5

Table A. 3 Volumetric Properties of Marshall Samples at 50 Blows Marshall for Section 902S

Asphalt Content, P_b(%) = 4.28

BSG Aggregates = 2.65

Theoretical Maximum Specific Gravity = 2.48

Sample Number	Weight in Air (g)	Weight in Water (g)	Weight Saturated Surface-Dry	BSG mix	Marshall Density (kg/m^3)	VTM (%)	VMA (%)	VFA (%)
1	1202.3	692.7	1205.3	2.35	2344.4	5.2	15.4	66.4
2	1198.1	691.1	1206.7	2.33	2322.6	6.0	16.2	62.6
3	1193.6	686.5	1196.8	2.34	2337.9	5.4	15.6	65.3
4	1193.2	687.5	1196.4	2.35	2343.5	5.2	15.4	66.3
Mean	1196.8	689.5	1201.3	2.3	2337.1	5.4	15.6	65.2
Std Dev	4.3	2.9	5.5	0.01	10.1	0.4	0.4	1.8
2 x Std Dev	8.6	5.9	10.9	0.02	20.2	0.8	0.7	3.5
Variance	18.4	8.6	29.8	0.0001	101.9	0.2	0.1	3.1
CV (%)	0.4	0.4	0.5	0.4	0.4	7.5	2.3	2.7

Table A. 4 Volumetric Properties of Marshall Samples at 75 Blows Marshall for Section 902S

Sample Number	Weight in Air (g)	Weight in Water (g)	Weight Saturated Surface-Dry	BSG mix	Marshall Density (kg/m^3)	VTM (%)	VMA (%)	VFA (%)
1	1198.1	694.0	1202.5	2.36	2355.0	4.7	15.0	68.5
2	1198.6	696.8	1200.8	2.38	2377.0	3.8	14.2	73.0
3	1196.4	694.9	1199.0	2.38	2372.2	4.0	14.4	71.9
4	1199.5	696.1	1204.7	2.36	2357.3	4.6	14.9	68.9
Mean	1198.2	695.5	1201.8	2.4	2365.4	4.3	14.6	70.6
Std Dev	1.3	1.2	2.4	0.01	10.9	0.4	0.4	2.2
2 x Std Dev	2.6	2.5	4.9	0.02	21.8	0.9	0.8	4.5
Variance	1.7	1.6	5.9	0.0001	118.3	0.2	0.2	5.0
CV (%)	0.1	0.2	0.2	0.5	0.5	10.2	2.7	3.2

Table A. 5 Volumetric Properties of Marshall Samples at 50 Blows Marshall for Section 903S

Asphalt Content, P_b(%) = 5.03

BSG Aggregates = 2.47

Theoretical Maximum Specific Gravity = 2.65

Sample Number	Weight in Air (g)	Weight in Water (g)	Weight Saturated Surface-Dry	BSG mix	Marshall Density (kg/m^3)	VTM (%)	VMA (%)	VFA (%)
1	1200.6	686.3	1203.6	2.32	2319.8	6.0	16.4	63.2
2	1202.0	688.0	1207.2	2.32	2314.0	6.3	16.6	62.3
3	1199.9	687.6	1203.4	2.33	2325.2	5.8	16.2	64.1
4	1201.0	686.6	1204.9	2.32	2316.1	6.2	16.6	62.6
Mean	1200.9	687.1	1204.8	2.3	2318.7	6.1	16.5	63.1
Std Dev	0.9	0.8	1.7	0.01	4.9	0.2	0.2	0.8
2 x Std Dev	1.8	1.6	3.5	0.01	9.8	0.4	0.4	1.6
Variance	0.8	0.6	3.1	0.00002	24.0	0.04	0.03	0.7
CV (%)	0.1	0.1	0.1	0.2	0.2	3.3	1.1	1.3

Table A. 6 Volumetric Properties of Marshall Samples at 75 Blows Marshall for Section 903S

Sample Number	Weight in Air (g)	Weight in Water (g)	Weight Saturated Surface-Dry	BSG mix	Marshall Density (kg/m^3)	VTM (%)	VMA (%)	VFA (%)
1	1192.1	690.2	1194.9	2.36	2360.9	4.4	14.9	70.7
2	1189.2	684.9	1191.6	2.35	2345.8	5.0	15.5	67.8
3	1186.9	684.0	1190.2	2.35	2343.6	5.1	15.6	67.4
4	1184.2	681.9	1187.4	2.35	2341.5	5.2	15.6	67.0
Mean	1188.1	685.3	1191.0	2.4	2347.9	4.9	15.4	68.2
Std Dev	3.4	3.5	3.1	0.01	8.8	0.4	0.3	1.7
2 x Std Dev	6.7	7.1	6.2	0.02	17.6	0.7	0.6	3.4
Variance	11.3	12.5	9.7	0.0001	77.2	0.1	0.1	2.9
CV (%)	0.3	0.5	0.3	0.4	0.4	7.3	2.1	2.5

Table A. 7 Volumetric Properties of Marshall Samples at 50 Blows Marshall for Section 959S

Asphalt Content, P_b(%) = 5.03

BSG Aggregates = 2.47

Theoretical Maximum Specific Gravity = 2.65

Sample Number	Weight in Air (g)	Weight in Water (g)	Weight Saturated Surface-Dry	BSG mix	Marshall Density (kg/m^3)	VTM (%)	VMA (%)	VFA (%)
1	1187.7	682.8	1192.9	2.33	2327.2	5.6	16.2	65.4
2	1186.0	678.4	1194.9	2.30	2295.1	6.9	17.4	60.2
3	1189.6	684.7	1195.9	2.33	2325.9	5.7	16.3	65.1
4	1187.0	681.7	1196.2	2.31	2306.0	6.5	17.0	61.8
Mean	1187.6	681.9	1195.0	2.3	2313.6	6.2	16.7	63.1
Std Dev	1.5	2.6	1.5	0.02	15.7	0.6	0.6	2.5
2 x Std Dev	3.0	5.3	3.0	0.03	31.4	1.3	1.1	5.1
Variance	2.3	7.0	2.2	0.0003	246.1	0.4	0.3	6.5
CV (%)	0.1	0.4	0.1	0.7	0.7	10.3	3.4	4.0

Table A. 8 Volumetric Properties of Marshall Samples at 75 Blows Marshall for Section 959S

Sample Number	Weight in Air (g)	Weight in Water (g)	Weight Saturated Surface-Dry	BSG mix	Marshall Density (kg/m^3)	VTM (%)	VMA (%)	VFA (%)
1	1189.1	686.9	1193.7	2.35	2345.2	4.9	15.6	68.6
2	1194.4	687.5	1199.9	2.33	2329.9	5.5	16.1	65.8
3	1188.8	684.7	1193.6	2.34	2334.9	5.3	15.9	66.7
4	1186.6	682.6	1191.4	2.34	2331.0	5.5	16.1	66.0
Mean	1189.7	685.4	1194.7	2.3	2335.2	5.3	15.9	66.8
Std Dev	3.3	2.2	3.7	0.01	7.0	0.3	0.3	1.3
2 x Std Dev	6.6	4.5	7.3	0.01	13.9	0.6	0.5	2.5
Variance	11.0	5.0	13.4	0.0001	48.4	0.1	0.1	1.6
CV (%)	0.3	0.3	0.3	0.3	0.3	5.3	1.6	1.9

Table A. 9 Volumetric Properties of Marshall Samples at 50 Blows Marshall for Section 960S

Asphalt Content, P_b(%) = 5.2

BSG Aggregates = 2.48

Theoretical Maximum Specific Gravity = 2.65

Sample Number	Weight in Air (g)	Weight in Water (g)	Weight Saturated Surface-Dry	BSG mix	Marshall Density (kg/m^3)	VTM (%)	VMA (%)	VFA (%)
1	1186.8	681.9	1191.2	2.33	2329.1	6.0	16.2	62.8
2	1191.9	682.5	1195.5	2.33	2322.3	6.3	16.5	61.6
3	1178.8	677.6	1181.8	2.34	2336.8	5.7	15.9	64.1
4	1184.0	678.2	1191.4	2.31	2306.0	7.0	17.0	59.1
Mean	1185.4	680.1	1190.0	2.3	2323.5	6.3	16.4	61.9
Std Dev	5.5	2.5	5.8	0.01	13.1	0.5	0.5	2.1
2 x Std Dev	10.9	5.0	11.6	0.03	26.3	1.1	0.9	4.2
Variance	29.9	6.3	33.6	0.0002	172.7	0.3	0.2	4.4
CV (%)	0.5	0.4	0.5	0.6	0.6	8.5	2.9	3.4

Table A. 10 Volumetric Properties of Marshall Samples at 75 Blows Marshall for Section 960S

Sample Number	Weight in Air (g)	Weight in Water (g)	Weight Saturated Surface-Dry	BSG mix	Marshall Density (kg/m^3)	VTM (%)	VMA (%)	VFA (%)
1	1172.3	676.7	1174.8	2.36	2352.4	5.1	15.4	66.8
2	1175.4	675.3	1177.5	2.34	2339.4	5.6	15.8	64.5
3	1168.7	676.9	1171.2	2.37	2363.2	4.7	15.0	68.9
4	1126.5	650.7	1128.8	2.36	2355.1	5.0	15.3	67.3
Mean	1160.7	669.9	1163.1	2.4	2352.5	5.1	15.4	66.9
Std Dev	23.0	12.8	23.0	0.01	9.9	0.4	0.4	1.8
2 x Std Dev	46.0	25.6	46.0	0.02	19.8	0.8	0.7	3.6
Variance	528.1	164.3	528.8	0.0001	97.9	0.2	0.1	3.3
CV (%)	2.0	1.9	2.0	0.4	0.4	7.8	2.3	2.7

Table A. 11 Volumetric Properties of Marshall Samples at 50 Blows Marshall for Section 961M

Asphalt Content, P_b(%) = 5.21

BSG Aggregates = 2.46

Theoretical Maximum Specific Gravity = 2.64

Sample Number	Weight in Air (g)	Weight in Water (g)	Weight Saturated Surface-Dry	BSG mix	Marshall Density (kg/m^3)	VTM (%)	VMA (%)	VFA (%)
1	1198.3	691.3	1199.2	2.36	2358.2	3.8	15.0	74.7
2	1195.5	692.3	1196.3	2.37	2370.9	3.3	14.5	77.5
3	1194.6	691.1	1195.4	2.37	2367.7	3.4	14.6	76.8
4	1196.9	693.9	1197.4	2.38	2376.0	3.1	14.3	78.7
Mean	1196.3	692.2	1197.1	2.4	2368.2	3.4	14.6	76.9
Std Dev	1.6	1.3	1.6	0.01	7.5	0.3	0.3	1.7
2 x Std Dev	3.2	2.6	3.3	0.02	15.0	0.6	0.5	3.3
Variance	2.6	1.6	2.7	0.0001	56.3	0.1	0.1	2.7
CV (%)	0.1	0.2	0.1	0.3	0.3	9.1	1.9	2.2

Table A. 12 Volumetric Properties of Marshall Samples at 75 Blows Marshall for Section 961M

Sample Number	Weight in Air (g)	Weight in Water (g)	Weight Saturated Surface-Dry	BSG mix	Marshall Density (kg/m^3)	VTM (%)	VMA (%)	VFA (%)
1	1204.1	699.4	1204.6	2.39	2382.3	2.8	14.1	80.1
2	1200.8	698.5	1201.5	2.39	2386.1	2.6	13.9	81.1
3	1201.2	695.6	1201.8	2.38	2371.6	3.2	14.5	77.7
4	1200.8	698.1	1201.2	2.39	2385.6	2.7	14.0	81.0
Mean	1201.7	697.9	1202.3	2.4	2381.4	2.8	14.1	80.0
Std Dev	1.6	1.7	1.6	0.01	6.8	0.3	0.2	1.6
2 x Std Dev	3.2	3.3	3.1	0.01	13.5	0.6	0.5	3.2
Variance	2.5	2.7	2.5	0.0001	45.7	0.1	0.1	2.5
CV (%)	0.1	0.2	0.1	0.3	0.3	9.7	1.7	2.0

Table A. 13 Volumetric Properties of Marshall Samples at 50 Blows Marshall for Section 962SR

Asphalt Content, P_b(%) = 4.69

BSG Aggregates = 2.49

Theoretical Maximum Specific Gravity = 2.65

Sample Number	Weight in Air (g)	Weight in Water (g)	Weight Saturated Surface-Dry	BSG mix	Marshall Density (kg/m^3)	VTM (%)	VMA (%)	VFA (%)
1	1167.0	677.0	1173.2	2.35	2350.7	5.3	15.0	64.7
2	1163.5	676.6	1171.4	2.35	2350.3	5.3	15.0	64.6
3	1132.2	655.8	1142.6	2.33	2324.7	6.3	15.9	60.2
4	1118.0	648.9	1126.5	2.34	2339.7	5.7	15.4	62.7
Mean	1145.2	664.6	1153.4	2.3	2341.4	5.7	15.3	63.1
Std Dev	23.9	14.4	22.8	0.01	12.2	0.5	0.4	2.1
2 x Std Dev	47.9	28.8	45.6	0.03	24.5	1.0	0.9	4.2
Variance	573.0	207.2	518.8	0.0002	149.7	0.2	0.2	4.5
CV (%)	2.1	2.2	2.0	0.5	0.5	8.7	2.9	3.4

Table A. 14 Volumetric Properties of Marshall Samples at 75 Blows Marshall for Section 962SR

Sample Number	Weight in Air (g)	Weight in Water (g)	Weight Saturated Surface-Dry	BSG mix	Marshall Density (kg/m^3)	VTM (%)	VMA (%)	VFA (%)
1	1172.2	680.6	1179.5	2.35	2348.4	5.4	15.0	64.3
2	1165.8	675.5	1171.0	2.36	2351.6	5.2	14.9	64.9
3	1164.0	675.1	1170.6	2.35	2348.0	5.4	15.1	64.2
4	1169.2	680.3	1177.2	2.36	2351.8	5.2	14.9	64.9
Mean	1167.8	677.9	1174.6	2.4	2350.0	5.3	15.0	64.6
Std Dev	3.6	3.0	4.5	0.002	2.0	0.1	0.1	0.4
2 x Std Dev	7.3	6.0	8.9	0.004	4.1	0.2	0.1	0.7
Variance	13.3	8.9	19.9	0.000004	4.2	0.01	0.01	0.1
CV (%)	0.3	0.4	0.4	0.1	0.1	1.6	0.5	0.6

APPENDIX B. VOLUMETRIC PROPERTIES OF SUPERPAVE™GYRATORY COMPACTOR SAMPLES

Table B. 1 Volumetric Properties of SHRP Gyratory Compactor Samples for 1.25° Angle of Gyration at $N_{initial}$ for Section 901M

Asphalt Content, P_b(%) = 5.21

BSG Aggregates = 2.64

Theoretical Maximum Specific Gravity = 2.46

Sample Number	G_{mb} corrected	VTM (%)	VMA (%)	VFA (%)
1	2.20	10.4	21.0	50.6
2	2.20	10.4	21.0	50.4
3	2.19	10.9	21.5	49.1
4	2.17	11.6	22.0	47.5
5	2.18	11.3	21.8	48.2
Mean	2.2	10.9	21.5	49.2
Std Dev	0.0	0.5	0.5	1.3
2 x Std Dev	0.0	1.0	0.9	2.7
Variance	0.00	0.27	0.21	1.81
CV (%)	0.59	4.79	2.15	2.73

Table B. 2 Volumetric Properties of SHRP Gyratory Compactor Samples for 1.25° Angle of Gyration at N_{design} for Section 901M

Sample Number	G_{mb} corrected	VTM (%)	VMA (%)	VFA (%)
1	2.38	3.1	14.6	78.9
2	2.38	3.0	14.5	79.4
3	2.36	3.8	15.2	74.8
4	2.35	4.2	15.6	72.8
5	2.36	4.0	15.4	73.7
Mean	2.4	3.6	15.1	75.9
Std Dev	0.01	0.6	0.5	3.0
2 x Std Dev	0.03	1.1	1.0	6.1
Variance	0.00	0.33	0.26	9.18
CV (%)	0.60	15.81	3.36	3.99

Table B. 3 Volumetric Properties of SHRP Gyratory Compactor Samples for 1.25° Angle of Gyration at $N_{maximum}$ for Section 901M

Sample Number	G_{mb} corrected	VTM (%)	VMA (%)	VFA (%)
1	2.42	1.6	13.3	87.8
2	2.41	1.7	13.3	87.5
3	2.41	1.7	13.4	87.0
4	2.41	1.8	13.5	86.3
5	2.41	1.8	13.5	86.3
Mean	2.4	1.7	13.4	87.0
Std Dev	0.00	0.1	0.1	0.7
2 x Std Dev	0.00	0.2	0.2	1.3
Variance	0.00	0.01	0.01	0.43
CV (%)	0.10	5.67	0.65	0.75

Table B. 4 Volumetric Properties of SHRP Gyratory Compactor Samples for 2.00° Angle of Gyration at $N_{initial}$ for Section 901M

Sample Number	G_{mb} corrected	VTM (%)	VMA (%)	VFA (%)
1	2.23	9.3	20.0	53.6
2	2.21	10.1	20.8	51.2
3	2.23	9.3	20.1	53.6
4	2.21	10.0	20.7	51.5
5	2.21	10.0	20.7	51.6
Mean	2.2	9.8	20.5	52.3
Std Dev	0.01	0.4	0.4	1.2
2 x Std Dev	0.02	0.8	0.7	2.4
Variance	0.00	0.17	0.14	1.42
CV (%)	0.46	4.29	1.80	2.28

Table B. 5 Volumetric Properties of SHRP Gyratory Compactor Samples for 2.00° Angle of Gyration at N_{design} for Section 901M

Sample Number	G_{mb} corrected	VTM (%)	VMA (%)	VFA (%)
1	2.40	2.1	13.7	84.4
2	2.38	3.3	14.7	77.9
3	2.40	2.4	13.9	83.0
4	2.38	3.2	14.7	78.2
5	2.38	3.0	14.5	79.2
Mean	2.4	2.8	14.3	80.5
Std Dev	0.01	0.5	0.4	3.0
2 x Std Dev	0.02	1.0	0.9	5.9
Variance	0.00	0.26	0.20	8.77
CV (%)	0.52	18.11	3.12	3.68

Table B. 6 Volumetric Properties of SHRP Gyratory Compactor Samples for 2.00° Angle of Gyration at $N_{maximum}$ for Section 901M

Sample Number	G_{mb} corrected	VTM (%)	VMA (%)	VFA (%)
1	2.44	0.6	12.4	94.8
2	2.44	0.7	12.5	94.4
3	2.43	0.8	12.6	93.4
4	2.43	1.0	12.7	92.5
5	2.44	0.6	12.4	94.8
Mean	2.4	0.8	12.5	94.0
Std Dev	0.00	0.1	0.1	1.0
2 x Std Dev	0.01	0.3	0.2	2.0
Variance	0.00	0.02	0.01	1.04
CV (%)	0.14	17.99	0.96	1.09

Table B. 7 Volumetric Properties of SHRP Gyratory Compactor Samples for 2.75° Angle of Gyration at $N_{initial}$ for Section 901M

Sample Number	G_{mb} corrected	VTM (%)	VMA (%)	VFA (%)
1	2.23	9.3	20.1	53.5
2	2.24	8.8	19.6	55.0
3	2.25	8.5	19.3	56.2
4	2.22	9.7	20.4	52.6
Mean	2.2	9.1	19.9	54.3
Std Dev	0.01	0.5	0.5	1.6
2 x Std Dev	0.03	1.1	0.9	3.2
Variance	0.00	0.28	0.22	2.56
CV (%)	0.58	5.86	2.36	2.95

Table B. 8 Volumetric Properties of SHRP Gyratory Compactor Samples for 2.75° Angle of Gyration at N_{design} for Section 901M

Sample Number	G_{mb} corrected	VTM (%)	VMA (%)	VFA (%)
1	2.40	2.4	13.9	83.0
2	2.40	2.3	13.9	83.6
3	2.41	1.6	13.3	87.7
4	2.38	3.3	14.7	77.9
Mean	2.4	2.4	14.0	83.0
Std Dev	0.02	0.7	0.6	4.0
2 x Std Dev	0.03	1.3	1.2	8.0
Variance	0.00	0.44	0.34	15.99
CV (%)	0.68	27.79	4.18	4.81

Table B. 9 Volumetric Properties of SHRP Gyratory Compactor Samples for 2.75° Angle of Gyration at $N_{maximum}$ for Section 901M

Sample Number	G_{mb} corrected	VTM (%)	VMA (%)	VFA (%)
1	2.44	0.5	12.3	95.6
2	2.44	0.4	12.2	96.4
3	2.45	0.4	12.2	96.8
4	2.45	0.2	12.1	98.0
Mean	2.4	0.4	12.2	96.7
Std Dev	0.00	0.1	0.1	1.0
2 x Std Dev	0.01	0.3	0.2	2.1
Variance	0.00	0.02	0.01	1.05
CV (%)	0.13	31.89	0.93	1.06

Table B. 10 Volumetric Properties of SHRP Gyratory Compactor Samples for 1.25° Angle of Gyration at $N_{initial}$ for Section 902S

Asphalt Content, P_b(%) = 4.82

BSG Aggregates = 2.65

Theoretical Maximum Specific Gravity = 2.48

Sample Number	G_{mb} corrected	VTM (%)	VMA (%)	VFA (%)
1	2.07	16.2	25.7	36.9
2	2.05	17.0	26.4	35.6
3	2.14	13.6	23.4	41.8
Mean	2.1	15.6	25.2	38.1
Std Dev	0.04	1.8	1.6	3.3
2 x Std Dev	0.09	3.5	3.1	6.5
Variance	0.00	3.13	2.46	10.62
CV (%)	2.10	11.32	6.23	8.56

Table B. 11 Volumetric Properties of SHRP Gyratory Compactor Samples for 1.25° Angle of Gyration at N_{dedign} for Section 902S

Asphalt Content, P_b(%) = 4.82

BSG Aggregates = 2.65

Theoretical Maximum Specific Gravity = 2.48

Sample Number	G_{mb} corrected	VTM (%)	VMA (%)	VFA (%)
1	2.30	7.2	17.7	59.4
2	2.27	8.3	18.6	55.8
3	2.36	4.6	15.4	70.1
Mean	2.3	6.7	17.3	61.8
Std Dev	0.05	1.9	1.7	7.5
2 x Std Dev	0.09	3.8	3.3	15.0
Variance	0.00	3.53	2.77	56.02
CV (%)	2.01	28.10	9.65	12.12

Table B. 12 Volumetric Properties of SHRP Gyratory Compactor Samples for 1.25° Angle of Gyration at $N_{maximum}$ for Section 902S

Sample Number	G_{mb} corrected	VTM (%)	VMA (%)	VFA (%)
1	2.35	5.0	15.8	68.4
2	2.34	5.5	16.3	65.9
3	2.36	4.8	15.6	69.4
Mean	2.3	5.1	15.9	67.9
Std Dev	0.01	0.4	0.4	1.8
2 x Std Dev	0.02	0.8	0.7	3.6
Variance	0.00	0.16	0.13	3.29
CV (%)	0.43	7.96	2.27	2.67

Table B. 13 Volumetric Properties of SHRP Gyratory Compactor Samples for 2.00° Angle of Gyration at $N_{initial}$ for Section 902S

Sample Number	G_{mb} corrected	VTM (%)	VMA (%)	VFA (%)
1	2.08	16.2	25.7	37.0
2	2.09	15.5	25.1	38.2
3	2.11	14.7	24.4	39.6
Mean	2.1	15.5	25.1	38.3
Std Dev	0.02	0.7	0.6	1.3
2 x Std Dev	0.04	1.5	1.3	2.6
Variance	0.00	0.53	0.42	1.74
CV (%)	0.86	4.71	2.58	3.45

Table B. 14 Volumetric Properties of SHRP Gyratory Compactor Samples for 2.00° Angle of Gyration at N_{dedign} for Section 902S

Sample Number	G_{mb} corrected	VTM (%)	VMA (%)	VFA (%)
1	2.31	6.7	17.3	61.2
2	2.32	6.2	16.9	63.0
3	2.33	5.8	16.5	64.8
Mean	2.3	6.2	16.9	63.0
Std Dev	0.01	0.5	0.4	1.8
2 x Std Dev	0.02	0.9	0.8	3.6
Variance	0.00	0.21	0.16	3.27
CV (%)	0.48	7.27	2.39	2.87

Table B. 15 Volumetric Properties of SHRP Gyratory Compactor Samples for 2.00° Angle of Gyration at $N_{maximum}$ for Section 902S

Sample Number	G_{mb} corrected	VTM (%)	VMA (%)	VFA (%)
1	2.36	4.5	15.4	70.4
2	2.37	4.2	15.0	72.2
3	2.39	3.3	14.3	76.8
Mean	2.4	4.0	14.9	73.1
Std Dev	0.02	0.6	0.6	3.3
2 x Std Dev	0.03	1.3	1.1	6.6
Variance	0.00	0.40	0.31	10.74
CV (%)	0.66	15.73	3.76	4.48

Table B. 16 Volumetric Properties of SHRP Gyratory Compactor Samples for 2.75° Angle of Gyration at $N_{initial}$ for Section 902S

Sample Number	G_{mb} corrected	VTM (%)	VMA (%)	VFA (%)
1	2.15	13.3	23.1	42.4
2	2.17	12.4	22.3	44.5
3	2.19	11.5	21.5	46.6
Mean	2.2	12.4	22.3	44.5
Std Dev	0.02	0.9	0.8	2.1
2 x Std Dev	0.05	1.8	1.6	4.2
Variance	0.00	0.83	0.66	4.31
CV (%)	1.04	7.36	3.63	4.66

Table B. 17 Volumetric Properties of SHRP Gyratory Compactor Samples for 2.75° Angle of Gyration at N_{dedign} for Section 902S

Sample Number	G_{mb} corrected	VTM (%)	VMA (%)	VFA (%)
1	2.35	5.2	15.9	67.6
2	2.37	4.1	15.0	72.4
3	2.38	4.0	14.9	73.2
Mean	2.4	4.4	15.3	71.1
Std Dev	0.02	0.6	0.6	3.0
2 x Std Dev	0.03	1.3	1.1	6.1
Variance	0.00	0.40	0.32	9.20
CV (%)	0.66	14.35	3.69	4.27

Table B. 18 Volumetric Properties of SHRP Gyratory Compactor Samples for 2.75° Angle of Gyration at $N_{maximum}$ for Section 902S

Sample Number	G_{mb} corrected	VTM (%)	VMA (%)	VFA (%)
1	2.41	2.5	13.6	81.3
2	2.43	2.0	13.1	85.0
3	2.43	1.8	12.9	86.0
Mean	2.4	2.1	13.2	84.1
Std Dev	0.01	0.4	0.3	2.5
2 x Std Dev	0.02	0.8	0.7	5.0
Variance	0.00	0.15	0.12	6.16
CV (%)	0.39	18.34	2.59	2.95

Table B. 19 Volumetric Properties of SHRP Gyratory Compactor Samples for 1.25° Angle of Gyration at $N_{initial}$ for Section 903S

Asphalt Content, P_b(%) = 5.03

BSG Aggregates = 2.65

Theoretical Maximum Specific Gravity = 2.47

Sample Number	G_{mb} corrected	VTM (%)	VMA (%)	VFA (%)
1	2.06	16.5	26.1	36.6
2	2.06	16.8	26.3	36.1
3	2.04	17.4	26.8	35.2
4	2.05	17.3	26.7	35.4
5	2.06	16.9	26.4	36.1
Mean	2.1	17.0	26.5	35.9
Std Dev	0.0	0.3	0.3	0.6
2 x Std Dev	0.02	0.7	0.6	1.1
Variance	0.00	0.12	0.09	0.32
CV (%)	0.42	2.03	1.15	1.57

Table B. 20 Volumetric Properties of SHRP Gyratory Compactor Samples for 1.25° Angle of Gyration at N_{design} for Section 903S

Sample Number	G_{mb} corrected	VTM (%)	VMA (%)	VFA (%)
1	2.28	7.7	18.3	57.7
2	2.27	8.1	18.6	56.6
3	2.26	8.6	19.1	54.7
4	2.27	8.0	18.5	56.7
5	2.28	7.7	18.2	57.9
Mean	2.3	8.0	18.5	56.7
Std Dev	0.0	0.4	0.3	1.3
2 x Std Dev	0.02	0.8	0.7	2.5
Variance	0.00	0.15	0.12	1.58
CV (%)	0.42	4.77	1.83	2.22

Table B. 21 Volumetric Properties of SHRP Gyratory Compactor Samples for 1.25° Angle of Gyration at $N_{dmaximum}$ for Section 903S

Sample Number	G_{mb} corrected	VTM (%)	VMA (%)	VFA (%)
1	2.33	5.8	16.5	65.2
2	2.32	6.2	16.9	63.5
3	2.31	6.6	17.3	61.9
4	2.32	6.1	16.8	63.8
5	2.33	5.9	16.7	64.6
Mean	2.3	6.1	16.8	63.8
Std Dev	0.0	0.3	0.3	1.2
2 x Std Dev	0.02	0.6	0.5	2.5
Variance	0.00	0.09	0.07	1.51
CV (%)	0.33	5.04	1.62	1.93

Table B. 22 Volumetric Properties of SHRP Gyratory Compactor Samples for 2.00° Angle of Gyration at $N_{initial}$ for Section 903S

Sample Number	G_{mb} corrected	VTM (%)	VMA (%)	VFA (%)
1	2.06	16.5	26.1	36.7
2	2.06	16.7	26.3	36.3
3	2.07	16.2	25.8	37.2
4	2.09	15.7	25.3	38.1
5	2.11	14.8	24.5	39.8
Mean	2.1	16.0	25.6	37.6
Std Dev	0.0	0.8	0.7	1.4
2 x Std Dev	0.04	1.6	1.4	2.8
Variance	0.00	0.61	0.48	1.93
CV (%)	0.93	4.89	2.70	3.70

Table B. 23 Volumetric Properties of SHRP Gyratory Compactor Samples for 2.00° Angle of Gyration at N_{design} for Section 903S

Sample Number	G_{mb} corrected	VTM (%)	VMA (%)	VFA (%)
1	2.31	6.8	17.4	61.2
2	2.31	6.7	17.4	61.5
3	2.30	6.8	17.5	60.9
4	2.33	5.8	16.6	65.0
5	2.34	5.5	16.3	66.2
Mean	2.3	6.3	17.0	63.0
Std Dev	0.0	0.6	0.5	2.5
2 x Std Dev	0.03	1.2	1.1	4.9
Variance	0.00	0.38	0.30	6.06
CV (%)	0.66	9.74	3.20	3.91

Table B. 24 Volumetric Properties of SHRP Gyratory Compactor Samples for 2.00° Angle of Gyration at $N_{maximum}$ for Section 903S

Sample Number	G_{mb} corrected	VTM (%)	VMA (%)	VFA (%)
1	2.37	4.3	15.2	71.9
2	2.37	4.1	15.1	72.8
3	2.36	4.5	15.4	71.1
4	2.38	3.7	14.7	74.8
5	2.39	3.3	14.4	76.8
Mean	2.4	4.0	15.0	73.5
Std Dev	0.0	0.4	0.4	2.3
2 x Std Dev	0.02	0.9	0.8	4.6
Variance	0.00	0.20	0.16	5.38
CV (%)	0.47	11.29	2.66	3.16

Table B. 25 Volumetric Properties of SHRP Gyratory Compactor Samples for 2.75° Angle of Gyration at $N_{initial}$ for Section 903S

Sample Number	G_{mb} corrected	VTM (%)	VMA (%)	VFA (%)
1	2.11	14.7	24.5	39.9
2	2.10	15.2	24.9	39.0
3	2.10	15.0	24.7	39.4
4	2.11	14.5	24.3	40.3
Mean	2.1	14.8	24.6	39.6
Std Dev	0.0	0.3	0.3	0.6
2 x Std Dev	0.02	0.6	0.5	1.2
Variance	0.00	0.10	0.07	0.34
CV (%)	0.36	2.08	1.11	1.48

Table B. 26 Volumetric Properties of SHRP Gyratory Compactor Samples for 2.75° Angle of Gyration at N_{design} for Section 903S

Sample Number	G_{mb} corrected	VTM (%)	VMA (%)	VFA (%)
1	2.34	5.5	16.3	66.4
2	2.33	5.7	16.5	65.4
3	2.34	5.5	16.3	66.3
4	2.34	5.4	16.3	66.6
Mean	2.3	5.5	16.3	66.2
Std Dev	0.0	0.1	0.1	0.5
2 x Std Dev	0.01	0.2	0.2	1.0
Variance	0.00	0.01	0.01	0.27
CV (%)	0.13	2.21	0.66	0.79

Table B. 27 Volumetric Properties of SHRP Gyratory Compactor Samples for 2.75° Angle of Gyration at $N_{maximum}$ for Section 903S

Sample Number	G_{mb} corrected	VTM (%)	VMA (%)	VFA (%)
1	2.40	3.0	14.1	78.5
2	2.39	3.2	14.3	77.4
3	2.39	3.3	14.3	77.2
4	2.40	2.8	13.9	79.7
Mean	2.4	3.1	14.2	78.2
Std Dev	0.0	0.2	0.2	1.2
2 x Std Dev	0.01	0.4	0.4	2.4
Variance	0.00	0.04	0.03	1.39
CV (%)	0.21	6.66	1.29	1.51

Table B. 28 Volumetric Properties of SHRP Gyratory Compactor Samples for 1.25° Angle of Gyration at $N_{initial}$ for Section 959S

Asphalt Content, P_b(%) = 5.12

BSG Aggregates = 2.65

Theoretical Maximum Specific Gravity = 2.47

Sample Number	G_{mb} corrected	VTM (%)	VMA (%)	VFA (%)
1	2.00	18.9	28.3	33.1
2	2.05	17.0	26.6	36.0
3	2.04	17.3	26.8	35.6
4	2.03	17.7	27.2	35.0
Mean	2.0	17.7	27.2	34.9
Std Dev	0.0	0.9	0.8	1.3
2 x Std Dev	0.04	1.7	1.5	2.6
Variance	0.00	0.73	0.57	1.71
CV (%)	1.04	4.83	2.78	3.74

Table B. 29 Volumetric Properties of SHRP Gyratory Compactor Samples for 1.25° Angle of Gyration at N_{design} for Section 959S

Sample Number	G_{mb} corrected	VTM (%)	VMA (%)	VFA (%)
1	2.23	9.6	20.1	52.0
2	2.28	7.6	18.3	58.4
3	2.28	7.9	18.5	57.5
4	2.27	8.1	18.7	56.8
Mean	2.3	8.3	18.9	56.2
Std Dev	0.0	0.9	0.8	2.8
2 x Std Dev	0.04	1.8	1.6	5.7
Variance	0.00	0.82	0.65	8.08
CV (%)	0.99	10.95	4.25	5.06

Table B. 30 Volumetric Properties of SHRP Gyratory Compactor Samples for 1.25° Angle of Gyration at $N_{maximum}$ for Section 959S

Sample Number	G_{mb} corrected	VTM (%)	VMA (%)	VFA (%)
1	2.31	6.4	17.2	62.8
2	2.33	5.7	16.6	65.7
3	2.32	5.9	16.8	64.8
4	2.32	6.1	16.9	64.1
Mean	2.3	6.0	16.9	64.3
Std Dev	0.0	0.3	0.3	1.2
2 x Std Dev	0.01	0.6	0.5	2.4
Variance	0.00	0.09	0.07	1.47
CV (%)	0.32	4.98	1.57	1.89

Table B. 31 Volumetric Properties of SHRP Gyratory Compactor Samples for 2.00° Angle of Gyration at $N_{initial}$ for Section 959S

Sample Number	G_{mb} corrected	VTM (%)	VMA (%)	VFA (%)
1	2.08	15.9	25.7	37.8
2	2.07	16.3	26.0	37.2
3	2.06	16.4	26.1	37.0
4	2.04	17.2	26.8	35.7
Mean	2.1	16.5	26.1	37.0
Std Dev	0.0	0.5	0.5	0.9
2 x Std Dev	0.03	1.1	0.9	1.8
Variance	0.00	0.28	0.22	0.80
CV (%)	0.64	3.24	1.81	2.42

Table B. 32 Volumetric Properties of SHRP Gyratory Compactor Samples for 2.00° Angle of Gyration at N_{design} for Section 959S

Sample Number	G_{mb} corrected	VTM (%)	VMA (%)	VFA (%)
1	2.32	6.0	16.9	64.4
2	2.32	6.2	17.0	63.6
3	2.32	6.2	17.1	63.5
4	2.30	6.9	17.7	60.8
Mean	2.3	6.3	17.2	63.1
Std Dev	0.0	0.4	0.4	1.5
2 x Std Dev	0.02	0.8	0.7	3.1
Variance	0.00	0.16	0.13	2.39
CV (%)	0.43	6.31	2.06	2.45

Table B. 33 Volumetric Properties of SHRP Gyratory Compactor Samples for 2.00° Angle of Gyration at $N_{maximum}$ for Section 959S

Sample Number	G_{mb} corrected	VTM (%)	VMA (%)	VFA (%)
1	2.38	3.6	14.7	75.7
2	2.37	3.8	15.0	74.3
3	2.37	3.9	15.0	74.1
4	2.36	4.5	15.5	70.9
Mean	2.4	4.0	15.0	73.7
Std Dev	0.0	0.4	0.4	2.0
2 x Std Dev	0.02	0.8	0.7	4.0
Variance	0.00	0.16	0.13	4.08
CV (%)	0.42	10.15	2.36	2.74

Table B. 34 Volumetric Properties of SHRP Gyratory Compactor Samples for 2.75° Angle of Gyration at $N_{initial}$ for Section 959S

Sample Number	G_{mb} corrected	VTM (%)	VMA (%)	VFA (%)
1	2.06	16.6	26.2	36.8
2	2.10	15.1	24.9	39.3
3	2.09	15.4	25.2	38.8
4	2.08	15.6	25.4	38.4
Mean	2.1	15.7	25.4	38.3
Std Dev	0.0	0.6	0.6	1.1
2 x Std Dev	0.03	1.3	1.1	2.2
Variance	0.00	0.40	0.31	1.23
CV (%)	0.75	4.02	2.19	2.90

Table B. 35 Volumetric Properties of SHRP Gyratory Compactor Samples for 2.75° Angle of Gyration at N_{design} for Section 959S

Sample Number	G_{mb} corrected	VTM (%)	VMA (%)	VFA (%)
1	2.31	6.6	17.4	62.1
2	2.35	4.7	15.7	70.0
3	2.33	5.5	16.4	66.4
4	2.34	5.4	16.3	66.9
Mean	2.3	5.6	16.5	66.4
Std Dev	0.0	0.8	0.7	3.2
2 x Std Dev	0.04	1.5	1.4	6.5
Variance	0.00	0.59	0.46	10.52
CV (%)	0.82	13.86	4.14	4.89

Table B. 36 Volumetric Properties of SHRP Gyratory Compactor Samples for 2.75° Angle of Gyration at $N_{maximum}$ for Section 959S

Sample Number	G_{mb} corrected	VTM (%)	VMA (%)	VFA (%)
1	2.38	3.6	14.8	75.4
2	2.41	2.5	13.7	82.1
3	2.40	2.8	14.0	80.3
4	2.40	2.7	13.9	80.8
Mean	2.4	2.9	14.1	79.7
Std Dev	0.0	0.5	0.5	2.9
2 x Std Dev	0.03	1.0	0.9	5.8
Variance	0.00	0.26	0.21	8.47
CV (%)	0.53	17.84	3.22	3.65

Table B. 36 Volumetric Properties of SHRP Gyratory Compactor Samples for 1.25° Angle of Gyration at $N_{initial}$ for Section 960S

Asphalt Content, P_b(%) = 5.20

BSG Aggregates = 2.65

Theoretical Maximum Specific Gravity = 2.48

Sample Number	G_{mb} corrected	VTM (%)	VMA (%)	VFA (%)
1	2.05	17.5	26.6	34.3
2	2.07	16.8	26.0	35.4
3	2.06	17.1	26.3	34.9
4	2.04	17.9	27.0	33.7
Mean	2.1	17.3	26.5	34.6
Std Dev	0.0	0.5	0.4	0.7
2 x Std Dev	0.02	0.9	0.8	1.5
Variance	0.00	0.21	0.17	0.53
CV (%)	0.56	2.66	1.55	2.10

Table B. 37 Volumetric Properties of SHRP Gyratory Compactor Samples for 1.25° Angle of Gyration at N_{design} for Section 960S

Sample Number	G_{mb} corrected	VTM (%)	VMA (%)	VFA (%)
1	2.29	7.9	18.1	56.4
2	2.29	7.7	17.9	57.2
3	2.29	7.6	17.9	57.3
4	2.27	8.5	18.6	54.4
Mean	2.3	7.9	18.1	56.3
Std Dev	0.0	0.4	0.4	1.3
2 x Std Dev	0.02	0.8	0.7	2.6
Variance	0.00	0.16	0.13	1.75
CV (%)	0.43	5.03	1.55	2.35

Table B. 38 Volumetric Properties of SHRP Gyratory Compactor Samples for 1.25° Angle of Gyration at $N_{maximum}$ for Section 960S

Sample Number	G_{mb} corrected	VTM (%)	VMA (%)	VFA (%)
1	2.34	5.9	16.3	63.8
2	2.33	6.0	16.4	63.5
3	2.34	5.8	16.2	64.4
4	2.32	6.5	16.8	61.6
Mean	2.3	6.0	16.5	63.3
Std Dev	0.0	0.3	0.3	1.2
2 x Std Dev	0.01	0.6	0.5	2.4
Variance	0.00	0.09	0.07	1.47
CV (%)	0.32	4.96	1.62	1.92

Table B. 39 Volumetric Properties of SHRP Gyratory Compactor Samples for 2.00° Angle of Gyration at $N_{initial}$ for Section 960S

Sample Number	G_{mb} corrected	VTM (%)	VMA (%)	VFA (%)
1	2.09	15.8	25.1	37.2
2	2.08	16.0	25.3	36.7
3	2.08	16.4	25.6	36.2
4	2.07	16.8	26.0	35.5
5	2.08	16.2	25.5	36.5
Mean	2.1	16.2	25.5	36.4
Std Dev	0.0	0.4	0.3	0.6
2 x Std Dev	0.02	0.7	0.7	1.3
Variance	0.00	0.14	0.11	0.40
CV (%)	0.44	2.29	1.29	1.73

Table B. 40 Volumetric Properties of SHRP Gyratory Compactor Samples for 2.00° Angle of Gyration at N_{design} for Section 960S

Sample Number	G_{mb} corrected	VTM (%)	VMA (%)	VFA (%)
1	2.33	6.2	16.6	62.5
2	2.33	6.3	16.7	62.1
3	2.32	6.7	17.0	60.8
4	2.31	7.1	17.4	59.0
5	2.32	6.4	16.8	61.8
Mean	2.3	6.6	16.9	61.2
Std Dev	0.0	0.4	0.3	1.4
2 x Std Dev	0.02	0.7	0.6	2.8
Variance	0.00	0.13	0.10	1.90
CV (%)	0.39	5.50	1.90	2.25

Table B. 41 Volumetric Properties of SHRP Gyratory Compactor Samples for 2.00° Angle of Gyration at $N_{maximum}$ for Section 960S

Sample Number	G_{mb} corrected	VTM (%)	VMA (%)	VFA (%)
1	2.38	4.0	14.7	72.5
2	2.38	4.1	14.8	72.0
3	2.38	4.3	14.9	71.1
4	2.38	4.2	14.8	71.7
5	2.37	4.3	15.0	70.9
Mean	2.4	4.2	14.8	71.6
Std Dev	0.0	0.1	0.1	0.6
2 x Std Dev	0.01	0.3	0.2	1.3
Variance	0.00	0.02	0.01	0.42
CV (%)	0.13	3.04	0.77	0.90

Table B. 42 Volumetric Properties of SHRP Gyratory Compactor Samples for 2.75° Angle of Gyration at $N_{initial}$ for Section 960S

Sample Number	G_{mb} corrected	VTM (%)	VMA (%)	VFA (%)
1	2.10	15.5	24.9	37.7
2	2.09	16.0	25.3	36.7
3	2.12	14.6	24.0	39.4
4	2.12	14.4	23.9	39.6
5	2.08	16.1	25.4	36.5
Mean	2.1	15.3	24.7	38.0
Std Dev	0.0	0.8	0.7	1.5
2 x Std Dev	0.04	1.6	1.4	2.9
Variance	0.00	0.64	0.50	2.12
CV (%)	0.94	5.21	2.87	3.83

Table B. 43 Volumetric Properties of SHRP Gyratory Compactor Samples for 2.75° Angle of Gyration at N_{design} for Section 960S

Sample Number	G_{mb} corrected	VTM (%)	VMA (%)	VFA (%)
1	2.34	5.8	16.2	64.3
2	2.32	6.5	16.9	61.4
3	2.36	4.8	15.3	68.8
4	2.36	5.0	15.5	67.7
5	2.33	6.2	16.6	62.7
Mean	2.3	5.7	16.1	65.0
Std Dev	0.0	0.7	0.7	3.2
2 x Std Dev	0.04	1.5	1.3	6.4
Variance	0.00	0.55	0.43	10.10
CV (%)	0.78	13.08	4.08	4.89

Table B. 44 Volumetric Properties of SHRP Gyratory Compactor Samples for 2.75° Angle of Gyration at $N_{maximum}$ for Section 960S

Sample Number	G_{mb} corrected	VTM (%)	VMA (%)	VFA (%)
1	2.40	3.4	14.1	75.9
2	2.39	3.6	14.3	75.0
3	2.40	3.3	14.0	76.5
4	2.40	3.2	14.0	76.8
5	2.40	3.5	14.2	75.4
Mean	2.4	3.4	14.1	75.9
Std Dev	0.0	0.1	0.1	0.7
2 x Std Dev	0.01	0.3	0.2	1.5
Variance	0.00	0.02	0.01	0.56
CV (%)	0.14	3.95	0.85	0.99

Table B. 45 Volumetric Properties of SHRP Gyratory Compactor Samples for 1.25° Angle of Gyration at $N_{initial}$ for Section 961M

Asphalt Content, P_b(%) = 5.21

BSG Aggregates = 2.64

Theoretical Maximum Specific Gravity = 2.46

Sample Number	G_{mb} corrected	VTM (%)	VMA (%)	VFA (%)
1	2.15	12.3	22.7	45.8
2	2.16	12.1	22.5	46.4
3	2.15	12.3	22.7	45.7
4	2.16	12.1	22.5	46.4
5	2.15	12.2	22.6	46.0
Mean	2.2	12.2	22.6	46.0
Std Dev	0.0	0.1	0.1	0.3
2 x Std Dev	0.01	0.3	0.2	0.6
Variance	0.00	0.02	0.01	0.10
CV (%)	0.15	1.10	0.53	0.68

Table B. 46 Volumetric Properties of SHRP Gyratory Compactor Samples for 1.25° Angle of Gyration at N_{design} for Section 961M

Sample Number	G_{mb} corrected	VTM (%)	VMA (%)	VFA (%)
1	2.34	4.8	16.1	70.1
2	2.34	4.7	16.0	70.5
3	2.33	5.0	16.3	69.0
4	2.33	5.3	16.5	68.1
5	2.33	4.9	16.2	69.5
Mean	2.3	5.0	16.2	69.4
Std Dev	0.0	0.2	0.2	0.9
2 x Std Dev	0.01	0.4	0.4	1.8
Variance	0.00	0.04	0.03	0.83
CV (%)	0.21	4.10	1.11	1.32

Table B. 47 Volumetric Properties of SHRP Gyratory Compactor Samples for 1.25° Angle of Gyration at $N_{maximum}$ for Section 961M

Sample Number	G_{mb} corrected	VTM (%)	VMA (%)	VFA (%)
1	2.37	3.5	15.0	76.3
2	2.37	3.4	14.8	77.2
3	2.37	3.6	15.0	76.3
4	2.36	3.9	15.3	74.7
5	2.37	3.5	15.0	76.3
Mean	2.4	3.6	15.0	76.2
Std Dev	0.0	0.2	0.2	0.9
2 x Std Dev	0.01	0.3	0.3	1.8
Variance	0.00	0.03	0.02	0.81
CV (%)	0.18	4.80	1.01	1.18

Table B. 48 Volumetric Properties of SHRP Gyratory Compactor Samples for 2.00° Angle of Gyration at $N_{initial}$ for Section 961M

Sample Number	G_{mb} corrected	VTM (%)	VMA (%)	VFA (%)
1	2.19	10.8	21.3	49.6
2	2.18	11.4	21.9	48.0
3	2.19	11.0	21.5	49.0
4	2.18	11.4	21.9	48.0
Mean	2.2	11.1	21.7	48.7
Std Dev	0.0	0.3	0.3	0.8
2 x Std Dev	0.02	0.6	0.5	1.6
Variance	0.00	0.09	0.07	0.61
CV (%)	0.35	2.76	1.25	1.60

Table B. 49 Volumetric Properties of SHRP Gyratory Compactor Samples for 2.00° Angle of Gyration at N_{design} for Section 961M

Sample Number	G_{mb} corrected	VTM (%)	VMA (%)	VFA (%)
1	2.36	3.7	15.2	75.3
2	2.36	4.0	15.4	73.8
3	2.36	3.8	15.2	75.1
4	2.36	4.0	15.4	73.8
Mean	2.4	3.9	15.3	74.5
Std Dev	0.0	0.2	0.1	0.8
2 x Std Dev	0.01	0.3	0.3	1.7
Variance	0.00	0.03	0.02	0.70
CV (%)	0.17	4.21	0.95	1.12

Table B. 50 Volumetric Properties of SHRP Gyratory Compactor Samples for 2.00° Angle of Gyration at $N_{maximum}$ for Section 961M

Sample Number	G_{mb} corrected	VTM (%)	VMA (%)	VFA (%)
1	2.40	2.3	13.9	83.2
2	2.39	2.5	14.0	82.5
3	2.40	2.3	13.9	83.4
4	2.39	2.5	14.0	82.5
Mean	2.4	2.4	14.0	82.9
Std Dev	0.0	0.1	0.1	0.5
2 x Std Dev	0.00	0.2	0.1	1.0
Variance	0.00	0.01	0.01	0.25
CV (%)	0.08	3.44	0.52	0.60

Table B. 51 Volumetric Properties of SHRP Gyratory Compactor Samples for 2.75° Angle of Gyration at $N_{initial}$ for Section 961M

Sample Number	G_{mb} corrected	VTM (%)	VMA (%)	VFA (%)
1	2.20	10.5	21.1	50.2
2	2.19	10.8	21.4	49.4
3	2.18	11.3	21.8	48.1
4	2.20	10.6	21.2	50.1
Mean	2.2	10.8	21.4	49.5
Std Dev	0.0	0.4	0.3	1.0
2 x Std Dev	0.02	0.7	0.7	1.9
Variance	0.00	0.14	0.11	0.92
CV (%)	0.42	3.46	1.54	1.94

Table B. 52 Volumetric Properties of SHRP Gyratory Compactor Samples for 2.75° Angle of Gyration at N_{design} for Section 961M

Sample Number	G_{mb} corrected	VTM (%)	VMA (%)	VFA (%)
1	2.36	3.8	15.2	75.2
2	2.36	3.9	15.3	74.5
3	2.35	4.1	15.5	73.3
4	2.36	3.7	15.1	75.5
Mean	2.4	3.9	15.3	74.6
Std Dev	0.0	0.2	0.2	0.9
2 x Std Dev	0.01	0.4	0.3	1.9
Variance	0.00	0.04	0.03	0.90
CV (%)	0.19	4.83	1.08	1.27

Table B. 53 Volumetric Properties of SHRP Gyratory Compactor Samples for 2.75° Angle of Gyration at $N_{maximum}$ for Section 961M

Sample Number	G_{mb} corrected	VTM (%)	VMA (%)	VFA (%)
1	2.41	2.0	13.6	85.1
2	2.40	2.2	13.8	83.9
3	2.40	2.1	13.7	84.6
4	2.40	2.1	13.7	84.9
Mean	2.4	2.1	13.7	84.6
Std Dev	0.0	0.1	0.1	0.5
2 x Std Dev	0.00	0.2	0.1	1.0
Variance	0.00	0.01	0.01	0.27
CV (%)	0.08	3.94	0.53	0.62

Table B. 54 Volumetric Properties of SHRP Gyratory Compactor Samples for 1.25° Angle of Gyration at $N_{initial}$ for Section 962SR

Asphalt Content, P_b(%) = 4.69

BSG Aggregates = 2.65

Theoretical Maximum Specific Gravity = 2.49

Sample Number	G_{mb} corrected	VTM (%)	VMA (%)	VFA (%)
1	2.06	17.0	26.0	34.8
2	2.06	16.9	26.0	34.8
3	2.06	17.2	26.2	34.4
Mean	2.1	17.0	26.1	34.7
Std Dev	0.0	0.1	0.1	0.2
2 x Std Dev	0.01	0.3	0.3	0.5
Variance	0.00	0.02	0.02	0.05
CV (%)	0.17	0.85	0.49	0.67

Table B. 55 Volumetric Properties of SHRP Gyratory Compactor Samples for 1.25° Angle of Gyration at N_{design} for Section 962SR

Sample Number	G_{mb} corrected	VTM (%)	VMA (%)	VFA (%)
1	2.31	7.2	17.3	58.4
2	2.32	6.8	17.0	59.9
3	2.30	7.6	17.7	57.1
Mean	2.3	7.2	17.3	58.4
Std Dev	0.0	0.4	0.3	1.4
2 x Std Dev	0.02	0.8	0.7	2.8
Variance	0.00	0.15	0.12	1.98
CV (%)	0.42	5.36	1.99	2.41

Table B. 56 Volumetric Properties of SHRP Gyratory Compactor Samples for 1.25° Angle of Gyration at $N_{maximum}$ for Section 962SR

Sample Number	G_{mb} corrected	VTM (%)	VMA (%)	VFA (%)
1	2.36	5.1	15.4	67.1
2	2.37	4.9	15.2	68.1
3	2.35	5.6	15.9	65.0
Mean	2.4	5.2	15.5	66.7
Std Dev	0.0	0.4	0.3	1.6
2 x Std Dev	0.02	0.7	0.6	3.2
Variance	0.00	0.13	0.10	2.59
CV (%)	0.38	6.91	2.05	2.41

Table B. 57 Volumetric Properties of SHRP Gyratory Compactor Samples for 2.00° Angle of Gyration at $N_{initial}$ for Section 962SR

Sample Number	G_{mb} corrected	VTM (%)	VMA (%)	VFA (%)
1	2.09	15.8	25.0	36.8
2	2.10	15.5	24.7	37.3
3	2.08	16.2	25.3	36.1
Mean	2.1	15.8	25.0	36.7
Std Dev	0.0	0.4	0.3	0.6
2 x Std Dev	0.02	0.7	0.6	1.2
Variance	0.00	0.13	0.10	0.38
CV (%)	0.42	2.24	1.26	1.68

Table B. 58 Volumetric Properties of SHRP Gyratory Compactor Samples for 2.00° Angle of Gyration at N_{design} for Section 962SR

Sample Number	G_{mb} corrected	VTM (%)	VMA (%)	VFA (%)
1	2.34	5.7	16.0	64.2
2	2.35	5.5	15.8	65.4
3	2.33	6.1	16.4	62.5
Mean	2.3	5.8	16.1	64.0
Std Dev	0.0	0.3	0.3	1.4
2 x Std Dev	0.02	0.7	0.6	2.8
Variance	0.00	0.11	0.09	2.03
CV (%)	0.36	5.84	1.87	2.22

Table B. 59 Volumetric Properties of SHRP Gyratory Compactor Samples for 2.00° Angle of Gyration at $N_{maximum}$ for Section 962SR

Sample Number	G_{mb} corrected	VTM (%)	VMA (%)	VFA (%)
1	2.39	3.7	14.2	74.1
2	2.41	3.1	13.7	77.0
3	2.38	4.1	14.6	71.7
Mean	2.4	3.7	14.2	74.3
Std Dev	0.0	0.5	0.4	2.7
2 x Std Dev	0.02	1.0	0.9	5.4
Variance	0.00	0.24	0.19	7.18
CV (%)	0.51	13.45	3.09	3.61

Table B. 60 Volumetric Properties of SHRP Gyratory Compactor Samples for 2.75° Angle of Gyration at $N_{initial}$ for Section 962SR

Sample Number	G_{mb} corrected	VTM (%)	VMA (%)	VFA (%)
1	2.12	14.9	24.2	38.4
2	2.09	15.9	25.1	36.5
3	2.09	15.9	25.1	36.6
Mean	2.1	15.6	24.8	37.2
Std Dev	0.0	0.6	0.5	1.1
2 x Std Dev	0.03	1.2	1.1	2.2
Variance	0.00	0.36	0.29	1.17
CV (%)	0.71	3.86	2.16	2.91

Table B. 61 Volumetric Properties of SHRP Gyratory Compactor Samples for 2.75° Angle of Gyration at N_{design} for Section 962SR

Sample Number	G_{mb} corrected	VTM (%)	VMA (%)	VFA (%)
1	2.35	5.3	15.6	66.2
2	2.34	5.8	16.1	64.0
3	2.34	5.7	16.0	64.4
Mean	2.3	5.6	15.9	64.8
Std Dev	0.0	0.3	0.2	1.2
2 x Std Dev	0.01	0.5	0.5	2.3
Variance	0.00	0.07	0.06	1.33
CV (%)	0.28	4.73	1.48	1.78

Table B. 62 Volumetric Properties of SHRP Gyratory Compactor Samples for 2.75° Angle of Gyration at $N_{maximum}$ for Section 962SR

Sample Number	G_{mb} corrected	VTM (%)	VMA (%)	VFA (%)
1	2.41	3.0	13.5	78.2
2	2.41	3.1	13.6	77.5
3	2.41	3.2	13.7	77.0
Mean	2.4	3.1	13.6	77.6
Std Dev	0.0	0.1	0.1	0.6
2 x Std Dev	0.0	0.2	0.2	1.2
Variance	0.0	0.0	0.0	0.4
CV (%)	2.4	3.3	0.7	0.8

APPENDIX C. MARSHALL STABILITY AND FLOW TEST RESULTS

M S = Marshall Stability

M F = Marshall Flow

Table C. 1 Marshall Stability and Flow at 50-Blow and 75-Blow Marshall for Test Section 901M

Specimen Number	M S 50-Blow (LBF)	M S 50-Blow (N)	M F 50-Blow (0.01inch)	M F 50-Blow (mm)	M S 75-Blow (LBF)	M S 75-Blow (N)	M F 75-Blow (0.01inch)	M F 75-Blow (mm)
1	140	5945	11	2.8	230	9744	12	3.1
2	150	6369	12	3.1	220	9324	11	2.8
3	180	7635	11	2.8	200	8481	9	2.3
4	170	7214	12	3.1	190	8057	11	2.8
Average	166.67	6791	11.5	2.9	210	8902	10.75	2.7
STDEV	15.28	771	0.58	0.2	18.26	770	1.26	0.3
2 x STDEV	30.6	1542	1.2	0.3	36.5	1540	2.5	0.6
variance	233.33	594740	0.33	0.0	333.3 3	592658	1.58	0.1
CV	9.17	11.4	5.02	5.1	8.69	8.6	11.71	11.6

Table C. 2 Marshall Stability and Flow at 50-Blow and 75-Blow Marshall for Test Section 902S

Specimen Number	M S 50-Blow (LBF)	M S 50-Blow (N)	M F 50-Blow (0.01inch)	M F 50-Blow (mm)	M S 75-Blow (LBF)	M S 75-Blow (N)	M F 75-Blow (0.01inch)	M F 75-Blow (mm)
1	180	7635	11	2.8	190	8057	13	3.1
2	135	5732	9	2.3	240	10167	16	4.1
3	185	7847	14	3.6	242	10252	15	3.8
4	161	6832	13	3.1	190	8057	12	3.1
Average	165.25	7012	11.75	2.9	215.5	9133	14	3.5
STDEV	22.66	958	2.22	0.5	29.46	1243	1.83	0.5
2 x STDEV	45.3	1917	4.4	1.1	58.9	2486	3.7	1.0
variance	513.58	918528	4.92	0.3	867.6 7	154512 4	3.33	0.3
CV	13.71	13.7	18.87	18.1	13.67	13.6	13.04	14.9

Table C. 3 Marshall Stability and Flow at 50-Blow and 75-Blow Marshall for Test Section 903S

Specimen Number	M S 50-Blow (LBF)	M S 50-Blow (N)	M F 50-Blow (0.01inch)	M F 50-Blow (mm)	M S 75-Blow (LBF)	M S 75-Blow (N)	M F 75-Blow (0.01inch)	M F 75-Blow (mm)
1	150	6369	12	3.1	180	7635	13	3.3
2	145	6156	9	2.3	180	7635	14	3.6
3	160	6790	11	2.8	176	7466	13	3.3
4	162	6874	12	3.1	162	6874	12	3.1
Average	154.25	6547	11	2.8	174.5	7402	13	3.3
STDEV	8.10	342	1.41	0.4	8.54	361	0.82	0.2
2 x STDEV	16.2	683	2.8	0.7	17.1	722	1.6	0.4
variance	65.58	116755	2.00	0.1	73.00	130442	0.67	0.0
CV	5.25	5.22	12.86	12.8	4.90	4.9	6.28	6.3

Table C. 4 Marshall Stability and Flow at 50-Blow and 75-Blow Marshall for Test Section 959S

Specimen Number	M S 50-Blow (LBF)	M S 50-Blow (N)	M F 50-Blow (0.01inch)	M F 50-Blow (mm)	M S 75-Blow (LBF)	M S 75-Blow (N)	M F 75-Blow (0.01inch)	M F 75-Blow (mm)
1	160	6790	13	3.3	200	8481	13	3.3
2	145	6156	11	2.8	181	7678	12	3.1
3	185	7847	14	3.6	175	7466	12	2.9
4	155	6580	15	3.8	180	7635	10	2.5
Average	161.25	6843	13.25	3.4	184	7815	11.6	3.0
STDEV	17.02	719	1.71	0.4	10.98	454	1.25	0.3
2 x STDEV	34.0	1439	3.4	0.9	22.0	907	2.5	0.6
variance	289.6	517437	2.9	0.2	120.7	205707	1.6	0.1
CV	10.55	10.5	12.89	13.0	5.97	5.8	10.75	10.7

Table C. 5 Marshall Stability and Flow at 50-Blow and 75-Blow Marshall for Test Section 960S

Specimen Number	M S 50-Blow (LBF)	M S 50-Blow (N)	M F 50-Blow (0.01inch)	M F 50-Blow (mm)	M S 75-Blow (LBF)	M S 75-Blow (N)	M F 75-Blow (0.01inch)	M F 75-Blow (mm)
1	180	7635	15	3.8	180	7635	14	3.6
2	165	7002	14	3.6	165	7002	11	2.8
3	178	7549	15	3.8	150	6369	10	2.5
4	140	5945	13	3.3	190	8075	17	4.3
Average	165.75	7033	14.25	3.6	171	7270	13	3.3
STDEV	18.41	777	0.96	0.2	17.50	745	3.16	0.8
2 x STDEV	36.8	1555	1.9	0.5	35.0	1490	6.3	1.6
variance	338.9	604333	0.9	0.1	306.3	555227	10.0	0.6
CV	11.11	11.1	6.72	6.7	10.22	10.2	24.33	24.4

Table C. 6 Marshall Stability and Flow at 50-Blow and 75-Blow Marshall for Test Section 961M

Specimen Number	M S 50-Blow (LBF)	M S 50-Blow (N)	M F 50-Blow (0.01inch)	M F 50-Blow (mm)	M S 75-Blow (LBF)	M S 75-Blow (N)	M F 75-Blow (0.01inch)	M F 75-Blow (mm)
1	153	6496	13	3.3	170	7214	13	3.3
2	170	7214	15	3.8	172	7298	15	3.8
3	143	6072	11	2.8	163	6916	13	3.3
4	175	7424	13	3.3	184	7805	14	3.6
Average	160.25	6801	13	3.3	172	7308	13.75	3.5
STDEV	14.86	628	1.63	0.4	8.73	370	0.96	0.2
2 x STDEV	29.7	1255	3.3	0.8	17.5	739	1.9	0.5
variance	220.92	393980	2.67	0.2	76.25	136664	0.92	0.1
CV	9.28	9.2	12.56	12.6	5.07	5.1	6.96	7.0

Table C. 7 Marshall Stability and Flow at 50-Blow and 75-Blow Marshall for Test Section 962SR

Specimen Number	M S 50-Blow (LBF)	M S 50-Blow (N)	M F 50-Blow (0.01inch)	M F 50-Blow (mm)	M S 75-Blow (LBF)	M S 75-Blow (N)	M F 75-Blow (0.01inch)	M F 75-Blow (mm)
1	160	6790	14	3.6	150	6369	16	4.1
2	125	5309	11	2.8	150	6369	17	4.3
3	115	4885	11	2.8	120	5098	14	3.6
4	130	5522	13	3.3	125	5309	13	3.3
Average	132.5	5626	12.25	3.1	136	5786	15	3.8
STDEV	19.36	820	1.50	0.4	16.01	678	1.83	0.5
2 x STDEV	38.7	1639	3.0	0.8	32.0	1356	3.7	0.9
variance	375.00	671873	2.25	0.1	256.2	460005	3.33	0.2
CV	14.62	14.6	12.24	12.4	11.75	11.7	12.17	12.2

APPENDIX D. TRIAXIAL FREQUENCY SWEEP TEST RESULTS AT 20°C

Vertical Traction = σ_1 (kPa)

Radial Traction = σ_3 (kPa)

Deviatoric Stress = σ_D (kPa)

Table D. 1 Triaxial Frequency Sweep Test results at 20°C, 1.25° Angle of Gyration and Deviatoric Stress of 200 kPa and 400 kPa for Test Section 901M

Sample Name	σ_1 kPa	σ_3 kPa	σ_D kPa	Freq (Hz)	Dyn Mod E_d (Mpa)	Phase Angle δ (°)	RAMS	RRMS	P Ratio, ν
901-1	450	250	200	10	3765	19.2	52.1	13.8	0.3
901-1	450	250	200	5	3340	19.5	59.1	16.9	0.3
901-1	450	250	200	1	2453	22.0	81.0	28.5	0.4
901-1	450	250	200	0.5	2044	22.2	92.6	40.2	0.4
901-2	450	250	200	10	3634	18.2	54.0	13.9	0.3
901-2	450	250	200	5	3205	18.9	61.7	15.7	0.3
901-2	450	250	200	1	2417	21.3	82.0	26.7	0.3
901-2	450	250	200	0.5	2066	21.4	95.6	35.4	0.4
901-3	450	250	200	10	3767	21.1	52.0	16.3	0.3
901-3	450	250	200	5	3508	20.4	56.3	19.4	0.3
901-3	450	250	200	1	2431	21.4	81.0	27.5	0.3
901-3	450	250	200	0.5	2064	22.2	95.3	38.6	0.4
901-1	650	250	400	10	4117	20.9	94.2	29.2	0.3
901-1	650	250	400	5	3519	21.0	112.2	37.7	0.3
901-1	650	250	400	1	2377	23.6	168.1	65.2	0.4
901-1	650	250	400	0.5	1976	23.7	201.3	82.0	0.4
901-2	650	250	400	10	3950	21.2	98.8	30.6	0.3
901-2	650	250	400	5	3445	21.0	114.7	37.4	0.3
901-2	650	250	400	1	2376	23.0	167.7	68.8	0.4
901-2	650	250	400	0.5	1994	23.1	199.1	80.3	0.4
901-3	650	250	400	10	4141	21.4	94.1	31.4	0.3
901-3	650	250	400	5	3521	21.0	112.3	37.4	0.3
901-3	650	250	400	1	2371	23.0	168.2	68.6	0.4
901-3	650	250	400	0.5	1982	23.6	200.6	81.3	0.4

Table D. 2 Triaxial Frequency Sweep Test results at 20°C, 1.25° Angle of Gyration and Deviatoric Stress of 600 kPa and 200 kPa (Fully Reversed) for Test Section 901M

Sample Name	σ_1 kPa	σ_3 kPa	σ_D kPa	Freq (Hz)	Dyn Mod E_d (Mpa)	Phase Angle δ (°)	RAMS	RRMS	P Ratio, ν
901-1	650	50	600	10	3306	20.7	176.0	54.3	0.3
901-1	650	50	600	5	2891	21.2	204.4	61.8	0.3
901-1	650	50	600	1	1883	24.2	317.5	122.6	0.4
901-1	650	50	600	0.5	1495	24.6	400.5	167.1	0.4
901-2	650	50	600	10	3219	20.5	181.0	59.4	0.3
901-2	650	50	600	5	2840	21.1	208.4	74.4	0.4
901-2	650	50	600	1	1887	23.4	317.2	124.2	0.4
901-2	650	50	600	0.5	1527	23.6	390.8	167.0	0.4
901-3	650	50	600	10	3491	21.6	167.1	62.4	0.4
901-3	650	50	600	5	3015	22.4	196.6	71.2	0.4
901-3	650	50	600	1	1949	24.4	307.2	125.8	0.4
901-3	650	50	600	0.5	1525	24.3	392.3	167.7	0.4
901-1	450	250	200	10	3194	26.8	124.5	36.1	0.3
901-1	450	250	200	5	2779	27.7	142.9	49.0	0.3
901-1	450	250	200	1	1720	32.2	231.0	95.3	0.4
901-1	450	250	200	0.5	1373	31.5	288.2	125.1	0.4
901-2	450	250	200	10	3072	24.6	129.4	40.1	0.3
901-2	450	250	200	5	2680	26.3	148.4	48.1	0.3
901-2	450	250	200	1	1735	30.8	229.2	87.9	0.4
901-2	450	250	200	0.5	1412	29.9	280.7	112.4	0.4
901-3	450	250	200	10	3421	24.2	116.2	37.6	0.3
901-3	450	250	200	5	2774	27.5	143.4	48.5	0.3
901-3	450	250	200	1	1743	31.3	228.1	91.9	0.4
901-3	450	250	200	0.5	1408	30.9	281.4	119.0	0.4

Table D. 3 Triaxial Frequency Sweep Test results at 20°C, 2.00° Angle of Gyration and Deviatoric Stress of 200 kPa and 400 kPa for Test Section 901M

Sample Name	σ_1 kPa	σ_3 kPa	σ_D kPa	Freq (Hz)	Dyn Mod E_d (Mpa)	Phase Angle δ (°)	RAMS	RRMS	P Ratio, ν
901-1	450	250	200	10	3774	23.6	51.7	13.7	0.3
901-1	450	250	200	5	3228	21.6	61.0	16.7	0.3
901-1	450	250	200	1	2237	25.1	88.7	31.0	0.3
901-1	450	250	200	0.5	1873	25.9	105.5	42.6	0.4
901-2	450	250	200	10	3659	22.2	53.6	18.6	0.3
901-2	450	250	200	5	3287	23.2	59.9	23.0	0.4
901-2	450	250	200	1	2154	25.5	91.5	36.2	0.4
901-2	450	250	200	0.5	1816	25.8	108.3	47.0	0.4
901-3	450	250	200	10	3930	23.0	49.7	18.8	0.4
901-3	450	250	200	5	3440	22.5	57.4	20.2	0.4
901-3	450	250	200	1	2386	24.8	82.8	31.7	0.4
901-3	450	250	200	0.5	1971	25.1	99.8	42.8	0.4
901-1	650	250	400	10	3980	22.9	97.2	30.8	0.3
901-1	650	250	400	5	3437	23.4	115.0	36.6	0.3
901-1	650	250	400	1	2235	25.5	178.4	69.9	0.4
901-1	650	250	400	0.5	1817	25.9	219.1	92.4	0.4
901-2	650	250	400	10	3914	23.0	99.6	34.0	0.3
901-2	650	250	400	5	3357	23.5	117.8	46.7	0.4
901-2	650	250	400	1	2161	25.7	183.8	77.6	0.4
901-2	650	250	400	0.5	1741	25.9	228.1	104.5	0.5
901-3	650	250	400	10	4106	22.3	94.8	31.8	0.3
901-3	650	250	400	5	3570	22.3	110.6	43.8	0.4
901-3	650	250	400	1	2350	25.0	169.6	70.7	0.4
901-3	650	250	400	0.5	1907	25.3	208.8	91.1	0.4

Table D. 4 Triaxial Frequency Sweep Test results at 20°C, 2.00° Angle of Gyration and Deviatoric Stress of 600 kPa and 200 kPa (Fully Reversed) for Test Section 901M

Sample Name	σ_1 kPa	σ_3 kPa	σ_D kPa	Freq (Hz)	Dyn Mod E_d (Mpa)	Phase Angle δ (°)	RAMS	RRMS	P Ratio, ν
901-1	650	50	600	10	3318	24.1	175.4	57.2	0.3
901-1	650	50	600	5	2821	22.8	209.5	71.0	0.3
901-1	650	50	600	1	1802	24.9	331.6	133.6	0.4
901-1	650	50	600	0.5	1437	25.2	415.9	184.8	0.4
901-2	650	50	600	10	3244	22.5	179.1	60.5	0.3
901-2	650	50	600	5	2809	22.9	210.7	75.0	0.4
901-2	650	50	600	1	1771	25.4	338.0	146.3	0.4
901-2	650	50	600	0.5	1415	25.3	422.6	203.0	0.5
901-3	650	50	600	10	3389	21.9	171.7	57.9	0.3
901-3	650	50	600	5	3032	22.3	195.2	73.3	0.4
901-3	650	50	600	1	1829	25.0	327.3	137.5	0.4
901-3	650	50	600	0.5	1257	35.9	315.2	137.3	0.4
901-1	450	250	200	10	3203	26.9	124.1	42.3	0.3
901-1	450	250	200	5	2658	29.5	149.5	51.7	0.3
901-1	450	250	200	1	1528	34.3	260.3	103.2	0.4
901-1	450	250	200	0.5	1156	36.1	342.9	138.6	0.4
901-2	450	250	200	10	3093	30.5	128.5	43.9	0.3
901-2	450	250	200	5	2542	29.8	156.2	60.7	0.4
901-2	450	250	200	1	1445	35.3	275.1	118.7	0.4
901-2	450	250	200	0.5	1082	36.9	366.0	164.9	0.5
901-3	450	250	200	10	3324	25.0	119.5	40.5	0.3
901-3	450	250	200	5	2826	27.8	140.7	54.2	0.4
901-3	450	250	200	1	1647	33.7	240.7	105.3	0.4
901-3	450	250	200	0.5	1257	35.9	315.2	137.3	0.4

Table D. 5 Triaxial Frequency Sweep Test results at 20°C, 2.75° Angle of Gyration and Deviatoric Stress of 200 kPa and 400 kPa for Test Section 901M

Sample Name	σ_1 kPa	σ_3 kPa	σ_D kPa	Freq (Hz)	Dyn Mod E_d (Mpa)	Phase Angle δ (°)	RAMS	RRMS	P Ratio, ν
901-1	450	250	200	10	3720	23.7	52.8	20.6	0.4
901-1	450	250	200	5	3226	25.6	61.3	23.3	0.4
901-1	450	250	200	1	2145	28.4	91.9	45.2	0.5
901-1	450	250	200	0.5	1700	28.6	116.1	56.1	0.5
901-2	450	250	200	10	4050	22.2	48.3	18.6	0.4
901-2	450	250	200	5	3415	24.8	57.8	20.2	0.3
901-2	450	250	200	1	2145	26.6	92.1	37.4	0.4
901-2	450	250	200	0.5	1788	27.9	110.2	46.5	0.4
901-3	450	250	200	10	4156	23.2	47.1	18.8	0.4
901-3	450	250	200	5	3527	23.9	55.9	21.2	0.4
901-3	450	250	200	1	2333	26.8	84.7	41.0	0.5
901-3	450	250	200	0.5	1878	27.4	104.7	51.7	0.5
901-1	650	250	400	10	4026	24.1	96.6	42.7	0.4
901-1	650	250	400	5	3403	24.6	116.0	51.3	0.4
901-1	650	250	400	1	2151	26.8	185.0	91.8	0.5
901-1	650	250	400	0.5	1703	27.8	233.6	117.6	0.5
901-2	650	250	400	10	4176	23.6	93.1	36.0	0.4
901-2	650	250	400	5	3509	24.3	112.6	44.8	0.4
901-2	650	250	400	1	2222	27.1	179.4	77.6	0.4
901-2	650	250	400	0.5	1780	27.3	223.9	102.8	0.5
901-3	650	250	400	10	4225	23.4	92.3	36.0	0.4
901-3	650	250	400	5	3634	24.8	108.6	43.9	0.4
901-3	650	250	400	1	2335	27.0	170.7	81.3	0.5
901-3	650	250	400	0.5	1867	27.0	212.7	107.8	0.5

Table D. 6 Triaxial Frequency Sweep Test results at 20°C, 2.00° Angle of Gyration and Deviatoric Stress of 600 kPa and 200 kPa (Fully Reversed) for Test Section 901M

Sample Name	σ_1 kPa	σ_3 kPa	σ_D kPa	Freq (Hz)	Dyn Mod E_d (Mpa)	Phase Angle δ (°)	RAMS	RRMS	P Ratio, ν
901-1	650	50	600	10	3406	23.4	170.9	63.8	0.4
901-1	650	50	600	5	2953	23.7	200.2	83.7	0.4
901-1	650	50	600	1	1833	26.3	326.0	160.9	0.5
901-1	650	50	600	0.5	1450	26.5	412.2	215.0	0.5
901-2	650	50	600	10	3408	23.2	170.7	57.2	0.3
901-2	650	50	600	5	2963	23.4	199.9	71.9	0.4
901-2	650	50	600	1	1851	25.8	323.3	140.4	0.4
901-2	650	50	600	0.5	1478	26.5	404.6	193.0	0.5
901-3	650	50	600	10	3737	23.3	155.5	61.1	0.4
901-3	650	50	600	5	3120	23.3	189.5	75.1	0.4
901-3	650	50	600	1	1964	25.6	304.7	147.1	0.5
901-3	650	50	600	0.5	1558	26.2	383.6	201.0	0.5
901-1	450	250	200	10	3178	29.5	125.1	49.3	0.4
901-1	450	250	200	5	2614	31.5	151.8	63.7	0.4
901-1	450	250	200	1	1357	39.2	292.7	147.3	0.5
901-1	450	250	200	0.5	950	41.7	417.0	217.5	0.5
901-2	450	250	200	10	3323	29.4	119.6	44.0	0.4
901-2	450	250	200	5	2838	31.9	139.9	56.0	0.4
901-2	450	250	200	1	1529	37.2	259.4	119.2	0.5
901-2	450	250	200	0.5	1107	40.3	357.1	167.4	0.5
901-3	450	250	200	10	3383	25.5	117.3	42.9	0.4
901-3	450	250	200	5	2755	30.6	144.2	60.3	0.4
901-3	450	250	200	1	1524	37.5	260.6	127.8	0.5
901-3	450	250	200	0.5	1093	40.6	362.3	183.1	0.5

Table D. 7 Triaxial Frequency Sweep Test results at 20°C, 1.25° Angle of Gyration and Deviatoric Stress of 200 kPa and 400 kPa for Test Section 902S

Sample Name	σ_1 kPa	σ_3 kPa	σ_D kPa	Freq (Hz)	Dyn Mod E_d (Mpa)	Phase Angle δ (°)	RAMS	RRMS	P Ratio, ν
902-1	450	250	200	10	2968	17.4	66.1	13.8	0.2
902-1	450	250	200	5	2721	17.8	72.3	16.9	0.2
902-1	450	250	200	1	2078	16.9	94.9	28.5	0.2
902-1	450	250	200	0.5	1829	16.9	108.1	40.2	0.2
902-2	450	250	200	10	2877	18.9	68.0	13.9	0.3
902-2	450	250	200	5	2617	18.6	75.3	15.7	0.3
902-2	450	250	200	1	1993	19.1	98.9	26.7	0.3
902-2	450	250	200	0.5	1739	17.9	113.6	35.4	0.3
902-3	450	250	200	10	2796	19.6	69.9	16.3	0.3
902-3	450	250	200	5	2496	17.9	79.0	19.4	0.3
902-3	450	250	200	1	1927	16.3	102.7	27.5	0.3
902-3	450	250	200	0.5	1707	16.9	115.3	38.6	0.3
902-1	650	250	400	10	3017	19.8	129.1	29.2	0.2
902-1	650	250	400	5	2612	19.0	151.1	37.7	0.2
902-1	650	250	400	1	1880	19.2	211.6	65.2	0.3
902-1	650	250	400	0.5	1626	18.8	244.8	82.0	0.3
902-2	650	250	400	10	2848	20.5	136.6	30.6	0.3
902-2	650	250	400	5	2533	20.4	155.8	37.4	0.3
902-2	650	250	400	1	1788	19.7	222.5	68.8	0.4
902-2	650	250	400	0.5	1541	19.2	258.1	80.3	0.4
902-3	650	250	400	10	2820	20.5	138.5	31.4	0.3
902-3	650	250	400	5	2539	19.7	155.7	37.4	0.3
902-3	650	250	400	1	1758	19.0	226.7	68.6	0.4
902-3	650	250	400	0.5	1567	18.9	254.1	81.3	0.3

Table D. 8 Triaxial Frequency Sweep Test results at 20°C, 1.25° Angle of Gyration and Deviatoric Stress of 600 kPa and 200 kPa (Fully Reversed) for Test Section 902S

Sample Name	σ_1 kPa	σ_3 kPa	σ_D kPa	Freq (Hz)	Dyn Mod E_d (Mpa)	Phase Angle δ (°)	RAMS	RRMS	P Ratio, ν
902-1	650	50	600	10	2287	21.4	254.5	54.3	0.2
902-1	650	50	600	5	1949	20.8	303.1	61.8	0.2
902-1	650	50	600	1	1367	20.3	437.3	122.6	0.3
902-1	650	50	600	0.5	1170	19.3	511.3	167.1	0.3
902-2	650	50	600	10	2193	22.1	265.4	59.4	0.3
902-2	650	50	600	5	1860	21.4	317.9	74.4	0.3
902-2	650	50	600	1	1285	20.4	465.1	124.2	0.4
902-2	650	50	600	0.5	1097	19.6	545.2	167.0	0.4
902-3	650	50	600	10	2036	22.2	286.5	62.4	0.3
902-3	650	50	600	5	1819	20.7	325.3	71.2	0.3
902-3	650	50	600	1	1285	20.0	464.6	125.8	0.4
902-3	650	50	600	0.5	1124	19.3	532.3	167.7	0.4
902-1	450	250	200	10	2192	23.9	181.1	36.1	0.2
902-1	450	250	200	5	1832	24.7	216.5	49.0	0.2
902-1	450	250	200	1	1222	25.0	324.5	95.3	0.3
902-1	450	250	200	0.5	1033	25.5	383.6	125.1	0.3
902-2	450	250	200	10	2074	24.1	191.5	40.1	0.3
902-2	450	250	200	5	1717	25.3	230.9	48.1	0.3
902-2	450	250	200	1	1114	26.0	356.3	87.9	0.4
902-2	450	250	200	0.5	930	25.1	426.1	112.4	0.4
902-3	450	250	200	10	2013	24.5	197.8	37.6	0.3
902-3	450	250	200	5	1749	25.4	227.0	48.5	0.3
902-3	450	250	200	1	1154	25.6	344.2	91.9	0.3
902-3	450	250	200	0.5	969	25.3	410.0	119.0	0.3

Table D. 9 Triaxial Frequency Sweep Test results at 20°C, 2.00° Angle of Gyration and Deviatoric Stress of 200 kPa and 400 kPa for Test Section 902S

Sample Name	σ_1 kPa	σ_3 kPa	σ_D kPa	Freq (Hz)	Dyn Mod E_d (Mpa)	Phase Angle δ (°)	RAMS	RRMS	P Ratio, ν
902-1	450	250	200	10	2729	19.4	71.5	15.1	0.2
902-1	450	250	200	5	2585	18.0	76.3	18.5	0.2
902-1	450	250	200	1	1965	17.6	101.1	30.4	0.3
902-1	450	250	200	0.5	1720	18.1	114.6	33.8	0.3
902-2	450	250	200	10	2778	18.2	70.7	17.1	0.2
902-2	450	250	200	5	2541	17.2	77.5	16.7	0.2
902-2	450	250	200	1	2029	17.3	97.1	27.8	0.3
902-2	450	250	200	0.5	1783	17.5	110.6	32.7	0.3
902-3	450	250	200	10	3038	18.1	64.3	20.8	0.3
902-3	450	250	200	5	2788	18.3	70.7	19.3	0.3
902-3	450	250	200	1	2086	17.0	94.9	29.6	0.3
902-3	450	250	200	0.5	1855	17.3	106.6	37.1	0.3
902-1	650	250	400	10	2848	19.8	135.9	40.1	0.3
902-1	650	250	400	5	2523	19.8	156.8	47.1	0.3
902-1	650	250	400	1	1805	20.0	220.9	74.9	0.3
902-1	650	250	400	0.5	1535	19.5	258.9	89.7	0.3
902-2	650	250	400	10	2948	20.6	131.9	37.3	0.3
902-2	650	250	400	5	2634	19.2	150.3	44.1	0.3
902-2	650	250	400	1	1900	20.3	209.5	69.7	0.3
902-2	650	250	400	0.5	1627	19.3	244.1	88.1	0.4
902-3	650	250	400	10	3224	20.9	120.5	36.1	0.3
902-3	650	250	400	5	2766	20.2	142.9	45.8	0.3
902-3	650	250	400	1	1978	20.5	201.5	73.3	0.4
902-3	650	250	400	0.5	1683	20.0	236.2	89.3	0.4

Table D. 10 Triaxial Frequency Sweep Test results at 20°C, 2.00° Angle of Gyration and Deviatoric Stress of 600 kPa and 200 kPa (Fully Reversed) for Test Section 902S

Sample Name	σ_1 kPa	σ_3 kPa	σ_D kPa	Freq (Hz)	Dyn Mod E_d (Mpa)	Phase Angle δ (°)	RAMS	RRMS	P Ratio, ν
902-1	650	50	600	10	1907	21.6	305.2	80.7	0.3
902-1	650	50	600	5	1808	21.1	326.7	104.6	0.3
902-1	650	50	600	1	1263	20.5	473.2	166.6	0.4
902-1	650	50	600	0.5	1082	19.7	552.9	222.4	0.4
902-2	650	50	600	10	2228	22.2	261.6	73.0	0.3
902-2	650	50	600	5	1954	21.0	302.6	95.3	0.3
902-2	650	50	600	1	1357	20.7	440.0	161.9	0.4
902-2	650	50	600	0.5	1163	19.8	514.1	202.3	0.4
902-3	650	50	600	10	2431	21.7	239.6	68.9	0.3
902-3	650	50	600	5	2059	21.6	287.0	91.5	0.3
902-3	650	50	600	1	1343	20.8	445.8	160.4	0.4
902-3	650	50	600	0.5	1071	26.2	369.9	144.2	0.4
902-1	450	250	200	10	1934	23.1	205.8	60.4	0.3
902-1	450	250	200	5	1687	25.8	235.8	73.4	0.3
902-1	450	250	200	1	1099	26.1	360.9	130.4	0.4
902-1	450	250	200	0.5	926	25.5	428.2	156.1	0.4
902-2	450	250	200	10	2126	24.0	187.0	53.6	0.3
902-2	450	250	200	5	1869	25.8	212.4	61.5	0.3
902-2	450	250	200	1	1236	27.1	321.7	114.3	0.4
902-2	450	250	200	0.5	1028	25.0	385.4	140.5	0.4
902-3	450	250	200	10	2342	27.1	169.4	52.2	0.3
902-3	450	250	200	5	1983	26.2	200.5	66.0	0.3
902-3	450	250	200	1	1291	26.8	307.3	117.2	0.4
902-3	450	250	200	0.5	1071	26.2	369.9	144.2	0.4

Table D. 11 Triaxial Frequency Sweep Test results at 20°C, 2.75° Angle of Gyration and Deviatoric Stress of 200 kPa and 400 kPa for Test Section 902S

Sample Name	σ_1 kPa	σ_3 kPa	σ_D kPa	Freq (Hz)	Dyn Mod E_d (Mpa)	Phase Angle δ (°)	RAMS	RRMS	P Ratio, ν
902-1	450	250	200	10	3034	23.7	64.6	17.1	0.3
902-1	450	250	200	5	2999	25.6	65.6	14.7	0.2
902-1	450	250	200	1	2342	28.4	84.4	21.8	0.3
902-1	450	250	200	0.5	2087	28.6	94.3	31.3	0.3
902-2	450	250	200	10	3440	22.2	57.0	15.0	0.3
902-2	450	250	200	5	3050	24.8	64.8	18.3	0.3
902-2	450	250	200	1	2381	26.6	82.8	28.5	0.3
902-2	450	250	200	0.5	2102	27.9	93.7	27.9	0.3
902-3	450	250	200	10	2700	23.2	73.0	12.7	0.2
902-3	450	250	200	5	2750	23.9	72.0	16.9	0.2
902-3	450	250	200	1	2273	26.8	86.9	28.6	0.3
902-3	450	250	200	0.5	2105	27.4	93.5	34.5	0.4
902-1	650	250	400	10	3462	24.1	112.4	32.3	0.3
902-1	650	250	400	5	3099	24.6	127.5	38.8	0.3
902-1	650	250	400	1	2233	26.8	178.2	62.8	0.4
902-1	650	250	400	0.5	1903	27.8	208.7	76.8	0.4
902-2	650	250	400	10	3714	23.6	104.8	32.5	0.3
902-2	650	250	400	5	3176	24.3	124.4	40.6	0.3
902-2	650	250	400	1	2314	27.1	171.9	63.9	0.4
902-2	650	250	400	0.5	1985	27.3	200.3	74.8	0.4
902-3	650	250	400	10	3607	23.4	108.0	35.1	0.3
902-3	650	250	400	5	3205	24.8	123.5	40.7	0.3
902-3	650	250	400	1	2295	27.0	173.8	62.9	0.4
902-3	650	250	400	0.5	1976	27.0	200.9	75.5	0.4

Table D. 12 Triaxial Frequency Sweep Test results at 20°C, 2.75° Angle of Gyration and Deviatoric Stress of 600 kPa and 200 kPa (Fully Reversed) for Test Section 902S

Sample Name	σ_1 kPa	σ_3 kPa	σ_D kPa	Freq (Hz)	Dyn Mod E_d (Mpa)	Phase Angle δ (°)	RAMS	RRMS	P Ratio, ν
902-1	650	50	600	10	2642	23.4	219.9	62.5	0.3
902-1	650	50	600	5	2354	23.7	251.0	76.8	0.3
902-1	650	50	600	1	1644	26.3	363.7	129.4	0.4
902-1	650	50	600	0.5	1379	26.5	433.2	168.3	0.4
902-2	650	50	600	10	2681	23.2	217.3	61.0	0.3
902-2	650	50	600	5	2446	23.4	241.9	72.5	0.3
902-2	650	50	600	1	1773	25.8	337.3	116.4	0.3
902-2	650	50	600	0.5	1512	26.5	395.2	153.8	0.4
902-3	650	50	600	10	2705	23.3	216.0	61.2	0.3
902-3	650	50	600	5	2399	23.3	246.7	73.4	0.3
902-3	650	50	600	1	1719	25.6	347.9	124.6	0.4
902-3	650	50	600	0.5	1474	26.2	405.0	151.8	0.4
902-1	450	250	200	10	2600	29.5	152.8	45.4	0.3
902-1	450	250	200	5	2253	31.5	176.1	55.7	0.3
902-1	450	250	200	1	1414	39.2	280.2	102.7	0.4
902-1	450	250	200	0.5	1145	41.7	346.0	128.6	0.4
902-2	450	250	200	10	2543	29.4	156.2	43.8	0.3
902-2	450	250	200	5	2207	31.9	180.0	53.5	0.3
902-2	450	250	200	1	1436	37.2	275.8	104.8	0.4
902-2	450	250	200	0.5	1145	40.3	346.1	139.9	0.4
902-3	450	250	200	10	2826	25.5	140.6	45.6	0.3
902-3	450	250	200	5	2415	30.6	164.6	56.0	0.3
902-3	450	250	200	1	1467	37.5	271.1	107.9	0.4
902-3	450	250	200	0.5	1146	40.6	345.7	144.0	0.4

Table D. 13 Triaxial Frequency Sweep Test results at 20°C, 1.25° Angle of Gyration and Deviatoric Stress of 200 kPa and 400 kPa for Test Section 903S

Sample Name	σ_1 kPa	σ_3 kPa	σ_D kPa	Freq (Hz)	Dyn Mod E_d (Mpa)	Phase Angle δ (°)	RAMS	RRMS	P Ratio, ν
903-1	450	250	200	10	2677	21.3	73.1	20.8	0.3
903-1	450	250	200	5	2316	20.1	85.1	25.7	0.3
903-1	450	250	200	1	1648	19.4	120.4	34.7	0.3
903-1	450	250	200	0.5	1435	19.1	137.0	46.9	0.3
903-2	450	250	200	10	2795	20.6	70.1	19.8	0.3
903-2	450	250	200	5	2487	20.3	79.2	25.9	0.3
903-2	450	250	200	1	1755	20.0	112.5	38.2	0.3
903-2	450	250	200	0.5	1529	19.4	129.0	45.2	0.4
903-3	450	250	200	10	2792	19.9	70.2	18.6	0.3
903-3	450	250	200	5	2423	19.6	81.5	23.8	0.3
903-3	450	250	200	1	1790	18.7	110.0	40.9	0.4
903-3	450	250	200	0.5	1513	18.5	130.4	48.9	0.4
903-1	650	250	400	10	2614	21.8	148.3	45.6	0.3
903-1	650	250	400	5	2238	21.0	176.7	59.8	0.3
903-1	650	250	400	1	1551	20.7	257.9	95.6	0.4
903-1	650	250	400	0.5	1321	19.9	301.1	120.4	0.4
903-2	650	250	400	10	2831	22.1	137.5	43.4	0.3
903-2	650	250	400	5	2376	21.2	166.4	56.0	0.3
903-2	650	250	400	1	1651	20.7	241.2	88.1	0.4
903-2	650	250	400	0.5	1404	19.9	283.3	108.0	0.4
903-3	650	250	400	10	2807	21.8	138.9	43.7	0.3
903-3	650	250	400	5	2327	21.2	170.1	58.3	0.3
903-3	650	250	400	1	1650	20.4	241.6	94.0	0.4
903-3	650	250	400	0.5	1377	19.8	289.2	113.5	0.4

Table D. 14 Triaxial Frequency Sweep Test results at 20°C, 1.25° Angle of Gyration and Deviatoric Stress of 600 kPa and 200 kPa (Fully Reversed) for Test Section 903S

Sample Name	σ_1 kPa	σ_3 kPa	σ_D kPa	Freq (Hz)	Dyn Mod E_d (Mpa)	Phase Angle δ (°)	RAMS	RRMS	P Ratio, ν
903-1	650	50	600	10	1992	23.5	291.9	101.8	0.3
903-1	650	50	600	5	1694	22.9	349.4	125.5	0.4
903-1	650	50	600	1	1128	21.4	530.1	208.4	0.4
903-1	650	50	600	0.5	958	20.1	623.9	267.1	0.4
903-2	650	50	600	10	2154	22.8	271.0	94.8	0.3
903-2	650	50	600	5	1824	22.7	324.3	115.4	0.4
903-2	650	50	600	1	1220	21.8	490.2	204.4	0.4
903-2	650	50	600	0.5	1026	20.4	582.8	253.1	0.4
903-3	650	50	600	10	2137	23.2	273.6	94.3	0.3
903-3	650	50	600	5	1786	22.1	331.7	115.7	0.3
903-3	650	50	600	1	1194	21.3	500.8	201.2	0.4
903-3	650	50	600	0.5	999	20.2	599.0	258.4	0.4
903-1	450	250	200	10	1949	24.3	204.1	61.7	0.3
903-1	450	250	200	5	1620	26.5	245.3	82.2	0.3
903-1	450	250	200	1	1035	27.2	384.1	147.1	0.4
903-1	450	250	200	0.5	870	25.7	455.3	183.1	0.4
903-2	450	250	200	10	2115	25.3	188.1	57.0	0.3
903-2	450	250	200	5	1811	25.9	219.3	75.9	0.3
903-2	450	250	200	1	1141	27.1	347.9	131.0	0.4
903-2	450	250	200	0.5	954	26.2	415.0	162.4	0.4
903-3	450	250	200	10	2035	25.7	195.2	61.6	0.3
903-3	450	250	200	5	1713	26.6	232.3	79.3	0.3
903-3	450	250	200	1	1090	26.9	365.2	139.9	0.4
903-3	450	250	200	0.5	915	26.1	433.4	172.7	0.4

Table D. 15 Triaxial Frequency Sweep Test results at 20°C, 2.00° Angle of Gyration and Deviatoric Stress of 200 kPa and 400 kPa for Test Section 903S

Sample Name	σ_1 kPa	σ_3 kPa	σ_D kPa	Freq (Hz)	Dyn Mod E_d (Mpa)	Phase Angle δ (°)	RAMS	RRMS	P Ratio, ν
903-1	450	250	200	10	2946	20.8	66.3	19.9	0.3
903-1	450	250	200	5	2597	19.9	76.0	23.8	0.3
903-1	450	250	200	1	1843	21.0	107.6	40.6	0.4
903-1	450	250	200	0.5	1582	20.5	124.3	47.3	0.4
903-2	450	250	200	10	3326	21.4	58.8	17.4	0.3
903-2	450	250	200	5	2826	20.5	69.9	25.4	0.4
903-2	450	250	200	1	2020	21.2	97.6	36.3	0.4
903-2	450	250	200	0.5	1760	21.2	111.9	41.8	0.4
903-3	450	250	200	10	2794	19.0	70.1	18.3	0.3
903-3	450	250	200	5	2610	18.9	75.5	19.0	0.3
903-3	450	250	200	1	2006	18.9	98.6	29.7	0.3
903-3	450	250	200	0.5	1770	19.9	111.2	39.0	0.4
903-1	650	250	400	10	3053	22.1	127.9	44.2	0.3
903-1	650	250	400	5	2601	21.9	152.1	55.4	0.4
903-1	650	250	400	1	1755	22.0	226.9	90.6	0.4
903-1	650	250	400	0.5	1486	21.6	267.3	111.6	0.4
903-2	650	250	400	10	3348	22.6	116.4	40.0	0.3
903-2	650	250	400	5	2794	21.6	141.4	54.0	0.4
903-2	650	250	400	1	1906	22.8	209.0	86.0	0.4
903-2	650	250	400	0.5	1580	22.0	252.0	109.7	0.4
903-3	650	250	400	10	3162	21.2	122.9	39.8	0.3
903-3	650	250	400	5	2814	21.7	140.4	47.2	0.3
903-3	650	250	400	1	1944	21.5	204.8	78.6	0.4
903-3	650	250	400	0.5	1643	21.8	241.8	100.4	0.4

Table D. 16 Triaxial Frequency Sweep Test results at 20°C, 2.00° Angle of Gyration and Deviatoric Stress of 600 kPa and 200 kPa (Fully Reversed) for Test Section 903S

Sample Name	σ_1 kPa	σ_3 kPa	σ_D kPa	Freq (Hz)	Dyn Mod E_d (Mpa)	Phase Angle δ (°)	RAMS	RRMS	P Ratio, ν
903-1	650	50	600	10	2327	23.7	250.1	77.1	0.3
903-1	650	50	600	5	1956	22.9	302.7	111.2	0.4
903-1	650	50	600	1	1280	22.6	466.9	197.0	0.4
903-1	650	50	600	0.5	1059	21.3	564.4	248.8	0.4
903-2	650	50	600	10	2559	22.9	227.5	78.0	0.3
903-2	650	50	600	5	2141	22.9	276.1	110.6	0.4
903-2	650	50	600	1	1383	22.9	432.3	199.8	0.5
903-2	650	50	600	0.5	1143	21.9	522.7	252.4	0.5
903-3	650	50	600	10	2291	21.3	254.5	73.1	0.3
903-3	650	50	600	5	2083	20.9	283.8	93.3	0.3
903-3	650	50	600	1	1355	22.5	441.9	185.4	0.4
903-3	650	50	600	0.5	918	22.0	473.1	167.3	0.4
903-1	450	250	200	10	2280	23.7	174.2	62.8	0.4
903-1	450	250	200	5	1904	28.3	208.5	76.7	0.4
903-1	450	250	200	1	1168	28.3	340.0	141.5	0.4
903-1	450	250	200	0.5	967	27.7	409.2	175.6	0.4
903-2	450	250	200	10	2464	26.7	161.4	62.0	0.4
903-2	450	250	200	5	2035	28.3	195.2	74.3	0.4
903-2	450	250	200	1	1275	28.7	311.3	135.5	0.4
903-2	450	250	200	0.5	1047	28.3	378.3	170.0	0.4
903-3	450	250	200	10	3286	22.2	59.7	21.3	0.4
903-3	450	250	200	5	2025	23.0	66.7	27.7	0.4
903-3	450	250	200	1	1231	22.2	97.8	144.7	0.4
903-3	450	250	200	0.5	918	22.0	473.1	167.3	0.4

Table D. 17 Triaxial Frequency Sweep Test results at 20°C, 2.75° Angle of Gyration and Deviatoric Stress of 200 kPa and 400 kPa for Test Section 903S

Sample Name	σ_1 kPa	σ_3 kPa	σ_D kPa	Freq (Hz)	Dyn Mod E_d (Mpa)	Phase Angle δ (°)	RAMS	RRMS	P Ratio, ν
903-1	450	250	200	10	3298	21.2	59.4	16.8	0.3
903-1	450	250	200	5	2846	21.1	69.4	24.4	0.4
903-1	450	250	200	1	1963	21.3	100.8	37.2	0.4
903-1	450	250	200	0.5	1717	21.5	114.5	46.0	0.4
903-2	450	250	200	10	3073	20.2	63.5	20.1	0.3
903-2	450	250	200	5	2804	21.7	70.4	23.2	0.3
903-2	450	250	200	1	1987	22.3	99.8	38.9	0.4
903-2	450	250	200	0.5	1687	21.7	116.8	46.7	0.4
903-3	450	250	200	10	3187	22.3	61.2	21.1	0.3
903-3	450	250	200	5	2882	22.3	68.4	23.9	0.3
903-3	450	250	200	1	2019	21.8	97.6	37.1	0.4
903-3	450	250	200	0.5	1726	21.3	113.9	45.3	0.4
903-1	650	250	400	10	3418	23.4	113.8	37.8	0.3
903-1	650	250	400	5	2854	23.0	138.4	50.2	0.4
903-1	650	250	400	1	1895	23.7	210.0	88.5	0.4
903-1	650	250	400	0.5	1578	23.3	251.5	112.5	0.4
903-2	650	250	400	10	3325	23.8	117.1	44.0	0.4
903-2	650	250	400	5	2785	23.0	141.8	53.2	0.4
903-2	650	250	400	1	1884	23.9	211.5	90.8	0.4
903-2	650	250	400	0.5	1574	23.1	252.1	109.1	0.4
903-3	650	250	400	10	3427	24.1	113.4	44.0	0.4
903-3	650	250	400	5	2903	23.7	136.1	53.2	0.4
903-3	650	250	400	1	1945	23.8	204.7	90.8	0.4
903-3	650	250	400	0.5	1612	23.3	246.5	109.1	0.4

Table D. 18 Triaxial Frequency Sweep Test results at 20°C, 2.75° Angle of Gyration and Deviatoric Stress of 600 kPa and 200 kPa (Fully Reversed) for Test Section 903S

Sample Name	σ_1 kPa	σ_3 kPa	σ_D kPa	Freq (Hz)	Dyn Mod E_d (Mpa)	Phase Angle δ (°)	RAMS	RRMS	P Ratio, ν
903-1	650	50	600	10	2592	23.3	225.0	78.4	0.3
903-1	650	50	600	5	2190	23.4	270.0	101.9	0.4
903-1	650	50	600	1	1402	23.2	426.6	186.1	0.4
903-1	650	50	600	0.5	1145	22.4	522.2	237.3	0.5
903-2	650	50	600	10	2557	23.1	227.9	83.6	0.4
903-2	650	50	600	5	2143	23.0	276.2	103.3	0.4
903-2	650	50	600	1	1380	23.1	432.9	188.7	0.4
903-2	650	50	600	0.5	1138	22.1	525.3	244.1	0.5
903-3	650	50	600	10	2579	23.7	225.6	83.6	0.4
903-3	650	50	600	5	2194	23.5	269.6	103.3	0.4
903-3	650	50	600	1	1411	23.6	424.0	188.7	0.4
903-3	650	50	600	0.5	1145	22.5	521.8	244.1	0.5
903-1	450	250	200	10	2608	27.3	152.3	55.3	0.4
903-1	450	250	200	5	2175	28.9	182.3	72.6	0.4
903-1	450	250	200	1	1328	30.0	298.8	137.4	0.5
903-1	450	250	200	0.5	1064	30.6	372.5	176.4	0.5
903-2	450	250	200	10	2516	27.1	158.0	54.1	0.3
903-2	450	250	200	5	2125	28.4	187.0	71.2	0.4
903-2	450	250	200	1	1307	30.4	303.4	138.1	0.5
903-2	450	250	200	0.5	1058	30.6	373.8	172.9	0.5
903-3	450	250	200	10	2537	29.1	156.9	53.8	0.3
903-3	450	250	200	5	2153	28.8	184.2	75.1	0.4
903-3	450	250	200	1	1307	30.7	302.9	137.1	0.5
903-3	450	250	200	0.5	1058	30.5	373.9	172.6	0.5

Table D. 19 Triaxial Frequency Sweep Test results at 20°C, 1.25° Angle of Gyration and Deviatoric Stress of 200 kPa and 400 kPa for Test Section 959S

Sample Name	σ_1 kPa	σ_3 kPa	σ_D kPa	Freq (Hz)	Dyn Mod E_d (Mpa)	Phase Angle δ (°)	RAMS	RRMS	P Ratio, ν
959-1	450	250	200	10	3119	20.2	62.8	18.3	0.3
959-1	450	250	200	5	2945	18.0	67.0	19.4	0.3
959-1	450	250	200	1	2171	19.3	91.3	30.7	0.3
959-1	450	250	200	0.5	1895	19.5	103.5	38.6	0.4
959-2	450	250	200	10	3193	18.6	61.4	17.1	0.3
959-2	450	250	200	5	3002	18.5	65.8	17.4	0.3
959-2	450	250	200	1	2296	19.2	85.7	32.2	0.4
959-2	450	250	200	0.5	1966	20.3	100.1	36.9	0.4
959-3	450	250	200	10	3335	19.4	58.5	18.3	0.3
959-3	450	250	200	5	2919	18.9	67.6	19.2	0.3
959-3	450	250	200	1	2184	19.7	90.4	29.4	0.3
959-3	450	250	200	0.5	1855	19.6	106.2	30.9	0.3
959-1	650	250	400	10	3328	19.9	117.1	32.9	0.3
959-1	650	250	400	5	2986	19.8	132.5	43.7	0.3
959-1	650	250	400	1	2102	20.8	189.7	67.9	0.4
959-1	650	250	400	0.5	1780	21.5	223.3	82.9	0.4
959-2	650	250	400	10	3492	19.8	111.4	31.2	0.3
959-2	650	250	400	5	3088	19.2	127.8	40.2	0.3
959-2	650	250	400	1	2148	20.8	185.6	65.5	0.4
959-2	650	250	400	0.5	1835	21.0	216.4	76.2	0.4
959-3	650	250	400	10	3381	20.8	115.3	33.7	0.3
959-3	650	250	400	5	3003	19.8	131.6	42.2	0.3
959-3	650	250	400	1	2064	21.4	193.3	66.4	0.3
959-3	650	250	400	0.5	1792	21.1	221.7	79.4	0.4

Table D. 20 Triaxial Frequency Sweep Test results at 20°C, 1.25° Angle of Gyration and Deviatoric Stress of 600 kPa and 200 kPa (Fully Reversed) for Test Section 959S

Sample Name	σ_1 kPa	σ_3 kPa	σ_D kPa	Freq (Hz)	Dyn Mod E_d (Mpa)	Phase Angle δ (°)	RAMS	RRMS	P Ratio, ν
959-1	650	50	600	10	2636	20.6	221.2	62.4	0.3
959-1	650	50	600	5	2363	20.3	250.3	85.0	0.3
959-1	650	50	600	1	1588	22.1	376.1	140.9	0.4
959-1	650	50	600	0.5	1321	22.1	452.2	185.1	0.4
959-2	650	50	600	10	2779	20.7	209.6	59.2	0.3
959-2	650	50	600	5	2425	20.7	243.5	74.6	0.3
959-2	650	50	600	1	1646	21.7	363.1	130.1	0.4
959-2	650	50	600	0.5	1373	21.5	435.1	168.3	0.4
959-3	650	50	600	10	2726	21.7	213.5	60.4	0.3
959-3	650	50	600	5	2343	21.1	252.6	81.6	0.3
959-3	650	50	600	1	1582	22.3	377.9	140.2	0.4
959-3	650	50	600	0.5	1339	21.7	446.2	178.6	0.4
959-1	450	250	200	10	2574	20.2	154.3	42.6	0.3
959-1	450	250	200	5	2241	24.1	177.0	54.4	0.3
959-1	450	250	200	1	1491	27.6	266.5	91.3	0.3
959-1	450	250	200	0.5	1233	26.8	321.2	111.6	0.3
959-2	450	250	200	10	2693	24.1	147.6	40.6	0.3
959-2	450	250	200	5	2301	23.4	172.6	50.9	0.3
959-2	450	250	200	1	1527	26.4	260.0	86.7	0.3
959-2	450	250	200	0.5	1263	26.4	313.5	110.1	0.4
959-3	450	250	200	10	2630	23.6	151.2	41.4	0.3
959-3	450	250	200	5	2258	23.9	175.7	53.0	0.3
959-3	450	250	200	1	1492	26.7	266.2	90.6	0.3
959-3	450	250	200	0.5	1242	26.4	318.9	111.4	0.4

Table D. 21 Triaxial Frequency Sweep Test results at 20°C, 2.00° Angle of Gyration and Deviatoric Stress of 200 kPa and 400 kPa for Test Section 959S

Sample Name	σ_1 kPa	σ_3 kPa	σ_D kPa	Freq (Hz)	Dyn Mod E_d (Mpa)	Phase Angle δ (°)	RAMS	RRMS	P Ratio, ν
959-1	450	250	200	10	3804	16.4	51.3	13.4	0.3
959-1	450	250	200	5	3241	17.5	60.8	14.9	0.2
959-1	450	250	200	1	2490	17.9	79.2	22.2	0.3
959-1	450	250	200	0.5	2155	18.9	91.5	29.4	0.3
959-2	450	250	200	10	3422	18.9	57.4	16.8	0.3
959-2	450	250	200	5	3199	19.5	61.8	16.4	0.3
959-2	450	250	200	1	2379	19.7	83.2	26.8	0.3
959-2	450	250	200	0.5	2216	19.9	89.0	30.4	0.3
959-3	450	250	200	10	3445	18.8	57.3	15.5	0.3
959-3	450	250	200	5	3313	18.6	59.6	14.1	0.2
959-3	450	250	200	1	2557	20.2	77.4	26.0	0.3
959-3	450	250	200	0.5	2142	20.7	92.1	28.3	0.3
959-1	650	250	400	10	3937	18.6	99.0	28.7	0.3
959-1	650	250	400	5	3371	18.8	117.2	33.5	0.3
959-1	650	250	400	1	2440	20.7	163.1	53.4	0.3
959-1	650	250	400	0.5	2086	20.4	190.6	67.3	0.4
959-2	650	250	400	10	3951	18.9	98.7	29.7	0.3
959-2	650	250	400	5	3430	19.7	115.3	37.3	0.3
959-2	650	250	400	1	2429	21.5	163.9	62.1	0.4
959-2	650	250	400	0.5	2060	21.6	192.8	73.6	0.4
959-3	650	250	400	10	3812	19.1	102.3	29.9	0.3
959-3	650	250	400	5	3474	19.5	113.9	32.8	0.3
959-3	650	250	400	1	2445	21.1	162.8	59.9	0.4
959-3	650	250	400	0.5	2090	22.5	190.3	75.1	0.4

Table D. 22 Triaxial Frequency Sweep Test results at 20°C, 2.00° Angle of Gyration and Deviatoric Stress of 600 kPa and 200 kPa (Fully Reversed) for Test Section 959S

Sample Name	σ_1 kPa	σ_3 kPa	σ_D kPa	Freq (Hz)	Dyn Mod E_d (Mpa)	Phase Angle δ (°)	RAMS	RRMS	P Ratio, ν
959-1	650	50	600	10	3091	18.5	188.5	51.4	0.3
959-1	650	50	600	5	2647	18.5	223.3	64.8	0.3
959-1	650	50	600	1	1842	20.8	324.2	116.6	0.4
959-1	650	50	600	0.5	1539	21.5	387.9	140.5	0.4
959-2	650	50	600	10	3135	19.4	186.0	55.2	0.3
959-2	650	50	600	5	2702	19.9	219.0	70.1	0.3
959-2	650	50	600	1	1836	21.7	325.9	115.6	0.4
959-2	650	50	600	0.5	1527	22.1	391.3	148.7	0.4
959-3	650	50	600	10	2998	19.4	194.8	57.3	0.3
959-3	650	50	600	5	2796	20.1	211.4	64.8	0.3
959-3	650	50	600	1	1862	21.5	321.3	114.3	0.4
959-3	650	50	600	0.5	1488	28.0	266.1	97.5	0.4
959-1	450	250	200	10	2866	18.5	138.5	31.6	0.2
959-1	450	250	200	5	2489	23.0	159.8	44.9	0.3
959-1	450	250	200	1	1713	26.9	231.7	75.0	0.3
959-1	450	250	200	0.5	1438	26.5	275.2	93.6	0.3
959-2	450	250	200	10	3034	20.9	131.1	38.0	0.3
959-2	450	250	200	5	2624	24.4	151.5	46.7	0.3
959-2	450	250	200	1	1753	27.0	226.5	77.9	0.3
959-2	450	250	200	0.5	1460	27.8	271.1	99.3	0.4
959-3	450	250	200	10	3133	19.8	126.9	38.0	0.3
959-3	450	250	200	5	2724	23.6	145.7	39.9	0.3
959-3	450	250	200	1	1790	27.7	222.1	79.3	0.4
959-3	450	250	200	0.5	1488	28.0	266.1	97.5	0.4

Table D. 23 Triaxial Frequency Sweep Test results at 20°C, 2.75° Angle of Gyration and Deviatoric Stress of 200 kPa and 400 kPa for Test Section 959S

Sample Name	σ_1 kPa	σ_3 kPa	σ_D kPa	Freq (Hz)	Dyn Mod E_d (Mpa)	Phase Angle δ (°)	RAMS	RRMS	P Ratio, ν
959-1	450	250	200	10	2878	16.9	67.7	12.6	0.2
959-1	450	250	200	5	2677	17.2	73.7	17.4	0.2
959-1	450	250	200	1	2142	18.3	92.3	26.6	0.3
959-1	450	250	200	0.5	1913	19.8	103.2	32.9	0.3
959-2	450	250	200	10	3308	16.4	59.2	13.7	0.2
959-2	450	250	200	5	3211	16.5	61.4	16.4	0.3
959-2	450	250	200	1	2446	19.9	81.0	26.7	0.3
959-2	450	250	200	0.5	2170	19.6	91.1	28.1	0.3
959-3	450	250	200	10	3366	17.5	58.0	16.2	0.3
959-3	450	250	200	5	3111	16.8	63.5	16.5	0.3
959-3	450	250	200	1	2518	18.6	78.4	21.2	0.3
959-3	450	250	200	0.5	2185	18.8	90.2	27.1	0.3
959-1	650	250	400	10	3494	17.9	110.8	23.7	0.2
959-1	650	250	400	5	3136	17.0	126.2	38.9	0.3
959-1	650	250	400	1	2299	20.6	173.5	60.2	0.3
959-1	650	250	400	0.5	1942	21.3	204.7	71.5	0.3
959-2	650	250	400	10	3910	18.5	99.6	26.4	0.3
959-2	650	250	400	5	3549	18.7	111.3	35.3	0.3
959-2	650	250	400	1	2529	20.7	157.4	56.7	0.4
959-2	650	250	400	0.5	2146	21.2	185.0	66.2	0.4
959-3	650	250	400	10	3821	18.9	101.9	23.7	0.2
959-3	650	250	400	5	3426	18.3	115.5	32.8	0.3
959-3	650	250	400	1	2504	20.7	159.2	52.5	0.3
959-3	650	250	400	0.5	2137	21.2	186.1	64.8	0.3

Table D. 24 Triaxial Frequency Sweep Test results at 20°C, 2.75° Angle of Gyration and Deviatoric Stress of 600 kPa and 200 kPa (Fully Reversed) for Test Section 959S

Sample Name	σ_1 kPa	σ_3 kPa	σ_D kPa	Freq (Hz)	Dyn Mod E_d (Mpa)	Phase Angle δ (°)	RAMS	RRMS	P Ratio, ν
959-1	650	50	600	10	2743	18.4	212.6	52.2	0.2
959-1	650	50	600	5	2471	18.8	239.3	66.8	0.3
959-1	650	50	600	1	1717	21.4	347.9	118.8	0.3
959-1	650	50	600	0.5	1423	22.0	419.8	159.9	0.4
959-2	650	50	600	10	3097	18.4	187.9	49.5	0.3
959-2	650	50	600	5	2773	18.8	213.3	60.9	0.3
959-2	650	50	600	1	1916	21.1	311.8	105.4	0.3
959-2	650	50	600	0.5	1583	22.0	378.0	138.0	0.4
959-3	650	50	600	10	2926	18.1	199.4	58.9	0.3
959-3	650	50	600	5	2725	19.1	216.8	60.5	0.3
959-3	650	50	600	1	1924	20.8	310.9	103.0	0.3
959-3	650	50	600	0.5	1606	21.7	372.4	132.3	0.4
959-1	450	250	200	10	2829	22.9	140.6	34.4	0.2
959-1	450	250	200	5	2500	23.4	158.8	43.6	0.3
959-1	450	250	200	1	1702	26.5	233.5	80.5	0.3
959-1	450	250	200	0.5	1413	27.3	280.3	103.6	0.4
959-2	450	250	200	10	3111	19.4	127.8	34.2	0.3
959-2	450	250	200	5	2665	23.5	149.1	43.7	0.3
959-2	450	250	200	1	1817	28.0	218.9	75.5	0.3
959-2	450	250	200	0.5	1517	27.7	261.1	96.6	0.4
959-3	450	250	200	10	2989	21.8	133.2	33.2	0.2
959-3	450	250	200	5	2712	23.9	146.2	40.4	0.3
959-3	450	250	200	1	1822	26.2	218.1	71.2	0.3
959-3	450	250	200	0.5	1526	27.4	259.4	88.9	0.3

Table D. 25 Triaxial Frequency Sweep Test results at 20°C, 1.25° Angle of Gyration and Deviatoric Stress of 200 kPa and 400 kPa for Test Section 960S

Sample Name	σ_1 kPa	σ_3 kPa	σ_D kPa	Freq (Hz)	Dyn Mod E_d (Mpa)	Phase Angle δ (°)	RAMS	RRMS	P Ratio, ν
960-1	450	250	200	10	2989	22.8	65.4	21.5	0.3
960-1	450	250	200	5	2688	20.4	73.3	19.6	0.3
960-1	450	250	200	1	1936	20.3	102.4	36.5	0.4
960-1	450	250	200	0.5	1642	19.1	120.4	42.6	0.4
960-2	450	250	200	10	2758	21.0	70.9	19.7	0.3
960-2	450	250	200	5	2424	19.6	81.3	26.7	0.3
960-2	450	250	200	1	1777	19.0	111.2	40.0	0.4
960-2	450	250	200	0.5	1531	18.9	128.6	45.2	0.4
960-3	450	250	200	10	3024	20.7	64.4	18.5	0.3
960-3	450	250	200	5	2575	19.9	76.5	23.4	0.3
960-3	450	250	200	1	1850	19.7	106.8	40.4	0.4
960-3	450	250	200	0.5	1640	18.4	119.9	48.2	0.4
960-1	650	250	400	10	2927	22.0	132.9	40.1	0.3
960-1	650	250	400	5	2551	21.6	155.0	53.5	0.3
960-1	650	250	400	1	1764	21.2	226.0	85.0	0.4
960-1	650	250	400	0.5	1487	19.9	267.5	99.9	0.4
960-2	650	250	400	10	2777	22.2	140.4	45.2	0.3
960-2	650	250	400	5	2359	21.9	167.2	56.4	0.3
960-2	650	250	400	1	1665	20.7	238.6	87.9	0.4
960-2	650	250	400	0.5	1422	19.9	280.0	107.1	0.4
960-3	650	250	400	10	2935	22.3	132.6	43.8	0.3
960-3	650	250	400	5	2465	21.8	160.5	55.3	0.3
960-3	650	250	400	1	1731	21.0	229.8	91.3	0.4
960-3	650	250	400	0.5	1458	20.1	272.9	106.4	0.4

Table D. 26 Triaxial Frequency Sweep Test results at 20°C, 1.25° Angle of Gyration and Deviatoric Stress of 600 kPa and 200 kPa (Fully Reversed) for Test Section 960S

Sample Name	σ_1 kPa	σ_3 kPa	σ_D kPa	Freq (Hz)	Dyn Mod E_d (Mpa)	Phase Angle δ (°)	RAMS	RRMS	P Ratio, ν
960-1	650	50	600	10	2259	23.8	257.9	86.2	0.3
960-1	650	50	600	5	1960	23.0	301.7	104.0	0.3
960-1	650	50	600	1	1289	22.2	463.7	185.3	0.4
960-1	650	50	600	0.5	1085	20.9	550.9	242.0	0.4
960-2	650	50	600	10	2119	23.3	275.6	90.4	0.3
960-2	650	50	600	5	1808	22.6	327.0	119.3	0.4
960-2	650	50	600	1	1213	21.5	493.2	205.7	0.4
960-2	650	50	600	0.5	1035	20.1	577.1	257.0	0.4
960-3	650	50	600	10	2249	23.6	258.8	89.7	0.3
960-3	650	50	600	5	1929	23.0	307.0	112.4	0.4
960-3	650	50	600	1	1282	21.9	466.4	195.3	0.4
960-3	650	50	600	0.5	1064	20.6	561.6	250.1	0.4
960-1	450	250	200	10	2187	24.9	181.8	53.7	0.3
960-1	450	250	200	5	1861	27.1	213.4	66.2	0.3
960-1	450	250	200	1	1170	27.7	340.1	126.2	0.4
960-1	450	250	200	0.5	966	26.8	410.3	155.4	0.4
960-2	450	250	200	10	2097	26.6	190.0	59.0	0.3
960-2	450	250	200	5	1730	26.7	230.1	77.3	0.3
960-2	450	250	200	1	1114	27.0	356.1	134.2	0.4
960-2	450	250	200	0.5	923	26.3	429.1	164.9	0.4
960-3	450	250	200	10	2170	28.0	183.2	63.5	0.3
960-3	450	250	200	5	1806	26.8	220.2	75.0	0.3
960-3	450	250	200	1	1145	27.3	347.1	135.2	0.4
960-3	450	250	200	0.5	948	26.6	418.1	164.0	0.4

Table D. 27 Triaxial Frequency Sweep Test results at 20°C, 2.00° Angle of Gyration and Deviatoric Stress of 200 kPa and 400 kPa for Test Section 960S

Sample Name	σ_1 kPa	σ_3 kPa	σ_D kPa	Freq (Hz)	Dyn Mod E_d (Mpa)	Phase Angle δ (°)	RAMS	RRMS	P Ratio, ν
960-1	450	250	200	10	2757	19.5	70.8	18.1	0.3
960-1	450	250	200	5	2580	19.1	76.4	20.7	0.3
960-1	450	250	200	1	1923	19.4	102.9	34.7	0.3
960-1	450	250	200	0.5	1692	19.2	116.7	39.0	0.3
960-2	450	250	200	10	2768	19.9	71.0	19.7	0.3
960-2	450	250	200	5	2487	19.7	79.4	27.0	0.3
960-2	450	250	200	1	1887	19.6	104.4	38.1	0.4
960-2	450	250	200	0.5	1640	19.8	120.5	45.1	0.4
960-3	450	250	200	10	2770	20.2	71.0	25.0	0.4
960-3	450	250	200	5	2592	20.2	76.2	25.9	0.3
960-3	450	250	200	1	1912	19.9	103.1	39.8	0.4
960-3	450	250	200	0.5	1630	20.4	121.0	49.3	0.4
960-1	650	250	400	10	3092	21.5	126.2	38.8	0.3
960-1	650	250	400	5	2688	21.3	146.9	51.1	0.3
960-1	650	250	400	1	1835	21.4	216.7	82.9	0.4
960-1	650	250	400	0.5	1555	21.1	256.0	102.8	0.4
960-2	650	250	400	10	3059	21.5	127.0	44.2	0.3
960-2	650	250	400	5	2592	21.7	152.5	54.9	0.4
960-2	650	250	400	1	1798	21.3	221.6	93.7	0.4
960-2	650	250	400	0.5	1516	21.1	262.6	106.2	0.4
960-3	650	250	400	10	3137	22.7	124.1	44.8	0.4
960-3	650	250	400	5	2652	21.9	149.0	56.9	0.4
960-3	650	250	400	1	1797	22.0	221.4	95.2	0.4
960-3	650	250	400	0.5	1514	21.5	262.7	111.4	0.4

Table D. 28 Triaxial Frequency Sweep Test results at 20°C, 2.00° Angle of Gyration and Deviatoric Stress of 600 kPa and 200 kPa (Fully Reversed) for Test Section 960S

Sample Name	σ_1 kPa	σ_3 kPa	σ_D kPa	Freq (Hz)	Dyn Mod E_d (Mpa)	Phase Angle δ (°)	RAMS	RRMS	P Ratio, ν
960-1	650	50	600	10	2318	22.0	250.8	73.0	0.3
960-1	650	50	600	5	2015	22.0	293.6	101.7	0.3
960-1	650	50	600	1	1346	22.0	443.9	174.9	0.4
960-1	650	50	600	0.5	1134	21.0	526.7	229.2	0.4
960-2	650	50	600	10	2253	22.2	258.1	85.1	0.3
960-2	650	50	600	5	1919	22.0	308.2	117.8	0.4
960-2	650	50	600	1	1288	21.5	464.0	201.6	0.4
960-2	650	50	600	0.5	1079	20.8	553.3	255.9	0.5
960-3	650	50	600	10	2403	22.6	242.5	80.6	0.3
960-3	650	50	600	5	2005	22.7	295.3	114.0	0.4
960-3	650	50	600	1	1315	22.1	454.6	190.1	0.4
960-3	650	50	600	0.5	989	28.2	400.3	169.2	0.4
960-1	450	250	200	10	2311	26.6	172.0	54.1	0.3
960-1	450	250	200	5	1968	26.4	201.5	69.3	0.3
960-1	450	250	200	1	1239	28.8	320.8	124.2	0.4
960-1	450	250	200	0.5	1022	27.9	388.2	155.1	0.4
960-2	450	250	200	10	2255	26.0	176.3	60.8	0.3
960-2	450	250	200	5	1904	27.4	208.7	71.8	0.3
960-2	450	250	200	1	1203	28.9	330.1	138.2	0.4
960-2	450	250	200	0.5	996	27.7	397.4	168.3	0.4
960-3	450	250	200	10	2312	28.1	171.9	62.9	0.4
960-3	450	250	200	5	1930	28.0	206.1	77.0	0.4
960-3	450	250	200	1	1199	28.9	331.2	136.9	0.4
960-3	450	250	200	0.5	989	28.2	400.3	169.2	0.4

Table D. 29 Triaxial Frequency Sweep Test results at 20°C, 2.75° Angle of Gyration and Deviatoric Stress of 200 kPa and 400 kPa for Test Section 960S

Sample Name	σ_1 kPa	σ_3 kPa	σ_D kPa	Freq (Hz)	Dyn Mod E_d (Mpa)	Phase Angle δ (°)	RAMS	RRMS	P Ratio, ν
960-1	450	250	200	10	3216	19.2	60.9	18.5	0.3
960-1	450	250	200	5	2756	19.9	71.7	24.1	0.3
960-1	450	250	200	1	2010	21.6	98.4	39.1	0.4
960-1	450	250	200	0.5	1765	21.4	111.4	44.2	0.4
960-2	450	250	200	10	3122	21.4	62.9	19.7	0.3
960-2	450	250	200	5	2817	21.6	70.1	24.3	0.3
960-2	450	250	200	1	2012	21.9	98.5	36.7	0.4
960-2	450	250	200	0.5	1714	22.0	114.7	45.8	0.4
960-3	450	250	200	10	3132	20.8	62.5	17.9	0.3
960-3	450	250	200	5	2788	20.7	70.8	22.8	0.3
960-3	450	250	200	1	2103	20.8	94.2	37.3	0.4
960-3	450	250	200	0.5	1794	20.6	109.6	45.5	0.4
960-1	650	250	400	10	3332	22.5	116.8	44.1	0.4
960-1	650	250	400	5	2890	22.4	136.7	52.4	0.4
960-1	650	250	400	1	1918	22.6	207.8	86.8	0.4
960-1	650	250	400	0.5	1604	22.5	247.9	108.3	0.4
960-2	650	250	400	10	3427	22.6	113.5	42.8	0.4
960-2	650	250	400	5	2876	23.0	137.3	50.3	0.4
960-2	650	250	400	1	1936	23.4	205.6	90.7	0.4
960-2	650	250	400	0.5	1607	23.4	247.6	110.7	0.4
960-3	650	250	400	10	3340	21.3	116.6	39.0	0.3
960-3	650	250	400	5	2866	21.8	137.9	50.9	0.4
960-3	650	250	400	1	1964	23.1	202.7	82.8	0.4
960-3	650	250	400	0.5	1646	22.5	241.6	108.1	0.4

Table D. 30 Triaxial Frequency Sweep Test results at 20°C, 2.75° Angle of Gyration and Deviatoric Stress of 600 kPa and 200 kPa (Fully Reversed) for Test Section 960S

Sample Name	σ_1 kPa	σ_3 kPa	σ_D kPa	Freq (Hz)	Dyn Mod E_d (Mpa)	Phase Angle δ (°)	RAMS	RRMS	P Ratio, ν
960-1	650	50	600	10	2589	22.9	225.1	76.9	0.3
960-1	650	50	600	5	2190	22.7	270.0	105.2	0.4
960-1	650	50	600	1	1433	22.9	417.1	181.3	0.4
960-1	650	50	600	0.5	1185	21.9	504.4	228.8	0.5
960-2	650	50	600	10	2698	22.7	216.0	72.3	0.3
960-2	650	50	600	5	2224	22.8	266.5	102.4	0.4
960-2	650	50	600	1	1430	23.0	417.7	172.6	0.4
960-2	650	50	600	0.5	1188	22.3	502.7	219.8	0.4
960-3	650	50	600	10	2595	22.3	224.4	71.5	0.3
960-3	650	50	600	5	2200	22.5	268.9	101.0	0.4
960-3	650	50	600	1	1440	22.8	415.3	178.5	0.4
960-3	650	50	600	0.5	1196	22.0	499.9	234.6	0.5
960-1	450	250	200	10	2546	27.6	156.1	57.0	0.4
960-1	450	250	200	5	2130	28.5	186.4	71.5	0.4
960-1	450	250	200	1	1285	31.1	308.7	134.1	0.4
960-1	450	250	200	0.5	1036	30.1	382.4	169.1	0.4
960-2	450	250	200	10	2657	30.1	149.5	57.5	0.4
960-2	450	250	200	5	2181	28.0	182.1	70.3	0.4
960-2	450	250	200	1	1292	32.1	307.4	135.3	0.4
960-2	450	250	200	0.5	1015	32.4	390.3	179.4	0.5
960-3	450	250	200	10	2506	27.5	158.3	58.6	0.4
960-3	450	250	200	5	2080	27.9	191.1	73.6	0.4
960-3	450	250	200	1	1289	30.1	308.0	133.5	0.4
960-3	450	250	200	0.5	1045	30.1	379.1	168.5	0.4

Table D. 31 Triaxial Frequency Sweep Test results at 20°C, 1.25° Angle of Gyration and Deviatoric Stress of 200 kPa and 400 kPa for Test Section 961M

Sample Name	σ_1 kPa	σ_3 kPa	σ_D kPa	Freq (Hz)	Dyn Mod E_d (Mpa)	Phase Angle δ (°)	RAMS	RRMS	P Ratio, ν
961-1	450	250	200	10	3027	20.5	64.7	18.7	0.3
961-1	450	250	200	5	2601	22.1	76.1	26.1	0.3
961-1	450	250	200	1	1824	20.8	107.9	39.1	0.4
961-1	450	250	200	0.5	1602	20.6	122.9	50.2	0.4
961-2	450	250	200	10	3069	22.4	64.1	23.3	0.4
961-2	450	250	200	5	2601	21.0	75.7	26.4	0.3
961-2	450	250	200	1	1853	22.1	106.9	44.3	0.4
961-2	450	250	200	0.5	1543	19.9	127.7	50.0	0.4
961-3	450	250	200	10	3037	22.4	64.7	21.9	0.3
961-3	450	250	200	5	2683	22.0	73.4	26.3	0.4
961-3	450	250	200	1	1881	20.6	104.7	38.8	0.4
961-3	450	250	200	0.5	1621	20.5	121.8	47.5	0.4
961-1	650	250	400	10	3002	24.3	129.6	45.3	0.3
961-1	650	250	400	5	2512	23.3	157.7	58.8	0.4
961-1	650	250	400	1	1713	22.1	232.6	99.3	0.4
961-1	650	250	400	0.5	1442	21.5	275.9	120.1	0.4
961-2	650	250	400	10	2985	24.5	130.4	47.8	0.4
961-2	650	250	400	5	2532	22.9	156.3	59.1	0.4
961-2	650	250	400	1	1718	22.7	231.8	98.8	0.4
961-2	650	250	400	0.5	1451	21.7	273.8	120.5	0.4
961-3	650	250	400	10	3023	22.7	129.2	44.6	0.3
961-3	650	250	400	5	2548	23.0	155.4	58.4	0.4
961-3	650	250	400	1	1761	22.1	226.5	92.8	0.4
961-3	650	250	400	0.5	1462	21.6	272.1	118.0	0.4

Table D. 32 Triaxial Frequency Sweep Test results at 20°C, 1.25° Angle of Gyration and Deviatoric Stress of 600 kPa and 200 kPa (Fully Reversed) for Test Section 961M

Sample Name	σ_1 kPa	σ_3 kPa	σ_D kPa	Freq (Hz)	Dyn Mod E_d (Mpa)	Phase Angle δ (°)	RAMS	RRMS	P Ratio, ν
961-1	650	50	600	10	2326	24.3	249.8	96.5	0.4
961-1	650	50	600	5	1952	23.8	302.7	124.7	0.4
961-1	650	50	600	1	1258	22.7	474.7	212.0	0.4
961-1	650	50	600	0.5	1051	21.4	569.0	269.6	0.5
961-2	650	50	600	10	2373	25.1	245.8	93.7	0.4
961-2	650	50	600	5	1986	24.7	297.3	123.3	0.4
961-2	650	50	600	1	1252	23.2	476.1	214.8	0.5
961-2	650	50	600	0.5	1038	21.5	576.3	270.0	0.5
961-3	650	50	600	10	2387	23.7	243.6	89.7	0.4
961-3	650	50	600	5	2023	23.7	292.1	110.6	0.4
961-3	650	50	600	1	1302	23.0	459.0	197.0	0.4
961-3	650	50	600	0.5	1056	21.6	566.0	264.0	0.5
961-1	450	250	200	10	2277	27.8	174.6	62.5	0.4
961-1	450	250	200	5	1847	28.1	214.6	81.3	0.4
961-1	450	250	200	1	1129	30.4	351.2	148.1	0.4
961-1	450	250	200	0.5	913	29.3	432.9	187.4	0.4
961-2	450	250	200	10	2285	29.4	174.1	64.8	0.4
961-2	450	250	200	5	1866	29.5	212.7	84.8	0.4
961-2	450	250	200	1	1129	30.8	351.8	152.7	0.4
961-2	450	250	200	0.5	912	29.2	434.2	191.5	0.4
961-3	450	250	200	10	2308	28.1	172.1	57.8	0.3
961-3	450	250	200	5	1867	28.8	212.4	80.9	0.4
961-3	450	250	200	1	1143	30.2	347.4	147.1	0.4
961-3	450	250	200	0.5	928	29.2	426.7	184.4	0.4

Table D. 33 Triaxial Frequency Sweep Test results at 20°C, 2.00° Angle of Gyration and Deviatoric Stress of 200 kPa and 400 kPa for Test Section 961M

Sample Name	σ_1 kPa	σ_3 kPa	σ_D kPa	Freq (Hz)	Dyn Mod E_d (Mpa)	Phase Angle δ (°)	RAMS	RRMS	P Ratio, ν
961-1	450	250	200	10	3095	23.8	63.2	20.9	0.3
961-1	450	250	200	5	2652	22.7	74.5	22.9	0.3
961-1	450	250	200	1	1837	22.4	107.9	40.5	0.4
961-1	450	250	200	0.5	1538	22.8	128.8	49.7	0.4
961-2	450	250	200	10	3297	21.9	59.0	19.5	0.3
961-2	450	250	200	5	2684	23.7	73.2	27.7	0.4
961-2	450	250	200	1	1846	24.2	106.8	41.8	0.4
961-2	450	250	200	0.5	1586	22.8	124.3	51.2	0.4
961-3	450	250	200	10	3040	24.0	64.3	21.2	0.3
961-3	450	250	200	5	2654	22.4	74.1	26.6	0.4
961-3	450	250	200	1	1838	23.7	107.2	45.5	0.4
961-3	450	250	200	0.5	1533	23.0	128.6	52.0	0.4
961-1	650	250	400	10	3163	24.4	121.9	39.8	0.3
961-1	650	250	400	5	2751	23.8	143.7	53.5	0.4
961-1	650	250	400	1	1791	24.3	222.4	86.6	0.4
961-1	650	250	400	0.5	1479	23.8	269.1	115.9	0.4
961-2	650	250	400	10	3292	24.2	118.0	45.5	0.4
961-2	650	250	400	5	2720	24.3	145.3	60.0	0.4
961-2	650	250	400	1	1774	24.4	224.1	99.3	0.4
961-2	650	250	400	0.5	1456	23.4	273.0	121.1	0.4
961-3	650	250	400	10	3185	23.9	122.1	43.3	0.4
961-3	650	250	400	5	2676	23.2	147.3	56.1	0.4
961-3	650	250	400	1	1758	23.9	226.3	98.5	0.4
961-3	650	250	400	0.5	1439	24.1	276.6	120.0	0.4

Table D. 34 Triaxial Frequency Sweep Test results at 20°C, 2.00° Angle of Gyration and Deviatoric Stress of 600 kPa and 200 kPa (Fully Reversed) for Test Section 961M

Sample Name	σ_1 kPa	σ_3 kPa	σ_D kPa	Freq (Hz)	Dyn Mod E_d (Mpa)	Phase Angle δ (°)	RAMS	RRMS	P Ratio, ν
961-1	650	50	600	10	2544	24.7	228.7	84.6	0.4
961-1	650	50	600	5	2212	23.7	267.5	100.9	0.4
961-1	650	50	600	1	1396	24.1	428.5	183.0	0.4
961-1	650	50	600	0.5	1133	23.1	527.6	243.0	0.5
961-2	650	50	600	10	2634	25.1	221.2	88.0	0.4
961-2	650	50	600	5	2129	24.2	278.1	108.9	0.4
961-2	650	50	600	1	1350	23.7	442.6	203.7	0.5
961-2	650	50	600	0.5	1109	22.5	538.9	264.4	0.5
961-3	650	50	600	10	2541	24.7	228.7	83.6	0.4
961-3	650	50	600	5	2143	24.1	275.6	106.3	0.4
961-3	650	50	600	1	1371	24.0	436.1	194.7	0.4
961-3	650	50	600	0.5	828	35.7	477.8	211.7	0.4
961-1	450	250	200	10	2495	28.7	158.9	55.6	0.3
961-1	450	250	200	5	2040	30.9	194.6	76.5	0.4
961-1	450	250	200	1	1121	34.9	354.3	150.6	0.4
961-1	450	250	200	0.5	846	35.7	467.8	204.6	0.4
961-2	450	250	200	10	2515	28.5	157.9	58.2	0.4
961-2	450	250	200	5	2048	30.9	193.4	80.6	0.4
961-2	450	250	200	1	1126	33.8	352.6	162.4	0.5
961-2	450	250	200	0.5	858	35.0	461.2	210.3	0.5
961-3	450	250	200	10	2424	29.1	163.5	53.1	0.3
961-3	450	250	200	5	1962	31.8	202.4	76.0	0.4
961-3	450	250	200	1	1099	35.3	361.3	153.9	0.4
961-3	450	250	200	0.5	828	35.7	477.8	211.7	0.4

Table D. 35 Triaxial Frequency Sweep Test results at 20°C, 2.75° Angle of Gyration and Deviatoric Stress of 200 kPa and 400 kPa for Test Section 961M

Sample Name	σ_1 kPa	σ_3 kPa	σ_D kPa	Freq (Hz)	Dyn Mod E_d (Mpa)	Phase Angle δ (°)	RAMS	RRMS	P Ratio, ν
961-1	450	250	200	10	3136	25.6	62.3	22.5	0.4
961-1	450	250	200	5	2689	24.6	73.5	25.4	0.3
961-1	450	250	200	1	1832	24.6	107.4	42.7	0.4
961-1	450	250	200	0.5	1514	25.1	130.1	56.8	0.4
961-2	450	250	200	10	3063	24.2	63.6	22.9	0.4
961-2	450	250	200	5	2720	23.7	72.3	26.7	0.4
961-2	450	250	200	1	1806	24.3	109.5	47.3	0.4
961-2	450	250	200	0.5	1499	24.4	131.1	60.8	0.5
961-3	450	250	200	10	3250	22.1	60.3	19.6	0.3
961-3	450	250	200	5	2757	23.8	71.3	23.3	0.3
961-3	450	250	200	1	1915	24.1	103.2	45.1	0.4
961-3	450	250	200	0.5	1585	24.1	124.2	51.1	0.4
961-1	650	250	400	10	3280	25.1	118.7	44.4	0.4
961-1	650	250	400	5	2752	24.8	143.5	56.8	0.4
961-1	650	250	400	1	1768	24.9	225.6	97.6	0.4
961-1	650	250	400	0.5	1440	25.1	275.9	123.8	0.4
961-2	650	250	400	10	3211	25.5	121.0	45.3	0.4
961-2	650	250	400	5	2712	24.6	145.5	59.7	0.4
961-2	650	250	400	1	1752	25.0	227.4	106.8	0.5
961-2	650	250	400	0.5	1438	24.9	276.3	131.4	0.5
961-3	650	250	400	10	3379	24.1	115.1	42.7	0.4
961-3	650	250	400	5	2807	24.3	140.5	56.4	0.4
961-3	650	250	400	1	1803	24.7	221.3	98.1	0.4
961-3	650	250	400	0.5	1491	24.5	266.1	199.6	0.8

Table D. 36 Triaxial Frequency Sweep Test results at 20°C, 2.75° Angle of Gyration and Deviatoric Stress of 600 kPa and 200 kPa (Fully Reversed) for Test Section 961M

Sample Name	σ_1 kPa	σ_3 kPa	σ_D kPa	Freq (Hz)	Dyn Mod E_d (Mpa)	Phase Angle δ (°)	RAMS	RRMS	P Ratio, ν
961-1	650	50	600	10	2732	24.5	213.0	85.0	0.4
961-1	650	50	600	5	2259	24.4	261.6	108.2	0.4
961-1	650	50	600	1	1410	24.8	423.6	198.0	0.5
961-1	650	50	600	0.5	1151	23.9	519.0	264.5	0.5
961-2	650	50	600	10	2627	24.4	221.0	93.9	0.4
961-2	650	50	600	5	2251	24.3	262.4	118.0	0.4
961-2	650	50	600	1	1408	24.7	424.3	211.6	0.5
961-2	650	50	600	0.5	1140	23.8	523.6	276.2	0.5
961-3	650	50	600	10	2668	23.8	218.0	86.2	0.4
961-3	650	50	600	5	2221	23.7	266.1	103.1	0.4
961-3	650	50	600	1	1412	23.9	423.8	188.6	0.4
961-3	650	50	600	0.5	1143	23.2	522.1	251.1	0.5
961-1	450	250	200	10	2574	31.3	154.1	56.6	0.4
961-1	450	250	200	5	2057	33.4	192.9	78.4	0.4
961-1	450	250	200	1	1064	36.9	371.9	167.9	0.5
961-1	450	250	200	0.5	773	38.5	512.0	235.2	0.5
961-2	450	250	200	10	2512	30.3	158.1	65.1	0.4
961-2	450	250	200	5	2019	33.1	196.6	86.7	0.4
961-2	450	250	200	1	1073	36.5	369.6	177.7	0.5
961-2	450	250	200	0.5	783	37.6	504.5	243.0	0.5
961-3	450	250	200	10	2580	28.9	154.1	56.4	0.4
961-3	450	250	200	5	2074	31.5	191.2	78.7	0.4
961-3	450	250	200	1	1151	34.6	344.1	157.3	0.5
961-3	450	250	200	0.5	856	36.7	462.1	212.8	0.5

Table D. 37 Triaxial Frequency Sweep Test results at 20°C, 1.25° Angle of Gyration and Deviatoric Stress of 200 kPa and 400 kPa for Test Section 962SR

Sample Name	σ_1 kPa	σ_3 kPa	σ_D kPa	Freq (Hz)	Dyn Mod E_d (Mpa)	Phase Angle δ (°)	RAMS	RRMS	P Ratio, ν
962-1	450	250	200	10	2242	19.5	87.8	27.3	0.3
962-1	450	250	200	5	2021	18.6	97.7	30.3	0.3
962-1	450	250	200	1	1528	17.6	129.6	44.4	0.3
962-1	450	250	200	0.5	1344	17.4	147.3	50.4	0.3
962-2	450	250	200	10	2294	19.2	85.5	26.5	0.3
962-2	450	250	200	5	2079	18.6	94.2	32.1	0.3
962-2	450	250	200	1	1592	17.0	124.2	43.9	0.4
962-2	450	250	200	0.5	1392	17.1	141.7	50.9	0.4
962-3	450	250	200	10	2137	19.4	92.1	27.4	0.3
962-3	450	250	200	5	1838	19.4	107.4	31.6	0.3
962-3	450	250	200	1	1383	17.6	142.5	45.5	0.3
962-3	450	250	200	0.5	1209	17.4	162.8	51.3	0.3
962-1	650	250	400	10	2259	21.6	172.4	58.8	0.3
962-1	650	250	400	5	1941	20.5	204.2	68.8	0.3
962-1	650	250	400	1	1413	18.6	281.8	104.4	0.4
962-1	650	250	400	0.5	1242	18.0	319.7	121.9	0.4
962-2	650	250	400	10	2277	21.8	171.4	58.9	0.3
962-2	650	250	400	5	1975	20.2	200.0	74.9	0.4
962-2	650	250	400	1	1450	18.8	274.8	113.8	0.4
962-2	650	250	400	0.5	1264	18.0	314.7	128.2	0.4
962-3	650	250	400	10	2006	22.2	193.9	64.1	0.3
962-3	650	250	400	5	1881	20.5	211.1	74.2	0.4
962-3	650	250	400	1	1258	18.7	316.7	115.6	0.4
962-3	650	250	400	0.5	1204	17.9	331.3	128.3	0.4

Table D. 38 Triaxial Frequency Sweep Test results at 20°C, 1.25° Angle of Gyration and Deviatoric Stress of 600 kPa and 200 kPa (Fully Reversed) for Test Section 962SR

Sample Name	σ_1 kPa	σ_3 kPa	σ_D kPa	Freq (Hz)	Dyn Mod E_d (Mpa)	Phase Angle δ (°)	RAMS	RRMS	P Ratio, ν
962-1	650	50	600	10	1668	22.9	349.3	110.6	0.3
962-1	650	50	600	5	1416	21.2	418.1	159.0	0.4
962-1	650	50	600	1	1027	19.1	582.2	244.9	0.4
962-1	650	50	600	0.5	912	17.8	654.9	291.1	0.4
962-2	650	50	600	10	1706	22.3	341.3	111.4	0.3
962-2	650	50	600	5	1445	21.3	409.1	159.9	0.4
962-2	650	50	600	1	1037	19.4	576.4	236.6	0.4
962-2	650	50	600	0.5	911	17.8	656.5	286.0	0.4
962-3	650	50	600	10	1479	24.2	394.2	119.2	0.3
962-3	650	50	600	5	1280	21.7	461.7	178.7	0.4
962-3	650	50	600	1	935	18.7	639.4	262.5	0.4
962-3	650	50	600	0.5	888	17.6	674.3	297.3	0.4
962-1	450	250	200	10	1621	26.3	245.5	82.7	0.3
962-1	450	250	200	5	1372	26.0	289.5	100.3	0.3
962-1	450	250	200	1	891	25.9	446.2	168.2	0.4
962-1	450	250	200	0.5	748	24.7	529.3	211.8	0.4
962-2	450	250	200	10	1657	26.8	240.2	85.9	0.4
962-2	450	250	200	5	1378	24.5	288.4	104.8	0.4
962-2	450	250	200	1	903	25.4	440.3	178.0	0.4
962-2	450	250	200	0.5	758	24.7	522.7	214.8	0.4
962-3	450	250	200	10	1473	27.9	270.4	84.7	0.3
962-3	450	250	200	5	1320	25.8	302.0	105.4	0.3
962-3	450	250	200	1	859	25.5	464.1	177.8	0.4
962-3	450	250	200	0.5	722	24.6	550.1	216.8	0.4

Table D. 39 Triaxial Frequency Sweep Test results at 20°C, 2.00° Angle of Gyration and Deviatoric Stress of 200 kPa and 400 kPa for Test Section 962SR

Sample Name	σ_1 kPa	σ_3 kPa	σ_D kPa	Freq (Hz)	Dyn Mod E_d (Mpa)	Phase Angle δ (°)	RAMS	RRMS	P Ratio, ν
962-1	450	250	200	10	2733	18.6	71.7	23.7	0.3
962-1	450	250	200	5	2420	19.4	81.5	30.3	0.4
962-1	450	250	200	1	1807	19.0	109.6	48.1	0.4
962-1	450	250	200	0.5	1561	19.0	126.4	54.3	0.4
962-2	450	250	200	10	2739	20.6	71.4	22.3	0.3
962-2	450	250	200	5	2350	19.6	84.0	27.0	0.3
962-2	450	250	200	1	1774	19.8	111.2	42.3	0.4
962-2	450	250	200	0.5	1565	18.6	125.7	51.0	0.4
962-3	450	250	200	10	2499	20.2	78.6	25.9	0.3
962-3	450	250	200	5	2263	18.3	87.2	27.4	0.3
962-3	450	250	200	1	1743	18.5	113.8	39.5	0.3
962-3	450	250	200	0.5	1522	18.0	129.4	45.3	0.4
962-1	650	250	400	10	2592	21.8	150.2	59.8	0.4
962-1	650	250	400	5	2245	21.2	175.9	69.2	0.4
962-1	650	250	400	1	1598	20.3	249.3	110.7	0.4
962-1	650	250	400	0.5	1369	19.5	290.6	132.8	0.5
962-2	650	250	400	10	2652	22.4	147.2	53.1	0.4
962-2	650	250	400	5	2279	21.6	173.5	68.4	0.4
962-2	650	250	400	1	1598	21.0	249.5	106.6	0.4
962-2	650	250	400	0.5	1374	20.5	289.1	124.9	0.4
962-3	650	250	400	10	2478	22.0	157.0	54.1	0.3
962-3	650	250	400	5	2153	20.8	183.3	70.3	0.4
962-3	650	250	400	1	1533	20.3	259.7	106.6	0.4
962-3	650	250	400	0.5	1319	19.4	301.0	123.3	0.4

Table D. 40 Triaxial Frequency Sweep Test results at 20°C, 2.00° Angle of Gyration and Deviatoric Stress of 600 kPa and 200 kPa (Fully Reversed) for Test Section 962SR

Sample Name	σ_1 kPa	σ_3 kPa	σ_D kPa	Freq (Hz)	Dyn Mod E_d (Mpa)	Phase Angle δ (°)	RAMS	RRMS	P Ratio, ν
962-1	650	50	600	10	1997	23.1	290.9	99.0	0.3
962-1	650	50	600	5	1681	21.9	351.7	132.7	0.4
962-1	650	50	600	1	1171	20.4	510.9	219.6	0.4
962-1	650	50	600	0.5	1013	19.0	590.3	275.1	0.5
962-2	650	50	600	10	2014	23.6	289.1	101.0	0.3
962-2	650	50	600	5	1691	22.0	349.8	137.0	0.4
962-2	650	50	600	1	1185	20.5	503.9	215.4	0.4
962-2	650	50	600	0.5	1020	19.5	585.3	264.2	0.5
962-3	650	50	600	10	1794	22.6	324.9	102.2	0.3
962-3	650	50	600	5	1530	21.6	386.7	142.2	0.4
962-3	650	50	600	1	1148	20.2	521.6	218.4	0.4
962-3	650	50	600	0.5	753	26.4	526.2	209.8	0.4
962-1	450	250	200	10	1853	28.1	214.4	81.8	0.4
962-1	450	250	200	5	1553	27.6	255.9	103.5	0.4
962-1	450	250	200	1	953	29.2	416.4	201.2	0.5
962-1	450	250	200	0.5	764	28.6	518.3	258.5	0.5
962-2	450	250	200	10	1905	28.2	208.9	77.3	0.4
962-2	450	250	200	5	1561	28.0	253.7	102.5	0.4
962-2	450	250	200	1	950	29.6	418.0	189.3	0.5
962-2	450	250	200	0.5	763	29.1	519.0	245.5	0.5
962-3	450	250	200	10	1732	27.3	229.5	80.2	0.3
962-3	450	250	200	5	1439	26.2	276.3	101.3	0.4
962-3	450	250	200	1	913	26.9	435.4	171.7	0.4
962-3	450	250	200	0.5	753	26.4	526.2	209.8	0.4

Table D. 41 Triaxial Frequency Sweep Test results at 20°C, 2.75° Angle of Gyration and Deviatoric Stress of 200 kPa and 400 kPa for Test Section 962SR

Sample Name	σ_1 kPa	σ_3 kPa	σ_D kPa	Freq (Hz)	Dyn Mod E_d (Mpa)	Phase Angle δ (°)	RAMS	RRMS	P Ratio, ν
962-1	450	250	200	10	2936	20.4	66.8	23.4	0.4
962-1	450	250	200	5	2532	20.8	77.8	29.8	0.4
962-1	450	250	200	1	1868	21.5	105.5	43.3	0.4
962-1	450	250	200	0.5	1652	19.8	119.3	50.4	0.4
962-2	450	250	200	10	2944	20.9	66.6	27.4	0.4
962-2	450	250	200	5	2660	19.8	74.1	28.7	0.4
962-2	450	250	200	1	1883	20.6	105.0	41.1	0.4
962-2	450	250	200	0.5	1650	19.4	119.4	48.6	0.4
962-3	450	250	200	10	2983	21.3	65.5	23.3	0.4
962-3	450	250	200	5	2590	21.1	76.1	26.8	0.4
962-3	450	250	200	1	1902	20.1	104.3	40.5	0.4
962-3	450	250	200	0.5	1643	20.1	120.3	49.3	0.4
962-1	650	250	400	10	2778	22.7	139.6	51.8	0.4
962-1	650	250	400	5	2386	22.1	165.6	67.3	0.4
962-1	650	250	400	1	1661	21.9	240.0	103.9	0.4
962-1	650	250	400	0.5	1421	21.1	279.3	127.1	0.5
962-2	650	250	400	10	2851	22.2	136.9	53.9	0.4
962-2	650	250	400	5	2427	22.3	162.8	66.7	0.4
962-2	650	250	400	1	1664	22.0	239.5	104.8	0.4
962-2	650	250	400	0.5	1429	21.3	277.8	127.8	0.5
962-3	650	250	400	10	2919	21.9	132.6	49.6	0.4
962-3	650	250	400	5	2469	21.6	160.4	61.7	0.4
962-3	650	250	400	1	1735	21.4	230.3	98.6	0.4
962-3	650	250	400	0.5	1453	20.9	273.5	122.4	0.4

Table D. 42 Triaxial Frequency Sweep Test results at 20°C, 2.75° Angle of Gyration and Deviatoric Stress of 600 kPa and 200 kPa (Fully Reversed) for Test Section 962SR

Sample Name	σ_1 kPa	σ_3 kPa	σ_D kPa	Freq (Hz)	Dyn Mod E_d (Mpa)	Phase Angle δ (°)	RAMS	RRMS	P Ratio, ν
962-1	650	50	600	10	2262	23.1	257.6	99.2	0.4
962-1	650	50	600	5	1807	22.2	327.0	135.3	0.4
962-1	650	50	600	1	1251	21.2	478.0	207.7	0.4
962-1	650	50	600	0.5	1073	19.9	557.1	256.6	0.5
962-2	650	50	600	10	2120	22.8	274.7	96.3	0.4
962-2	650	50	600	5	1783	22.0	331.5	138.8	0.4
962-2	650	50	600	1	1237	21.1	483.9	211.6	0.4
962-2	650	50	600	0.5	1055	19.8	566.5	259.3	0.5
962-3	650	50	600	10	2166	22.5	268.5	90.1	0.3
962-3	650	50	600	5	1833	21.9	322.3	125.5	0.4
962-3	650	50	600	1	1264	20.8	473.1	202.5	0.4
962-3	650	50	600	0.5	1081	19.8	553.1	252.7	0.5
962-1	450	250	200	10	1970	27.9	201.6	77.0	0.4
962-1	450	250	200	5	1584	29.4	251.0	96.2	0.4
962-1	450	250	200	1	916	31.1	433.1	194.2	0.4
962-1	450	250	200	0.5	703	31.9	563.5	261.1	0.5
962-2	450	250	200	10	1970	28.5	201.7	77.5	0.4
962-2	450	250	200	5	1600	28.7	248.6	100.3	0.4
962-2	450	250	200	1	931	30.6	426.5	190.2	0.4
962-2	450	250	200	0.5	727	30.7	544.1	255.3	0.5
962-3	450	250	200	10	1973	27.8	201.6	77.2	0.4
962-3	450	250	200	5	1620	29.2	245.3	98.1	0.4
962-3	450	250	200	1	954	30.5	416.3	191.9	0.5
962-3	450	250	200	0.5	739	31.0	535.7	248.2	0.5